



HAL
open science

Contribution of multitones to ultrawide band software defined radar

Julien Le Kerneç

► **To cite this version:**

Julien Le Kerneç. Contribution of multitones to ultrawide band software defined radar. Other [cs.OH]. Paris 6, 2011. English. NNT: . tel-03249827

HAL Id: tel-03249827

<https://theses.hal.science/tel-03249827>

Submitted on 4 Jun 2021

HAL is a multi-disciplinary open access archive for the deposit and dissemination of scientific research documents, whether they are published or not. The documents may come from teaching and research institutions in France or abroad, or from public or private research centers.

L'archive ouverte pluridisciplinaire **HAL**, est destinée au dépôt et à la diffusion de documents scientifiques de niveau recherche, publiés ou non, émanant des établissements d'enseignement et de recherche français ou étrangers, des laboratoires publics ou privés.



**THESE DE DOCTORAT DE
L'UNIVERSITE PIERRE ET MARIE CURIE**

Spécialité Electronique

EDITE de Paris – Ecole Doctorale Informatique, Télécommunication et Électronique

Présenté par

M. LE KERNEC Julien

Pour obtenir le grade de

DOCTEUR de l'UNIVERSITÉ PIERRE ET MARIE CURIE

Sujet de la thèse :

Contribution of Multitones for Ultra-Wide Band Software Defined Radar

Soutenue le 08/07/2011

Rapporteurs : Prof. Jacques David
Prof. Alain Mérigot

Directeur de thèse : Prof. Patrick Garda

Examineurs : Prof. Pascal Chevalier
Prof. Victor Fouad Hanna
Dr. Martin Klepal
Dr. Julien Denoulet
M. Philippe Dreuillet

Invités : Prof. Olivier Romain
M. Gérard Bobillot



**THESE DE DOCTORAT DE
L'UNIVERSITE PIERRE ET MARIE CURIE**

Spécialité Electronique

EDITE de Paris – Ecole Doctorale Informatique, Télécommunication et Électronique

Présenté par

M. LE KERNEC Julien

Pour obtenir le grade de

DOCTEUR de l'UNIVERSITÉ PIERRE ET MARIE CURIE

Sujet de la thèse :

Contribution of Multitones for Ultra-Wide Band Software Defined Radar

Soutenue le 08/07/2011

Rapporteurs : Prof. Jacques David
Prof. Alain Mérigot

Directeur de thèse : Prof. Patrick Garda

Examineurs : Prof. Pascal Chevalier
Prof. Victor Fouad Hanna
Dr. Martin Klepal
Dr. Julien Denoulet
M. Philippe Dreuillet

Invités : Prof. Olivier Romain
M. Gérard Bobillot

Acknowledgements

Après ces cinq années de doctorat bien remplies passées à l'Onera, à l'UPMC-LIP6 et au CNAM-EASY, le temps des remerciements est venu pour les personnes et institutions qui ont de près ou de loin contribué à la réussite de cette aventure.

Ma thèse s'est déroulée au sein du département Electromagnétisme et Radar de l'Onera, et je souhaite remercier les personnes qui sont à l'origine de cette thèse dans le domaine du radar logiciel. Merci donc à mes encadrants, Philippe Dreuillet, Gérard Bobillot et Juan-Carlos Castelli. Tous les trois m'ont beaucoup apporté sur le plan scientifique et personnel.

Je tiens également à remercier Patrick Garda, Julien Denoulet et Olivier Romain de l'UPMC-LIP6 qui ont encadré la thèse du côté universitaire. Plus particulièrement pour leur apport dans la structuration scientifique, la rédaction du manuscrit et en termes de communications.

J'adresse également mes sincères remerciements aux deux rapporteurs, Jacques David, Professeur à l'ENSEEIH et Alain Mérigot, Professeur à l'Institut Electronique Fondamentale – Université d'Orsay. J'ai fortement apprécié leur intérêt pour ces travaux et la justesse de leurs commentaires.

Merci également à Pascal Chevalier, Professeur de Chaire au CNAM-EASY et Martin Klepal, Chercheur au Cork Institute of Technology – Nimbus centre, pour leur participation au jury de thèse et leur intérêt pour ces travaux.

Merci également à Victor Fouad Hanna, Professeur à l'UPMC-L2E pour la présidence du jury de thèse, pour ses conseils et son intérêt pour ces travaux.

Dans ce travail, l'expérimentation a été la partie la plus stimulante et a demandé de relever de nombreux défis. Merci donc à Patrick Méchin de Techway pour le support technique sur numériseur, Matthias Charriot de Tektronix pour sa réactivité et son support technique sur les générateurs de signaux, à Anil Cheraly, Luc Picard, Sylvain Attia et Christophe Coudrain de l'Onera pour leur aide et leur expertise technique.

Je tiens aussi à remercier Antoine Ghaleb, Luc Vignaud, Jean-Philippe Ovarlez et Eric Chaumette pour leur expertise dans le domaine du traitement du signal et surtout pour leur pédagogie.

Je tiens aussi à remercier les personnes qui ont participé aux expérimentations en tant que cibles ou pour la logistique : Edouard Demaldent, Huy Khang Phan, Antoine Ghaleb, Ghilem Pailloux, Christophe Coudrain, Francois Tardivel, Jean-Francois Petex, Juan-Carlos Castelli, Gérard Bobillot, Jennifer Bourguignon, Severine Molko, Jean-Paul Marcellin, Jérôme Simon, Sophie Langlet, Béatrice Fromentin et David Levadoux.

Je souhaite également remercier Emmanuel Rosencher et Jean-Marc Boutry de m'avoir accueilli dans leurs locaux.

Merci également à Françoise Ricci et Elisabeth Bertheau pour leur aide sur les aspects administratifs.

Je tiens également à remercier le CNAM et plus particulièrement Michel Terré, Daniel Roviras et Catherine Algani et l'UPMC-LIP6 et plus particulièrement Patrick Garda, Julien Denoulet et Olivier Romain, qui m'ont accueilli au sein de leurs équipes respectivement EASY et SYEL en tant qu'ATER ce qui m'a permis d'achever ce manuscrit.

Je tiens à remercier mes collègues de l'Onera avec qui j'ai partagé de très bons moments : Aurore Risacher, Jérôme Simon, Huy Khang Phan, Béatrice Fromentin, Sophie Langlet, Jennifer Bourguignon, Séverine Daugas, Edouard Demaldent, Marc Le Khiem et Anil Chéry. Merci à vous.

Merci aussi à mes collègues de l'équipe SYEL à l'UPMC que j'ai grandement apprécié pour ces moments autour d'un café : Johan Mazeyrat, Anthony Kolar, Sylvain Viateur, Mehdi Terosiet, Olivier Romain, Julien Denoulet, Cedric Champion, Sylvain Feruglio, Patrick Garda, Farouk Valette, Ruomin Wang, Alex Goguin, Khalil Hachicha, Annick Alexandre, Brunel Happi et Abraham Suissa. Merci à vous.

Merci aussi à mes collègues de l'équipe EASY au CNAM pour leur accueil chaleureux : Catherine Algani, Michel Terré, Daniel Roviras, Christophe Alexandre, Didier Le Ruyet, Mylène Pischella, Pierre Provent, Yahia Medjadhi, Rostom Zakaria, Iness Ahriz et Berna Ozbek. Merci à vous.

Je remercie aussi Christopher Robert, Coach, qui m'a aidé à développer mes aptitudes de communications et à mieux maîtriser mon environnement professionnel.

Je dois remercier aussi mes amis Thomas Noël, Cédric Vignaud, Renaud Bellais et Vincent Foley pour leur soutien dans les bons et les mauvais moments.

Je dois remercier ma famille sans quoi rien de cela n'aurait été possible mes parents Catherine et Louis, mes frères Franck et Sébastien ainsi que tous les autres et surtout mon épouse Fei et ma fille Lou-Ann. Merci à vous pour votre soutien et vos encouragements.

Contents

Chapter 1. Introduction.....	1-1
Chapter 2. Context & Objectives.....	2-1
A. Onera’s missions and activities.....	2-2
B. Overview of radar evolution and background.....	2-3
1. History.....	2-3
2. Radar notions.....	2-4
3. Evolution of RF front ends.....	2-6
C. General Background on Multitones and OFDM.....	2-8
1. Definition of Multitones and OFDM.....	2-8
2. History of multicarrier waveforms.....	2-9
3. Advantages and Drawbacks of multi-carriers.....	2-10
D. New radar concepts.....	2-12
E. Contribution of Multitones for UWB Radar.....	2-17
Chapter 3. State of the Art.....	3-1
A. Existing RF platform analysis.....	3-2
1. PANDORA.....	3-2
2. HYCAM: Microwave Camera for Multi-Dimensional Analysis of the RCS of Time-Varying targets.....	3-3
3. Dual use SAR imaging and telecommunication system.....	3-4
4. IDROMel.....	3-5
5. Synthesis on the state of the art of RF platform architectures.....	3-6
B. What is the impact of RF components on the performances?.....	3-8
1. Linearization in radar systems involving multicarrier.....	3-8
2. RF Equipment & Multicarrier.....	3-11
3. Synthesis on RF equipment in the state of the art.....	3-14
C. What are the performances of Multitones and/or OFDM signals compared to classic waveforms?.....	3-15
1. Ambiguity Function.....	3-15
2. New Signal Processing Algorithms using Multi-carrier structure.....	3-18
3. Synthesis on the multitone performances compared to classic radar waveforms in the state of the art.....	3-24
D. Conclusions.....	3-26
1. Which architecture for the experimental test bench?.....	3-26
2. What is RF equipment impact on performances?.....	3-26
3. What are the performances of Multitones and/or OFDM signals compared to classic waveforms?.....	3-27

4. Redefinition of the Objectives.....	3-27
Chapter 4. Theoretical study of radar architectures for HYCAM-research test bench implementation 4-1	
A. Radar architecture	4-2
1. Radar front end architecture description	4-3
B. Generic Signal Processing Algorithms	4-6
1. Radix-2 FFT algorithm for parallel and time-interleaved architectures	4-6
2. DFT algorithm for frequency-interleaved architecture	4-8
3. Doppler processing.....	4-8
C. Radar architecture comparison.....	4-9
1. Minimum orthogonal time and Doppler ambiguity	4-9
2. Processing power and data throughput.....	4-10
3. Transfer Function Compensation	4-11
4. Dynamic range	4-14
5. Reference channel	4-15
6. Synthesis.....	4-15
D. Design rules for intermodulation.....	4-17
1. Intermodulation avoidance.....	4-18
2. 3 rd order intermodulation power level control in non-linear components.....	4-19
E. Conclusion	4-20
Chapter 5. Waveform simulations	5-1
A. Signal definitions.....	5-4
1. Multitones with Newman Phase codes.....	5-5
2. Linear Frequency Modulated Signal – Linear Chirp	5-7
B. Simulation processes and performance criteria.....	5-8
1. Simulated processes	5-8
2. Performance criteria	5-10
3. Synthesis of performance criteria.....	5-14
C. Simulated PMEPR	5-14
1. Effect of the number of quantization bits on PMEPR.....	5-15
2. Effect of saturation on PMEPR.....	5-15
D. Simulated Power Efficiency simulations	5-18
1. Effect of the number of quantization bits on Power Efficiency	5-18
2. Effect of saturation on Power Efficiency	5-19
E. Simulated Ambiguity Function.....	5-22
1. Simulated Ambiguity Function of Chirp and Multitones	5-22
2. Effect of the number of quantization bits on Distance Compression.....	5-24

3.	Effect of saturation in an amplifier on Distance Compression	5-27
F.	Discussion on simulations.....	5-27
G.	System level performances.....	5-31
H.	Synthesis and Conclusion.....	5-31
Chapter 6.	Radar Implementation and Experiment Design	6-1
A.	Radar Implementation	6-2
1.	Hardware and Design Constraints.....	6-2
2.	Frequency planning	6-4
3.	System Overview	6-5
4.	Radar characteristics	6-8
5.	Expected radar performances	6-9
B.	Experiment design for waveform comparison	6-9
1.	Description of the experimentation environment.....	6-9
2.	Radar Evolution.....	6-11
3.	Radar basic capabilities	6-12
4.	Experiment Design for Waveform Comparison.....	6-13
C.	Conclusions	6-20
Chapter 7.	Experimental Results	7-1
A.	Closed-loop DAC-Filter-ADC	7-2
1.	PMEPR.....	7-2
2.	Power efficiency.....	7-5
3.	Pulse compression DAC-ADC measurements	7-7
4.	Synthesis.....	7-8
B.	Experiment on static targets: Stability measurements.....	7-9
C.	Doppler Experiments.....	7-10
D.	Experiments on Saturation	7-13
1.	Test channel recovery algorithm	7-13
2.	PMEPR.....	7-15
3.	Power Efficiency	7-17
4.	Compression.....	7-18
5.	Synthesis on saturation.....	7-22
E.	Conclusions.....	7-23
Chapter 8.	Conclusion	8-1
A.	Conclusions	8-2
B.	Perspectives	8-3
C.	Publications & Communications.....	8-5
Chapter 9.	Appendix.....	9-1

A.	Multicarrier advantages and drawbacks	9-2
B.	PMEPR reduction techniques.....	9-3
C.	IDROMel.....	9-4
D.	Processing Power calculations	9-5
1.	Frequency Interleaved Architecture	9-5
2.	Parallel Architecture.....	9-6
3.	Time Interleaved Architecture	9-7
E.	Transfer Function Compensation.....	9-7
1.	Frequency-interleaved.....	9-8
2.	Parallel.....	9-10
3.	Time interleaved.....	9-10
F.	Spurious and Intermodulation avoidance.....	9-11
1.	Upconversion	9-11
2.	Downconversion.....	9-13
G.	Model for the AFD2-010020-23P-SP	9-14
H.	Ambiguity function algorithm validation.....	9-15
I.	Experimental test bench.....	9-17
1.	System Overview	9-17
2.	Transmitter	9-17
3.	Amplification stage 1	9-19
4.	Amplification stage 2	9-21
5.	2 nd oscillator and reference channel	9-24
6.	Test Channel.....	9-27
7.	Digitizer.....	9-29
8.	1 st local oscillator	9-30
J.	Parking Experiment Model	9-33
K.	RMS quantization noise floor	9-37
L.	Micro-Doppler Experiment.....	9-39
M.	Amplifier gain measurement and input power range for the saturation experiment.	9-44
N.	Stability	9-46
O.	Saturation Measurements	9-50
1.	PMEPR.....	9-50
2.	Power efficiency.....	9-50
3.	Mainlobe 3dB width.....	9-51
4.	Sidelobes' amplitudes	9-52
5.	Sidelobes' positions.....	9-54

Chapter 10. Bibliography..... 10-1

Table of figures

Figure 1: Ambiguity function examples: a) unmodulated pulse, b) linear frequency modulated, c) train of unmodulated pulses and d) train of phase coded pulse barker code	2-5
Figure 2: illustration of the ambiguity function concept (13).....	2-5
Figure 3: classic monostatic conventional radar block diagram (15)	2-6
Figure 4: digital monostatic digital radar block diagram.....	2-7
Figure 5: software Radio/Radar block diagram	2-7
Figure 6: OFDM representation infrequency domain.....	2-9
Figure 7: Block diagram of (top) transmitter (bottom) receiver - section of multicarrier Modulation-FFT radar scheme (14).....	2-12
Figure 8: OFDM agile radar transceiver block-scheme (37).....	2-14
Figure 9: System block diagram of PANDORA (43).....	3-2
Figure 10: HYCAM experimental test bench (9)	3-3
Figure 11: block diagram of the designed OFDM (top) performances (bottom) (45).....	3-4
Figure 12: IDROMel (left) architecture block diagram (right) prototype(www.openairinterface.org).....	3-5
Figure 13: Partial Ambiguity Function of a multi-frequency complementary phase-coded based on consecutive order cyclic shifts of a P4. $N = M = 15$. Equal carrier Amplitude (12). 3-16	3-16
Figure 14: multifrequency complementary phase-coded concept illustrating the spectrum shape, phase coding, autocorrelation and frequency weighting (69).....	3-17
Figure 15: ambiguity function of pulse burst with frequency agile OFDM patterns (top) random grouped (middle) Costas grouped (bottom) random spread subcarriers (37).....	3-18
Figure 16: ambiguity function of 8 tones signal with $F_c = 10\text{GHz}$, $B = 5\text{MHz}$, QPSK modulation (left) partial 3D ambiguity function (right) zero-delay cut (70).....	3-20
Figure 17: the processing scheme block diagram (71)	3-22
Figure 18: bistatic architecture.....	4-2
Figure 19: Frequency interleaved radar front end for 2 channels	4-4
Figure 20: Parallel radar front end for 2 channels	4-5
Figure 21: Time interleaved front end for 2 channels.....	4-5
Figure 22: Pulse compression algorithm (left) radix-2 FFT for parallel and time-interleaved architectures (right) DFT for frequency-interleaved architecture.....	4-7
Figure 23: digital downconversion to baseband	4-8
Figure 24: Doppler processing.....	4-9
Figure 25: processing power comparison of radar architectures with 2 channels and a sample frequency @ 2GS/s with 2 channels and a refresh rate of 100Hz for the time-interleaved architecture.....	4-11
Figure 26: Transfer functions block diagram for frequency interleaved architecture	4-12
Figure 27: Transfer functions block diagram for parallel architecture	4-13
Figure 28: Transfer functions block diagram for time interleaved architecture	4-14
Figure 29: Which architecture \rightarrow the parallel architecture	4-17
Figure 30: 3 rd order interception point and power levels for 3 rd order intermodulation power level control e.g 70dB below main signal (9).....	4-20
Figure 31: Chirp and Multitones with low $B = 1\text{MHz}$ and $\text{PRP} = 5\ \mu\text{s} \rightarrow \text{BT} = 5$	5-4
Figure 32: Multitones' samples generation algorithm.....	5-6
Figure 33: Newman Phase Coded Multitones $\text{BW} = 800\text{MHz}$ $\text{PRP} = 500\text{ns}$. Top: time domain Bottom: frequency domain.	5-7
Figure 34: Linear Chirp $\text{BW} = 800\text{MHz}$ $\text{PRP} = 500\text{ns}$ (top) time domain (bottom) frequency domain.....	5-7

Figure 35: algorithms used to study the performance criteria wrt quantization	5-9
Figure 36: algorithms used to study the performance criteria wrt saturation	5-10
Figure 37: domain of validity of each signal configuration.....	5-12
Figure 38: pulse compression measurements in distance for multitones and chirp when PRP = 500ns and B = 800MHz	5-13
Figure 39: nominal PMEPR values in dB of the tested signals: left) Chirp right) multitones	5-15
Figure 40: simulated PMEPR of Chirp and multitones with B = [1MHz (left), 800MHz (right)] wrt number of quantization bits. Top: Chirp, Bottom: multitones	5-16
Figure 41: simulated PMEPR of Chirp and multitones with B = [1MHz (left), 800MHz (right)] wrt saturation. Top: upC, Mid: multitones and Bottom: difference	5-17
Figure 42: nominal power efficiency values in % of the tested signals.....	5-18
Figure 43: simulated power efficiency of Chirp and multitones with B = [1MHz (left), 800MHz (right)] wrt number of quantization bits. Top: upC, Mid: multitones and Bottom: relative error on power efficiencies between waveforms	5-20
Figure 44: simulated power efficiency of Chirp and multitones with B = [1MHz (left), 800MHz (right)] wrt saturation. Top: upC, Mid: multitones and Bottom: relative error between on power efficiencies between waveforms.....	5-21
Figure 45: Simulated ambiguity function for Chirp and Multitones (B = 800MHz, PRP = 500ns, radial velocity @ 10.4GHz) (top) Chirp (middle) Multitones (bottom) ambiguity function difference for multitones and chirp with bandwidth time product equal to 400 (B 800MHz; T 500ns; velocity validity 2984m/s).....	5-23
Figure 46: main ridge cut of multitones and chirp signals for raw and Hamming windowed data and their differences for multitones and chirp with bandwidth time product equal to 400 (B800MHz; T500ns; velocity validity 2984m/s).....	5-24
Figure 47: (left) ambiguity function zero-Doppler cut (top) raw (bottom) Hamming window (right) zero-distance cut (top) raw (bottom) Hamming window for multitones and chirp with bandwidth time product equal to 400 (B800MHz; T500ns; velocity validity 2984m/s).....	5-24
Figure 48: effect of quantization on Chirp and Multitones for B = 800MHz and PRP= 50 μ s \rightarrow BT = 40000.....	5-25
Figure 49: Equation 20 vs simulated data: A) minimum number of bits, B) mean error, C) max error on pulse compression and D) mean error on pulse compression vs number of quantization bits.....	5-26
Figure 50: impulse responses wrt saturation and sampling frequency for signals with B = 800MHz and PRP = 50us.....	5-28
Figure 51: spectra at P1dB-6dB of chirp for B = 10MHz, PRP = 50us - positions and bandwidths of the strongest odd order intermodulations	5-29
Figure 52: spectra of chirp with PRP = 500us wrt saturation and sampling frequency.....	5-30
Figure 53: Bandpass sampling and Nyquist bands – $F_s = F_s_digitizer$	6-3
Figure 54: Signal generation with DAC - defined signal and its mirrored image around $Fs2 - Fs_generator = Fs$	6-4
Figure 55: Experimental test bench system overview - schematic	6-6
Figure 56: Experimental test bench system overview - lab experimental test bench set-up .	6-7
Figure 57: parking experiment (top) schematic and dimensions (bottom) lab and parking set-up.....	6-10
Figure 58: evolution of the radar view (top) optical camera view (bottom) radar view (left) first try (right) final stage.....	6-12
Figure 59: cat lying in the center of the scene (left) optical camera view (right) radar view..	6-13

Figure 60: pedestrian standing still while swinging his left arm slowly (left) optical camera view (right) radar view.....	6-13
Figure 61: direct measurement DAC filter ADC for waveform evaluation	6-14
Figure 62: experimental set-up for waveform experiments.....	6-15
Figure 63: static targets (left) calibrator position (right) calibrator placed at 5.197meter from the calibrator on the 0 °axis	6-15
Figure 64: stability measurement protocol	6-16
Figure 65: set up inside the anechoic chamber (top) optical view (bottom) radar view.....	6-18
Figure 66: saturation experiment synoptic.....	6-19
Figure 67: measured chirp and Multitones signals at 1MHz and 800MHz	7-2
Figure 68: top: PMEPR @ 10 bits for chirp and multitones, middle: difference between multitones and Chirp @ 8 and 10bits, bottom: difference between measurement and simulation @ 10 bits for chirp and multitones.....	7-4
Figure 69: Measured spectrum of chirp and Multitones at 1MHz and 800MHz.....	7-5
Figure 70: top: power efficiency @ 10 bits for chirp and multitones, middle: relative error between multitones and Chirp @ 8 and 10bits, bottom: relative error between measurement and simulation @ 10 bits for chirp and multitones.....	7-6
Figure 71: Compression in Distance of Chirp and multitones with (B 1MHz, PRP 500us) and (B 800MHz, PRP 5us) with Hamming window	7-7
Figure 72: stability on the peak response of the pulse compression of a trihedral reflector placed @ 27m from the antenna for chirp (right) and multitones (left) @ 1MHz over 16ms with digital replica	7-10
Figure 73: Doppler-distance images of the Doppler experiment top) Doppler-distance images bottom-left) zero-Doppler cut bottom-right) distance-cut	7-11
Figure 74: Amplitude of the modulation peaks of a 700Hz square-wave in the distance cuts @ BW 1MHz & 800MHz.....	7-12
Figure 75: echo reconstruction algorithm from distance compression.....	7-13
Figure 76: reversal algorithm effect on signal time and frequency domain, PMEPR and power efficiency for multitones with 800MHz bandwidth and 500ns PRP	7-14
Figure 77: measured PMPER from saturation experiment and difference between measured and simulated data.....	7-15
Figure 78: measured power efficiency from saturation experiment and error between measured and simulated data for multitones.....	7-17
Figure 79: impulse response of a chirp with 10MHz bandwidth and PRP 5us @ IP1dB ...	7-19
Figure 80: relative error and differences between measurement and simulation of the impulse response characteristics for multitones	7-20
Figure 81: Difference between multitones and Chirp impulse response on the saturation experiment.....	7-22
Figure 82: guard interval principle (5).....	9-2
Figure 83: schematic of the IDROMEL architecture (46)	9-4
Figure 84: Common Transmitter transfer function block diagram	9-7
Figure 85: AFD2-010020-23P-SP gain wrt input power measurement, model and IP1dB	9-15
Figure 86: Comparison of the analytical versus the numerical ambiguity function function for chirp (B = 800MHz, PRP = 500ns) (top) theoretical (middle) simulated (bottom) difference	9-16
Figure 87: Detailed architecture of the transmitter	9-17
Figure 88: Detailed architecture of amplification stage 1	9-19
Figure 89: Horn antenna dimensions	9-21
Figure 90: Detailed architecture of amplification stage 2.....	9-22
Figure 91: Detailed architecture of the 2 nd local oscillator and the reference channel	9-24

Figure 92: Detailed architecture of the test channel	9-27
Figure 93: Detailed architecture of the 1 st Local Oscillator.....	9-31
Figure 94: set-up for the parking experiment	9-33
Figure 95: Difference between target in line of sight and target travelling inside the antenna gain pattern.....	9-35
Figure 96: antenna main beam footprint for clutter calculation	9-36
Figure 97: Clutter to Noise ratio over the Parking area	9-36
Figure 98: a pedestrian sprinting on the 45 ° axis (left) optical camera view (right) radar view	9-40
Figure 99: a car circling very slowly around the center of the scene (left) optical camera view (right) radar view	9-40
Figure 100: synchronization and reproducibility issues with experiments on moving targets on a straight line over the 45 ° axis (a) car (b) sprinter (c) cyclist in free wheel (d) two joggers on.....	9-41
Figure 101: Doppler experiment with rotating fan facing forward on the 45 ° axis.....	9-42
Figure 102: distance cut at -0.2064m of radar view (left) full distance cut (right) zoom of left view (Figure 101).....	9-43
Figure 103: vector network analyzer measurement setup (top) reference measurement (bottom) amplifier gain measurement.....	9-44
Figure 104: IP1dB and gain for saturation experiment: amplifier ITS electronics PA-95105-4050.....	9-45

Table of tables

Table 1: Advantages and drawbacks of multitone and OFDM	2-10
Table 2: New radar concepts and implications in digital and analogue parts.....	2-16
Table 3: IDROMel basic features	3-5
Table 4: Synthesis of the known OFDM platform features	3-7
Table 5: linearization techniques and their improvement capabilities and drawbacks.....	3-10
Table 6: linearization techniques and their compensation capabilities and system implications (49).....	3-11
Table 7: evaluation of linearization techniques based on components, input power, waveform and performance criteria improvements	3-13
Table 8: simulated improvements for ADC with multicarrier signals.....	3-14
Table 9: maximum allowed speed wrt number of carriers for 1dB compression loss for $f_0 = 10GHz$ and $B = 5MHz$	3-21
Table 10: Synthesis of the new concepts advantages and drawbacks	3-24
Table 11: processing power required for all the architectures – real multiplications and additions.....	4-10
Table 12: Radar architectures synthesis.....	4-16
Table 13: n^{th} order intermodulation avoidance rules for upconversion	4-19
Table 14: n^{th} order intermodulation avoidance rules for downconversion	4-19
Table 15: (top) bandwidth settings (bottom) Pulse Repetition Periods	5-3
Table 16: eliminated waveform configurations	5-4
Table 17: main characteristics of the distance compression – raw data	5-22
Table 18: system level performances from simulation of quantization @ 10bits and saturation @ IP1dB.....	5-31
Table 19: DA and AD converters main characteristics	6-2
Table 20: Filters for image removal after upconversion.....	6-5
Table 21: estimated digitizers’ maximum achievable SNR.....	6-8
Table 22: radar characteristics	6-9
Table 23: measured targets for micro-Doppler experiments	6-11
Table 24: radar settings for micro-Doppler experiments – first try and final stage.....	6-11
Table 25: comparison of the experimental UWB reconfigurable radar HYCAM v2 to the RF platforms from the literature review	6-20
Table 26: Main characteristics of the pulse compression wrt bandwidth.....	7-8
Table 27: relative error on 3dB mainlobe width, sidelobes’ positions and difference in sidelobes’ amplitudes between measurements and simulations	7-8
Table 28: worst case relative error on stability wrt bandwidth with digital replica	7-9
Table 29: measured compression characteristics from saturation experiment	7-19
Table 30: Comparison of PMEPR reduction techniques	9-4
Table 31: number of operations per second for frequency interleaved architecture for DFT	9-5
Table 32: number of operations per second for frequency interleaved architecture for FFT	9-6
Table 33: number of operations per second for frequency parallel architecture	9-6
Table 34: number of operations per second for frequency time-interleaved architecture	9-7
Table 35: estimated digitizer dynamic range	9-38
Table 36: relative error in dB in amplitude and phase of the peak of the impulse response with a digital reference – raw.....	9-46
Table 37: difference in dB between multitone and Chirp in relative error in amplitude and phase of the peak of the impulse response with a digital reference – raw.....	9-46
Table 38: relative error in dB in amplitude and phase of the peak of the impulse response with a digital reference – Hamming.....	9-46

Table 39: difference in dB between multitones and Chirp in relative error in amplitude and phase of the peak of the impulse response with a digital reference – Hamming.....	9-47
Table 40: relative error in dB in amplitude and phase of the peak of the impulse response with a measured reference – raw	9-47
Table 41: difference in dB between multitones and Chirp in relative error in amplitude and phase of the peak of the impulse response with a measured reference – raw.....	9-47
Table 42: relative error in dB in amplitude and phase of the peak of the impulse response with a measured reference – Hamming	9-48
Table 43: difference in dB between multitones and Chirp in relative error in amplitude and phase of the peak of the impulse response with a measured reference – Hamming.....	9-48
Table 44: difference in dB between relative errors on stability obtained with measured reference and digital reference – raw	9-48
Table 45: difference in dB between relative errors on stability obtained with measured reference and digital reference - Hamming	9-49
Table 46: Measurement results on PMEPR in dB	9-50
Table 47: Measurement results on power efficiency in %	9-51
Table 48: Measurement results on 3dB main lobe width	9-52
Table 49: Measurement results on left sidelobe amplitude	9-53
Table 50: Measurement results on right sidelobe amplitude	9-54
Table 51: Measurement results on left sidelobe position.....	9-55
Table 52: Measurement results on right sidelobe position	9-56

Table of equations

Equation 1: TD – Total Distortion	3-12
Equation 2: Compression Loss for multitones (70)	3-19
Equation 3: maximum target speed for 1dB compression loss (70)	3-21
Equation 4: SNR improvement with Doppler subcarriers processing (37)	3-23
Equation 5: SNR Loss range for frequency interleaved architectures	4-14
Equation 6: 3 rd order interception point output back off for 3 rd order intermodulation power levels at XdB below the main signal power (9)	4-20
Equation 7: ambiguities and resolutions	5-2
Equation 8: fractional bandwidth (82)	5-2
Equation 9: Multitones generation rules for intermodulation-free digital signal	5-5
Equation 10: Newmann Phase Coded Multitones definition (real)	5-5
Equation 11: Newman Phase Codes	5-5
Equation 12: Linear Chirp definition (real)	5-7
Equation 13: simple radar equation (13).....	5-8
Equation 14: Peak to Mean Envelope Power Ratio	5-10
Equation 15: Maximum achievable signal to noise ratio (9)	5-11
Equation 16: power efficiency	5-11
Equation 17: Narrowband Ambiguity Function (84).....	5-12
Equation 18: Wideband Ambiguity Function (84)	5-12
Equation 19: upper bound of the phase error in the integrand caused by the NB ambiguity function approximation (85)	5-12
Equation 20: minimum number of useful bits necessary to digitize a signal with a given bandwidth-time product for pulse compression.....	5-27
Equation 21: 3dB percentage Bandwidth	6-3
Equation 22: Friis formula for noise figure & total gain	6-8
Equation 23: Noise power.....	6-8
Equation 24: AFD2-010020-23P-SP amplification model – 7 th order polynomial	9-14
Equation 25: Linear Chirp ambiguity function Analytical equation	9-15
Equation 26: IF sampling spatial speck	9-16
Equation 27: Triangle Corner Reflector RCS	9-33
Equation 28: Monostatic Signal to Noise Ratio.....	9-34
Equation 29: sinc ² approximation of the horn antenna gain pattern.....	9-34
Equation 30: clutter surface calculation (13)	9-35
Equation 31: relative clutter RCS with respect to grazing angle (13)	9-35
Equation 32: Maximum SNR achievable per ADC channel	9-37
Equation 33: Processing gain.....	9-37
Equation 34: FFT gain	9-37
Equation 35:bandpass sampling losses caused by aliased noise.....	9-37
Equation 36: SNR limitation caused by the total RMS aperture jitter.....	9-38
Equation 37: Gain versus input power.....	9-44

Glossary

A

AANF	Adaptive Analogue Notch Filter
ACPR	Adjacent Channel Power Ratio
AD	Analog to Digital
ADC	Analog to Digital Converter
ADSL	Asymmetric Digital Subscriber Line
AF	Ambiguity Function
AGC	Automatic Gain Control
AM	Amplitude Modulation
APAR	Active Phased Array Radar
AWG	Arbitrary Waveform Generator
AWGN	Additive White Gaussian Noise

B

BER	Bit Error Rate
BLER	Block Error Rate
BPSK	Binary Phase Shift Keying
BT	Bandwidth Time

C

CDMA	Code Division Multiple Access
CFAR	Constant False Alarm Rate
CNR	Clutter to Noise Ratio
COCS	Consecutive Order Cyclic Shift
COFDM	Coded Orthogonal Frequency Division Multiplexing
CR	Cognitive Radio/Radar
CW	Continuous Wave

D

DA	Digital to Analog
DAB	Digital Audio Broadcasting
DAC	Digital to Analog Converter
dBFS	dB @ Full Scale
dBsqm	dB square meter
DEMUR	Electromagnetism and Radar Department
DFT	Discrete Fourier Transform
DSP	Digital Signal Processing
DVB	Digital Video Broadcasting

E

ENOB	Effective Number Of Bits
------	--------------------------

F

FFT	Fast Fourier Transform
FM	Frequency Modulation

FMCW	Frequency Modulation Continuous Wave
FPGA	Field Programmable Gate Array
G	
GMACS	Giga Multiply-Accumulate Operations per Seconds
H	
HPA	High Power Amplifier
I	
IBO	Input Back Off
IDFT	Inverse Discrete Fourier Transform
IEEE	Institute of Electrical and Electronics Engineers
IF	Intermediate Frequency
IFFT	Inverse Fast Fourier Transform
IM3	3 rd Order Intermodulation
IP1dB	1dB compression point
L	
LFM	Linear Frequency Modulation
LO	Local Oscillator
LSL	Left Side Lobe
M	
MIMO	Multiple Input Multiple Output
MSC	Modulated Single Carrier
MT	Multitones
N	
NB	Narrowband
NF	Noise Figure
O	
OBO	Output Back Off
OFDM	Orthogonal Frequency Division Multiplexing
OOB	Out Of Band
P	
P3	the Lewis and Kretschmer Polyphase code P3
P4	the Lewis and Kretschmer Polyphase code P4
PANDORA	Parallel Array for Numerous Different Operational Research Activities
PAPR	Peak to Average Power Ratio
PER	Packet Error Rate
PM	Phase Modulation

PMEPR Peak to Mean Envelope Power Ratio
PTS Partial Transmit Sequence

Q

QPSK Quadrature Phase Shift Keying

R

RCS Radar Cross Section
RF Radio Frequency
RMS Root Mean Square
RSL Right Side Lobe
Rx Receiver

S

SAR Synthetic Aperture Radar
SFDR Spurious Free Dynamic Range
SIR Signal to Interference Ratio
SLM Selected Mapping
SNR Signal to Noise Ratio
SSPA Solid State Power Amplifier

T

TD Total Distortion
TI Tone Injection
TR Tone Reservation
TWTA Traveling Wave Tube Amplifier
Tx Transmitter

U

UHF Ultra High Frequency
UWB Ultra Wide Band

V

VSWR Voltage Standing Wave Ratio
VHF Very High Frequency

W

wrt with respect to

Chapter 1. Introduction

In the last two decades, telecommunications went through a fast evolution pushed by increasing demands on throughput, quality of service, etc... This led to the development of numerous standards in diverse applications to meet these requirements.

The evolution of processing power and AD/DA converters' bit-resolution according to Moore's Law made all of this possible.

One of the major advances in waveform design for telecommunications was the Orthogonal Frequency Division Multiplexing (OFDM). This waveform also called multitones is composed of a number of sine-waves or tones sent simultaneously. Each of these sine-waves is coded to carry information and allows increased throughputs and better quality of service.

Also the advent of digital technologies allows minimizing the number of components in the RF front end by replacing them partially by digital functions. In telecommunications, the received signal is now often fully digitized and processed directly in the digital core.

Nowadays, many communication standards are in use and until a few years back, a device was dedicated to use one standard and one standard only. With the development in digital architectures, the idea of merging several standards onto the same device came up. The best example is the smartphone that can use several communications modes: Wireless LAN, mobile phone communication standards ... To date, there is a RF front end and a dedicated for each function. As the technology evolves a growing number of functions are integrated onto the main chip. These devices adapt to their environment by modifying signal strength, changing communication standard, etc..

The next evolution of this approach would be adaptive systems that could emit, receive and process any kind of signal. This is called software radio.

When comparing the evolution of telecommunications to radar applications, radar technologies are a little behind radio technologies. Indeed defense applications usually require highly reliable systems and thus little risk is put into new technologies that have not proven their potential and reliability.

The digital architectures have improved greatly in terms of reliability and robustness in the last decade. Also the prospect of reconfigurable signal processing is extremely valuable in radar applications. This enables multifunction radars which could switch between different radar modes.

There is an opportunity for new advances in radar systems taking advantage of the progresses of the technologies and of the innovations in radio.

Multitones present many advantages; also they are easily configured and generated digitally. Such waveform presents appealing advantages for digital radar applications.

Onera - the French Aerospace Lab undergoes research in radar technologies since the 1960s. Its mission is to develop the radar systems of tomorrow. And in this perspective, Onera is researching and developing digital radar systems to replace the analogue systems currently used. The objective in the long term is to develop a software radar system.

This study is part of this research and aims at determining the contribution of multitones to ultra wide band software defined radar. Software defined radar is agile, reconfigurable and multifunction. The functions on the software defined radar are first radar modes such as surveillance, tracking and imaging and communications. For communications, multitones allow their implementation and present numerous advantages that can be applied for radar applications.

The objective is to quantify the performances of multitones for radar applications. This will be compared to the performances of the reference in radar applications: the chirp in order to position the multitones with respect to it. For this a reconfigurable radar platform is required which is able to support any kind of waveforms Two questions are raised. The first question is: **which architecture for the implementation?** The second is underlying to the first: **what is the impact of RF components on radar performances?**

This thesis work is composed of eight chapters. Chapter 2 introduces the context of the study from the perspective of radar, the waveforms (multitones and OFDM) and new radar concepts for the fusion of front ends. From the context emerges the need to design an Ultra Wide Band (UWB) Reconfigurable Radar platform, in order to experimentally compare waveforms, and quantify the performances of these new waveforms compared to classic ones. Chapter 3 presents the results of the State of the Art survey on the existing UWB Software Defined Radar platforms and their performances, the effect of RF equipment on system performances and multitones/OFDM performances with respect to classic radar waveforms.

Chapter 4 and Chapter 5 regroup theoretical studies and simulations. Chapter 4 is the theoretical study of radar architectures for the implementation of the test bench. This chapter deals with the RF front end architecture as well as the processing algorithm that will be used to process all the tested waveforms. Then in Chapter 5, the performances of two waveforms: multitones with Newman Phase Codes and Chirp are evaluated using simulation. Those simulations include a parametric study on bandwidth and pulse repetition period as well as the influence of RF equipment with quantization and saturation processes included. Three criteria were chosen to evaluate the performances Peak to Mean Power Ratio, power efficiency and compression.

Chapter 6 and Chapter 7 deal with experimental implementation and results. Chapter 6 shows the design of the UWB Software Defined Radar platform based on the theoretical studies, the performances of the system are drafted from theoretical analysis and measurements. Also this chapter presents the experimental protocol to allow an unbiased comparison of several waveforms. The proposed experiments are used to study the waveform performances wrt quantization, saturation and Doppler. Also an experiment is proposed to measure the stability of the platform. Finally in Chapter 7, an analysis of the measured performances PMEPR, power efficiency and compression of both waveforms is proposed wrt quantization, saturation and Doppler as well as system stability. The performances of the tested waveforms are compared to simulations and between each other.

Finally, Chapter 8 will present the conclusions and perspectives of this thesis.

Chapter 2. Context & Objectives

This chapter will introduce the context of the study and the objectives that were set. The aim is to give a comprehensive overview of the main notions used throughout this study and introduce the objectives. This work was conducted at Onera – the French Aerospace Lab. Onera’s mission and activities will be presented in the first part of this chapter. Next, the multicarrier waveforms will be introduced. This section will cover its development, background and current applications. Then a brief overview of radar will be given from the perspective of its evolution throughout history and some background knowledge. This chapter will then conclude on Software Defined Systems which fuses several functions such as communications and radar for which Orthogonal Frequency Division Multiplexing (OFDM) is foreseen as a valid candidate.

A. Onera’s missions and activities

Onera (1) is the French national aerospace research center. It is a public research establishment, with eight major facilities in France and about 2,000 employees, including 1,500 scientists, engineers and technicians.

The research conducted at Onera whether it has short, medium or long-term goals, is designed to support the competitiveness and creativity of the aerospace and defense industries. The research carried out at Onera results in computation codes, methods, tools, technologies, materials and other products and services which are used to design and manufacture everything to do with aerospace such as Civil aircraft, Military aircraft, Helicopters and Tilt-rotors, Propulsion systems, Orbital systems, Space transport, Missile systems, Defense systems and Networked systems and security systems.

The Electromagnetism and Radar Department (DEMR) missions are to improve existing systems and define future systems in the main areas of application of electromagnetism, i.e. radar, stealth, electromagnetic compatibility, electronic warfare and telecommunications. The DEMR aims at taking the concept radar from the analog era to the digital era.

At Onera, the first experiments involving distributed multitones were implemented in 1984. Onera developed a Synthetic Antenna and Impulse Radar (RIAS) (2) (3) (4) for surveillance and tracking. This VHF radar uses a network of 25 emitters and 25 receivers distributed on two concentric circles of a few hundreds of meters in diameter. This radar was simultaneously emitting and receiving 25 orthogonal signals, which is equivalent to multitones combined after emission.

Onera started investigating Multi-carrier radars from 2002 which is my research subject. And two major research trends can be identified: Passive Detection using Digital Audio Broadcasting conducted by Dominique Poullin and Marc Flécheux (5) (6) (7) and Yohann Paichard’s thesis on a Microwave Camera for Multi-Dimensional Analysis of the Radar Cross Section of Time-Varying targets : HYCAM experimental test bench (8) (9). Those projects will be presented further in the state of the art. The feasibility study of UWB digital radar with Multitones is the next step in the HYCAM research trend.

This project aims at developing a radar platform to evaluate the waveforms’ performances, thus an overview of the radar evolution and background is proposed.

B. Overview of radar evolution and background

In this section, the radar evolution throughout history will be first introduced to give an overview of radar developments since its creation. Some radar notions will then be introduced, followed by the evolution of front ends from analogue to digital

1. History

The first applications in radio-electricity were telecommunications then radio-navigation. However in the early 1900s, pioneers thought up the possibility to detect the presence of metallic objects using electromagnetic waves, such as the telemobiloscope (10). It was necessary to detect the objects without their cooperation to avoid collisions for e.g. maritime navigation. The principal advances were made to fulfill the military aerial and maritime defense needs from the thirties. (11).

Although the technology rapidly evolved during World War II (WWII), radar immensely improved following the war, the principal advances being higher power outputs, greater receiver sensitivity, and improved timing and signal-processing circuits.

The pulse compression techniques were invented in the 40s to provide higher range resolution while maintaining good signal to noise ratio: binary phase coding, Linear Frequency Modulation and stepped frequency.

In the 60s, following the development of semiconductor devices and digital computers, new advances appeared for radar applications: A lot of efforts on waveform design led to good compression and improved detection capabilities. Levanon's work is a good example of such research on a quest for the thumbtack Ambiguity Function which is the radar "Holy Grail". He studied Costas Signal, Non-Linear Frequency Modulations, Polyphase codes and especially trains of coherent pulses. Up until the late 1990s, polyphase codes and linear chirp were considered the best radar signals. (12)

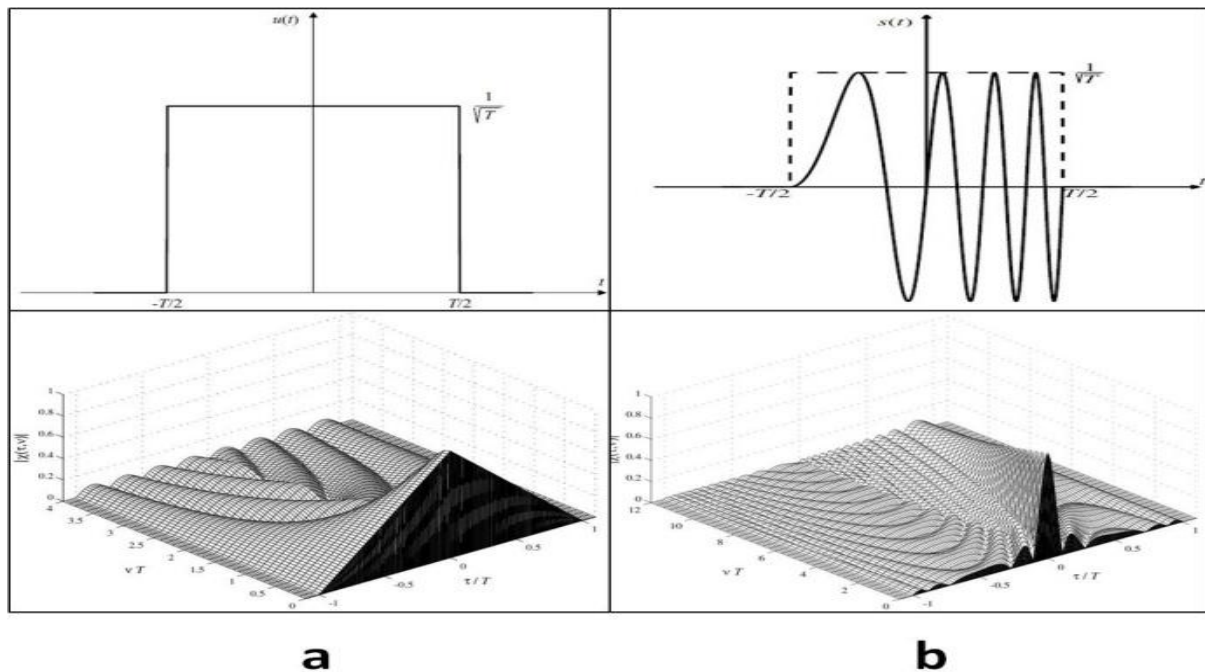
Radar nowadays faces several technological challenges. The race for ever higher spatial resolution, which demands larger and larger bandwidth, puts a strain on the evolution of analog/digital, hardware, waveform design and software. These radars with large bandwidth also need to adapt to the local spectrum regulations. The electromagnetic spectrum being overcrowded, the radar will have to deal with user interferences and emission limits. The major challenge yet to be faced is the multifunction radar. In other words, the radar of tomorrow will have to handle various radar modes such as: surveillance, tracking, imaging and identifying, fire support, use of electronic counter counter-measures, etc ... Also, it should be able to function in a network or communicate its data with a remote base station. On top of this, to avoid redundant hardware, the radar and communication front ends must be fused together. Thus the multifunction radar system must allow dynamic reconfigurability. Other requirements, such as stealth may be needed by the use of low probability of interception schemes, or even passive radar using opportunistic broadcasters.

The history shows the technological evolution of radar systems which went from full analog to hybrid analog/digital architectures. The next section will briefly introduce radar principles and the difference between classic and digital architectures.

2. Radar notions

The word **RADAR** (derived from “radio detection and ranging”) summarizes the two main tasks of radar: detecting a target and determining its range. Fairly early range has expanded to include direction to the target and radial velocity between the radar and the target. Presently, more information on the target can be sought, such as its shape, size, and trajectory. (12)

In radar, the detection is realized using a matched filter. This processing technique allows maximizing the signal-to-noise ratio considering Additive White Gaussian Noise (AWGN). The matched filter is implemented using the complex conjugate of the received signal as reference for the correlation with the received signal (13). One way to evaluate the radar waveform performances for detection is to use the ambiguity function as illustrated in Figure 1.



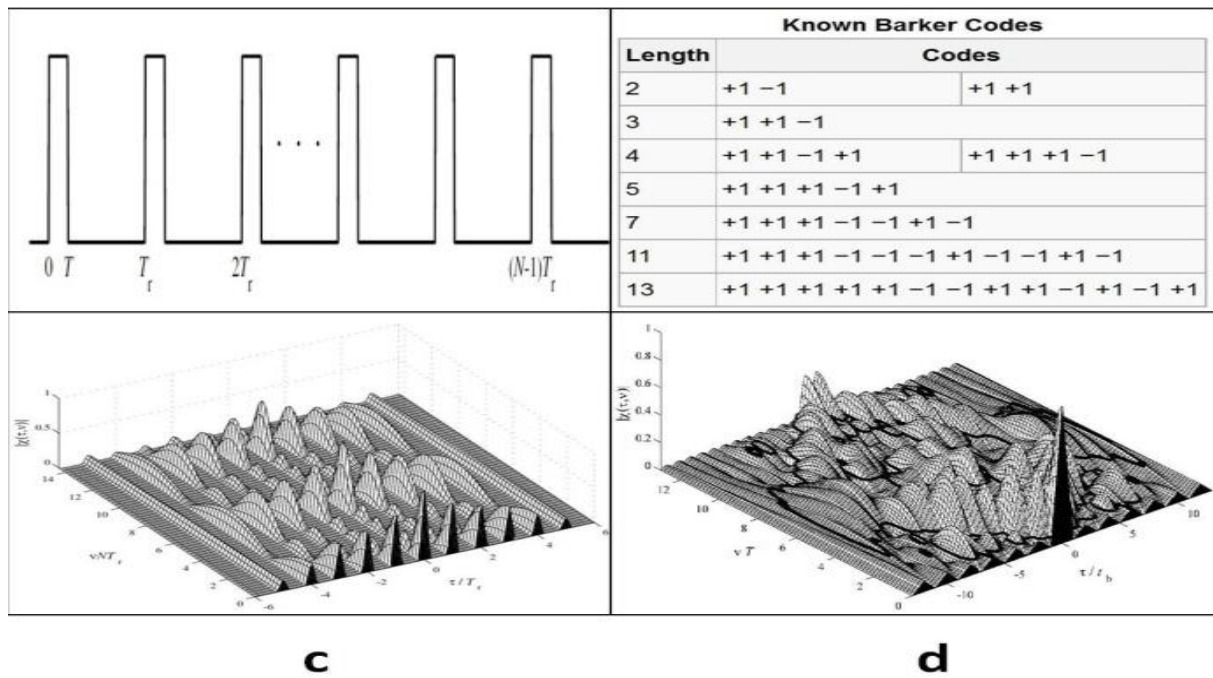


Figure 1: Ambiguity function examples: a) unmodulated pulse, b) linear frequency modulated, c) train of unmodulated pulses and d) train of phase coded pulse barker code

The ambiguity function represents the time response of a filter matched to a given finite energy signal when the signal is received with a delay τ and a Doppler shift v relative to the nominal values (zeros) expected by the filter (12). In other words, it represents the maximum Radar Cross Section (RCS) contrast between two targets. Beyond that, a target with a high RCS will mask the target with a smaller RCS as shown in Figure 2. (13)

Also the ambiguity function can have several maxima, which in presence of noise, may be interpreted as absolute maxima. This confusion may lead to detecting multiple targets when there is only one (Figure 2). (13)

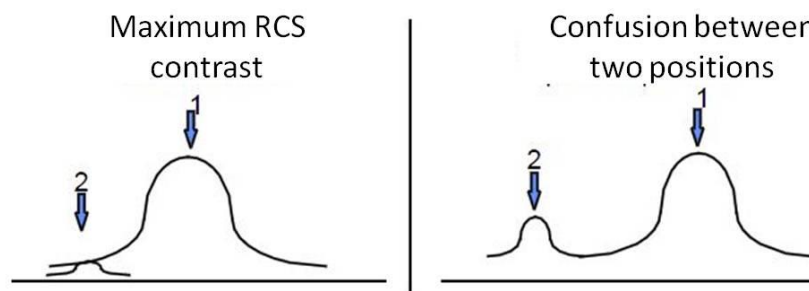


Figure 2: illustration of the ambiguity function concept (13)

Levanon et al.’s work mainly focuses on ambiguity function shaping through radar waveform design, aiming at an ideal thumbtack. (12). This led to the development of an analytic formula to derive the periodic ambiguity function. In (14), they showed that to achieve pulse compression with good peak main lobe to side lobe ratios, Pulse coded Doppler radars use different types of transmission codes such as a complementary code pair which gives ideally zero side lobes.

3. Evolution of RF front ends

In a conventional single carrier pulse-coded Doppler-radar system, all the code bits are transmitted on a selected carrier using a desired modulation scheme. Then, this signal is up-converted and amplified by a transmitter and sent through a transmitting antenna. Note that the two local oscillators in this architecture are synchronized to avoid frequency drift between them. The echoes from targets are picked up through a receiving antenna and are downconverted in the receiver. The most common signal processing scheme of single carrier radar systems is given in Figure 3. After processing the signals through a matched filter, integration and FFT, the detection threshold is applied for constant false alarm rate (CFAR). The detected target plots are given to the data processor for tracking and other functions. There are different constant false alarm rate techniques available.

Nowadays, wireless systems favor digital implementations over analog for most functions. A digital radar is described in Figure 4. The principle is similar. The Analog to Digital and Digital to Analog Converters are used to interface both realms. Note that all the detection functions have been moved into the digital realm. This allows the use of Digital Signal Processing to implement advanced algorithms for target recognition, tracking and performance enhancements with post processing. The signal generator is now replaced by a sample table and synthesized with a digital to analog converter. The digital functions are managed with a digital core (either PC, FPGA or other controllers) allowing dynamic reconfigurability, real-time processing and multi-tasking.

Such reconfiguration in analog radar would require changing a piece of circuitry either to modify the waveform or the signal processor. With the advent of digital technologies, all these can be digitally managed without redesigning the system for the new features.

Also the architecture shown in Figure 4 is bound to evolve with the improvement in analog bandwidth, sampling frequency and bit resolution. Indeed the super-heterodyne architecture in RF front ends will be pushed higher in the frequency spectrum. Thus the architecture, shown in Figure 5, will be replacing the super-heterodyne architecture up to the full X band in the 2012 horizon and moving upward in the future.

Also in digital radar, a reference signal must be stored in order to execute the pulse compression. A digital or measured reference can be used; the advantage of measuring the reference is the transfer function compensation. Thus either a calibration procedure or reference channel should be considered during the design of the radar.

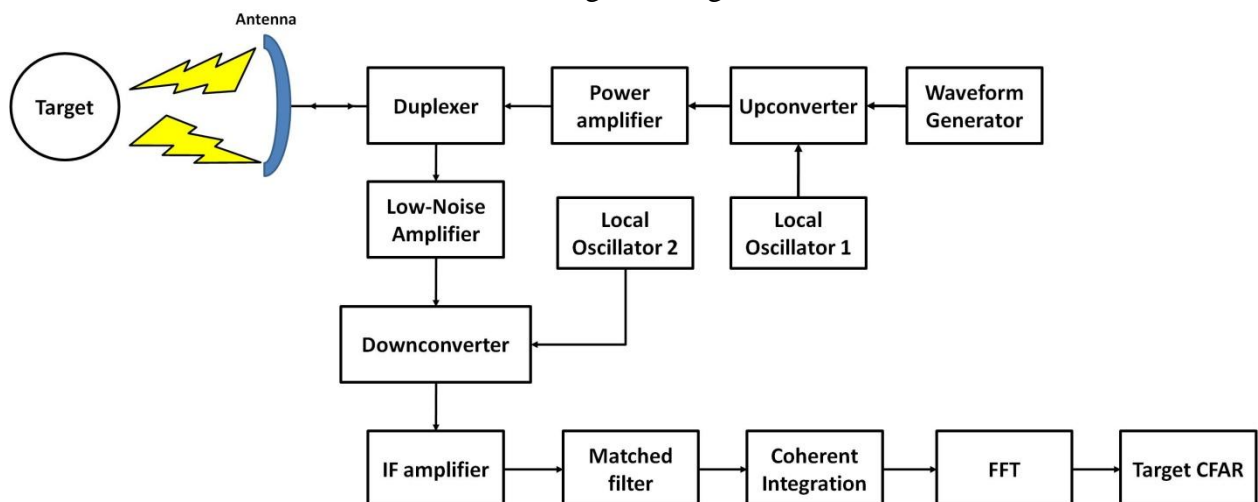


Figure 3: classic monostatic conventional radar block diagram (15)

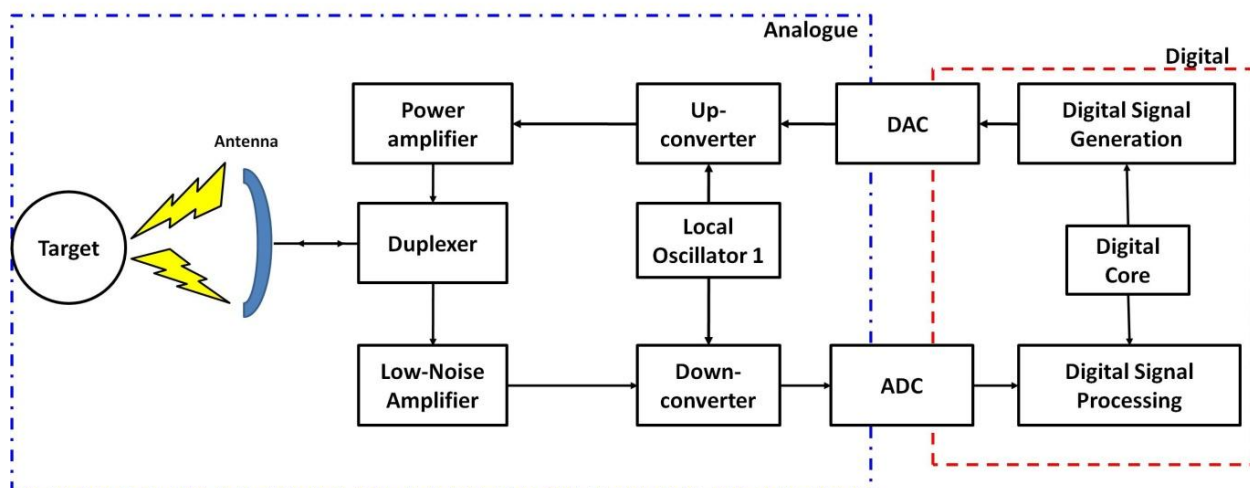


Figure 4: digital monostatic digital radar block diagram

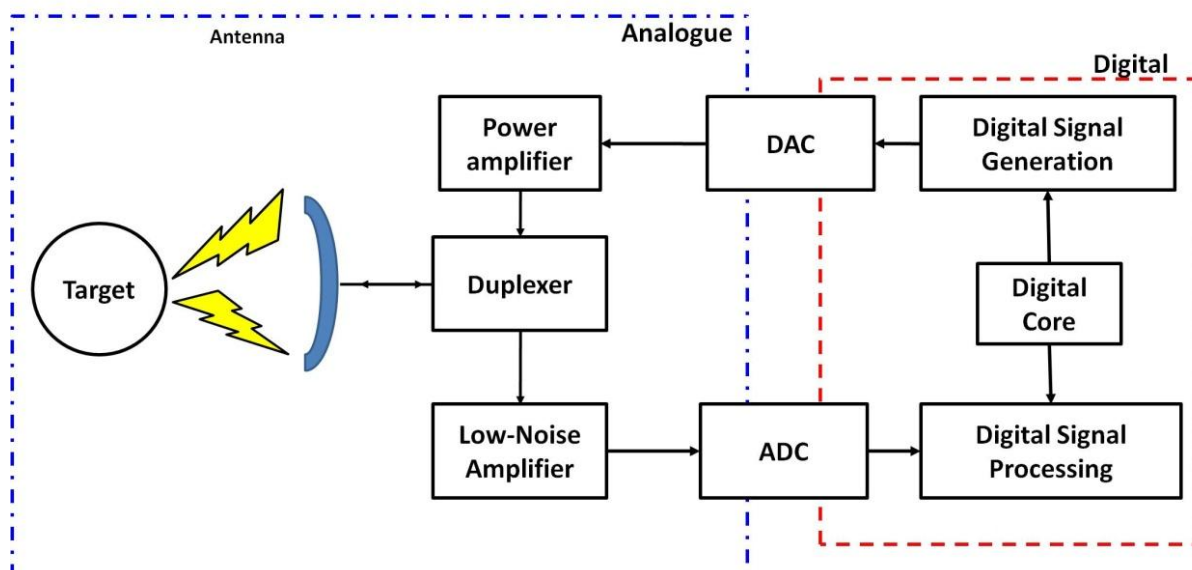


Figure 5: software Radio/Radar block diagram

In telecommunications, the evolution of RF architectures from analogue to digital gave rise to new radio concepts: Software-Defined Radio and Cognitive Radio.

The principle of software defined radio is to get a RF platform to execute several different radio functions. As the A2D or D2A converters get closer to the antenna for transmitters as well as for receivers, software defined radio can fully exploit the flexibility and the advanced conception tools from the digital world (16). For a software defined radio system to be useful as an adaptable future-proof solution, and to cover both existing and emerging standards, it is required to have elements of reconfigurability, intelligence and software programmable hardware. In addition, the emerging user requirements on reconfigurable mobile systems and networks are paving the way for the introduction of reconfigurability in future mobile systems (17).

Cognitive radio is an evolution of software radio. Software defined radio indeed is an enabling technology for cognitive radio new concept. A cognitive radio communication system matches its behavior to the environment A cognitive radio system is made of a terminal : the driver, a sensor bubble to adapt to its environment and the software defined

radio to use the available networks such as Wifi, WiMax, 3GPP, The sensor bubble provides the terminal with all the necessary information to take adequate decisions concerning its optimal (in terms of available resources use) and secure (in terms of quality of service) operation. (16)

These concepts, emerging from telecommunications, could be adapted to radar systems for signal agility, passive detection and opportunistic broadcasting. Some new radar concepts are presented in section Chapter 2.D.

OFDM has recently been introduced as a strong multicarrier modulation scheme candidate to be applied in cognitive radio (18). Cognitive radio requires sensing the spectrum and thus performs a spectral analysis. OFDM efficiently uses FFT for spectral analysis and demodulation. It also has the ability of OFDM to notch some carriers to avoid interference or licensed users band (19). Thus the next section will present in more details the OFDM and related modulation techniques.

C. General Background on Multitones and OFDM

In this section, the concept of Multitones and the OFDM will be presented. First a definition of multicarrier signals will be given. Then a brief history review of multitones will be presented. Finally the advantages and drawbacks of such waveforms will be introduced.

1. Definition of Multitones and OFDM

The first multichannel modulation systems appeared in the 1950's as military radio links, systems best characterized as frequency-division multiplexed systems. The first OFDM schemes were presented in (20) and (21). Actual use of OFDM was limited and the practicability of the concept was questioned. However, OFDM was made more practical through the works of Chang and Gibby (22), Weinstein and Ebert, (23), Peled and Ruiz, (24), and Hirotsuki, (25). The OFDM that is described in (23) uses the discrete Fourier transform (DFT) with a cyclic prefix (24). The DFT (implemented with a fast Fourier transform (FFT)) and the cyclic prefix have made OFDM both practical and attractive to the radio link designer. A similar multichannel modulation scheme, discrete multitone modulation, has been developed for static channels such as the digital subscriber loop (26). discrete multitones also uses DFTs and the cyclic prefix but has the additional feature of bit-loading which is generally not used in OFDM, although related ideas can be found in (27).

In this work, we will differentiate the terms Multitones and OFDM which stands for Orthogonal Frequency Division Multiplexing. (12):

Multitone signals are, in definition, the simultaneous emission of subcarriers or tones regardless of the modulation overlaid on those carriers, or transmission protocol. Thus OFDM is a special case of Multitones, used for telecommunications and implementing a communication protocol with cyclic prefixes. Thus throughout the thesis, we will call Multitones, signals with multiple equally spaced (orthogonal) subcarriers overlaid with a phase modulation.

OFDM is a method of transmitting data simultaneously over multiple equally spaced carrier frequencies, using Fourier transform processing for modulation and demodulation. The method has been proposed for many types of radio systems, such as wireless local area networks and digital audio and video broadcasting. By dividing the bandwidth into many small orthogonal frequencies (efficiently achievable using the fast Fourier transform), the

data can be transmitted across multiple narrowband channels having overlapping frequency spectra.

Orthogonality is a mathematical concept derived from the vector representation of time-dependent waveforms. If the waveforms to be compared are laid out on the time axis, if the average of the integral of the products of pairs of values for all instances of time extending over their common period is taken, and if this average is found to be zero, then the waveforms are said to be orthogonal.

In OFDM, the various time-dependent waveforms are selected to lie on carriers separated by the inverse of the signal duration t_b as illustrated in Figure 6.

Due to the rectangular pulse shaping of the signal, the spectra of the subcarriers are $(\sin x)/x$ functions with a first null at the inverse of the signal duration t_b as shown in Figure 6. In a practical application, the OFDM signal is generated in a first step as a discrete-time signal in the DSP part of the transmitter. The bandwidth of the OFDM system with N subcarriers, is N/t_b . Thus the signal must be sampled with the sampling time t_b/N .

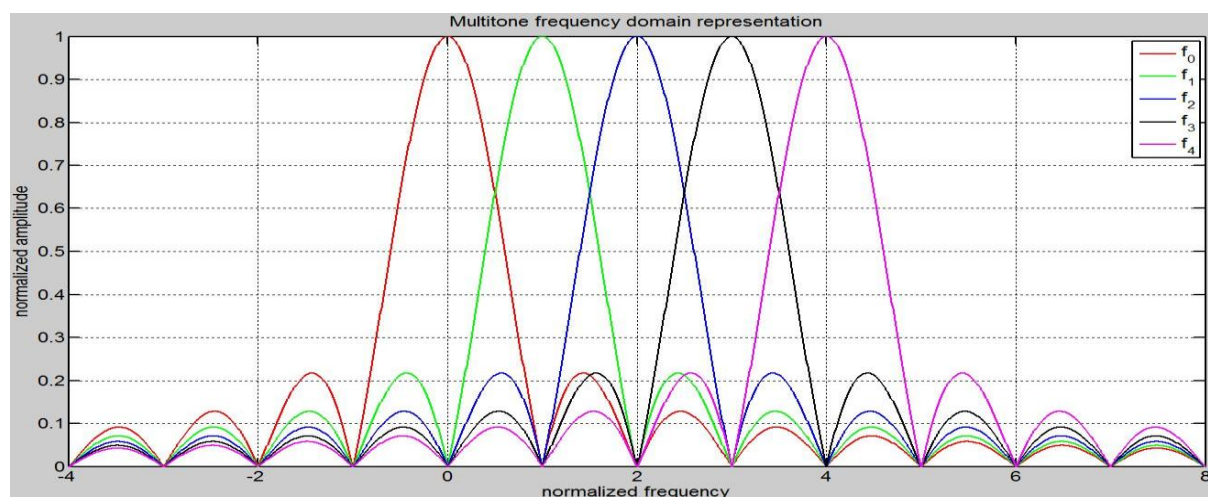


Figure 6: OFDM representation in frequency domain

Synchronization at the receiver is an important topic in OFDM transmission systems, since time and frequency synchronization errors disturb the orthogonality of the subcarriers. For radar, the sensitivity to exact synchronization is beneficial, since the receiver knows what were the transmitted “data”, and measures the delay time and Doppler frequency shifts between the transmitted signal and the received echo.

OFDM signals are trains of multicarrier chips or pulses. Every t_b , the complex modulation changes according to the incoming data. Multitone signals will be defined as a train of multicarriers with identical complex modulation. In other words, the same symbol will be continuously transmitted.

The concept of multitones and OFDM waveform now understood, the next section will give an overview of the history of OFDM.

2. History of multicarrier waveforms

In the late 1950s and early 1960s, telecommunications engineers developed multi-carrier communications for higher data rate HF military communications in parallel of radar research.

After that time, OFDM emerged as a special case of multi-carrier modulation using densely spaced subcarriers and overlapping spectra. But this principle couldn't be implemented until several technological breakthroughs occurred, such as oscillator stability in the transmitter and receiver, linearity of the power amplifiers, compensation of channel effects, Doppler spreading. (28).

As these issues were solved, the development of coded multicarrier modulation in the 90s allowed the implementation of OFDM in various telecommunication protocols that we now use in our everyday life, such as internet protocols or broadband and many others¹.

OFDM principles being understood, the next section will show the advantages of such a waveform.

3. Advantages and Drawbacks of multi-carriers

Advantages	Drawbacks
Resistance to frequency selective fading	Peak to Mean Envelope Power Ratio (PMEPR)
Efficient bandwidth usage	
Immunity to delay spread and multipath	
Simple equalization	
Sub-band independence	
Diversity	
Low probability of Interception	
Time-varying targets – stationarity	

Table 1: Advantages and drawbacks of multitones and OFDM

The different advantages and drawbacks of multitones are listed in Table 1. (further details can be found in Annex Chapter 9.A).

For classic radar waveforms with frequency or phase modulation, fading results in the loss of portions of the modulation. This deteriorates the detection both in distance and velocity. Multitones would have attenuated frequencies in the signal bandwidth but all the signal modulation would be picked up.

In telecommunications, guard intervals are used to insure immunity to delay spread and multipath, these would reduce compression gain. Radar applications alone do not require guard intervals as they do not require transmitting data, the same symbol can be transmitted over and over again. Thus the guard interval for the radar would be the preceding symbol resulting in no loss in compression.

In the radar context, sub-band independence allows the implementation of several radar functions within the same signal, also notches can be applied easily to the signal to avoid interferences or other licensed applications. The independence of sub-bands means that the radar function can keep working even if one or several sub-bands are turned off.

Multitones enables signal diversity. A coherent train of diverse pulses whose detection capabilities in distance and Doppler have increased contrast compared to a coherent train of

¹ Asymmetric Digital Subscriber Line (ADSL) services, Digital Audio Broadcast (DAB), Digital Terrestrial Television Broadcast (DVB) in Europe, Integrated Services Digital Broadcasting in Japan, IEEE 802.11a/g (WiFi), 802.16a (WiMax), Power Line Networking (HomePlug). Since OFDM is suited for high data rate systems, it is considered as a viable technology for the implementation of the fourth generation (4G) wireless services, IEEE 802.11n (high speed 802.11) and IEEE 802.20 (MAN).

identical pulses. The orthogonality reduces susceptibility to mutual or intentional interference. Using Code Division Multiple Access (CDMA) with multitones gives way to spectral reuse and allows several systems to broadcast within close vicinity with negligible interferences. (29) The development of radar networks with no perturbation between one another using the same frequency band is thus possible.

Garmatyuk et al. determined OFDM pulse is evidently the hardest to intercept and predict compared to FM and Frequency Hopping signals. In fact, its uniqueness is such that no amount of oversampling and no size of a fractional sample window will allow the interceptor to precisely resolve the time-frequency characteristics of an OFDM signal. (30)

In (9), Paichard proposed a RCS measurement technique adapted for time-varying targets. This technique uses multitones. It involves the emission and reception of all the frequencies over a short time to keep stationarity conditions. This method has the advantage to be adapted to every type of modulations: periodic and aperiodic. Using chirp or step frequency signals means that the frequencies are sequentially emitted. Thus the different states of the modulations are not recorded over all the frequencies but rather sampled by the frequencies as they are emitted. This compromises the stationarity over the emission time and is not adapted to aperiodic modulations.

The high Peak to Mean Envelope Power Ratio (PMEPR) of OFDM signals is a fundamental drawback when compared to single-carrier modulation. Practical power amplifiers are linear only over a finite range of input amplitudes. (31). When all the N tones in multitones are in phase, the signal PMEPR is maximum and equal to N . This means that the average power effectively emitted is $1/N$. Thus for a radar, it reduces the maximum attainable radar slant range. Moreover, in order to avoid spectral growth in the form of intermodulations among subcarriers or out-of-band radiation, the transmit power amplifier must be operated in its linear region where the transmitted power is lower than the maximum output power. (32). Also, the peak emitted power is limited by regulatory constraints e.g. European Communications Office (33), European Telecommunications Standards Institute (34), IEEE standards (35), or application constraints. The effect is to reduce the transmitted average power of multicarrier signal. Generally, there are two solutions to reduce PMEPR for OFDM: coding either in amplitude and/or in phase, or linearization of the amplifier. (31) (32). Details on PMEPR reduction techniques can be found in Annex Chapter 9.B. The most popular techniques are the amplitude clipping & filtering and coding. Generally, those solutions usually increase software complexity or necessitate training sequences. However using polyphase codes e.g. P3 and P4 codes (36) allows yielding at PMEPR of the order of 5dB (12). There is much less computation required but no data can be encoded.

Telecommunication terminals require synchronization to receive multitones as the transmitter and receiver are connected via a wireless connection. In monostatic or bistatic radar with a transmitter and a receiver on the same platform, this synchronization is not required.

Multitones used for radar purposes present undeniable advantages and few drawbacks. However a couple of questions remain on their Doppler tolerance and their ambiguity functions. This question will be looked at in the state of the art Chapter 3.C.

The evolution of RF front ends and the many advantages of multitones explain the ever growing interest of the radar community for these waveforms. In the following section, modern radar concepts will be introduced.

D. New radar concepts

Digital radar concepts in literature, either passive or active, flourish. Three concepts will be presented: a generic digital radar, an agile multitone radar and a passive coherent location system using digital audio broadcasting signals.

a) Digital radar using multicarrier signals

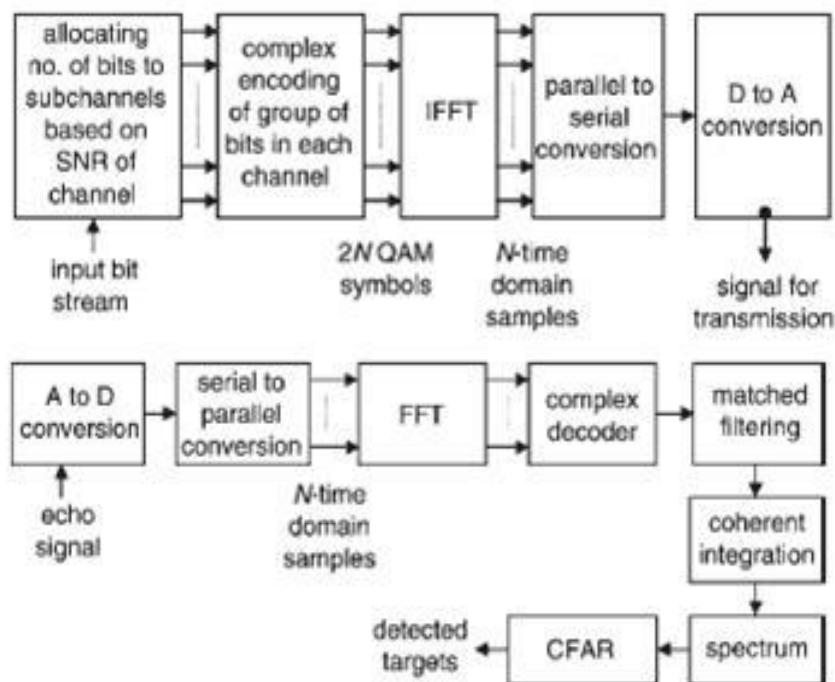


Figure 7: Block diagram of (top) transmitter (bottom) receiver - section of multicarrier Modulation-FFT radar scheme (14)

In (14), the authors introduce the differences between single carrier and multicarrier radars. The authors describe the necessary steps for generating and processing OFDM signals for a digital radar. The modulation of the carriers by the code sequence is digitally performed, using an orthogonal transformation (IFFT) at the receiver to recover the code. In the radar system based on multicarrier modulation, the input bit-stream of a radar signal waveform is divided among the number of sub-channels that are selected for transmission. The allocation of these bits depends on the signal-to-noise ratio (SNR) of each individual channel. After allocating bits to a sub-channel, the complex encoding based on the chosen modulation such as QAM, binary phase shift keying, QPSK, is carried out for each sub-channel. Inverse fast Fourier transform (IFFT) is performed on these symbols and the parallel data are converted to serial data. A digital to analog converter (DAC) is used to convert these digital data into analog signals for amplification and transmission as radar signals through suitable antennas. The block diagram of processing steps that are involved in the transmitter for multicarrier modulation based radar employing FFTs is given in Figure 7. (14)

The received echoes from targets, after proper detection and amplification, are converted to digital form using an ADC in the receiver. The schematic of processing steps that are involved in the receiver for multicarrier modulation-FFT based radar is given in Figure 7. The digital data in serial form are converted to parallel data. The FFT is performed on these samples for demodulation, which corresponds to reverse process of modulation using IFFTs in a transmitter. Using a complex decoder, the data bits are decoded and further processing is performed on this data as shown in Figure 7. The FFT of the output sampler is calculated after discarding the cyclic prefixed samples. The sub-symbols are recovered using the maximum likelihood criterion. The bit stream is recovered using a suitable decoding technique. (14)

b) Agile multitone radar

Van Genderen et al. published in (37) research on frequency agile radar using multitone signals, as shown in Figure 8. Frequency agility is an important feature when radar operates in jammed environments. With the development of OFDM in communications, the opportunity for a new generation of digital agile radar rises. Old and expensive multi-channel analog agile front ends could be replaced by simpler and cost effective single channel transceivers where the coherent switches in frequency are no longer in analog circuits but in the digital architecture. The frequency agility can be digitally controlled in the IFFT block of the transmitter by selecting at any given time the desired sub-bands. Narrowband jamming/Interference can be avoided by turning off certain sub-bands. The structure of OFDM signals could enable both concepts of pulse-to-pulse agility and Doppler processing to coexist in the same system. The generated radar waveform doesn't need a cyclic prefix if the communication is not implemented.

These principles could be transposed to any other waveforms given a few tweaks to the processing chain after the ADC.

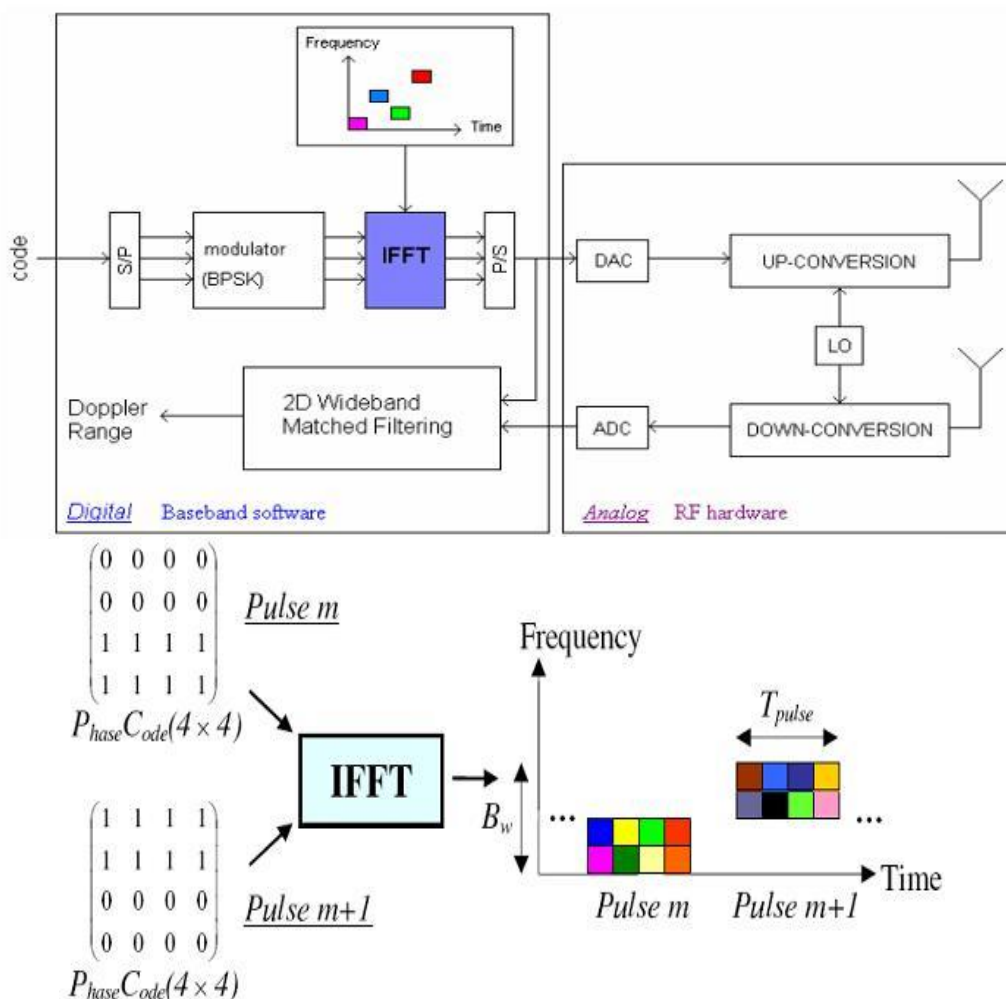


Figure 8: OFDM agile radar transceiver block-scheme (37)

c) Passive coherent location system using digital audio broadcasting signals

In 1998, Lockheed-Martin Mission Systems (38) first announced a commercial system, “the Silent Sentry system” that exploited FM radio and analogue television transmitters. In 1999, (39) proposed a target tracking system, thus proving the feasibility of using non-cooperative broadcasters to track targets in the same fashion as bi-static radars.

At Onera, Passive Detection using Digital Audio Broadcasting is investigated since 2005 by Dominique Poullin and Marc Flécheux (5) (7) (6). Since the development of new communication protocols in Europe such as Digital Audio Broadcasting and Digital Video Broadcasting, opportunity transmitters for radar detection and location became a topic of interest. First it allows complete discretion and gives access to Very High Frequency (VHF) and Ultra High Frequency (UHF). Second, the available bandwidth with these protocols, e.g. digital audio broadcasting 1.5MHz in VHF and 7.5MHz in UHF gives interesting range resolutions respectively of 100m and 20m. Third, with Coded OFDM, two network configurations can be implemented: Single Frequency Network and Multiple Frequency Network.

There are a few basic rules to follow to implement passive detection using digital broadcasters with Coded OFDM modulation. For all Passive Coherent Location systems, the main path must be cancelled in order to detect targets despite the main path sidelobes. And for digital broadcasters using Coded OFDM in single frequency network configuration, the

cancellation process must also cancel the main fixed echoes, the single frequency network broadcasters and their multipaths. It was also shown that the antenna array should be composed of at least 4 elements in order to get accurate location and tracking capabilities (7). The emission time is long and the radar needs to receive signals simultaneously. This requires a bi (multi)-static operation and also implicates a strong isolation between the emitting and receiving antennas. Bi (multi)-static operation also requires the synchronization of the remote receivers and thus suffers from beat error, carrier and phase offset.

It is important to notice that communication and radar applications have different requirements. In communications, e.g. digital audio broadcasting, convolutional or concatenated codes with PMEPR of 15dB are preferred over Reed-Muller with complementary Golay codes with lower PMEPR. Despite a higher PMEPR, a greater range is achieved in presence of multipath because they are more resistant to Rayleigh fading. They also have a lower information redundancy, thus a higher throughput. On the other hand, digital audio broadcasting carries higher noise levels which may degrade radar detection. Thus for radar applications, coding schemes such as Reed-Muller with lower PMEPR will be preferred over digital audio/video broadcasting signals to optimize detection range and accuracy.

The advantage of such waveforms either for passive or active coherent location, is the easy implementation of differential decoding for detection.

d) Technological Developments and new concepts

From 2000, authors started publishing about the use OFDM signals based on high data rates communications, for digital radar and especially the fusion of front ends.

Advances in Software defined radio allow considering the implementation of a significant portion of signal generation and processing in software, leaving analog front end and antenna system as the only hardware components in the design. High spectral efficiency and possibility of orthogonal multi-channel processing of UWB-OFDM signaling, as opposed to LFM or short-pulse waveforms, allow it to consider for a combination of imaging and Doppler radar, data/voice transmission capabilities, implementation of frequency-hopping for improved interference/jamming protection, thus reducing the effects of radar interference on radar performance (40).

Also relatively recent advent of unmanned aerial vehicles into battlefield operations has brought about new challenges and opportunities for radar sensing platforms. Particularly, in light of the increasing importance of military operations in urban terrain, the gap between short and long range radar imaging scenarios appears to narrow, as target ranges may be as short as 100m or less (30).

OFDM has recently been introduced as a strong multicarrier modulation scheme candidate to be applied in Cognitive RF systems. The rationale is that they need to sense the spectrum and that involves some sort of spectral analysis. Fast Fourier Transform (FFT) can be used for spectral analysis while at the same time acting as an OFDM demodulator. OFDM also has the capability to notch the parts of its carriers which are coincidentally within the region of the Licensed User's band. Such OFDM flexibility simplifies the application of dynamic spectrum access for RF systems. (19)

For communications, OFDM is used as a modulation scheme enabling high data rates and a good usage of the bandwidth. For radar, it will be used as a modulation for pulse compression in the receiver to extract range and Doppler. Its immunity to multipath, by using guard intervals, makes it very attractive for short-range network scenario. (41)

Garmatyuk et al. aim at determining the minimum SNR for a dual use radar/communication system, to successfully transmit a high resolution image to a remote system, and study the effects of carrier offset on range profile reconstruction. They determined that for SNRs higher than -15dB, range profile recovery is successfully performed. With range resolution below -20dB, range imaging starts to deteriorate significantly. (40)

In imaging radar processing, carrier synchronization is not as important as in telecommunications, albeit it is certainly desired to avoid signal recovery errors associated with carrier offset. Accurate carrier synchronization is of paramount importance to data communications, and it was also found to affect point target recovery. The target-to-clutter ratio is 6dB with perfect synchronization and drops to 2dB in the worst-case scenario of phase offset being around π (40).

The fusion of both radar and communication into one single system has traditionally been tackled by means of separated infrastructures. However, being both RF systems, their combination could be possible. OFDM is considered for the fusion of both radar and communication in a single system. Nikoogar et al. analyzed a squared set-up of 2.5km side and focused on the physical layer. The number of target reports collected at each radar station that can be communicated to fellow radars depends on the volume of the report. They determined that the Omni directional joined with directional radar implementation with rotating antennas has a higher throughput than only directional to directional. (41)

All these authors aim at developing the reconfigurable radar platforms supporting functions such as SAR imaging and communications. This implies the development of an agile and generic RF architecture and a reconfigurable processing architecture.

	Concepts based on software defined RF systems	Concepts based on Cognitive RF systems	Evolution of front ends
Emission	Signal: - flexibility - agility - diversity	- Opportunistic Broadcasting - Spectrum Insertion	- Fusion of front ends: comms/radar - More Generic & Simpler RF
Reception	- DSP reconfigurability - Multifunction e.g SAR, Comms - Passive detection	- Opportunistic Detection - Interference Avoidance - Spectrum analysis	- Architectures for signal diversity, agility and reconfiguration

Table 2: New radar concepts and implications in digital and analogue parts

Table 2 summarizes the new radar concepts, it can be observed that these concepts are based on notions from the telecommunications. The general trend is however multifunction radar, meaning that the enabling radar architectures will have to evolve from dedicated platforms to multifunction platforms. Also the digital architecture evolution, in power and capabilities, leads to simpler and more generic architectures, bringing the D/A and A/D converters closer and closer to the antennas. The digital architecture now allows the implementation of

multifunction systems such as SAR imaging, Passive Detection and Communications, on a single generic RF platform. Thus this leads to a lower hardware complexity but a higher software complexity.

E. Contribution of Multitones for UWB Radar

This thesis work conducted in Onera, contribution of multitones for UWB radar, aims at developing an experimental test bench to evaluate the performances of Multitones and/or OFDM signals compared to classic radar signals such as chirp.

The design of a digitally reconfigurable radar with multitones raises several questions on the implementation and performances of the required architecture and also on the performances of multitones compared to classic radar signals.

The issues that will be addressed, are:

- Which architecture should be implemented for this study?
- What are the performances of Multitones and/or OFDM signals compared to classic radar signals?

The issue of implementation raises another issue at the component level. It is thus important to investigate, using simulations and measurements, the influence of RF components characteristics on multicarrier signal performances. This may allow us to predict architecture performances based on component choices. So the third issue addressed in this thesis will be:

- What is the impact of RF components on the performances of OFDM signals and radar performances?

The **State of the Art** will be investigated in order to answer those questions. It will be split in 3 sections. The first section will focus on existing radar platforms implementing multicarrier signals, to allow for a wiser choice of architecture. The second section will look at the impact of RF equipment on performances through the linearization issue in general, and then more specifically on the performances of equipment, such as power amplifiers and ADC, used with multitones signals. Finally the performances of OFDM will be compared to other waveforms on detection, ambiguity function and signal processing.

Following the State of the Art, the **radar modeling** will be presented in chapter IV. Building on the conclusions of the state of the art, the characteristics of 3 architectures will be compared before choosing the most suitable candidate. Then, some design considerations will be presented on intermodulations avoidance and power control with non-linear components.

In chapter V, **waveform simulations** will be developed. The waveform-independent performance criteria (PMEPR, power efficiency and Ambiguity Function) will be defined. The performances will be evaluated on three basis perfect signal, quantization and saturation. The simulation results will then be analyzed and the limitations of simulations will be discussed.

Chapter VI will deal with the **implementation of the radar and the experiments**. First the design constraints will be exposed, followed by the frequency planning. Then an overview of the radar will be presented followed by its measured performances. The experiments to

compare the multitones with chirp signals in closed-loop, with static targets, Doppler shift and saturation will then be developed

Chapter VII will present the **experimental results of the comparison** between multitones and chirp. The sections will be broken down in terms of performance criteria, first with respect to PMEPR, then power efficiency, and finally pulse compression.

Chapter 3. State of the Art

In this chapter, the state of the art survey aims at finding answers to the issues raised in this thesis. The first one will concern the radar architecture and will look at the OFDM radar platforms that are already implemented. Then the impact of RF equipment will be investigated at every level of the architecture, through papers dealing with linearization, and papers dealing with OFDM associated with power amplifiers and A/D or D/A converters. Finally, the performances of OFDM/Multitones signals will be collected either as standalone or compared to classic waveforms.

A. Existing RF platform analysis

It is important to note that even though some radar implementations can be found in the literature, they are very few. In this section, four radar platforms implementing multicarrier signals will be reviewed and compared: the PANDORA (1998) which is the first experimental OFDM radar, HYCAM which is a RCS measuring system developed at Onera (2005), a dual use SAR imaging and telecommunications system (2008) and finally a reconfigurable Software Defined Radio platform IDROMel (2009).

1. PANDORA

In 1998, Van Genderen et al. presented an experimental radar named PANDORA (42) (43), which stands for Parallel Array for Numerous Different Operational Research Activities. The radar operates on 2 antennas, one for Transmission (Tx), one for Reception (Rx), and a minimum of 60dB isolation between antennas is required. The radar is composed of the following building blocks: FM-continuous wave waveform generator, Power Combiner Block, Wideband Low Noise amplifier, Power resolver Block, Range FFTI (Stretch processing for each FM-continuous wave channel). As for signal processing, two functions are implemented: Non-coherent processor, High Resolution FFT or Channel FFT. The schematic of PANDORA system is given in Figure 9.

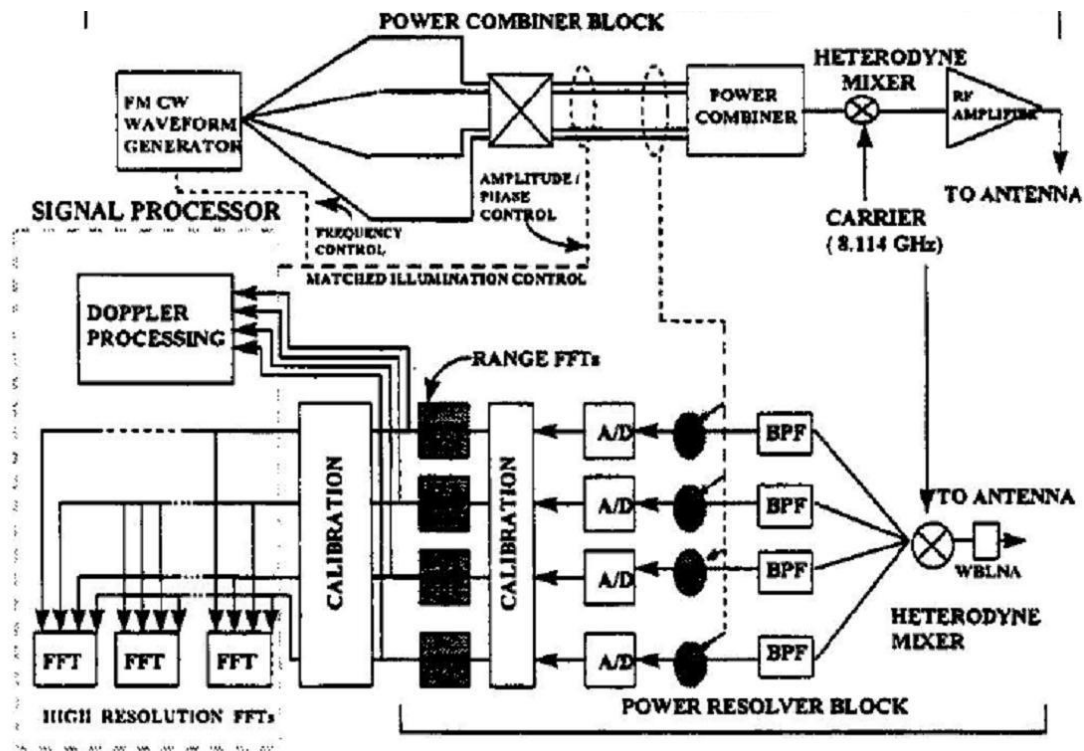


Figure 9: System block diagram of PANDORA (43)

The guard band was used to achieve a higher range resolution than what can be obtained by the sweeps alone. At the receiver end, the signals are split into their constituents and collectively processed to obtain an extremely high resolution synthetic image of the target. This radar, operating in the X band, generates 8 separate signals, either Frequency Modulation Continuous Wave (FMCW) or Single Frequency Continuous Wave, which are then additively mixed and radiated (Note that parallel single frequency continuous wave gives stepped multitones). Adding both signal and guard bands, the radar total bandwidth is 776MHz. The result yields 0.19m in spatial resolution if we include the guard bands. Breaking down the wideband signal in several narrowband signals allows for high signal purity, meaning little amplitude distortion and simple correction of phase shifts and group delays.

2. HYCAM: Microwave Camera for Multi-Dimensional Analysis of the RCS of Time-Varying targets

From 2000 to 2006, Onera investigated the OFDM for radar applications. In 2005, a working prototype of a Microwave Camera for Multi-Dimensional Analysis of the RCS of Time-Varying targets (9) (8) was implemented.

With multitones, the extraction of the backscattered coefficients can be made via polyphase filter structures (FFT), hence reducing the computation load. The multitones are less sensitive to filter non-linearities. This robustness allows reducing the overlap between the receiver channels, which is a major advantage for the digital architecture. Finally it is possible with multitones to interleave the test and reference signals as well as several sub-bands in the receiver thus reducing the cost of the test bench.

The experimental test bench (Figure 10) had a receiver bandwidth of 2 x 400MHz and allowed validating the simultaneous emission of phase-coded multitones, the reception with multi-channel architecture with interleaved test and reference signals, and that the modulation of time-varying targets (active modulator) can be extracted.

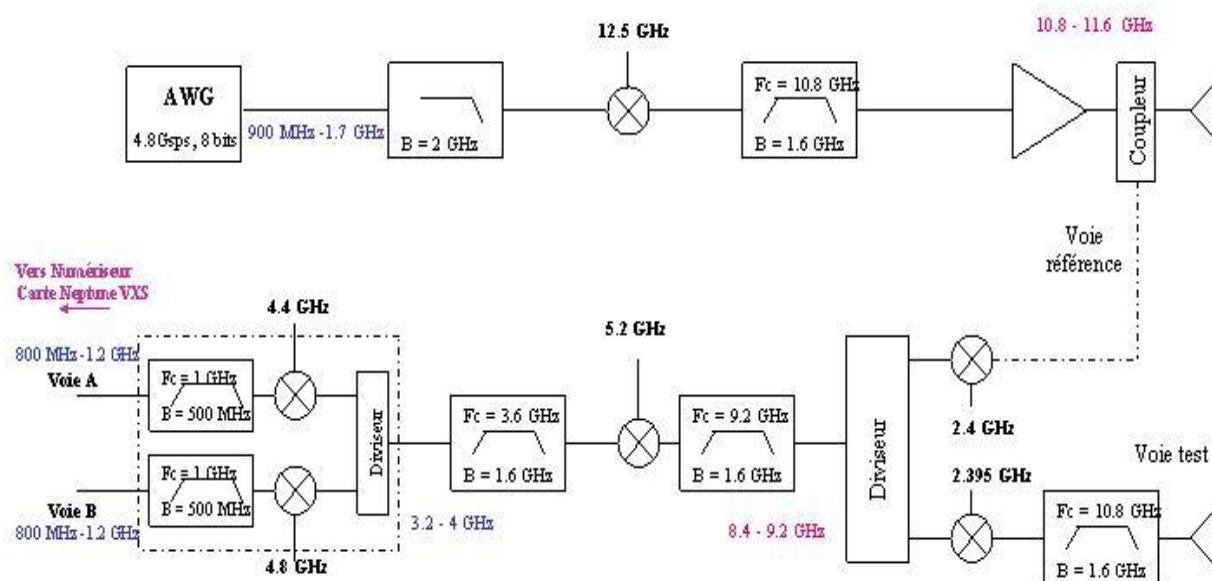
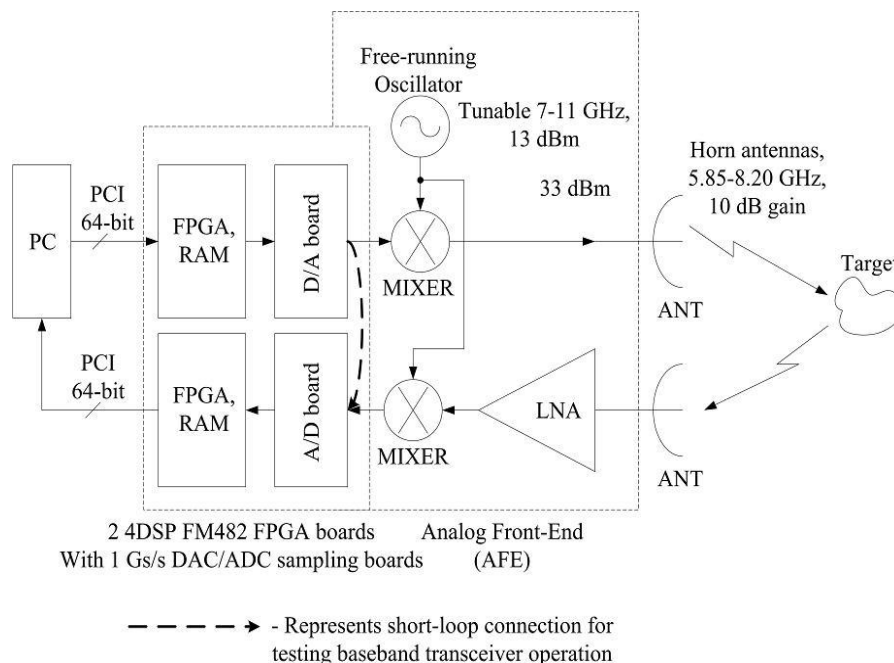


Figure 10: HYCAM experimental test bench (9)

3. Dual use SAR imaging and telecommunication system

In 2008, Garmatyuk et al. described the design and architecture of an experimental radar test bench based on OFDM (30) (44) (45), see Figure 11. The radar signal is digitally generated by forming an arbitrary-length vector of OFDM sub-carrier amplitudes and translating it in analog format via 1GS/s DA conversion. It also displays pulse to pulse reconfigurability by varying the number and composition of sub-carriers. The signal is upconverted to 7.5 GHz carrier frequency and emitted via small-form horn antenna. The receiver includes 1 Gs/s A/D converter and processing is performed in frequency domain. The system is currently configured for short-range applications (3-5 m) and can be used as radar or communication unit without any changes to hardware and with very minimal changes to software. UWB OFDM benefits is scalable, as implementing a faster D/A and A/D converters would allow to instantly upgrade the resolution of such a radar system.

The system’s useful bandwidth is 500 MHz, which allows it to perform as high-resolution radar with range resolution of approximately 0.30 meter. The system can also be used as a communication unit with experimental data rate of 57 Mb/s, enabling image communications. Its performances are shown in Figure 11.



Parameter	Value	Units
Baseband signal bandwidth	500	MHz
Transmitted signal bandwidth	7.0...8.0	GHz
Standard pulse width	513	ns
Transmit power, approximately	25	mW
Experimental radar range, as tested	1.5...5	meters
Number of bits in commun. configuration	19	Per pulse
Experimental range resolution	0.30	meter

Figure 11: block diagram of the designed OFDM (top) performances (bottom) (45)

4. IDROMel

From 2006 to 2009, Open Air Interface’s IDROMel project (46) developed a reconfigurable Software Defined Radio platform. The project investigates the feasibility of agile spectrum management, including propagation aspects and radio resources' management. The prototypes RF front end have transmitter and receiver physical layers functioning in real-time with the possibility to dynamically change part or all of the processing such as modulation and channel coding. It can commute from a UMTS type physical layer to a IEEE.802.16/11.

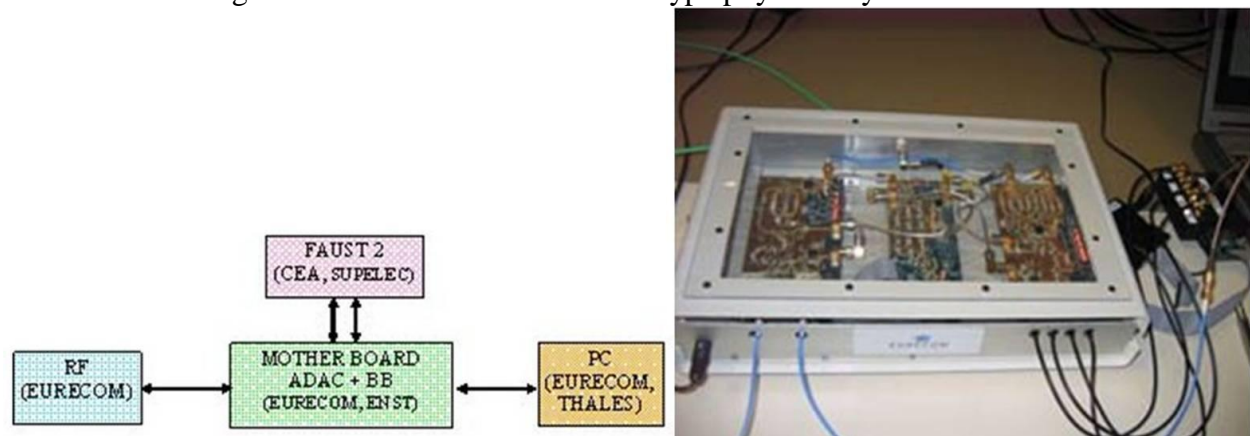


Figure 12: IDROMel (left) architecture block diagram (right) prototype(www.openairinterface.org)

The four blocks composing the platform in Figure 12 are the Motherboard, the PC, the Hardware Accelerator and the RF front end. The Mother board integrates baseband DSP ADCs and DACs. The PC is equipped with a real time operating system and all MAC layer essentials. The software allows the dynamic partial or full reconfiguration of the mobile and base stations for real time communications and processing, implementation of IP applications, and the management of vertical handover. The Hardware Accelerator is a Network on Chip. The RF platform features are listed in Table 3.

Frequency tuning range	400MHz-7.5GHz
Maximum instantaneous bandwidth	20MHz
Max Tx power	20dBm if $B_{tx} \in [2GHz - 7GHz]$ 15dBm otherwise
NF	8dB
Frequency raster	500kHz

Table 3: IDROMel basic features

This architecture has three key features. The first is an integrated baseband DSP, handling advanced resampling, fine frequency adjustment, I/Q amplitude/phase compensation and Power Amplifier linearization. The second is the ability to handle concurrent communication in different bands and with different waveforms. Finally, using the same front end, it can use time-division or frequency-division schemes.

The RF front end, shown in Figure 83 in section Chapter 9.A, is composed of three sections, the wideband frequency synthesizer; the transmitter and the receiver. The local oscillator synthesizer directly generates within the $[1.9GHz, 4.1GHz]$ range, a frequency doubler is added to obtain the $[3.8GHz, 8.2GHz]$ local oscillator range. The transmitted signals between 4 and 7.5GHz are directly upconverted in the Tx from baseband, while signals below 4GHz are downconverted with the second 8.2GHz local oscillator after upconversion. The receiver

section splits the tuning range in four sub bands because off-the-shelf wideband low noise amplifiers have high noise figures and non-constant gain versus frequency. It results in 4 sub-bands [400MHz,1.2GHz] , [1.2GHz,2GHz] , [2GHz,4GHz] and [4GHz-8GHz] . This approach is used to decrease the amount of outer band interference. After this part, the architecture uses the same principle as for the transmitter section.

This prototype achieved a completely flexible baseband processing, a network on chip integration, FPGA partial reconfiguration support , very wide band RF from 400MHz to 7.5GHz , 4x4 MIMO support and flexible MAC design for vertical handover support .

5. Synthesis on the state of the art of RF platform architectures

Table 4 references the main features of the 4 experimental multicarrier platforms investigated. Comparing the platforms' features, the use of a super-heterodyne structure is common to all of them. Two reasons explain this choice. First, at the transmitter level, the commercially available DACs have limited sampling frequencies which limits the frequency tuning range. The upconverters are used to bring the generated signals up to the desired frequency range. Secondly, at the receiver level, the ADC analog bandwidth are limited, furthermore bandpass sampling degrades the ADCs resolution. Thus the downconverters bring the received signal frequencies within the ADC's bandwidth and sampling frequency.

Radar systems are designed for sub-meter resolution thus wide bandwidth, as opposed to a pure communication system that presents 20MHz bandwidth which is the maximum bandwidth allocated in UMTS and unlicensed IEEE.802.11/16.

The PANDORA splits the total bandwidth at the reception, applies an analog demodulation technique known as stretch processing before digitization. Since the received bandwidth is split, processed and digitized separately, it is similar to sub-Nyquist sampling. The information from the sub bands must be digitally recombined. PANDORA is a reconfigurable platform, it can generate FMCW or stepped-OFDM without changing the hardware configuration. Using stretch processing to demodulate stepped-OFDM is only possible because each frequency is split on a different receiver channel. This architecture can only be implemented for a limited number of carriers.

Platform	PANDORA APAR	HYCAM	Garmatyuk et al.	IDROMel
Instantaneous Bandwidth	384MHz 776MHz with guard bands	800MHz	500MHz	20MHz
Experimental range resolution	0.39m 0.19m	X	0.3m	X
Tested range	X	10m	1.5m – 5m	X
Sampling scheme	Shannon	Sub-Nyquist Bandpass	Shannon	Shannon
Sampling frequency	X	1.35GS/s	1GS/s	X
resolution	X	10bits	8bits	X
Frequency Tuning range	8GHz-12GHz	10GHz-11.6GHz	7GHz-8GHz	400MHz-7.5GHz
Max Tx Power	X	10dBm	14dBm	15dBm 21dBm
architecture	Super-heterodyne Stretch-Processing	Super-heterodyne Frequency-interleaving	Super-heterodyne	Super-heterodyne 4x4 MIMO I/Q channels
waveforms	Stepped-Multitones, Multiband-FMCW	Phase-Coded Multitones	Phase-coded OFDM	UMTS, GSM, IEEE.802.11/16
Pulse width	3.125ms per step	100ns-200ns	128ns-513ns	Dependent on standard

Table 4: Synthesis of the known OFDM platform features

HYCAM in reception combines the received signal and reference signal, which is shifted in frequency domain by half a frequency step, thus the signals are frequency-interleaved. This architecture allows using half the IF channels and thus ADCs. However despite the economic advantage, this technique leaves the reference signal completely exposed to any interferences that may be added to the received signal. The second disadvantage of this technique is the increase of the minimum record length to have an integer number of signal periods. The third disadvantage is the limitation in frequency step: when the step size decreases, so does the Doppler tolerance of such architecture. The signal is then split into two sub-bands for sub-Nyquist and bandpass sampling, and the total bandwidth is digitally reconstructed.

The dual use SAR imaging and communication system is completely generic, it can generate and receive any signals. However there isn't a single filter in the radar architecture which will result in intermodulations and image signals within the system, thus resulting in decreased accuracy.

IDROMel is a communication system but given a few tweaks, it turns into a 4x4 MIMO radar. This architecture is generic and the tuning range is very wide from UHF up to C band. It uses 2 transmission paths to bring IF band up to the desired frequency range, depending on the target frequency range. The receiver has 4 paths to downconvert the received bandwidth to the IF band, in order to optimize performances. This choice of architecture takes advantage of components designed on one octave rather than broadband components. This offers better gain flatness and noise figure. The problem is the multiple down-converting stages increasing distortions and I/Q channels that can be a handful to balance.

From the different architectures, the conclusion is that this technology for reconfigurable radars is still in its early stage. Either the reconfiguration is limited in the number of carriers, in step size or in bandwidth, or its hardware architecture needs to be split into several sub-bands. These reconfiguration capabilities are usually at the cost of increased hardware complexity or increasing interferences in the receiver.

Still a few design rules can be drawn from these architectures. First, if the ADC-DAC IF bandwidths aren't high enough for the application, a super-heterodyne structure to bring the IF band up to the desired bandwidth and the received signal into the ADC IF bandwidth will be required. From the perspective of Ultra Wideband, sub-Nyquist schemes should be adopted when the ADC Nyquist bands are not wide enough to digitize the entire bandwidth. Furthermore, frequency interleaving should be avoided because in live situations, the system will not be located in an anechoic chamber. Thus any perturbations from the received signal may affect the reference channel, which is normally used to correct the received signal from hardware distortions. Also, this technique decreases the reconfiguration capabilities of the radar.

The design of the architecture should be kept simple, with as little components as possible, one or two down-conversions at most. Unlike chirp signal, stretch processing isn't applicable to multitones thus whichever waveform is used, it should be fully digitized.

Now that architecture basic design rules have been explored through the few implementations found in the literature, the impact of RF equipment on the performances has to be investigated.

B. What is the impact of RF components on the performances?

The underlying issue of implementation is the impact of the RF equipment on performances. Note that the literature is lacking on this particular subject and that the use of multitones is mainly dealing with linearization and/or component characterization. The rare results from this survey mostly come from simulations, although a few experimental validations are reported in this section.

The influence of RF components will be investigated from two perspectives. The first section deals with the general topic of linearization for radar systems, involving multicarrier through simulations, and experimental results from Roke Manor Research Limited. The second section will be focused on the association of multicarrier with RF equipment, such as power amplifiers and ADCs, mostly through simulations.

1. Linearization in radar systems involving multicarrier

At Roke Manor Research Limited, research is focused on increasing the dynamic range of RADAR system to see deeper into clutter. In order to do so, one can increase the illumination on the target or the power output, either by increasing the power from the transmitter or by increasing the pulse length. In a Phased Array Radar system, increasing the power can be at the expense of higher thermal dissipation, and increased pulse length have varying deleterious effects on phase and gain from pulse to pulse. This can lead to the array pattern either moving pointing angle or getting broader, neither of which are desired. The linearization techniques exposed below are valid if the power amplifiers are working in saturation and there is no AM component in the RADAR waveform. (47)

The classic solution is to use Automatic Gain Control (AGC) or Sensitivity Time Control. Unfortunately this produces changes in receiver sensitivity, which the operator in many situations may not be aware of. (48). The easiest linearization technique is to back off the amplifier so that it is almost working in small signal. This can lead to a 100W amplifier specified for 10W mean power channels. (47). Pre-Distortion is a commonly used technique in which the signal is first distorted, so that the distortion in the amplifier is cancelled. Amplitude pre distortion is not recommended for RADAR. (47). Harmonic Injection is similar to Pre-Distortion in that a harmonic of the input signal is also added to the signal. This harmonic is phased so that the resultant output harmonics are cancelled. The controlling of this phasing over all conditions has meant that this technique is not used so much in practice. (47)

Roke Manor Research Limited proposes several linearization techniques studied first through simulations and then implemented on an experimental test bench. The compensation capabilities of each of the previous methods and system implications are listed in Table 5 and Table 6 (49). In Table 5, the techniques highlighted in orange have been experimentally tested; the other techniques' performances in white are based on simulations. The abbreviations used in Table 5 are listed below:

AOA	Angle Of Arrival
BF	BeamForming
dBFS	Difference between input signal power and maximum ADC input power (full scale)
IM2	2 nd Order Intermodulations
IM3	3 rd Order intermodulations
IMD	Intermodulation Distortion
OOB	Out-Of-Band
PRP	Pulse Repetition Period
SFDR	Spurious Free Dynamic Range

Multi-channel test scenario (49) is composed of a Linear array with 8 receivers which are uniformly spaced by half a wavelength. The antenna bandwidth is centered at 3GHz and the receiver baseband is 20MHz. The noise level input is -70dB.

Linearization techniques	Tested Signals	Test conditions	Criteria	Improvements	Drawbacks
Digital Post Distortion (50) (51) (49)	NB 2-tones WB FMCW	Roke's RRT experimental set-up	IM 3	15dB 3-5dB	- SFDR improvement dependence on input signal, receiver front-end characteristic - temperature sensitive
	NB 2-tones with temperature-dependent LUT	Roke's RRT experimental set-up	IM3	34.4dB ±2.5dB	Temperature dependent LUT with calibration data
	Signal@0dBFS NB 2-tones WB FMCW	RMRL's Bistatic Radar	IM3/IMD IMD	15dB/11-16dB 0.5-3dB	
	NB 2 tones ADC resolution @8bits @10bits @12bits	RMRL's MFR Test-Bed	IM3/DR/noise floor	18dB/10dB/12dB 38dB/20dB/4dB 52dB/22dB/1dB	SFDR improvement dependence on number of bits
	NB 2-tones WB FMCW	RMRL's Advanced MFR Test-Bed	IM3	[15-35dB] [2-6dB]	
Frequency Retranslation Mixer (51)	WB/NB 2-tones WB FMCW	adaptive closed loop control	IM3 IMD	20-25dB 16-18dB	application dependent
ADC linearization (51) (49)	NB 2-tones	3-tone dither with 50 harmonic Code Map	SFDR	≤ 30dB 13dB@0dBFS	- longer word length - sensitive to noise - IM2
3bit DI with 3-tone dither and code mapping		≤ 35dB 16dB@0dBFS			
7bit DI with 3-tone dither, code mapping and compressive sampling		≤42dB 25dB@0dBFS			
Spatial Diversity (49)	NB 2 tones	Multi-channel test scenario	IMD	10dB	- Implementation of AM @ each Rx channel - Augmented Adaptive BF - Limited AOA - Estimation requires 10 ⁸ samples to converge on IMD of -60dB -Viable for high stability of the order of a few hrs, only a few samples are required for PRP 8kHz
Distortion Correction Processing (51) (49)	NB 2 tones	Multi-channel test scenario	IMD	10-30dB 18dB	Post distortion processing reintroduces OOB IM3

Table 5: linearization techniques and their improvement capabilities and drawbacks

	Digital post-distortion	Frequency Retranslation mixer linearization	ADC linearization	Spatial diversity	Distortion Correction Processing
Distortion components					
In-band mixer products	No	Yes	No	No	Yes
In-band intermodulation distortion	Yes	Yes	Yes	Yes	No
Out-of-band IMD & harmonics	Yes	Yes	Yes	Yes	Yes
Phase noise, local oscillator spurs	No	No	No	No	Yes
Quantization noise	No	No	Yes	No	Yes
System					
Channels	Single/Multiple	Single/Multiple	Single/Multiple	Multiple	Multiple
Hardware complexity	Low	High	Moderate	Moderate	Moderate
Processing complexity	Moderate	Moderate	High	Moderate	Low

Table 6: linearization techniques and their compensation capabilities and system implications (49)

The review shows that the different linearization techniques offer a great potential for NB-2tones intermodulation distortion improvements, in the order of tens of dBs. Also they emphasize the fact that performances are application specific. The simulated techniques give an idea of expected improvements, but unless the RF components characteristics are known and implemented in the simulation process, the results won't be fully accurate. Thus the simulated linearization techniques will be left aside. The methods that were experimentally validated digital post distortion and frequency retranslation mixer, are now analyzed. Digital Post Distortion can correct harmonics, in-band and out-of-band intermodulation distortion at the cost of moderately higher processing power. The improvements require high performance DSP/FPGA and are dependent on temperature, input signal, RF front end characteristics and the ADC bit resolution. Also the improvements for WB cases are limited to a few dBs. The retranslation mixer linearization shows improvements greater than 20dB for NB, and 10dB for WB case. However, Table 6 shows that the hardware complexity is high and the improvements are application-dependent. This means that the practical implementation of such techniques for software defined RF systems may be intractable, given the wide range of configurations required for such applications. However for radar with few targets, it would increase the detection probability of small targets in the presence of big targets.

The linearization from a general perspective has been investigated. The investigation will now focus on multicarrier interactions with RF equipment.

2. RF Equipment & Multicarrier

In this section, the impact of RF equipment on multicarrier signals will be studied, first with respect to power amplifiers and then to ADC. Note that in this section, the results mostly

come from simulations and were not experimentally validated. Also, there is no reference of DACs associated with multitone signals in the literature.

a) Power Amplifier & Multicarrier

For this section, the linearization techniques used for telecommunication applications are presented in Table 7. A color code is used to differentiate simulated from measured performances: white means that the performances are based on simulation results, orange means that it has been experimentally validated. In Table 7, only the results from (52) have been validated. The abbreviations used in Table 7 are listed below and in Equation 1

ACPR	Adjacent Channel Power Ratio which is the ratio of the total power of intermodulations to the useful signal power
HPA	High Power Amplifier
IP1dB	Amplifier 1dB compression point
N-OFDM/tones	N is the number of subcarriers
OOB power	Out Of Band power used to measure the spectral regrowth
SSPA	Solid State Power Amplifier
TD	Total Distortion (see Equation 1)
TWTA	Traveling-Wave Tube Amplifier

Equation 1: TD – Total Distortion

$$TD = SNR_{SSPA} - SNR_{linear} - OBO$$

Where SNR_{linear} (53) is the SNR required to get a Bit Error Rate (BER) of 10^{-3} on a linear channel, SNR required to get a bit error rate of 10^{-3} with solid state power amplifier and OBO is the output power back off compared to saturated power

Linearization Techniques	Component	Input power	Waveform	Performance Criteria	Improvements
Iterative Clipping (53)	SSPA	IP1dB-4dB IP1dB-8dB	96-OFDM-QPSK 96-OFDM -64QAM	TD/OOB Power TD/OOB Power	0.32dB/≈10dB 2.1dB/≈10dB

Baseband Digital Pre-distortion with Tone-Injection (54)	PA	0dBm	WiMax (256-OFDM-64QAM)	OOB Power ACPR	21dB 8-10dB
Pre-distorter with tracking (55)	SSPA: > Cst Param > Param(t)	IP1dB-7dB	128-OFDM-16QAM	BER@SNR 14dB	> 9dB () > 28dB
Limiter (56)	TWTA Linearized-TWTA	> IP1dB	2/4/N-tones	multicarrier/s single carrier saturated Pout ratio	0.6/1/1.2dB 1/2/2.3dB
Interleaving & peak windowing (57)	HPA	IP1dB- 3.5dB	16QAM : > 256-OFDM > 512-OFDM > 1024-OFDM	SNR@BER 10^{-3}	3dB 3.5dB 5dB
Compression @ Tx & expansion @ Rx (58)	HPA	IP1dB- 3.5dB	QPSK/16QAM /64QAM: >256-OFDM > 512-OFDM > 1024-OFDM	SNR@BER 10^{-3}	≈5dB ≈5.3dB ≈5.5dB
Tone Reservation (52)	Class A SSPA	IP1dB- 3.5dB	256-OFDM-32- reserved-64nulls	OOB Power	8dB

Table 7: evaluation of linearization techniques based on components, input power, waveform and performance criteria improvements

In (59) and from Table 7, the effects of amplifier back-off on OFDM are discussed based on both simulations and experimental results. For 6dB of back-off, the signal is almost completely unaffected, even at 3dB or even 2dB back-off, the degradation is still quite tolerable. The required OBO is shown to be somewhat application specific.

The performances are mostly estimated in simulations, thus it may be enough to dimension the system but not fully accurate.

b) ADC & Multicarriers

The association of multicarriers signals with ADC yielded two publications on bit error rate improvement. Table 8 presents the improvements obtained with the two techniques found in the literature: clip correction (60) and Interference Mitigation (61). The first technique allows relaxing the constraints on the ADC resolution and the second allows bit error rate improvements when experiencing low levels of NB Interferences. The same color code used in the previous table is implemented for Table 8, it can be observed that all the results are simulated. The abbreviations used in Table 8 are listed below:

SIR	Signal to Interference Ratio
AGC	Automatic Gain Control
AANF	Adaptive Analogue Notch Filter
MB	Multi Band
ZP	Zero-Padding
PER	Packet Error Rate
BLER	block error rate

Techniques	Solutions	Waveform	Performance Criteria	Parameters	Improvements
Clip Correction (60)	DSP simple DSP complex	64-OFDM-11nulls IEEE.802.11a (35)	PER wrt SNR simple complex	SNR = 35dB AGC back off @IBO = 3dB @IBO = 5dB @IBO = 7dB AGC back off	Clipping threshold -1dB PER 0.55 → 0.41 PER 0.28 → 0.2 PER 0.09 → 0.05 Clipping threshold -3dB
Interference Mitigation (61)	Valid for low SIR Conventional DSP + AGC DSP+AANF +AGC	128-ZP-OFDM MB_OFDM IEEE 802.15.3a (35)	BLER wrt SIR	BLER =0.1	SIR > 12dB SIR > -3dB SIR > -12dB

Table 8: simulated improvements for ADC with multicarrier signals

In (62), the ADC resolution of multi-band and pulsed-OFDM ultra wideband systems (IEEE 802.15.3a (35)) is derived using simulation results. They show that in both, 4-bit resolution is enough to obtain a bit error rate wrt SNR performances quasi-identical to the ideal case with infinite resolution.

None of these linearization techniques or bit resolution performances for telecommunication applications were experimentally validated, hence the system performances can't be predicted in advance.

3. Synthesis on RF equipment in the state of the art

The linearization techniques can improve the intermodulation distortions by tens of dBs, which results in a real improvement in detection in the NB case. However, these techniques have limited effects for wideband signals and increase processing and/or hardware complexity. (50) (51). Also the linearization techniques require receiver bandwidth greater than the useful signal bandwidth to collect data on the out of band intermodulations for post processing (51). The techniques for linearization proposed in (49) through (51) use multitones to identify intermodulations to improve Chirp performances. Their focus is on intermodulation products and dynamic range. Those performances are essential for radar performances to maximize the detection. However the techniques that are proposed add complexity on the hardware and processing and several techniques have to be combined to obtain optimum performances. These improvements are waveform dependent; thus it is interesting for operational radar systems that do not dynamically change their waveforms on a regular basis. Indeed, some techniques require fine tuning and larger receiver bandwidth compared to the signal instantaneous bandwidth. The latter will limit the spatial resolution of the radar to a fraction of the actual receiver bandwidth. These constraints might be intractable for agile radars that may dynamically change their waveforms to avoid interferences, and change functions from surveillance to high resolution for target identification. Also, the increased processing complexity imposes more efficient DSP for real time processing.

The review on power amplifier and ADC with multicarrier displays a strong focus on telecommunication applications. Various techniques have been presented to improve the performances in terms of spectral regrowth, output power or bit error rate with valuable results. However, performances in radar applications are assessed in a completely different

manner. The focus in radar systems is on maximizing SNR for detection and maximizing detection range.

Moreover, most results from the literature concern analytical or simulation results and weren't experimentally validated. The experimental results collected in the literature show that the performances are application specific. Thus the estimated performances allow a general characterization of a system, but can't be accurately predicted until they are measured. So simulation results should be used with care and experimentally validated to evaluate their real potential.

Note also the absence of literature on DACs and the scarce articles on ADCs with multitones. This shows that the matter is still quite unexplored and that the performances of multitones with DAC/ADC are not yet quantized.

C. What are the performances of Multitones and/or OFDM signals compared to classic waveforms?

In this section, the performances of multicarrier signals will be presented. First, they will be studied with respect to the ambiguity function improvements that can be implemented with coherent trains of multicarrier pulses. Then, the advances in terms of Doppler signal processing for multicarrier signals will be introduced.

Note that this section only presents simulated or analytical results. The literature has more publications on Multi-carriers performances for radar applications. However, many of these publications e.g. (63) (44) (41) concern the communication aspect of multi-carriers in radar, leaving radar performances with multicarrier signals aside. A comparison of performances is found in terms of detection in (14) . The authors compared single carrier and multicarrier radar systems in simulations. They found that for target detection in radar based on multicarrier modulation, the required constant false alarm rate detection threshold is lower than for a single carrier radar system.

1. Ambiguity Function

LFM uses spectrum efficiently and has a constant envelope. It is easier to implement than phase coded modulation and it can use stretch processing. Finally, it has zero correlation sidelobes. On the other hand, it doesn't have a perfect periodic autocorrelation and it exhibits a range-Doppler ridge in the single pulse ambiguity function and it suffers from some level of range sidelobes. (64)

For a coherent train of LFM, Levanon shows in (65) (66) how to completely remove most of the autocorrelation sidelobes about the mainlobe peak, without any increase to the mainlobe width. The pulse diversity is obtained by overlaying them with orthonormal coding. A byproduct of this design is reduced autocorrelation recurrent lobes. However, the overlaid signal affects the signal's Doppler resistance, which can be a drawback for some applications. Multi-frequency complementary phase-coded signals (67) are a train of modulated OFDM symbols. The subcarriers are phase modulated by different sequences that constitute a complementary set. (68) allowing spectrum reuse and achieving lower autocorrelation sidelobes as shown in Figure 13 in (12). PMEPR reaches about 2 dB (12) when a polyphase code is used over the frequencies of a multitones symbol.

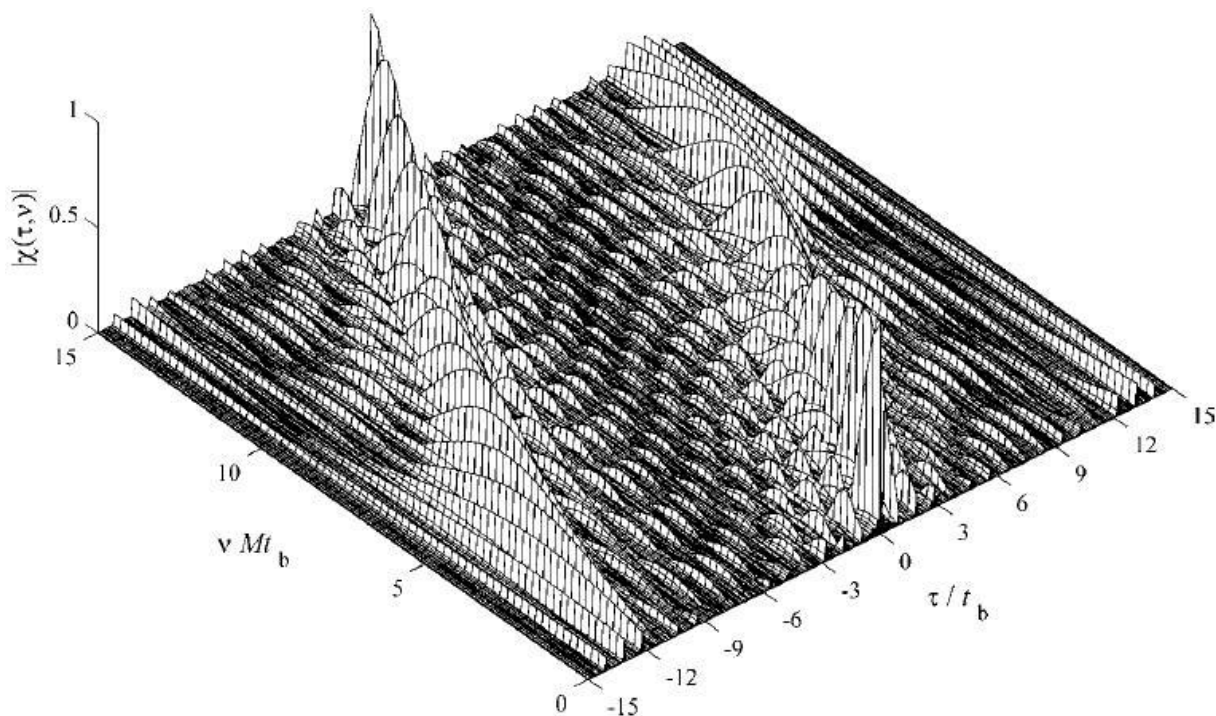


Figure 13: Partial Ambiguity Function of a multi-frequency complementary phase-coded based on consecutive order cyclic shifts of a P4. $N = M = 15$. Equal carrier Amplitude (12)

This coherent train of diverse pulses presents an ambiguity function devoid from most of the recurrent lobes found in a coherent train of identical pulses. The volume of the ambiguity function removed from the recurrent sidelobes is spread all over the ambiguity function area, thus raising the pedestal level. Multi-frequency complementary phase-coded is a pulse signal, however it benefits from the periodic autocorrelation of the signal it is based on to achieve favorable aperiodic autocorrelation. Different codes yield different performances (29). The entire concept of $M \times M$ multi-frequency complementary phase-coded with complementary set and frequency weighting is best summarized by Figure 14 (69).

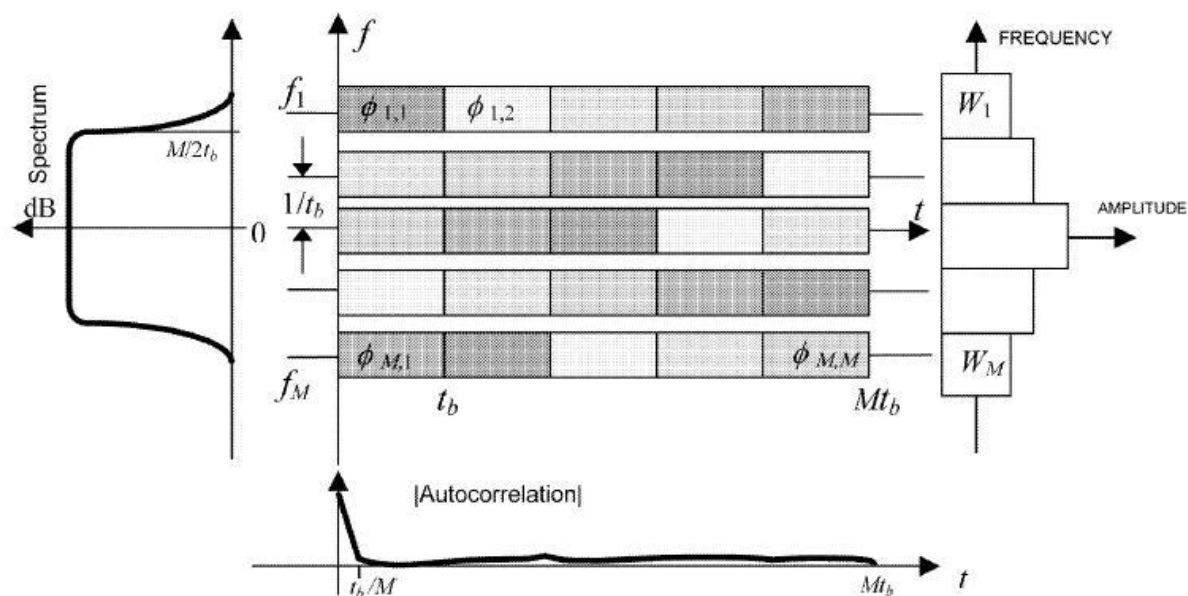
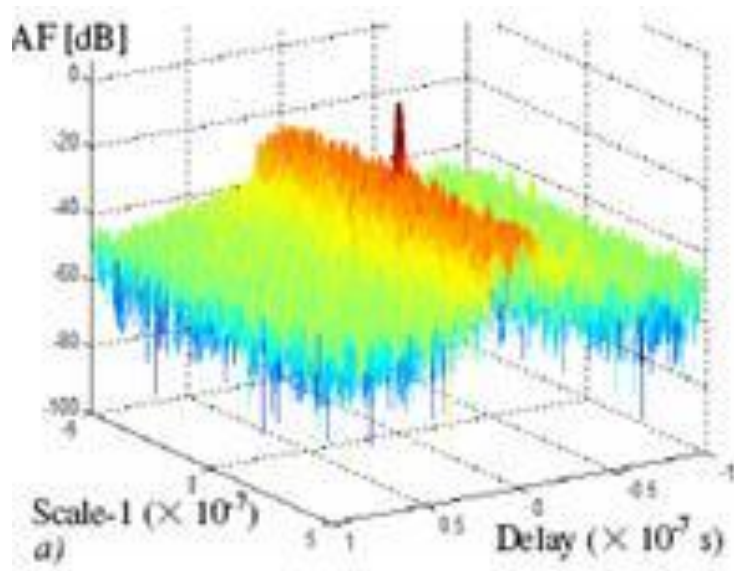


Figure 14: multifrequency complementary phase-coded concept illustrating the spectrum shape, phase coding, autocorrelation and frequency weighting (69)

In (37), the authors determined by simulations that when using agility with multitones, random spread subcarriers pattern provides the best ambiguity function in terms of sidelobe levels and speed ambiguities compared to the random grouped subcarriers and repeated Costas grouped subcarriers (see Figure 15). However, it does not benefit from any instantaneous bandwidth reduction as the other two cases. The agile random spread carrier has the advantage of decreasing the probability of interception and giving rise to a near thumbtack ambiguity function.



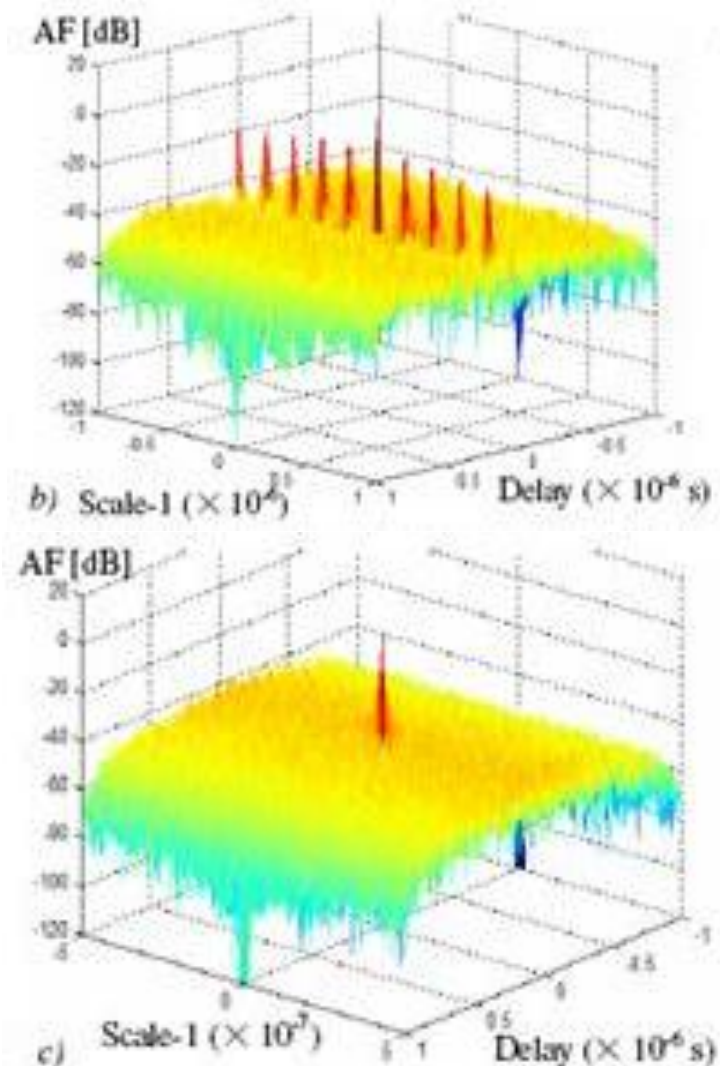


Figure 15: ambiguity function of pulse burst with frequency agile OFDM patterns (top) random grouped (middle) Costas grouped (bottom) random spread subcarriers (37)

2. New Signal Processing Algorithms using Multi-carrier structure

This section presents new signal processing algorithms using the multicarrier structure. This subsection will present processing technique concepts and simulation results used to solve Doppler either more efficiently or in cases that did not allow Doppler resolution with classic waveforms. First, a solution using Doppler Filter banks related to the Doppler resistance for OFDM signals (70) is proposed. Then a technique allowing Doppler ambiguity resolution for OFDM (71) is presented. It will be followed by a novel technique enabling Doppler resolution for agile OFDM (37). Finally, the issue of Wideband OFDM Doppler processing (72) is discussed.

a) Doppler Filter banks and Doppler resistance for OFDM signals (70)

Doppler tolerance of multitones is investigated using simulations in (70). Considering an 8 carrier signal with a centre frequency at 10GHz, a bandwidth of 5MHz and coded with QPSK, the ambiguity function shown in Figure 16 is obtained. The result is the same as the zero delay cut of the ambiguity diagram of an unmodulated pulse with the same pulse length. This means that the pulse compression is achieved without change in the Doppler resolution.

Unlike pulse compression using Linear Frequency Modulation, the ambiguity diagram of an OFDM Radar signal is symmetrical around the delay axis as well as around the Doppler axis. This means that OFDM Radar signals do not experience Range-Doppler coupling, which is the main disadvantage of pulse compression using LFM. They derived the compression loss, which is a function of the Doppler frequency and the delay (Equation 2).

Equation 2: Compression Loss for multitones (70)

$$\frac{1}{L_{PC}(\tau, f_d)} = \text{sinc}(\pi f_d(T - |\tau|))$$

Where f_d is the Doppler Frequency, τ is the delay and T is the signal period.

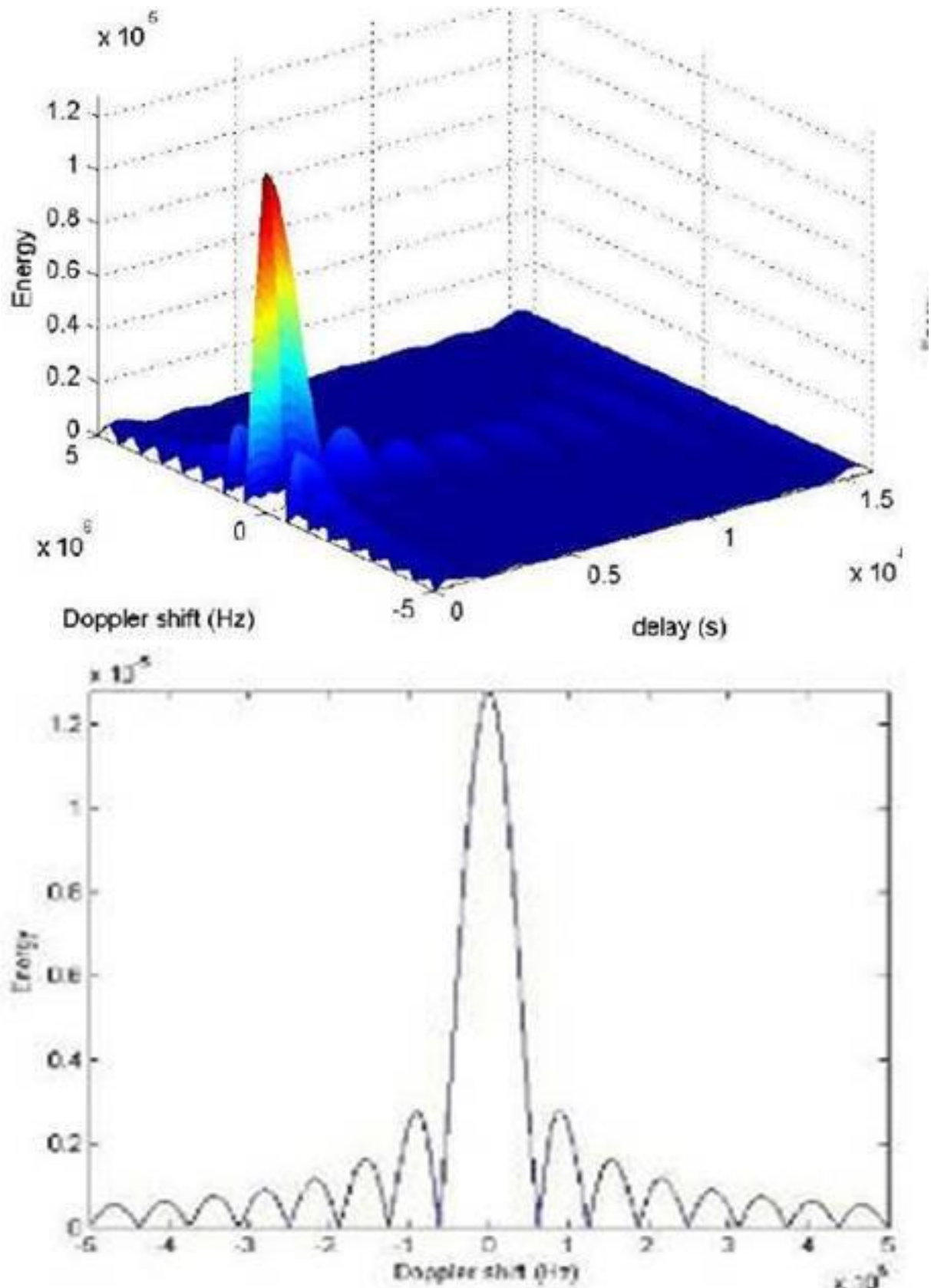


Figure 16: ambiguity function of 8 tones signal with $F_c = 10\text{GHz}$, $B = 5\text{MHz}$, QPSK modulation (left) partial 3D ambiguity function (right) zero-delay cut (70)

The effect of a higher number of carriers for a constant bandwidth renders the compression losses of the main lobe and first side lobe about equal. Van Genderen et al. determined that if we want to set a maximum compression loss of 1dB, there is a limit to the target speed. The expression for the Doppler frequency can be used to calculate the maximum target speed (Equation 3).

Equation 3: maximum target speed for 1dB compression loss (70)

$$|v_{r_{max}}| = \frac{1}{2} \frac{f_l}{4} \frac{c}{f_0} = \frac{Bc}{8Nf_0}$$

Where f_0 is the center frequency, c is the speed of light, f_l is the lower frequency, B is the bandwidth and N is the number of carriers.

For $f_0 = 10GHz$, $B = 5MHz$ and a QPSK modulation, the maximum allowed speeds with respect to the number of carriers are given in Table 9.

Number of carriers	V_{max} (m/s)	$F_{doppler}$ (Hz)
8	2343.75	156250
16	1171.88	78125
32	585.94	39062.67
64	292.97	19531.33
128	146.48	9765.333
256	73.24	4882.667
512	36.62	2441.333
1024	18.31	1220.667
2048	9.16	610.6667
4096	4.58	305.3333

Table 9: maximum allowed speed wrt number of carriers for 1dB compression loss for $f_0 = 10GHz$ and $B = 5MHz$

To measure larger Doppler within a single pulse, the authors proposed a concept based on a compression filter bank. It should be implemented just like a Doppler filter bank. For the NB case, the banks are constructed by using a reference signal in the compression filter that is frequency shifted compared to their neighboring compression filters cross at their 1dB compression loss points. (70)

b) Doppler ambiguity resolution for OFDM (71)

A novel processing technique using the structure of OFDM signals allows solving Doppler ambiguity by Doppler sensitive pulse compression (71). It executes the Doppler matched filter bank digitally, and solves the ambiguity in the radial velocity measurements in one train of multicarrier pulses. This results in lower Doppler sidelobes in the ambiguity function. The processing technique is independent of the phase coding on the subcarriers thus it can be implemented either for communication or radar waveforms.

The Doppler Effect on the multitones can be considered as the shift of the carriers by an amount determined by the radial velocity of the target. The structure of multicarrier signals allows the Doppler compensation by implementing a cyclic shift of the FFT output in the receiver and no extra hardware is required. The processing scheme is given as block diagrams in Figure 17.

Radial velocity is measured through the phase variation from pulse to pulse for a range bin, the same as the other pulse compression techniques. Thus multitones' structure offers an opportunity to solve the ambiguity in the radial velocity measurements without the need to transmit multiple trains of pulses, reducing the required time on target remarkably. The Doppler compensation of multi-carrier waveform is accomplished in a more efficient manner than that of single-carrier phase-coded waveforms. The simulation results show that this signal and associated processing scheme seem valid for use in radar networks responsible for surveillance of areas for slow moving targets and persons, and implement simultaneously a communication function as the processing is independent of phase coding. The multifunction of the waveform and system provides the radar network with robust communications infrastructure.

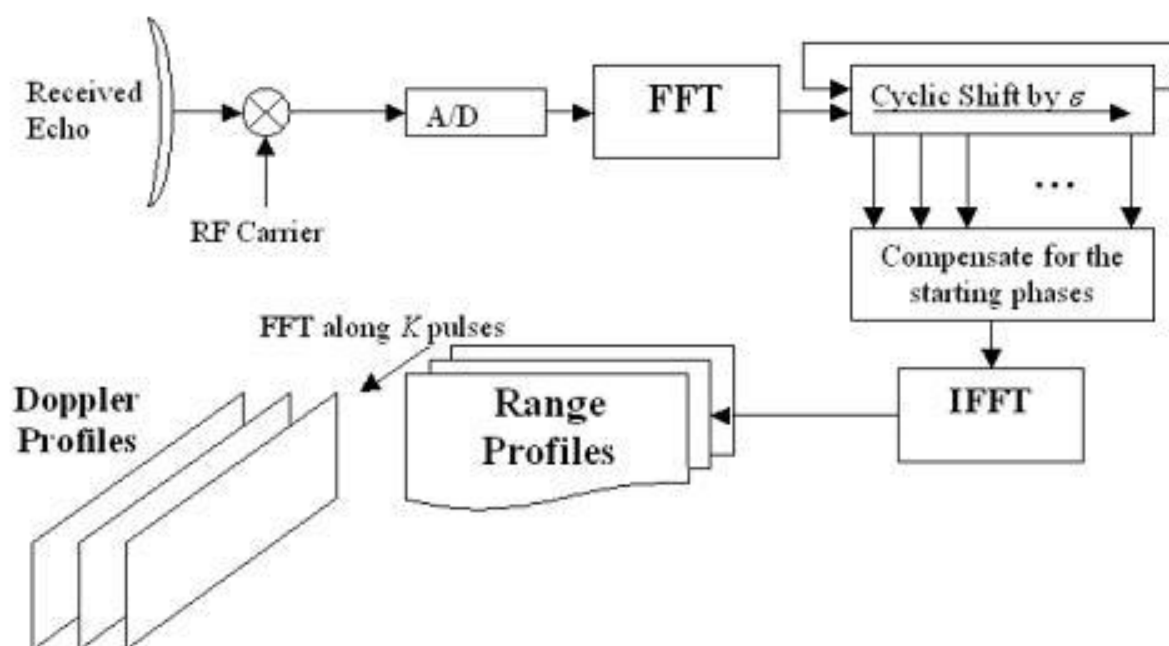


Figure 17: the processing scheme block diagram (71)

c) Doppler resolution for agile OFDM (37)

When radar agility is used, the Doppler frequency shift has a linear dependency on the carrier frequency. In the NB assumption, this difference is ignored and $\Delta f_{Doppler}$ is the same for all frequencies. Obviously, the NB assumption is violated during the whole pulse burst but not during one pulse. Thus, the Doppler scaling will result in a stretching or compressing of the pulse repetition period but its effect will be negligible on the pulse time that is short enough. If such radars were to operate in proximity occupying the same BW, frequency agility would be a good way to prevent fading due to the propagation channel, jamming from unwanted sources and interferences from the system itself. Multicarrier waveforms can enable solving the Doppler ambiguity and also estimating the Doppler shift more accurately. In particular, if Doppler would be estimated per subcarrier, there should be favorite combinations of the narrowband estimates that enable higher accuracy and also an unambiguous solution in shorter time. A single burst could be enough to retrieve the Doppler shift. Recall that in single carrier RF agile radar, the Doppler frequency varies from pulse-to-pulse and makes it impossible to use conventional FFT techniques. The Doppler processing concept for OFDM keeps the same number of subcarriers to measure Doppler all along the burst, while the rest contributes to agility. It relies on very low speeds such that the narrowband hypothesis is valid.

This Doppler frequency spans over the whole burst, and if no phase coding is applied on these N_{Dopp} subcarriers, all of them will have their starting phase modified by the Doppler phase φ_{D_M} , at each pulse m . The concept of multicarrier Doppler processing, where the Doppler processing is done per subcarrier, improves the Signal-to-Noise Ratio (SNR) in the Doppler spectrum when all Doppler spectrums are averaged compared to single carrier as shown in Equation 4. (37)

Equation 4: SNR improvement with Doppler subcarriers processing (37)

$$(S/N)_{MC\ dB} = (S/N)_{SC\ dB} + 10\log_{10}(N_{Dopp})$$

d) Wideband OFDM Doppler processing (72)

For the wideband Doppler processing, there is dilation due to the Doppler Effect. In radar terminology, a pulse burst is said to be wide band when the amount of scaling is not negligible compared to the range resolution when there is range walk. As soon as one pulse suffers one or more range gates displacement, the quality of the Doppler spectrum drops accordingly. A more appropriate wideband processing that would be able to deal with this displacement is then required. The concept proposed and evaluated deviates from the conventional one, in the sense that the pulse is first transformed from time to frequency by means of FFT, so that Doppler is seen per subcarrier. The folded part of the Doppler frequency is correctly retrieved. Ideas to recover the unambiguous Doppler are suggested by making use of the spectrum of the received pulse. As soon as the scaling of the spectrum can be noticed, the radial speed can be estimated. (72)

3. Synthesis on the multitone performances compared to classic radar waveforms in the state of the art

Concepts	Advantages	Drawbacks
multifrequency complementary phase-coded ambiguity function Coherent train of diverse pulses (12)	Near Thumbtack No recurrent sidelobes Diversity Spectrum reuse No range-doppler coupling	Higher Pedestal Waveform Dependent Performances
Agile OFDM (37) Processing ambiguity function <ul style="list-style-type: none"> • Random grouped • Costas grouped • Random spread 	Doppler Resolution with agility Lower Instantaneous Rx BW low probability of interception non-constant PRI Lower Instantaneous Rx BW Best ambiguity function near thumbtack Jamming resistant – low probability of interception	Low Doppler Resistance High ridge in ambiguity function along zero-delay cut Lower contrast Lower Doppler Ambiguity Higher pedestal Full Instantaneous Rx BW
Doppler filter banks (70) @ 1dB compression loss	Compensation of OFDM Doppler resistance for the detection of large Doppler	The smaller the frequency spacing, the more filters required
Doppler ambiguity resolution in one train of multicarrier pulses (71)	Reduced dwell time Processing is independent of phase coding Multifunction Enabling Digital Doppler Filter banks to compensate low Doppler resistance	Only for NB signals Low Doppler tolerance
Wideband OFDM Doppler processing (72)	Solves spectrum dilation due to High Speed No Doppler Ambiguity Unambiguous Doppler recovered	Oversampling Requires longer dwell time The scaling of the spectrum needs to be determined with a high reliability

Table 10: Synthesis of the new concepts advantages and drawbacks

Table 10 summarizes the different techniques presented for improved ambiguity functions and new processing techniques for OFDM signals.

As opposed to LFM, OFDM can't use stretch processing, but OFDM have improved detection capabilities compared to single carrier waveforms. Also the Ambiguity function of train of diverse OFDM pulses do not display range-Doppler coupling, or any of the recurrent sidelobes observed in classic waveforms. The OFDM waveform is polyvalent, it doesn't outperform the classic waveforms in a particular domain, but it has the best overall performances. The OFDM signals can be compared to a triathlon athlete: though the multi-frequency complementary phase-coded signal does not have the lowest PMEPR, the lowest autocorrelation function sidelobes, or the highest efficiency frequency spectrum, we could not find other signals that outperform it when all three aspects are considered (68). All the results on ambiguity functions are solely based on simulation.

Although OFDM isn't as Doppler resistant as Chirp signals, these new techniques show through simulations results the enormous potential of multicarrier signals for Doppler processing. They demonstrate improved efficiency, shortened dwell time. Doppler can also be resolved while using agility, which is a great advantage for electronic warfare or using opportunistic broadcasting. The major limitation to these new techniques seems to be the low Doppler tolerance. These new conceptual algorithms' performances will have to be evaluated on experimental data before assessing their real potential.

When analyzing the signals that were used in these publications, the algorithm use multitones derived from telecommunications. Concerning the ambiguity function improvement in (12), using a train of diverse OFDM symbols allows a near thumbtack ambiguity function, rather than the bed of nails ambiguity function. The correlation of orthogonal codes results in low response, thus explaining an ambiguity function with near thumbtack shape with a higher pedestal.

The multitones phase code is changed on every period. It has been shown in (73) that the choice of phase coding is important for Doppler tolerance². Thus the number of filters in (70) could be reduced if Doppler resistant codes, such as polyphase codes (Newman, Schroeder or Narahashi-Nojima), are overlaid on the multitones

The processing schemes proposed in (71) and (37) are based on FFT processing and thus are very efficient. These techniques suffer from low Doppler tolerance and are limited to NB signals, because they use NB approximation for Doppler and enable the simplifications for the processing. However, these are not suitable for UWB signals.

In (37), the agility allows the low probability of interception, while solving Doppler for low velocity targets. However, the tones used for solving Doppler have to be unmodulated and transmitted continuously, which would be intercepted quite easily. Also the gain on Doppler processing depends on the number of fixed tones. The more tones are dedicated for solving Doppler, the easier it is to intercept the signal.

In (72), the biggest disadvantages are the oversampling and the longer dwell time. Indeed, while using UWB signals, the ADC converters are usually used at their fullest. Using such a technique would require the use of sub Nyquist sampling, thus increasing hardware complexity. Also the longer dwell time on target required might be hindering for the radar, in case of high velocity targets.

² Note that all OFDM codes aren't as Doppler sensitive as can be announced in literature. Indeed, bi-phase, such as Reed-Muller or Barker codes, relying on exact phase matching to achieve near perfect correlation, present a strong degradation in the compression when carrier/phase offset is present. This causes strong sidelobes to appear in the ambiguity function. However, some polyphase codes overlaid over multitones are by definition "chirp-like" codes, such as Newman and Schroeder or Narahashi-Nojima. They mimic the chirp instantaneous phase variation by mean of a phase code, and thus are Doppler resistant. (73)

D. Conclusions

In this chapter, the state of the art was investigated and three main issues were answered partially. This section will conclude on all three issues: the RF architecture, the effect of RF equipment on performances and the comparison of multitones with classic radar waveforms. Finally the objectives set for this thesis are refined based on the results of the survey.

1. Which architecture for the experimental test bench?

Very **few** experimental radar systems implementing multicarrier waveforms are documented in the literature. Indeed, the first implementations only date from the late 90s/early 2000. The technology for reconfigurable radar is still in its infancy and needs to undergo several evolutions before using its potential at the fullest.

Studying the existing platforms allowed learning basic rules for the next reconfigurable radar. Simplicity is the key word. Also, AD/DA converters have considerably improved their sampling frequencies and resolutions over the last decade. In a near future the full X band will be reached without any mixers, and wideband signals will be fully digitized using one AD/DA converter. Until such improvements are achieved, the reconfigurable radar will have to resort to super-heterodyne architectures and sub-Nyquist and/or bandpass sampling to overcome technological constraints.

2. What is RF equipment impact on performances?

It was shown that the linearization techniques in (49) through (51) increase hardware and/or software complexity for the reconfigurable platform. Also the performances are dependent on both waveform and hardware, and have limited impact on wideband signals, and require larger receiver bandwidth wrt signal bandwidth. For dynamically reconfigurable radar, where speed is of the essence, such techniques would hinder the radar detection, as a training time is required for compensation. The extra processing power required will decrease the radar reactivity, and larger receiver bandwidth will increase the hardware constraints on AD/DA converters. These techniques should be kept for radar systems operating with a fixed set of waveforms, the foreseeable improvements brought by these techniques on reconfigurable platforms do not outweigh the disadvantages they present.

The impact of amplifier and ADC with multitones on performances for telecommunication applications is well documented in the literature. However the evaluation of performances in the telecommunications and for radar systems is completely different. The techniques for improving telecommunications performances will have to be re-evaluated from the perspective of radar systems, focusing on maximizing detection range and contrast. Once again, the improvements brought by the techniques show a dependence on hardware and waveform.

This confirms the need to experimentally evaluate the impact of RF components on radar performances. However, simulations may be enough to dimension a system and give general performance trends.

3. What are the performances of Multitones and/or OFDM signals compared to classic waveforms?

The literature focuses on OFDM signals derived from telecommunication waveforms; however, radar applications do not necessarily need to carry information, and thus can continuously repeat the same symbol. In that case guard bands aren't necessary. With no data to carry, simpler PMEPR reduction techniques such as P3 or P4 codes can be used. They reduce the PMEPR sufficiently and work for any number of carrier. Also since P3 or P4 codes are Doppler tolerant thus the weakness in Doppler resistance of OFDM signals would be solved. The processing techniques to solve Doppler are phase code independent, thus they could still be used with a combination of various P3/P4 codes. Using such signals repeatedly will have an influence on the ambiguity function which will have to be studied.

4. Redefinition of the Objectives

This literature review brought partial answers for all the objectives. Comparing performances of two waveforms in simulations and experimentally is different. To date, very few experimental platforms have been implemented. First of all, the circuit non linearities will affect the signals differently, and assuming identical signal characteristics and linear operation, the performances may differ. Also for a valid comparison, two separate systems, one dedicated for chirp and the other for multitones, would be biased since the systems would differ.

Hence the **first** objective is to **design and implement a reconfigurable radar platform able to support any kind of waveforms**. The choice of radar architecture must enable the comparison of any waveform without any RF modifications

The **second** objective will be to study **the effects of ADC-DAC bit resolution and amplifier saturation on performances**. Indeed, those are key components, and their impacts on system performances are the most important. Thus, the thesis work will focus on two processes: quantization and saturation, which will be studied through simulated and experimental results. The quantization will determine the effects of ADC-DAC bit resolution on overall performances. The saturation will be applied at the Power Amplifier in the transmitter, and its effects on overall performances will be studied.

The **third** objective is to **compare the performances of multitones versus classic radar signals, using the same platform**. To date, the chirp is the most implemented waveform in radar systems. The LFM will thus be used as a reference to compare the multitones' performances for radar applications. In the literature, the authors often refer to what multitones can do compared to linear chirp or other waveforms, but numerical results are often simulated and mostly based on communication capabilities. This work will compare those signals using waveform independent criteria to evaluate their performances for radar applications.

Using multitones rather than OFDM signals from telecommunications, has never been implemented on a software defined radar platform. The performances' comparison of both multitones and chirp for radar applications will be based on both simulated and measured data from the same reconfigurable radar platform.

Chapter 4. Theoretical study of radar architectures for HYCAM- research test bench implementation

Based on the basic rules drawn from the state of the art and the evolution of RF architecture to digital, three architectures will be devised in this chapter: frequency-interleaved, parallel and time-interleaved. The first is inspired from the architecture proposed in (9), the second does not use interleaving and has an ADC dedicated to the reference channel and another to the test channel, the third is an evolution of the previous architectures. In the first part of this chapter, the different radar architectures will be described, studied and evaluated against each other with respect to these thesis objectives. The best suited architecture will be chosen for implementation. The second part of this chapter will deal with radar design rules concerning intermodulations in non-linear components: intermodulation avoidance and power level control for third order intermodulations.

A. Radar architecture

Here the word architecture refers to the entire radar system, from the RF front end to the processing algorithm. Let's review together the architectures, their characteristics and performances.

Radar RF front ends usually have one antenna for both transmission and reception, as shown in Figure 5 in Chapter 1. This kind of architecture implies a pulsed emission and a discontinued reception during the emission of this pulse, known as blind range and limited isolation between transmitter and receiver channels. This means that all the echoes returning during the pulse emission time t_p are not received. Thus from the antenna to $D = \frac{c \cdot t_p}{2}$, the radar is blind and can't detect any targets.

Before studying radar architectures for implementation, a few parameters have to be considered, such as the experimental range ($\approx 50m$) and logistics.

For short range, the pulse should be less than 100ns to keep a monostatic architecture for such ranges. This would greatly limit the compression gain: the bandwidth-time product. Thus, the pulsed emission monostatic architectures will be replaced by continuous wave emission bistatic architectures, as shown in Figure 18. The radar operates in continuous wave mode and to decouple the emission from reception, two antennas are required: one for transmission and one for reception. This option eliminates the blind range at the cost of antenna coupling.

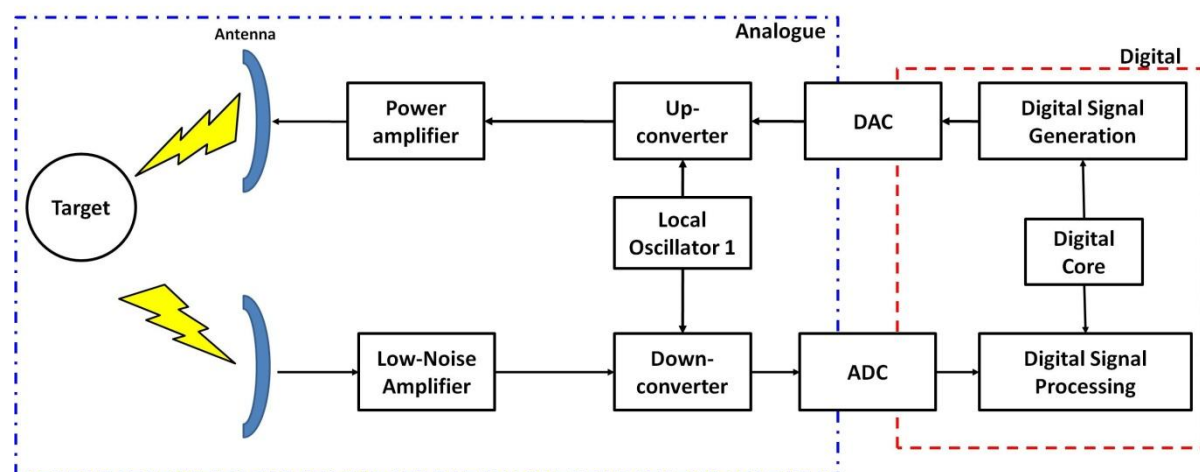


Figure 18: bistatic architecture

The choice of architecture is crucial for the parametric study of various waveforms. The architecture must be selected according to requirements on reconfigurability and overall performances. The radar reconfigurability will be its ability to change the waveform or power levels, the quality of an architecture will be judged on the reconfiguration ranges. The performances of each architecture will be compared on processing power, transfer function cancellation, expected dynamic range and reference channel usage.

Three architectures are proposed: frequency-interleaved, parallel and time-interleaved. The frequency-interleaved architecture is inspired from Paichard's work on RCS measurement (9). It is investigated because it reduces the number of components and the number of ADC channels. The parallel architecture was derived from the frequency interleaved architecture. Although it requires more components, it has a potential for more versatile usage. The time-interleaved architecture is an optimization of the parallel architecture. It combines the quality of the previous architectures: versatility and component reduction. Hence, they'll be compared with respect to each other based on the characteristics mentioned above.

Each one of the architectures incorporates a reference channel that enables the radar to record variations after the amplification stage, and use the recorded signal as a reference rather than the digital replica. The measured replica is used to compensate for hardware transfer functions.

1. Radar front end architecture description

The three architectures' front ends are described below. First the frequency-interleaved front end, then the parallel front end and finally the time-interleaved front end.

a) *Frequency interleaved front end*

Since the radar operates in continuous wave mode, the frequency spectra of generated and received signals are discrete. We will exploit this property to design the frequency interleaved architecture. The periodicity is T , which corresponds for multitone signal to the orthogonal time T_{orth} . T_{orth} is defined as the inverse of the frequency spacing Δf .

In Figure 19, the frequency interleaved front end is depicted. The signal is generated in IF and a low pass filter removes the image signal. The IF signal is upconverted in RF by F_{LO} . The upconverted signal goes through a band pass filter to remove the image frequency after upconversion. The signal is then amplified either by a low noise amplifier for short range applications, or a power amplifier for applications requiring longer ranges. A directional coupler (DC) is plugged at the output of the amplifier. The coupled output of this DC is used as reference channel and the direct path output is directly plugged to the antenna. The backscattered signal is received by the second antenna. This path is the test channel. A low noise amplifier is used to amplify the signal before downconversion, with the local oscillator frequency used for upconversion. The signal in the reference channel is attenuated and downconverted with a local oscillator frequency equal to $F_{LO} + \Delta f/2$. With this operation, the reference channel is shifted by $\Delta f/2$ with respect to the test channel. Both signals are sent to a power combiner, thus both signals merge together, and the frequency spacing is now $\Delta f/2$. The signal goes through an anti-aliasing band pass filter, is amplified and finally digitized by an ADC. This architecture presents the advantage of digitizing the reference and test signals on the same ADC, thus reducing by half the number of required ADC channels.

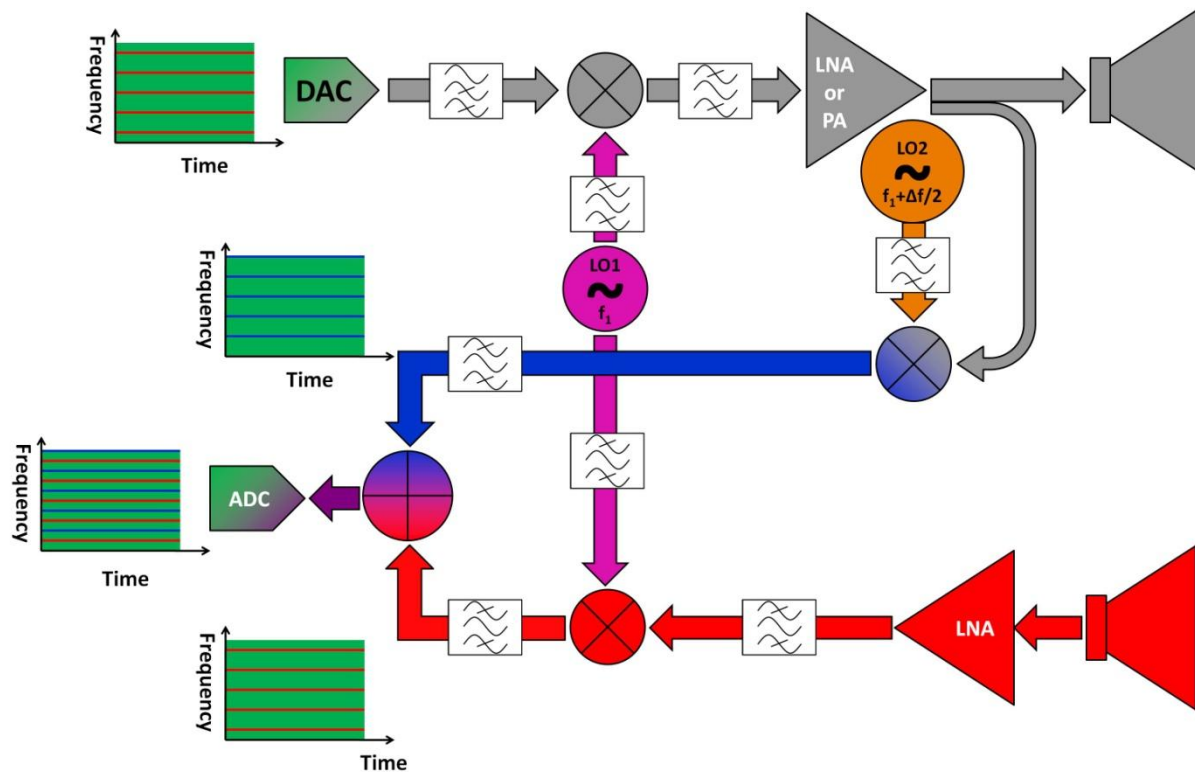


Figure 19: Frequency interleaved radar front end for 2 channels

b) Parallel front end

In Figure 20, the parallel front end is depicted. Compared to the frequency interleaved front end, the modifications occur at the reference and test channels' downconversions. Both reference and test channels are downconverted by the same local oscillator frequency used for upconversion. Both test and reference signals go through anti-aliasing band pass filters, are amplified and finally digitized by two ADCs.

c) Time interleaved front end

In Figure 21, the time interleaved front end is depicted. Compared to the parallel front end, after the transmitter's amplifier and before the receiver's amplifier, a switching circuit is implemented. The switches allow two modes: calibration mode and measurement mode. The calibration mode is enabled when the switches shunt the antennas creating a direct path from the transmitter to the receiver with some attenuation. The measurement mode is enabled when the switches connect the antennas for emission and reception of the signal backscatter. Thus by time sharing the channels, the hardware from the test channel is reused for the reference channel and avoids doubling components at the price of interrupted test channel measurement.

As introduced earlier, the architecture is composed of the front end and the signal processing algorithm. Three architectures were presented frequency-interleaved, parallel and time-interleaved. To complete the architecture, the associated algorithms required to process the data will be presented next.

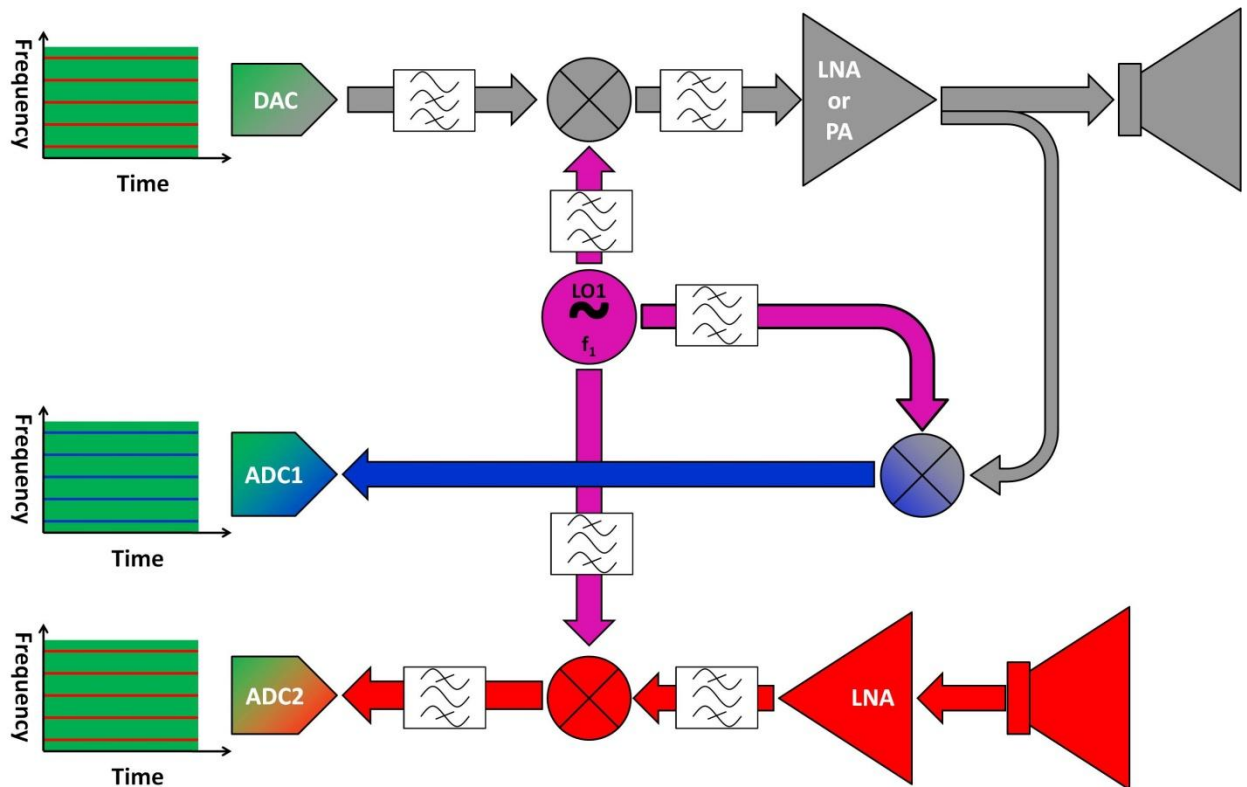


Figure 20: Parallel radar front end for 2 channels

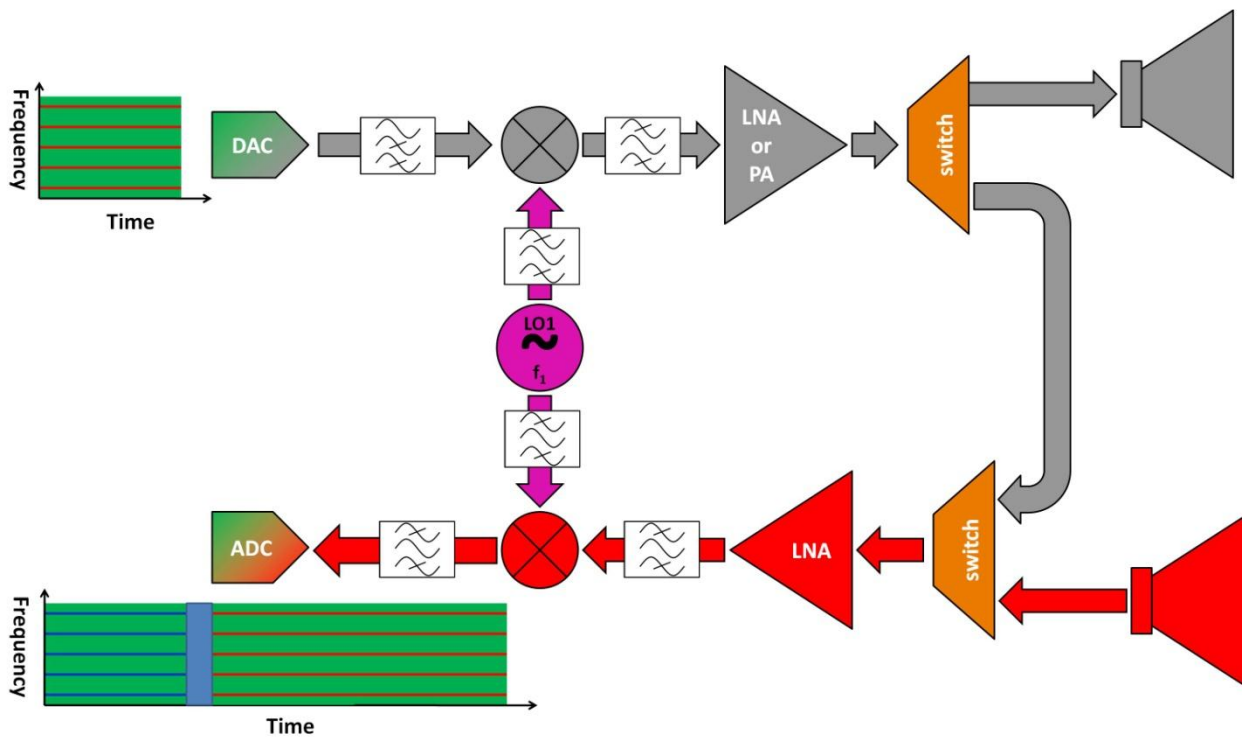


Figure 21: Time interleaved front end for 2 channels

B. Generic Signal Processing Algorithms

Generic algorithms were devised, according to the architecture characteristics, and with the objective to compare waveforms. The processing power required to analyze the waveforms will be evaluated in each case. It is one of the characteristics which will determine the choice of architectures.

The algorithms are implemented to process any kind of waveforms. This allows comparing two distinct signals on waveform independent criteria. Radar systems use pulse compression in order to “see” the targets within the antenna beam, the optimum match filtering process in white Gaussian Noise was chosen for implementation. The matched filter for any signals is its complex conjugated spectra. The concept consists in passing the tested signal through a matched filter to obtain the impulse response.

Two algorithms (Figure 22) are proposed to execute this task. The first one uses radix-2 FFT and is suitable only for the parallel and the time-interleaved-architectures. The second uses DFT because of constraints on data extraction for frequency-interleaved signals.

1. Radix-2 FFT algorithm for parallel and time-interleaved architectures

The principle of the pulse compression algorithm using radix-2 FFT is described in Figure 22 (left). Two input signals are necessary: the reference signal and the test signal. The reference signal is used to generate the matched filter. It can either be a digital replica or a measured replica of the generated signal.

Since the signal delay is unknown a priori, a sliding window that is three times the signal period is implemented for the test channel. This guarantees that the full target return is within this range and that the continuous emission of the signal is taken in account during correlation. Taking three times the symbol period insures that whatever the signal returns delays are, a complete impulse response is generated without losses on the edges of the pulse compression. The reference replica used for cross correlation can be implemented in several manners. It can be implemented using a fixed digital replica of the emitted signal. It could also be implemented using the reference channel data stream. The replica can either be fixed or refreshed at a given frequency, or even replaced continuously. Hence, this algorithm is suitable for either the parallel or the time-interleaved architectures.

Both vectors have unit sizes equal to $M = \text{orthogonal time} \times \text{sampling frequency}$. In order to speed up the processing time, FFT-radix2 is used. Thus the digitized vector length $3M$ for the test channel and M for the reference channel are zero padded up to $2^P > 4M - 1$. The zero padding is used to create a support for correlation equal to the sum of both test and reference vectors. Zero-padding up to the next power of two allows using efficient FFT algorithm: radix-2.

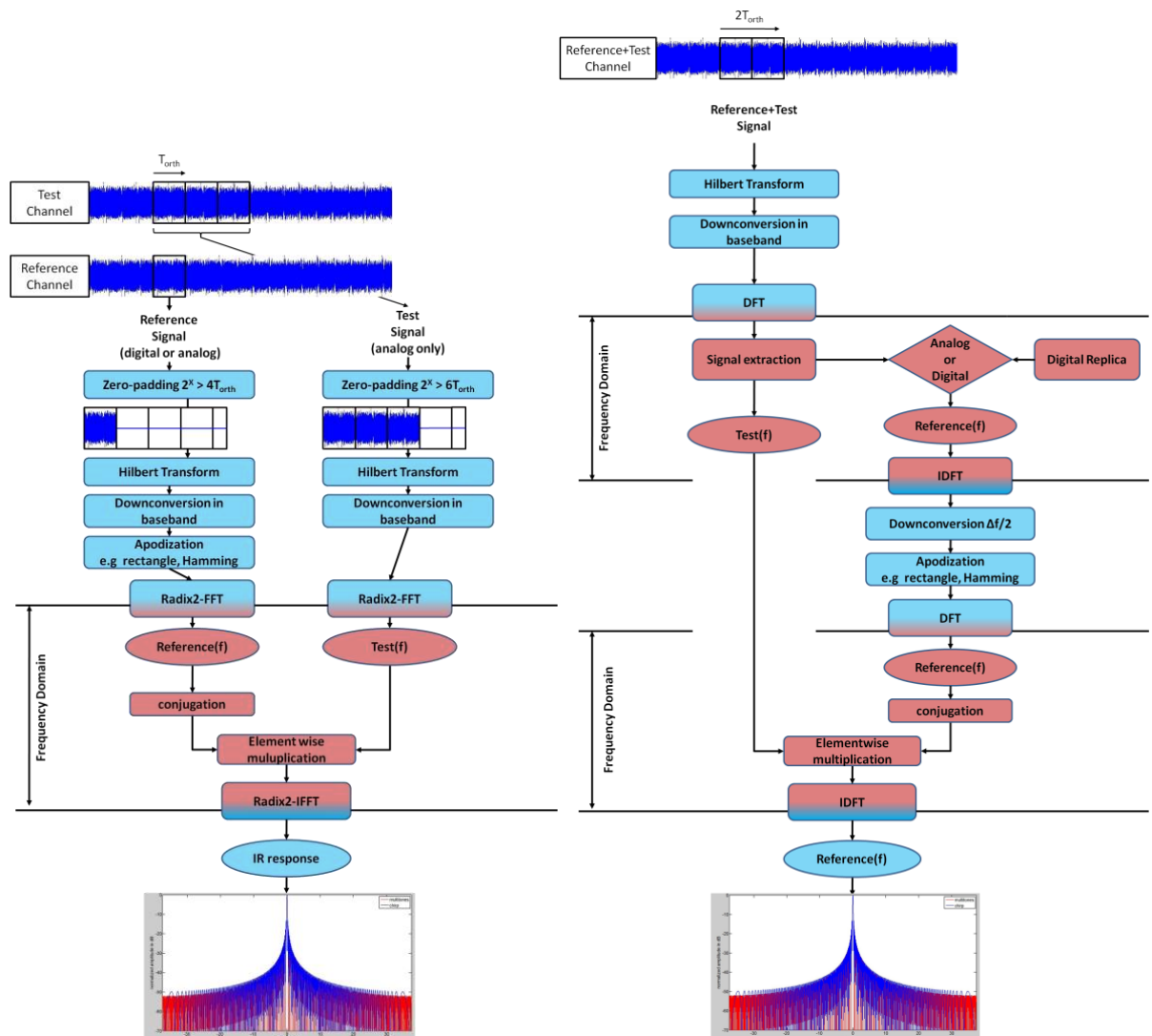


Figure 22: Pulse compression algorithm (left) radix-2 FFT for parallel and time-interleaved architectures (right) DFT for frequency-interleaved architecture

The radar system only generates the real part of the signal. The complex values of the signal must therefore be reconstructed. The Hilbert transform is used to reconstitute the complex part of the digitized vector.

The signals are digitally downconverted to base band, as shown in Figure 23. Then, a window function, such as Rectangle or Hamming, is applied over the pulse length M on the replica used as reference. The apodization is done in time domain to take into account live operation of the radar with OFDM signals. The apodization window (Hamming) limits the effect of inter-symbol interference (ISI) and increases the contrast of the impulse response at the cost of a 38% wider main lobe at 3dB.

A radix-2 FFT is applied on both test and reference signals to switch from time to frequency domain. The complex conjugate of the reference signal is multiplied element by element by the test signal. This operation is equivalent to a cross correlation in time domain.

Then, to return in time domain and get the impulse response, a radix-2 IFFT is applied on the cross correlated data to obtain the pulse compression. The complete pulse compression ranges from $\frac{M}{2}$ up to $\frac{3M}{2}$, giving a zero delayed response centered within that window.

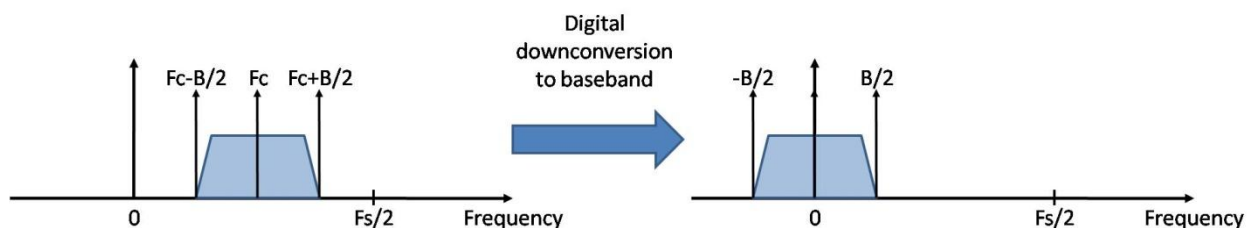


Figure 23: digital downconversion to baseband

2. DFT algorithm for frequency-interleaved architecture

The frequency interleaved architecture intertwines both reference and test signals into a common signal. The reference is shifted in frequency by half the inverse of the pulse repetition period ($\frac{1}{2T_{orth}} \equiv \frac{\Delta f}{2}$) compared to the test signal. The principle of the pulse compression algorithm for frequency-interleaved signals is described in Figure 22 (right). The algorithm first extracts the reference and the test signals before realizing the pulse compression.

Since the frequency step of the signal is now $\frac{\Delta f}{2}$, the orthogonal period is doubled. At least $2M$ samples are necessary for the extraction of both signals. A Hilbert transform is applied to this vector to reconstruct the complex part, since the radar only generates real samples. The signal is then downconverted in baseband.

A regular FFT aka DFT is used to switch from time to frequency domain. Odd samples go to the test channel vector and even samples go to the reference channel. The reference channel can be replaced at that moment by a digital replica if required. The reference signal on M samples is then switched back to time domain using an IDFT.

This operation enables the final downconversion to compensate for the slight phase modulation resulting from the frequency shift. A downconversion by $\frac{\Delta f}{2}$ is applied and a window can be applied in time domain over the full vector length which matches the symbol period.

The reference channel is once more switched to frequency domain with a DFT. The reference's complex conjugate is multiplied element by element to the text vector. This realizes the equivalent of a time domain cross-correlation. Finally an IDFT is applied to obtain the pulse compression.

3. Doppler processing

The Doppler processing shown in Figure 24, is common to all architectures. To form a distance-velocity image, the system accumulates impulse responses over time. This way, the phase modulation caused by target velocity is sampled over a fixed period T_{orth} , fixing the

frequency ambiguity $\Delta f = \frac{1}{T_{orth}}$. The integration time is an integer multiple N_{IT} of the phase modulation sampling period. It fixes the frequency resolution, which is equal to $\delta f = \frac{1}{N_{IT} \cdot T_{orth}}$. The Doppler frequency is directly related to the emitted frequency $F_D = \frac{2 \cdot \text{velocity} \cdot \text{emitted frequency}}{\text{speed of light}}$.

Given a vector size M in the time direction, another Hamming window of size M is applied. The vectors are then zero-padded up to $2M$ and then further zero-padded up to the next power of 2. This way, an IFFT radix-2 can be used to finally obtain a distance Doppler image.

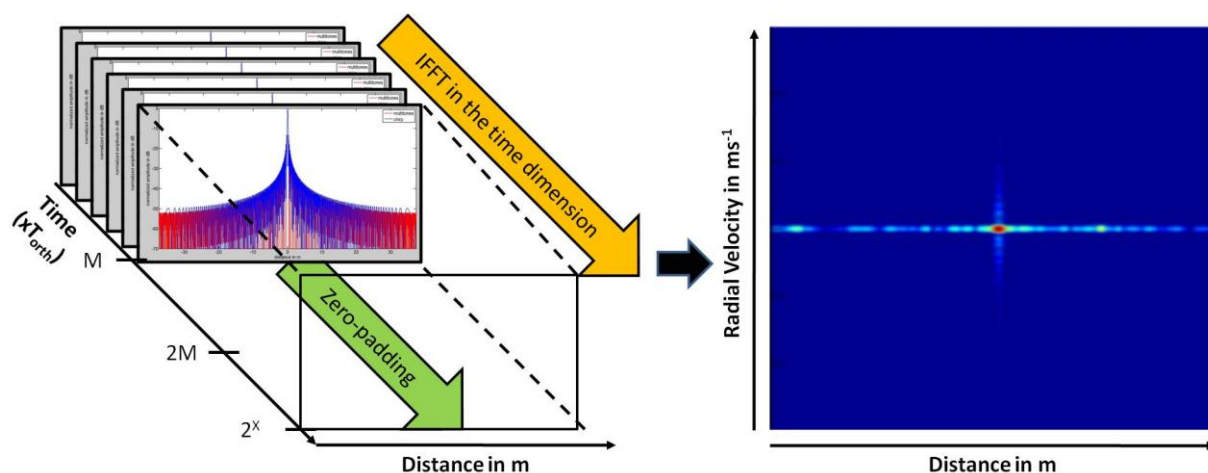


Figure 24: Doppler processing

C. Radar architecture comparison

The architectures' performances will be studied based on the signal configuration (pulse repetition period and bandwidth). Then the processing power and data-throughput requirements to execute a single FFT will be evaluated, based on the signal length. The third criteria will be the transfer function cancellation capabilities of the various architectures. The expected dynamic range losses and finally the reference channel constraints will be evaluated in each case.

1. Minimum orthogonal time and Doppler ambiguity

The orthogonal time of the emitted signal is $T_{orth} = 1/\Delta f$.

Frequency Interleaved Architecture

When $2n$ channels (n reference channels and n test channels) are frequency interleaved, then the minimum orthogonal time in reception is $2nT_{orth}$. The n reference channels are fixed, they don't have Doppler components. However the test channels do. The Doppler shift must not exceed $\Delta f/2n$. The more channels are frequency interleaved, the more the Doppler shift recoverable is reduced. Even though Shannon's theorem is respected to sample the Doppler modulation after extraction, the Doppler beyond $\Delta f/2n$ won't be recovered because the Doppler shift overlaps the reference frequencies and has a deleterious effect on them. A polluted reference reduces overall performances of the radar.

Parallel and Time-interleaved architecture

When $2n$ channels (n reference channels and n test channels) are recorded in parallel or with time interleaving, the minimum orthogonal time in reception doesn't change. Thus the Doppler ambiguity is Δf .

2. Processing power and data throughput

In order to quantify the required processing power, the characteristics of the Neptune VXS 2 (74) ADC that will be implemented in the radar will be used for the estimations. The ADC Neptune VXS 2 encodes the samples on 10 bits, meaning that the data is encoded on 2 bytes. Thus the data flux is 4GB/s per channel @ 2GS/s when digitizing continuously.

The orthogonal time of the emitted signal is $T_{orth} = 1/\Delta f$. When digitized in reception, the orthogonal time is represented by a vector of length M . A Hilbert transform is used to reconstruct the imaginary signal from the digitized real signal to get the complex signal. Also note that a complex multiplication needs 4 real multiplications and 2 real additions. A complex addition needs 2 real additions.

The comparison in processing power will be based on the number of operations required to obtain one distance pulse compression, since once the pulse compression is obtained, the Doppler processing is common to all architectures.

 The processing operations linked to sub-Nyquist sampling for a number of channels greater than 2 will be purposely excluded. Indeed, a reconstruction algorithm needs to be implemented. However my expertise doesn't go that far. Thus it is left out of the processing power calculations.

	Real Multiplications	Real Additions
Frequency Interleaved Architecture – Case 1- $M \neq 2^Z$	$\frac{2M(15nM + 4)}{T_{orth}}$	$\frac{3M(10nM - 1)}{T_{orth}}$
Frequency Interleaved Architecture – Case 2 - $M = 2^Z$	$\frac{2^{Z-1}(9Z + 11)}{nT_{orth}}$	$\frac{2^{Z-2}(27Z + 9)}{nT_{orth}}$
Parallel Architecture $4M < 2^Y$	$\frac{4M + 2^{Y+1}n(7Y + 10)}{T_{orth}}$	$\frac{2M + 2^Yn(21Y + 15)}{T_{orth}}$
Time Interleaved Architecture $4M < 2^Y$	$\frac{2^{Y+2}(2Y + 3)}{T_{orth}} + 4rM$	$\frac{2^{Y+2}n(3Y + 2)}{T_{orth}} + r(2M + 2^Yn)$

Table 11: processing power required for all the architectures – real multiplications and additions

Figure 25 was plotted using the required processing power referenced in Table 11 (see details in Appendix Chapter 9.D). The frequency interleaved architecture requires much more computation than the other two architectures, except when its vector length reaches a power of 2. In this case, the frequency-interleaved architecture is interesting, as it requires one ADC and less computation power for the same result. Thus it reduces the data throughput and the required processing power. So it is most likely that this architecture will be limited to short range, in order to process Doppler within the tolerance imposed by this architecture and

relatively low radial Doppler shifts. In terms of performances in relatively low interference environments, if the requirements can be met with the limited set of operating points, this architecture is advantageous.

The parallel architecture requires more computation power than the time interleaved architecture. And any vector length is tolerated, guaranteeing efficient calculation. Thus these architectures allow more flexibility in waveform design. The same remarks stated above hold true when the number of channels is increased.

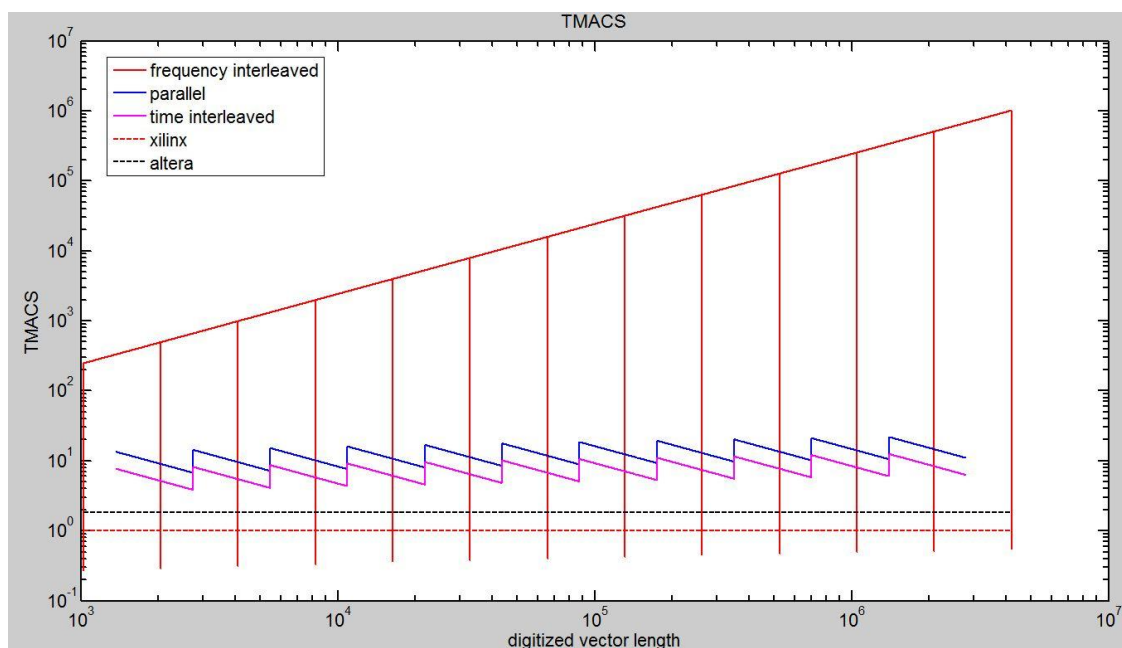


Figure 25: processing power comparison of radar architectures with 2 channels and a sample frequency @ 2GS/s with 2 channels and a refresh rate of 100Hz for the time-interleaved architecture

The processing power is high but not far from the announced capabilities of FPGAs. The Altera Stratix V (75) performs up to 1.840 Tera Multiply-Accumulate Operations per Second (TMACS) and Xilinx Virtex 6 (76) performs over 1 TMACS. In Figure 25, it can be seen that a few FPGAs will be needed to perform the full processing for any vector length in real time. And FPGA capabilities will continue to increase in the future.

The bottleneck today is the communication bus throughput and storage capabilities. Considering the 2 channels case, the system must handle 8GB/s for the parallel architecture and 4GB/s for the time-interleaved and frequency interleaved architectures. The latest performances announced by National Instruments (77) in bus communications (NI-PXIE-1075) is up to 4GB/s and for data storage with the (NI-HDD-8264) up to 600MB/s. At present, the off-the-shelf equipment data throughput can only handle the time interleaved and frequency interleaved architectures with two channels on 1 ADC @2GS/s. Also, the data needs to be decimated to reduce the data throughput for storage. These conclusions are for raw data only; the implementation of pre-processing can dramatically reduce the calculation power. And, if the radar uses pulse bursts rather than continuous wave emission, these requirements would be reduced proportionally with the PRP at a given pulse length.

3. Transfer Function Compensation

Frequency Interleaved

In the frequency interleaved architecture, the transmitter transfer function can be fully compensated. The IF stage transfer function is cancelled out, if the amplitude and phase variations over $\Delta f/2$ do not differ significantly. If the components are matched in the downconverters and in the paths linking the downconverters to the power combiners, then further compensation can be accomplished in those parts. However, because of the phase difference between the two local oscillator frequencies, there is a phase component that can't be cancelled out.

This architecture also requires extra calculations. First to extract the complex coefficient of both channels from the frequency interleaved signal. Then, to digitally downconvert the reference signal and compensate for the $\Delta f/2$ frequency modulation.

In Figure 19 and Figure 26, the signals from the reference path and the test channel are summed in the power combiner. This means that if any interference appears in one of the combined channels, they will corrupt the other one. So this limits the use of such architecture to short range applications or environments with low interference levels such as an anechoic chamber.

The transfer functions of the frequency interleaved architecture are shown in Figure 26. And the demonstration of transfer function cancellation is available in Chapter 9.E.1Appendix page 9-8.

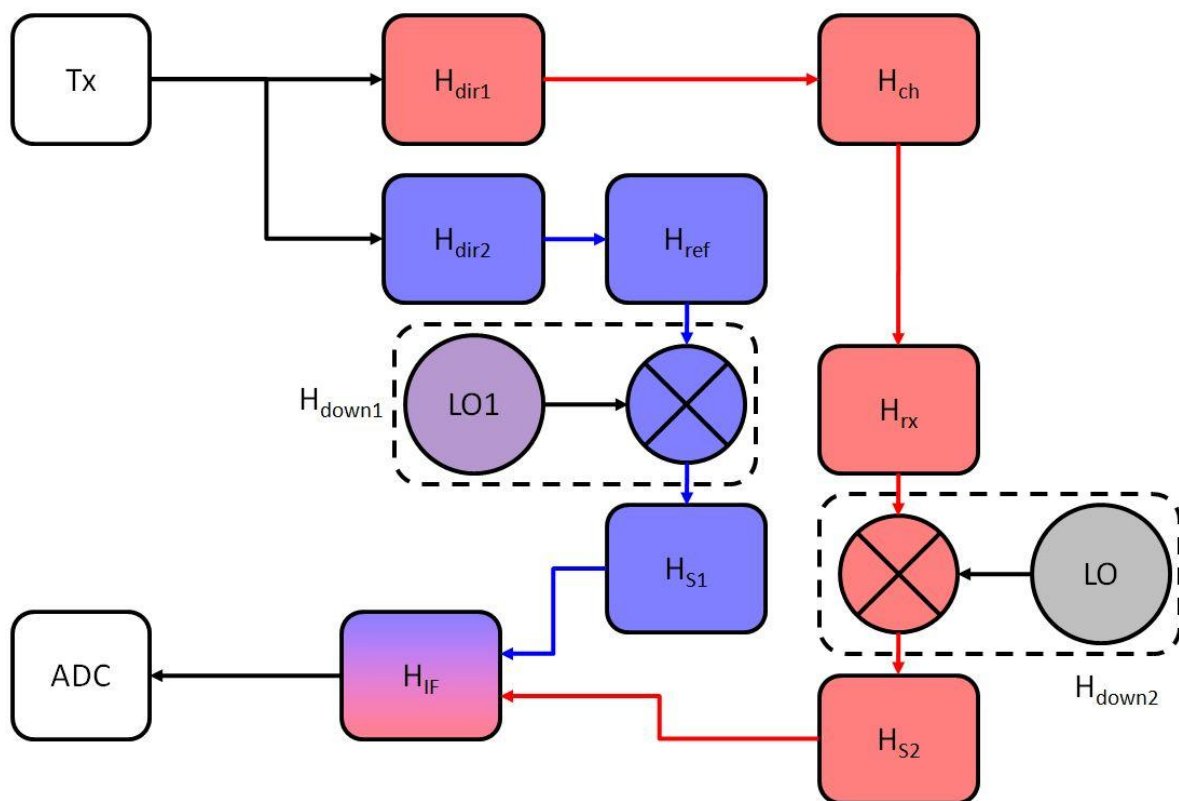


Figure 26: Transfer functions block diagram for frequency interleaved architecture

Parallel Architecture

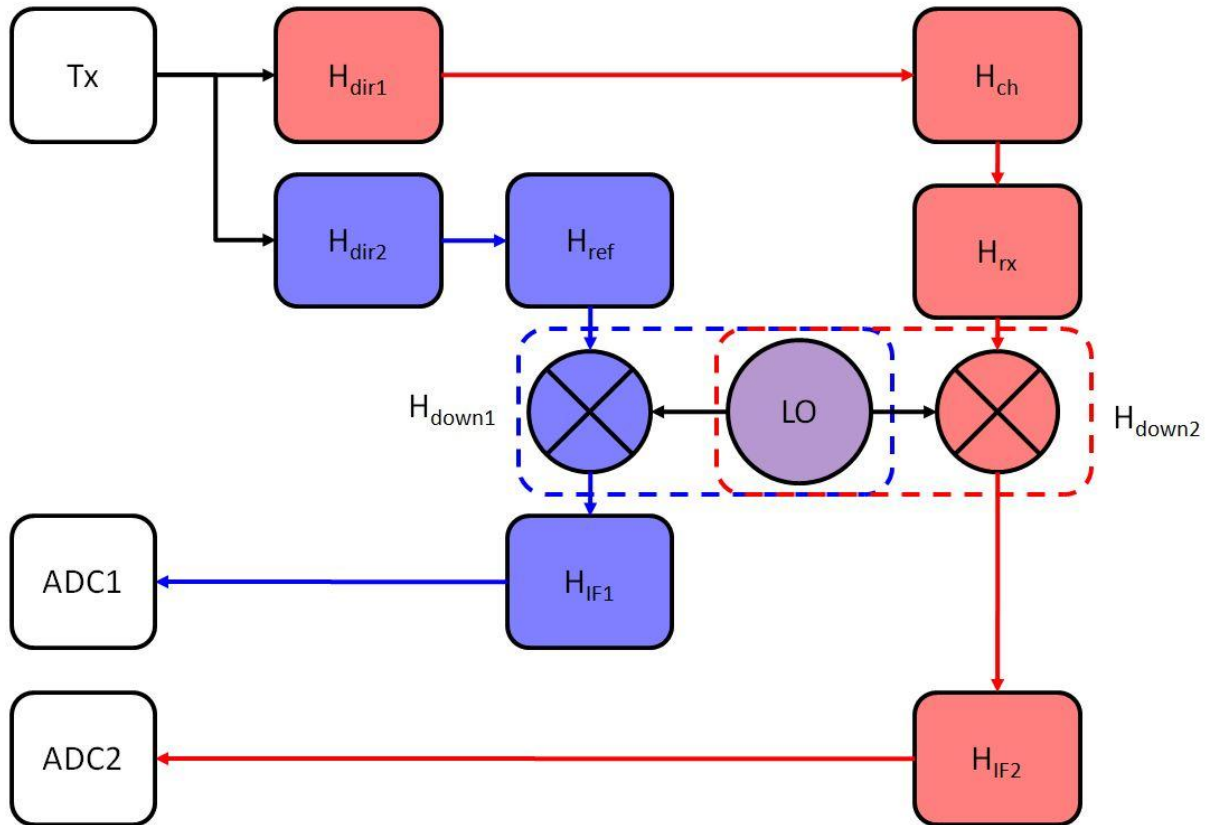


Figure 27: Transfer functions block diagram for parallel architecture

In this case the reference and the test channel are demodulated by the same local oscillator frequency, so if the components are matched in the IF stages and downconverters, their transfer function can potentially be compensated. And here the transmitter transfer function is fully compensated. This analysis shows that the reference and test channels are completely decorrelated, so any interference affecting one of the channels will not contaminate the other.

The transfer functions of the parallel architecture are shown in Figure 27. The demonstration is available in Chapter 9.E.2 Appendix page 9-10

Time interleaved

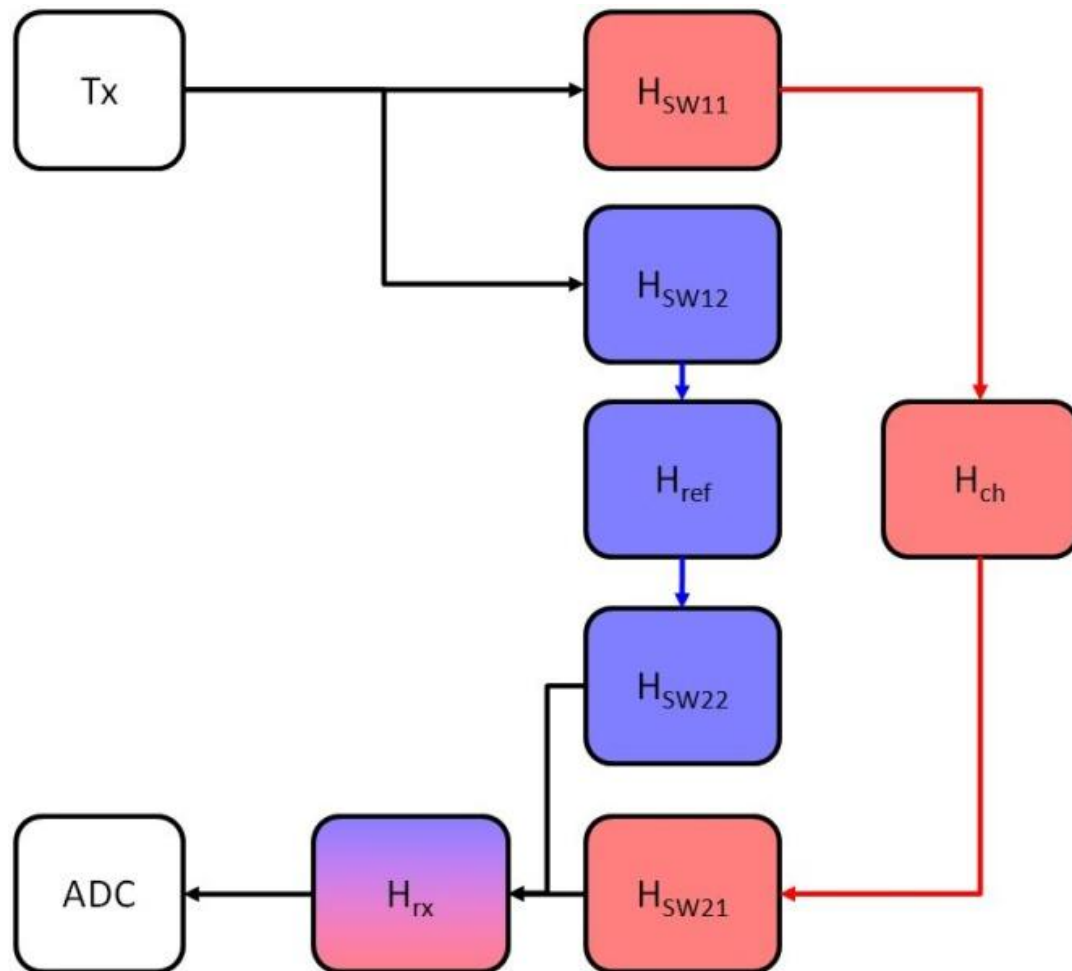


Figure 28: Transfer functions block diagram for time interleaved architecture

In this case, both signals are downconverted with the same local oscillator frequency. The transfer functions from the transmitter and receiver are cancelled out. Only remains transfer functions from the reference path and the test path. In other words, the difference lies in the switches' positions and between the bypass and the channel with aeriels. Here the isolation between the channels is as good as the isolation in the switches. Therefore the designer should take this into account when selecting the switches.

The transfer functions of the time interleaved architecture are shown in Figure 28. The demonstration is available in Chapter 9.E.3 Appendix page 9-10.

4. Dynamic range

The time-interleaved and parallel architecture use the ADC full scale, but not the frequency interleaved architecture. The worst case scenario is when the frequency interleaved signals have equal amplitudes, and the best case is when the other channel is zero. The number of channels considered is always even.

Equation 5: SNR Loss range for frequency interleaved architectures

$$\begin{aligned} 10\log_{10}(\text{number of channels}/2) &\leq SNR_{loss} \\ &\leq 10\log_{10}(\text{number of channels}) \text{ (dB)} \end{aligned}$$

For a system with two channels, the SNR loss ranges from 0dB to 3dB and deteriorates with the number of channels. Since the SNR is of paramount importance for radar detection, this will limit the frequency-interleaved architecture to short ranges or it will require higher resolution ADCs for equivalent performances.

5. Reference channel

The pulse compression consists in multiplying the test channel with the complex conjugate of the reference channel. The reference channel is available at any time in both the parallel and frequency interleaved architecture. The reference coefficients can be obtained at any time, the refresh rate of these coefficients can be modulated to fit performance requirements. The minimum refresh rate is determined by the system stability $RR_{min} = 1/T_{stable}$. The stability can be evaluated by the evolution of the subtraction of impulse response peaks over time with either a sliding reference or a fixed reference. The maximum refresh rate is the time required to process the FFT coefficients for the reference channel and conjugate them $RR_{min} = 1/T_{calc min}$. In the time-interleaved architecture however, the reference is not always available. The refresh rate must be calculated to avoid having too many interruptions as it blinds the radar to eventual targets, thus the target speeds must be taken into account. but it shouldn't fall below $RR_{min} = 1/T_{stable}$. So if the calculated refresh rate for the application of interest is lower than RR_{min} , then another configuration has to be chosen.

As for time-interleaved architecture, there is an additional drawback concerning the synchronization requirements and the switching time. The switching time for X band switches varies depending on the power class of the radar. Up to 30dBm, pin switches can be used. The switching time is in tens of nanoseconds, the isolation in the range of 30-60dB and the insertion loss from 0.5-3dB (78). However for high power radar, electro-mechanical switches are required. The switching time then goes up to tens of milliseconds, the isolation is in the range 40-80dB and the insertion loss from 0.1 to 1dB (79).

During switching time, the signal is truncated, so all the sampled periods surrounding the switching time will be dismissed. This requires a very accurate trigger and synchronization in the data storage to avoid corrupting the data.

6. Synthesis

	Frequency Interleaved		Parallel	Time Interleaved
ADC channels	1		$2n$	n
Data stream	4GB/s		$2n \times 4\text{GB/s}$	$n \times 4\text{GB/s}$
Min integration time	$2nT_{orth}$		T_{orth}	T_{orth}
Doppler Ambiguity	$\Delta f/4n$		$\Delta f/2$	$\Delta f/2$
Vector Length	$M \neq 2^Z$	$M = 2^Z$	$M \rightarrow 4M < 2^Y$	$M \rightarrow 4M < 2^Y$
Processing <ul style="list-style-type: none"> • Intensity • Multiplications • Additions 	+ + + + + $2M(15nM + 4) /$ $3M(10nM - 1) /$	+ $2^{Z-1}(9Z + 11)/T_o$ $2^{Z-2}(27Z + 9)/T_o$	Any size + + + $4M$ $+ 2^{Y+1}n(7Y$ $+ 10)$ $2M$ $+ 2^Yn(21Y$ $+ 15)$	Any size + + $2^{Y+2}(2Y + 3)/T_{orth}$ $+ 4rM$ $2^{Y+2}n(3Y + 2)/T_{orth}$ $+ r(2M$ $+ 2^Yn)$
Transfer function cancellation <ul style="list-style-type: none"> • Complete • Partial 	Emitter + IF stage after power combiner Downconverter + IF stage before power combiner		Emitter Downconverter + IF stage	Emitter + Receiver
Isolation	None		$> 80\text{dB}$	$> 60\text{dB}$
Signals	Any		Any	Any
Other	Dynamic range reduction $SNR_{loss} = [10\log_{10}(n); 10\log_{10}(2n)]\text{dB}$		Data stream and storage	Data stream and storage Switching time dependent on radar power class
Applications	Short range applications Anechoic chambers		Short Acquisition Applications	Low power radar <100W

Table 12: Radar architectures synthesis

For radar applications, any level of interferences can be expected, so a high level of isolation between the reference channel and the test channel is required. The frequency interleaved architecture is thus dismissed. Only remain the time-interleaved and parallel architectures. The time-interleaved architecture clearly outperforms the parallel architecture in terms of processing power and transfer function cancellation. However, if a high power amplifier is required, the switching time in the time-interleaved architecture becomes problematic, since it reaches tens of milliseconds.

So for applications up to medium range sensing, the time-interleaved architecture is the most appropriate architecture. The only thing that might be limiting its use is the calibration time versus time of exposure.

And for any applications from short to long range, the parallel architecture can be implemented at the cost of a higher processing power and lower transfer function cancellation capability.

The parallel architecture doesn't have the best performances in terms of processing power and transfer function cancellation, however it is clearly the most versatile and robust to equipment influences and instabilities. It measures the test and reference channels

continuously, thus allowing uninterrupted detection and the matched filter update on a pulse to pulse basis.

The time interleaved architecture is also very versatile. However there are constraints on synchronization for switching operations and stability to limit the frequency of the calibration cycle. This means that the radar will be blinded during calibration time. Although it is limited to powers up to a few tens of Watts, the time interleaved architecture offers a processing power that is halved and a system with a reduced number of components.

After implementation, the radar will be used to test various waveforms with a wide range of bandwidths and pulse repetition periods. Since the radar system stability is not known in advance, the parallel architecture shown in Figure 29 will be chosen for its robustness to equipment imperfections.

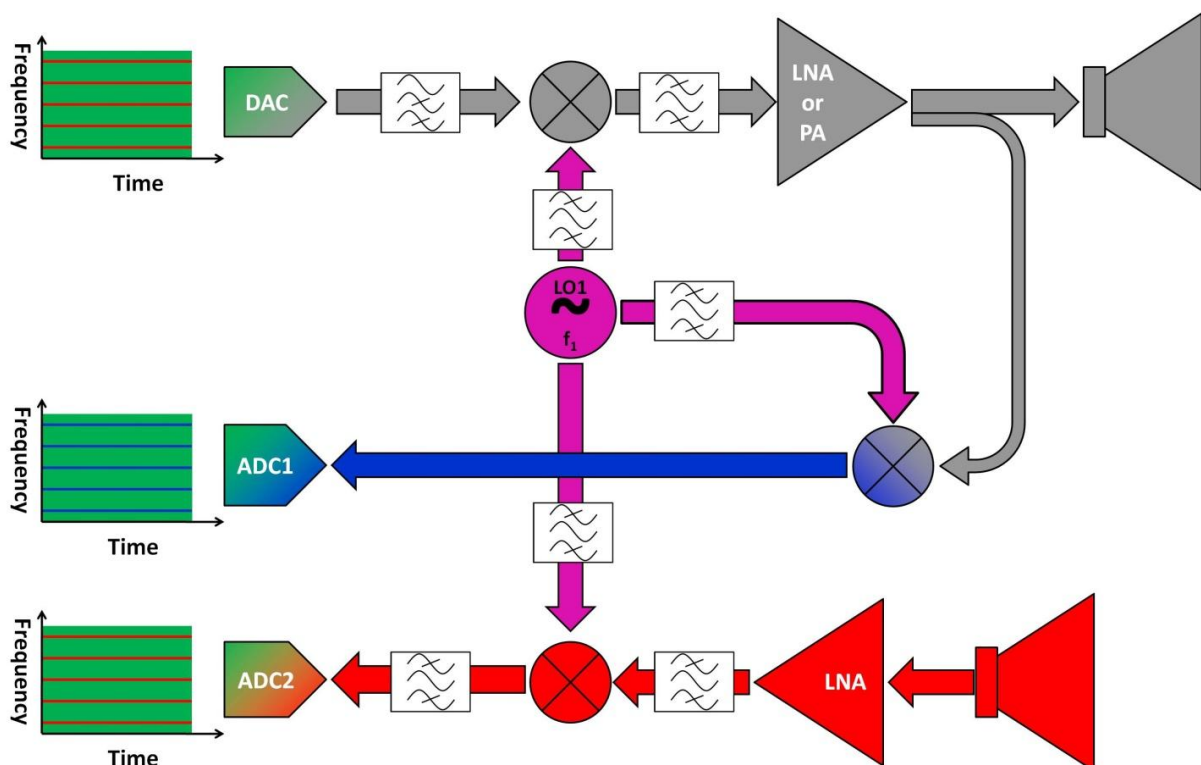


Figure 29: Which architecture → the parallel architecture

The architecture for this project has been selected. The following section will focus on general design rules for the radar, more specifically for intermodulations. Intermodulations are caused by non-linear components; hence the next section also addresses the second issue of this thesis: the effect of RF components on radar performances.

D. Design rules for intermodulation

This section focuses on the effect of RF components for radar performances. Intermodulations are generated when a signal goes through non-linear components such as mixers, amplifiers and DACs/ADCs.

These intermodulations decrease the overall performances of the signals. If they fall inside the useful bandwidth, they cause in-band distortions and affect the amplitudes and phases of

the signals. This is problematic if the signal carries information, since amplitude or phase distortion can cause losses. In the radar case, it is more a question of loss of compression, as the signal will be mismatched with its replica.

Intermodulations are also generated outside the useful bandwidth, thus raising the power level in adjacent bands. These out of band intermodulations waste energy that should be concentrated in the useful bandwidth to extend range. This could also interfere with neighboring RF systems operating in the same frequencies; furthermore the radar might not be authorized to transmit because of power emission regulations.

This section will set design rules for the implementation of a frequency planning which avoids intermodulations inside the useful bandwidth, and guidelines for signal input back off to limit the 3rd order intermodulation power levels.

1. Intermodulation avoidance

Concerning the upconversion and downconversion for UWB signals, great care has to be taken to avoid intermodulations. These will degrade signal purity and provoke amplitude modulation (AM) and phase modulation (PM). From the mixer characteristics and the theoretical digitizer dynamic range, the order of the IM avoidance has to be determined. The formulas for intermodulation avoidance of the nth order for up and down conversions are derived in Appendix A.

F_{LO}	Local Oscillator
$F_{l1} < F_l < F_{l2}$	Intermediate Frequency (IF) Range present at the mixer IF port
$F_{H1} < F_H < F_{H2}$	Radio Frequency (RF) Range present at the mixer RF port

From the perspective of maximizing the bandwidth at upconversion, the designer should choose a local oscillator frequency greater than the RF upper bound. However, the IF input should remain in the linear operation range of non-linear devices, otherwise the pure intermodulations (nF) won't be negligible anymore. If the IF input is driven near or in saturation, it is recommended to choose a local oscillator frequency smaller than the RF range lower bound. Also in both cases, the maximum bandwidth achievable can't exceed by the IF range lower bound. In other words, the bandwidth can't exceed an octave with respect to the IF range lower bound. See Table 13.

From the perspective of maximizing the bandwidth at downconversion, the designer should choose a local oscillator frequency greater than the RF upper bound up to 3rd order intermodulation avoidance. For IM4 avoidance, both schemes yield identical maximum bandwidth. And from 5th order intermodulation avoidance, the local oscillator frequency should be smaller than the RF range lower bound. See Table 14. If the bandwidth is greater than one octave and if the circuit contains any non-linear components, the designer must make sure that the IM2 products do not exceed the minimum power detectable by the ADC.

Case	$F_{l1} < F_{l2} < F_{LO} < F_{H1} < F_{H2} < 2F_{LO}$	$F_{l1} < F_{l2} < F_{H1} < F_{H2} < F_{LO}$
Basics	$F_{l2} < 2F_{l1}$	$F_{l2} < 2F_{l1}$ $F_{l2} < F_{LO}/2$ & $F_{l1} < F_{LO}/4$

validity	$n \geq 3$	$n \geq 4$
Linear	$(n - 1)F_{l1} + (n - 1)B < F_{LO}$	$(n - 3)F_{l1} + (n - 2)B < F_{LO}$
	$F_{l1_max} = B_{max} = \frac{F_{LO}}{2(n - 1)}$	$F_{l1_max} = B_{max} = \frac{F_{LO}}{2n - 5}$
Saturated	$(n - 1)F_{l1} + nB < F_{LO}$	$(n + 1)F_{l1} + (n + 1)B < F_{LO}$
	$F_{l1_max} = B_{max} = \frac{F_{LO}}{2(n + 1)}$	$F_{l1_max} = B_{max} = \frac{F_{LO}}{2(n + 1)}$

Table 13: n^{th} order intermodulation avoidance rules for upconversion

Case	$F_{l1} < F_{l2} < F_{LO} < F_{H1} < F_{H2} < 2F_{LO}$	$F_{l1} < F_{l2} < F_{H1} < F_{H2} < F_{LO}$
Basics	X	$F_{l2} < F_{LO}/2$
validity	$n \geq 4$ and n even	$n \geq 4$ and n even
	$F_{l2} < 2F_{l1}$	$F_{l2} < 2F_{l1}$
validity	$n \geq 3$ and n odd	$n \geq 3$ and n odd
	$F_{l2} < 2F_{LO}/(n + 1)$	$F_{l2} < 2F_{LO}/(n + 3)$
$n = 3$	$B_{max} = 2F_{LO}/(n + 1)$	$B_{max} = F_{LO}/2$
$n = 4$	$B_{max} = F_{L1}$	$B_{max} = F_{L1}$
$n \geq 5$	$F_{l1_max} = B_{max} = \frac{F_{LO}}{(n + 1)}$	$F_{l1_max} = B_{max} = \frac{F_{LO}}{(n + 3)}$

Table 14: n^{th} order intermodulation avoidance rules for downconversion

These rule will be used when the frequency planning will be defined. See section Chapter 6.A.2.

2. 3rd order intermodulation power level control in non-linear components

In (9), the author derived a formula to set the 3rd order intermodulation products power level at the non-linear component output based on (80). Equation 6 defines the maximum output power and input power to set 3rd order intermodulation power levels at XdB below the main signal output power:

Equation 6: 3rd order interception point output back off for 3rd order intermodulation power levels at XdB below the main signal (9)

$$P_{out_dB} = IP3_{dB} - X_{dB}/2$$

where $IP3$ is the 3rd order interception point and X_{dB} is 3rd order intermodulation power levels.

This value X will have to be determined based on the component with the lowest dynamic range. This will determine the maximum power level tolerable in the system. To illustrate, 3rd order intermodulation products and higher order are rejected below 70dB if the output signal power is 35dB below the 3rd order interception point, as shown in Figure 30.

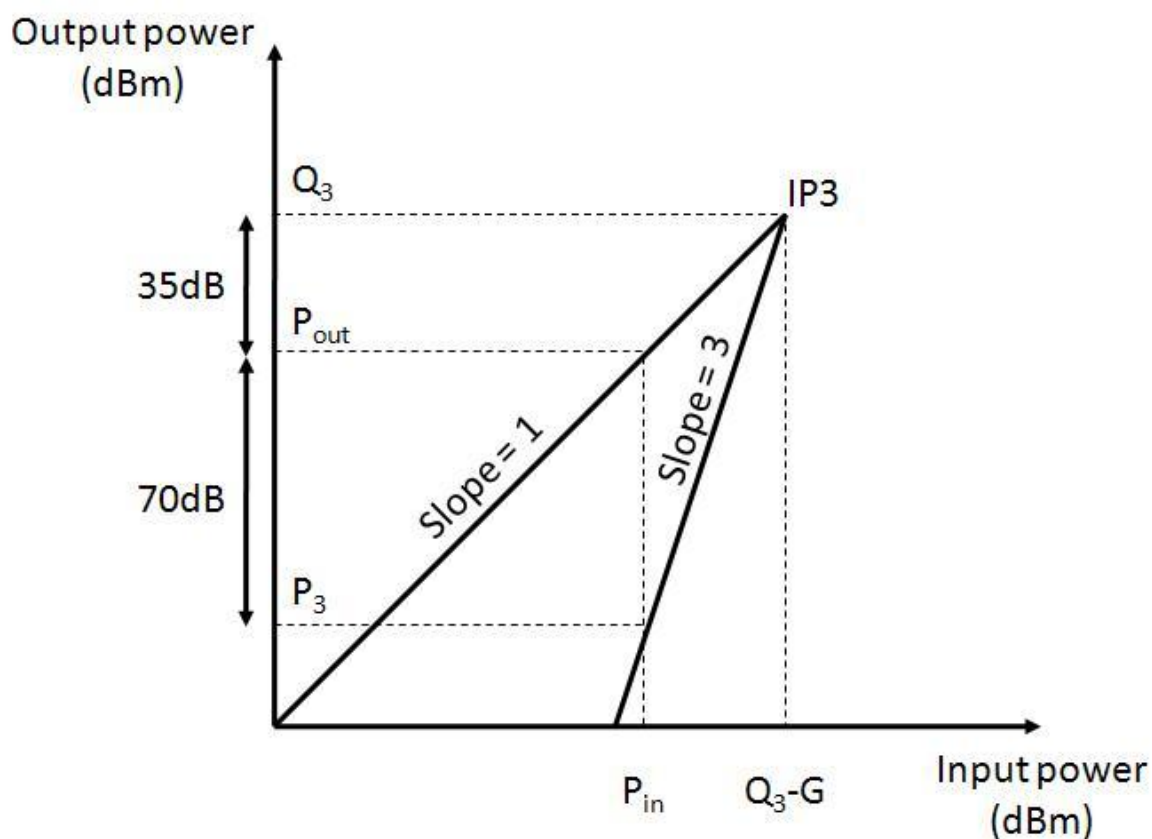


Figure 30: 3rd order interception point and power levels for 3rd order intermodulation power level control e.g 70dB below main signal (9)

E. Conclusion

According to Table 12, the parallel architecture was chosen for implementation compared to frequency-interleaved and time-interleaved architectures, because it is the most versatile and robust to equipment influences and instabilities. It measures the test and reference channels continuously, thus allowing uninterrupted detection and the matched filter can be refreshed on a pulse to pulse basis. On the other hand, it comes with higher processing time, data throughput and storage. It was chosen to implement a reference channel in the test bench and to record a reference signal from the power amplifier output; the necessity of this channel will be evaluated based on the comparison of simulated and measured reference signals.

A narrowband distance-Doppler processing algorithm was proposed for operational use in the experimentation. To keep the error caused narrowband approximations within a set limit; the range of velocities will have to be defined. Using NB algorithms allow a practical implementation for real time processing. The solution would be to use wavelet transforms for processing, however the required processing power is on a different level, and thus a practical implementation is not feasible at the moment.

It was established through demonstration how to design the frequency plan, in order to avoid intermodulation to any desired order for up and down conversion. The basic rule is to keep the signal bandwidth under an octave. This limit is the achievable bandwidth for direct generation when using a super-heterodyne architecture for any waveform. The mixer stage is the bottleneck in generating wideband. High spectral purity requirements with a mixer stage tend to reduce the signal bandwidth that can be generated. When AD/DA converters allow direct signal synthesis and digitization in the frequency band of interest, multitones and chirp will still be limited to one octave because of the amplifier. Avoiding intermodulations is a key feature in the design of the radar, as they can deteriorate in band properties, and out of band intermodulations results in a waste of energy. This could result in compression losses due to signal mismatch at the receiver level, and a shorter detection range because of a drop of SNR caused by out of band intermodulations. Both of these would result in decreased detection capabilities, thus great care must be put to the frequency planning and the amplifier input power level.

Now that the reconfigurable radar platform architecture for this study has been defined, the performances of multitones in the context of radar applications have to be investigated. The next chapter studies the multitones' performances in simulations.

Chapter 5. Waveform simulations

In this chapter, the waveform performances of chirp and multitones will be studied through simulations. The study will focus on two processes: quantization and saturation which are linked to key components in the radar: DA/AD converters and the power amplifier.

This thesis work aims at determining the contribution of Multitones for software defined radar. This study focuses on a special case of multitones with Newman Phase codes. The performances of multitones for radar applications need to be compared to a reference in order to gauge its potential for radar applications. Linear Frequency Modulation is the first and probably still the most popular pulse compression method (12). So the Chirp was selected to be the basis for a comparison with multitones.

The waveforms (Multitones and Chirp) used for the comparison will be introduced and their intrinsic properties, such as PMEPR, power efficiency and ambiguity functions characteristics, will be compared for different Bandwidth, Pulse Repetition Period. These characteristics will also be compared wrt quantization and saturation.

Since the study is about radar waveforms, the multitones will be implemented with a PMEPR reduction technique known as Newman Phase codes (81). This was chosen for three reasons: low complexity of generation, Doppler resistance (73) and for radar only applications, no data needs to be encoded.

In order to cover various radar signal configurations from primary radar to high resolution radar, various combinations of radar ambiguities and resolutions were tested. Studying various configurations may allow determining if some are more favorable to one or the other waveform. The parameters are the bandwidth (BW) and the pulse repetition period (PRP) (see Equation 7 and Table 15).

Equation 7: ambiguities and resolutions

$$\begin{aligned}
 \text{Range Ambiguity } \Delta R &= \frac{c \times PRP}{2} \\
 \text{Doppler Frequency Ambiguity } \Delta f_D &= \pm \frac{1}{2 \times PRP} \\
 \text{Spatial Resolution } \delta R &= \frac{c}{2 \times BW} \\
 \text{Doppler Resolution } \delta f_D &= \pm \frac{1}{2 \times \text{integration time}} = \pm \frac{1}{2 \times K \times PRP}
 \end{aligned}$$

Where c is the speed of light, and K is an integer.

In 2002, Federal Communications Commission (FCC) (82), under the part 15 limits, stated that an UWB device should have a fractional bandwidth η of at least 0.2 or occupy 500MHz or more of the spectrum. The fractional bandwidth η is defined by Equation 8.

Equation 8: fractional bandwidth (82)

$$\eta = 2 \frac{f_H - f_L}{f_H + f_L}$$

Where f_H and f_L are respectively the upper and lower frequency of the -10dB bandwidth.

For the values of fractional bandwidth shown in Table 15, the 3dB bandwidth lower and upper frequencies is used instead. As shown in Chapter 6.A.2, the emitted frequency range that was chosen for the experimentation is in X band. The frequency tuning range is between 10GHz and 11.6GHz. However, the intermediate frequency range is in L band, between 1.1GHz and 1.9GHz, giving a 800MHz instantaneous receiver bandwidth.

Note that in IF band at 1MHz and 10MHz, the system is considered NB. However at 150MHz, it is in the grey area between NB and UWB, and at 800MHz, the system is considered UWB. In X band, from 1MHz to 150MHz, the system is considered NB and UWB at 800MHz.

Bandwidth	1MHz	10MHz	150MHz	800MHz
Spatial Resolution	150m	15m	1m	0.1875m
Fractional bandwidth in X band	0.0001	0.001	0.014	0.076
Classification in X band	NB	NB	NB	UWB
Fractional bandwidth in L band	0.00067	0.0067	0.1	0.533
Classification in L band	NB	NB	NB/UWB	UWB

Pulse Repetition Period	0.5μs	5μs	50μs	500μs	1ms
Range ambiguity	75m	750m	7.5km	75km	150km
Doppler frequency ambiguity	2MHz	200kHz	20kHz	2kHz	1kHz

Table 15: (top) bandwidth settings (bottom) Pulse Repetition Periods

Note that signals with Bandwidth-Time products lower than 40 won't be studied because of their limited detection capabilities. For example with a bandwidth of 1MHz and a pulse repetition period of 5 μs, the bandwidth-time product is 5, the spatial resolution is 150m and the distance ambiguity is 750m, the detection is limited to five spatial resolutions and separating multiple targets would be problematic. Also the signal is not well defined, especially for multitones, giving rise to distortions when using Hamming apodization in the compression, as shown in Figure 31. Thus three configurations are discarded from the study as shown in Table 16.

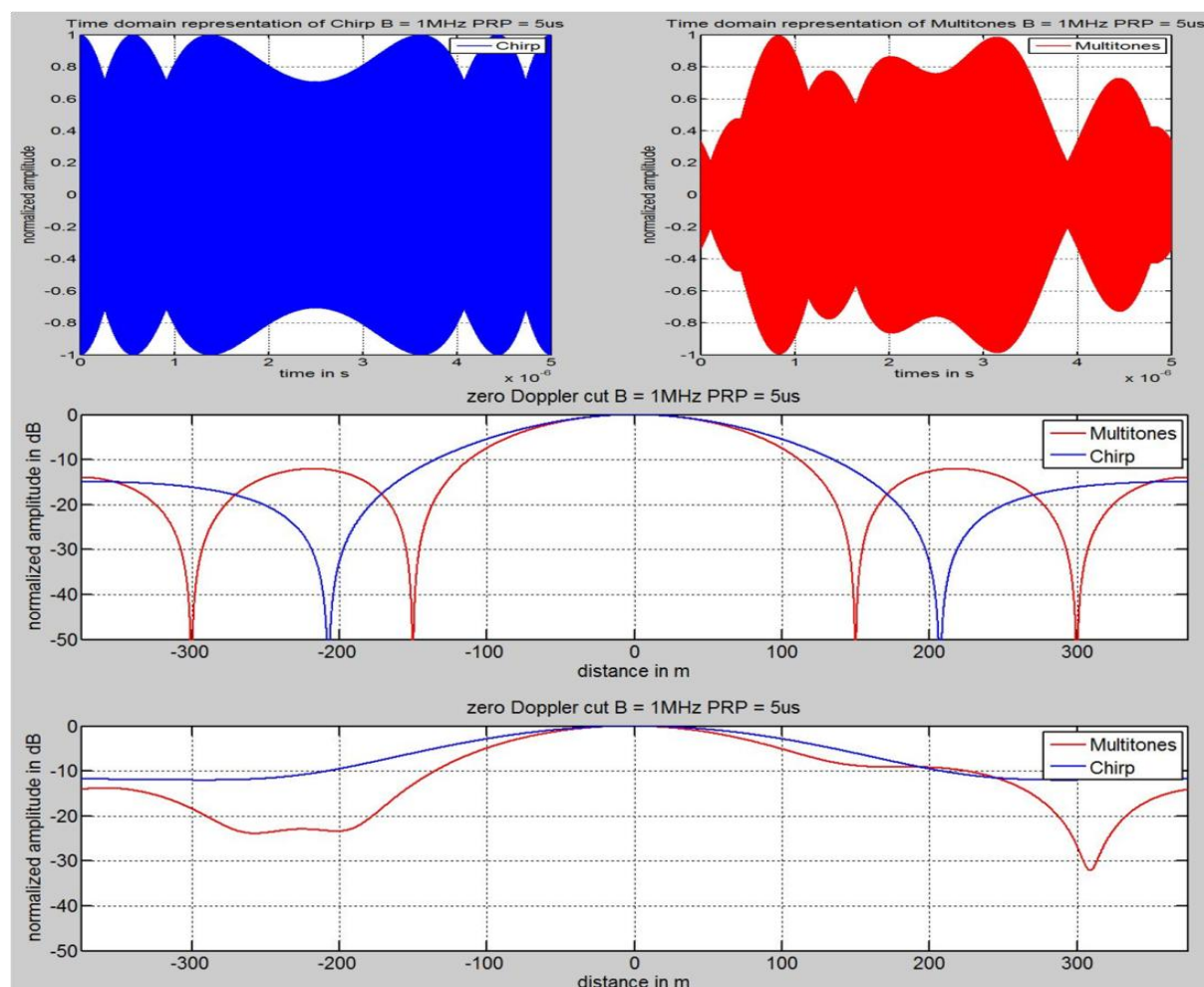


Figure 31: Chirp and Multitones with low $B = 1\text{MHz}$ and $\text{PRP} = 5\ \mu\text{s} \rightarrow \text{BT} = 5$

Bandwidth	Pulse Repetition Period	bandwidth-time product
1MHz	5 μs	5
1MHz	500ns	No resolution
10MHz	500ns	5

Table 16: eliminated waveform configurations

In the next sections, the Multitones and Chirp signals that will be used for the experiments will be first defined. Then their respective ambiguity functions will be simulated and compared. Next, the signals will be tested against saturation over performance criteria that are waveform independent. Following the simulations on saturation, the limitations of the model will be discussed. Finally the performances at the system level will be presented.

A. Signal definitions

The radar emits in continuous wave and the waveforms will cover the bandwidths of 1MHz, 10MHz, 150MHz and 800MHz, and pulse repetition period of 500ns, 5 μs, 50 μs, 500 μs and 1ms. Each bandwidth value will be tested with every PRP values. It can't be done in one case as 500ns pulse already produces 2MHz instantaneous bandwidth, thus the combination 1MHz with 500ns is not possible. The IF sampling frequency is 2GS/s, the IF frequency range is centered around 1.5GHz and the instantaneous bandwidth varies from 1MHz to 800MHz.

1. Multitones with Newman Phase codes

Multitones are composed of N sinewaves simultaneously generated. A multitude of phase codes exist to reduce PMEPR for multitones such as Reed-Muller with complementary Golay codes, bi-phase codes, Newman phase codes, etc...Bi-phase codes tend to be Doppler intolerant and have significantly reduced range sidelobes. On the contrary, **polyphase codes** tend to be more **Doppler tolerant** and have **higher range sidelobes** (73). Since for radar application, Doppler tolerance is important to detect moving targets and avoid the multiplication of filters to process the data, **Newman** polyphase codes (12) (81) were chosen, because they are **easy to implement** and the **PMEPR reduction is sufficient**. Furthermore this code is compatible with **any vector size**. Other codes may be more efficient but Newman phases code were chosen because they fit the requirements for radar applications, the aim is to evaluate the contribution of multitones for radar, not to optimize the waveform phase code.

Equation 9 presents the generation constraints to obtain intermodulation-free multitones. These constraints are respected for signal generation and digitization throughout the thesis.

Equation 9: Multitones generation rules for intermodulation-free digital signal

$$\begin{aligned} T &= M t_s \equiv \delta f = F_s / M \\ BW &= N \delta f, N \in \mathbb{N} \\ F_0 &= n_0 \delta f, n_0 \in \mathbb{N} \end{aligned}$$

Where M, N, n_0 are all **integers**. M is the number of sampling time t_s in the orthogonal period T , and the sampling frequency F_s is equal to M times the frequency spacing δf . The number of tones N in the signal times the frequency spacing δf gives the signal bandwidth. Finally, the index n_0 times the frequency spacing δf gives the starting frequency. All variables in the multitones are related by integer multiples.

 These constraints imply that in presence of Doppler, the orthogonality is broken and intermodulation products may appear. The issue of interferences caused by Doppler on Multitones has been discussed in (9).

Equation 10 presents the real part of the multitones signal.

Equation 10: Newmann Phase Coded Multitones definition (real)

$$MT(m) = \Re \left[\frac{1}{\sqrt{N}} e^{j \frac{2\pi n_0 m}{M}} \sum_{n=0}^{N-1} e^{j \frac{2\pi n m}{M} + j \phi_n} \right] = \frac{1}{\sqrt{N}} \sum_{n=0}^{N-1} \cos \left(\frac{2\pi (n_0 + n) m}{M} + \phi_n \right)$$

Where n_0 is an **integer** and the index of the first carrier, n is the frequency index $n \in [0, N - 1]$, M is the number of samples in the signal period, $m \in [0, M - 1]$ is an integer and the time index inside the period and ϕ_n is the Newman phase code, defined in Equation 11, that is overlaid on the frequencies.

Equation 11: Newman Phase Codes

$$\phi_n = j \frac{\pi n^2}{N}; n \in [0, N - 1]$$

Where N is an integer and is the number of subcarriers, and n is an integer and the subcarrier index.

In order to generate the samples for generation and simulation, the signal is defined in frequency domain. The amplitude and phase information are defined for each point from $[-\frac{F_s}{2}; \frac{F_s}{2} - \delta f]$ and $\delta f = \frac{F_s}{M}$ is the frequency step in frequency domain. The frequencies are thus defined between $[n_0, n_0 + N - 1]$ with amplitude 1 and phase defined by ϕ_n . Then the algorithm applies a Fast Fourier Transform (FFT) on this vector, and the real part of the time domain signal is extracted to obtain the final samples. Then the signal is normalized between $\pm 1V$. The resulting samples are defined with a precision of 32bits. The generation algorithm is illustrated in Figure 32 and the result is shown in Figure 33. The spectrum displayed in Figure 33 is the result of a zero-padded FFT.

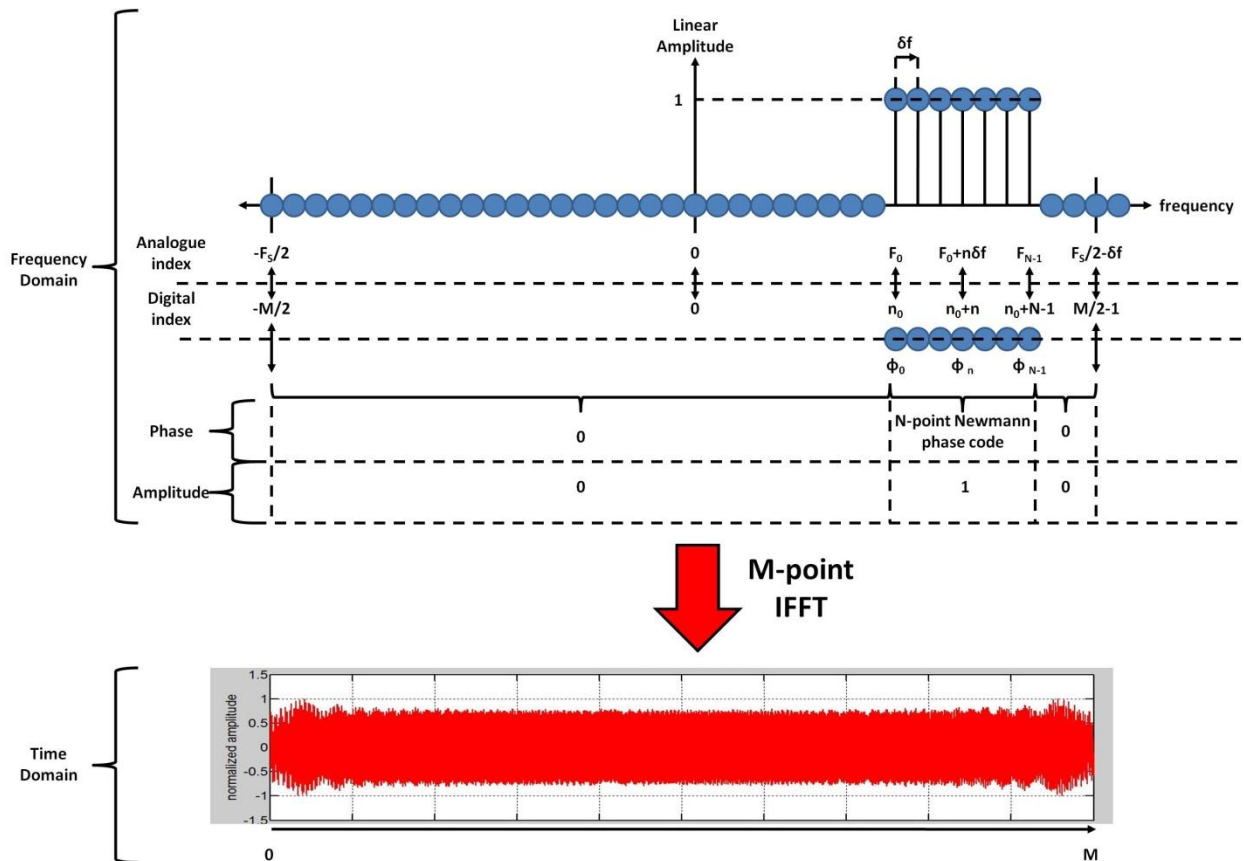


Figure 32: Multitones' samples generation algorithm

 Note the difference between the frequency vector used for generation with a DFT in Figure 32 and the spectrum displayed in Figure 33. The roll-off shown in the latter comes from the zero-padding used to perform the frequency analysis with a radix-2 FFT.

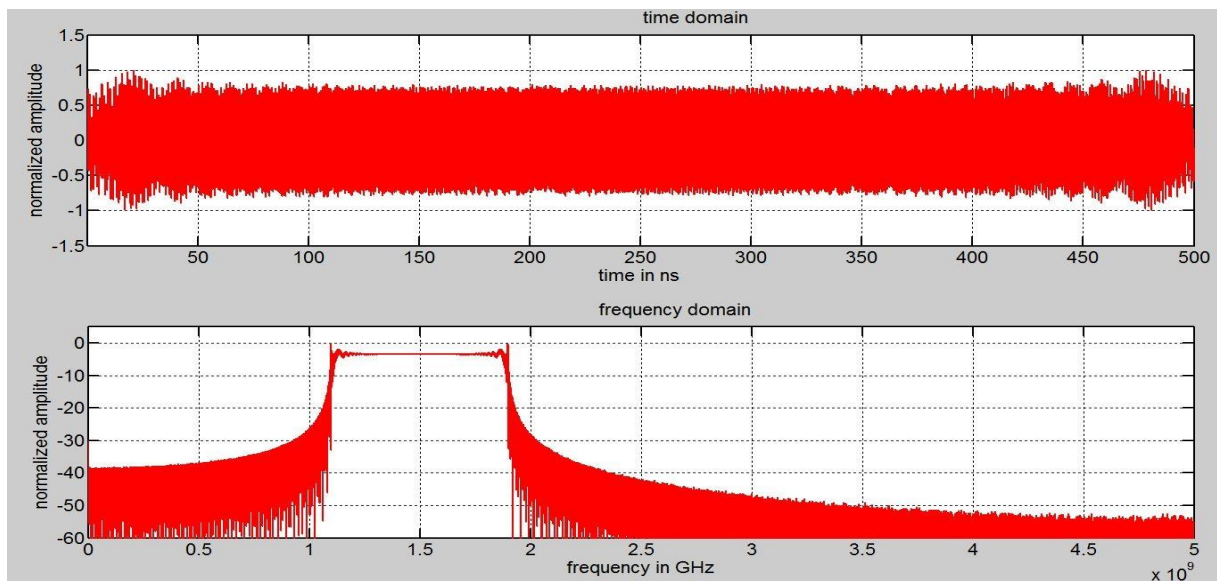


Figure 33: Newman Phase Coded Multitones BW = 800MHz PRP = 500ns. Top: time domain Bottom: frequency domain.

2. Linear Frequency Modulated Signal – Linear Chirp

The Linear Chirp is a signal whose frequency linearly increases over its period. It is described by Equation 12. The signal is directly generated in time domain with Equation 12. The rest of the algorithm is the same as stated in the previous section. Figure 34 shows the normalized Chirp with 10bit-resolution generated @ 10GHz with this algorithm and the spectrum obtained with the zero-padded FFT algorithm shown in Figure 22.

Equation 12: Linear Chirp definition (real)

$$Chirp(m) = \Re \left[e^{j\frac{2\pi n_0 m}{M}} e^{j\frac{2\pi}{M} \left(\frac{Nm}{2M} \right) m} \right] = \cos \left(2\pi \left(n_0 + \frac{Nm}{2M} \right) \frac{m}{M} \right)$$

Where M is the number of samples per signal period, $m \in [0, M - 1]$ is the sample index, n_0 is the carrier index frequency, and N is the bandwidth size.

 For chirp, using either a DFT or a radix-2 FFT does not affect the frequency spectrum. Chirp waveforms are well known for presenting spectral roll-off.

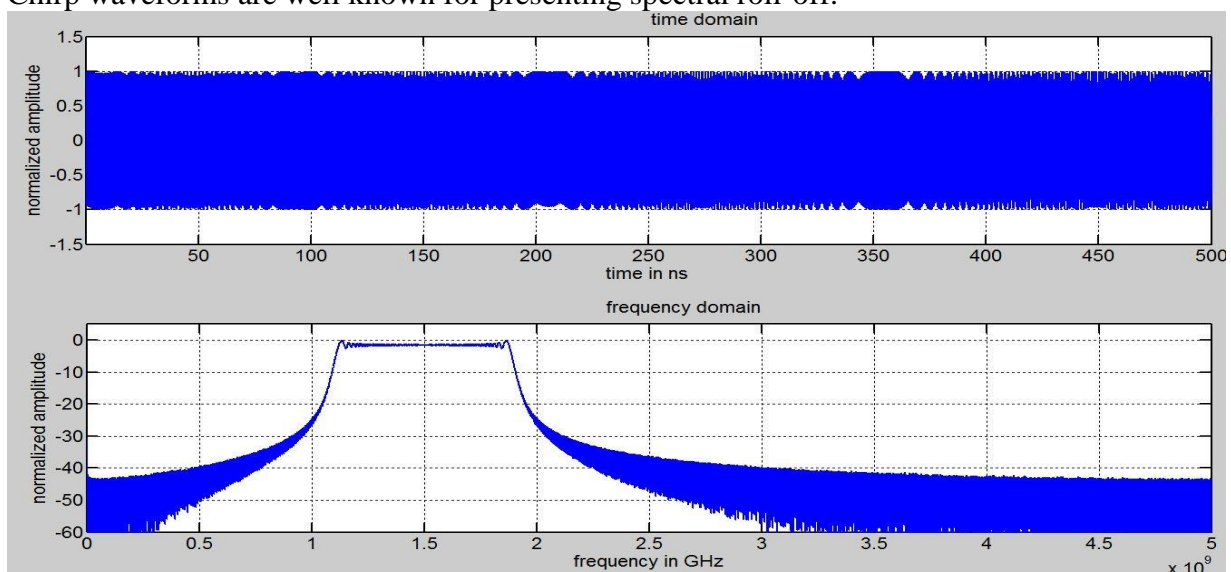


Figure 34: Linear Chirp BW = 800MHz PRP = 500ns(top) time domain (bottom) frequency domain

B. Simulation processes and performance criteria

This section presents the simulated processes and waveform-independent performance criteria that are used in the evaluation of radar waveforms for this thesis.

1. Simulated processes

In the Radar community, the ultimate goal is always to improve detection. Two of the key components in the radar chain are strongly related to the capacity of a radar to detect on longer ranges and with a higher sensitivity. They are respectively the Power Amplifier and the ADC. To increase the radar slant range, the transmitter must emit as much power as possible within the useful bandwidth. The link between emitted power and detection range is easily explained by the simple radar equation on received power.

Equation 13: simple radar equation (13)

$$P_{Rx} = P_{Tx} \frac{G_{Tx} \cdot G_{Rx} \cdot \lambda^2 \cdot \sigma_0}{(4\pi)^3 \cdot R_{Tx}^2 \cdot R_{Rx}^2}$$

Where P_{Rx} & P_{Tx} are the Rx and Tx Power, G_{Tx} & G_{Rx} are the Tx and Rx Antenna Gain, λ is the signal wavelength, σ_0 is the target Radar Cross Section, and R_{Tx} & R_{Rx} are the Tx-to-target and target-to-Rx distances.

The smallest received power also depends on receiver sensitivity which is closely related to the ADC resolution. We've seen in the State of the Art on linearization in section Chapter 3.B.1 from (48) (49) (50) (51), that the rationale behind their study of linearization techniques was to increase radar receiver dynamic ranges for the detection of small targets in highly cluttered background.

In order to determine the best operating point for a power amplifier, a study on the saturation at the power amplifier level is proposed.

Also to determine the best ADC resolution for a given application, the effects of quantization on performances must be investigated.

The performance criteria proposed in this section are PMEPR, Power efficiency and Pulse compression. They are waveform-independent to avoid judging on biased criteria for one waveform or the other.



In order to model the signals, the vectors were generated with a 10GHz sampling clock. This allows sufficiently large Nyquist bands to avoid the folding of intermodulation products. The strongest intermodulations are odd orders and with a low sampling frequency, all the intermodulations will fold over the useful bandwidth. (see section Chapter 5.F on the limitations of simulation)

Thus in the following subsections, the quantization process synoptic followed by the saturation process synoptic in amplifiers is presented. The quantization process will allow determining the limits of utilization of a given hardware with respect to power efficiency, PMEPR and compression. Then the saturation process will allow determining the best

operating range on a specific amplifier configuration with respect to power efficiency, PMEPR and compression.

For the study the data will be filtered to simulate a 1GHz bandwidth.

a) Effect of quantization on performance criteria

The signal vectors are quantized in bit resolutions ranging from 2 to 24. The quantization process chosen for simulations is the same as the equipment. In other words, the encoded value on n bits is floored to the nearest signed integer. Thus the quantized values range from $[-2^{n-1}; 2^{n-1} - 1]$. The algorithms used to study the performance criteria (PMEPR, power efficiency and compression) wrt quantization are presented in Figure 35.

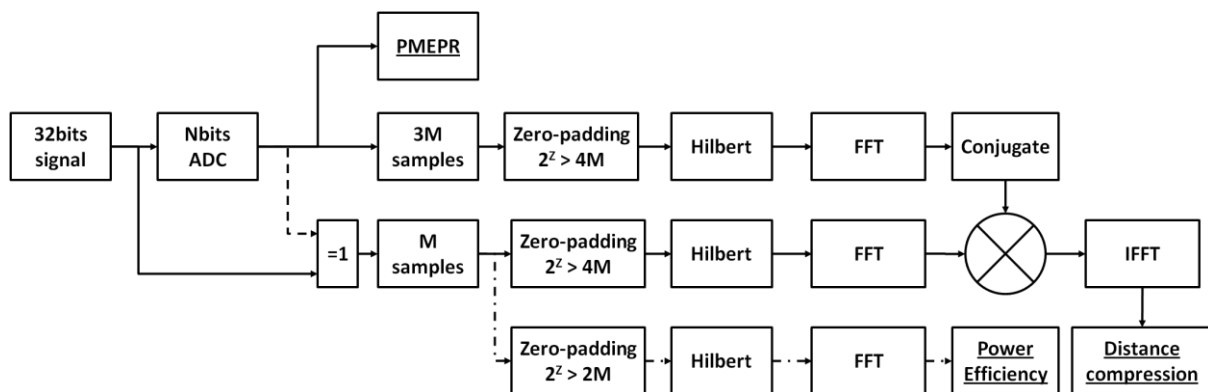


Figure 35: algorithms used to study the performance criteria wrt quantization

b) Effect of saturation in an amplifier on performance criteria

The signal vectors will be studied against saturation in an amplifier. The saturation will range ± 6 dB with respect to the amplifier IP1dB (1dB-compression point IBO).

In order to get a realistic model of amplification, an AFD2-010020-23-P (component 24) gain was measured with respect to input power. This amplifier has a gain of 25dB and a frequency range from 1GHz to 2GHz. The model and measurement for this component are available in Appendix Chapter 9.G.

Furthermore the gain with respect to input frequency will be assumed constant to avoid in-band distortion and add further perturbations in the simulation of the saturation process. The saturated data is then filtered from with a rectangular filter in frequency domain between 1GHz and 2GHz.

The algorithms used to study the performance criteria (PMEPR, power efficiency and compression) wrt saturation are presented in Figure 36.

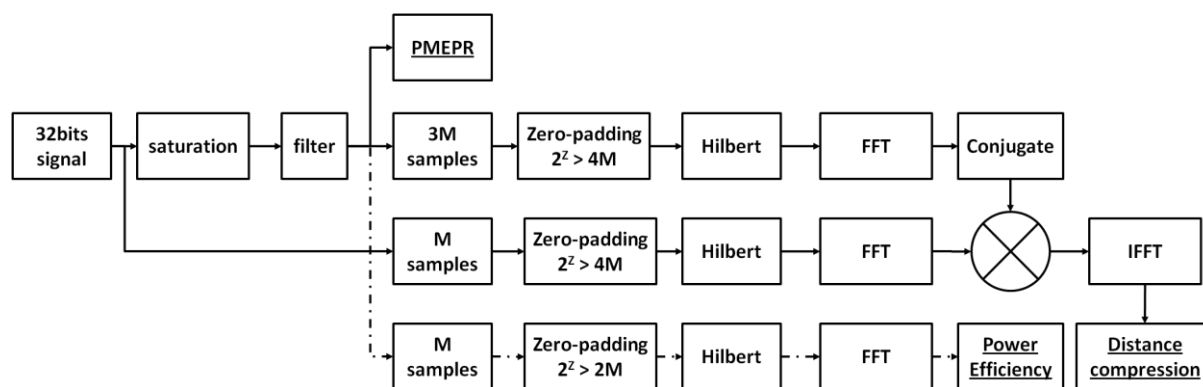


Figure 36: algorithms used to study the performance criteria wrt saturation

2. Performance criteria

Several characteristics were chosen to determine the optimum operating point: power efficiency, peak to mean envelope power ratio (PMEPR) and pulse compression characteristics.

a) PMEPR – Peak to Mean Envelope Power Ratio

Definition

If the digitized signal is represented by M points and $n \in [0; M - 1]$ then PMEPR is defined in Equation 14.

Equation 14: Peak to Mean Envelope Power Ratio

$$PMEPR = \frac{\max(|s(n)|^2)}{\frac{1}{M} \sum_{n=0}^{M-1} |s(n)|^2}$$

Why choosing PMEPR?

PMEPR allows the evaluation of three performance criteria at the radar system level: consumption, detection range and SNR.

The PMEPR is linked in the literature to Power Amplifier and ADC power consumption (60), thus a lower PMEPR reduces the power consumption of a radar system.

Besides, a high PMEPR may reduce the average power transmitted by the power amplifier (52). Also Multitones main drawback is its high PMEPR, which limits the power efficiency of solid state power amplifier (55). The transmitted power in Equation 13, which is essential to radar slant range, is function of the amplifier gain function and input power wrt to IBO. The IBO is defined with respect to the peak input power. Thus a higher PMEPR at the power amplifier input would result in a lower transmitted power.

At the ADC level, the maximum input power set by the constructor determines the maximum SNR after digitization. This SNR decreases as the PMEPR increases (9), so the PMEPR will set the maximum achievable signal to noise ratio without clipping.

Equation 15: Maximum achievable signal to noise ratio (9)

$$SNR_{max} = P_{FS} - PMEPR - N_0 - F - B_{Rx} - G \text{ [dB]}$$

Where P_{FS} is the full scale ADC maximum input power, N_0 is the noise density, B_{Rx} is the receiver bandwidth, F is the receiver noise figure, G is the receiver gain.

b) Power Efficiency

Definition

The power efficiency is defined in Equation 16.

Equation 16: power efficiency

$$\eta = \frac{\text{in band power}}{\text{total power}}$$

The in-band power is the useful power for the detection, in other words this is the energy that will be emitted from and received by the radar system. The total power is the power contained within the amplifier's operating frequency range. This includes useful signal power, and all the power carried by non-linearities generated by the amplification outside the useful bandwidth. Thus the total power will be measured before filtering the amplifier output signal. It will be evaluated over a full ADC Nyquist band.

Why choosing Power Efficiency?

Power Efficiency allows looking at four performance criteria at the radar system level: spectral leakage, consumption, detection range and SNR.

The output spectrum nowadays is heavily regulated by frequency range and emission limits by regulatory bodies such as ITU (83). Thus when amplifying before emitting, the amplifier output has to be filtered to respect the emission limits.

The PMEPR gives an evaluation of the amplifier efficiency when converting supply power into transmitted power. However, power efficiency will evaluate the transmitted power that is actually transmitted after filtering the spectral leakage.

Power efficiency is of primary importance especially in radar where every dB counts and is costly. Also maximizing in-band power will increase the detection range and SNR.

c) Pulse compression & Ambiguity Function

Definition

The definitions of ambiguity function and thus pulse compression were given in section Chapter 2.B.2 on radar notions. The ambiguity function of a signal can be defined either using NB approximation or the WB definition as shown in Equation 17 & Equation 18.

Equation 17: Narrowband Ambiguity Function (84)

$$NB\ AF\chi(f_d, \tau) = \int_{-\infty}^{+\infty} \tilde{s}(t)\tilde{s}^*(t - \tau)e^{-j2\pi f_d t} dt$$

where $\tilde{s}(t)$ complex baseband signal
 $s(t) = \text{Re}\{\tilde{s}(t)e^{j2\pi f_c t}\}$
 f_c carrier frequency
 f_d Doppler frequency
 τ delay
 $*$ denotes the complex conjugate

Equation 18: Wideband Ambiguity Function (84)

$$WB\ AF\chi(\alpha, \tau) = \frac{1}{\sqrt{\alpha}} \int_{-\infty}^{+\infty} x(t)x^*\left(\frac{t}{\alpha} - \tau\right) dt$$

where $x(t) = \tilde{s}(t)e^{j2\pi f_c t}$
 $\alpha = (c + v)/(c - v)$ is the scaling
 v uniform target speed
 c speed of light

Equation 19: upper bound of the phase error in the integrand caused by the NB ambiguity function approximation (85)

$$\varepsilon \leq 2\pi \frac{2|v|BT}{c + v}$$

Equation 19 is the upper bound of the error, however in (85) an exact formula is proposed. Using Equation 19 and considering that a 5% error in the integrand is acceptable, Figure 37 gives the range of velocities where the NB ambiguity function approximation is valid.

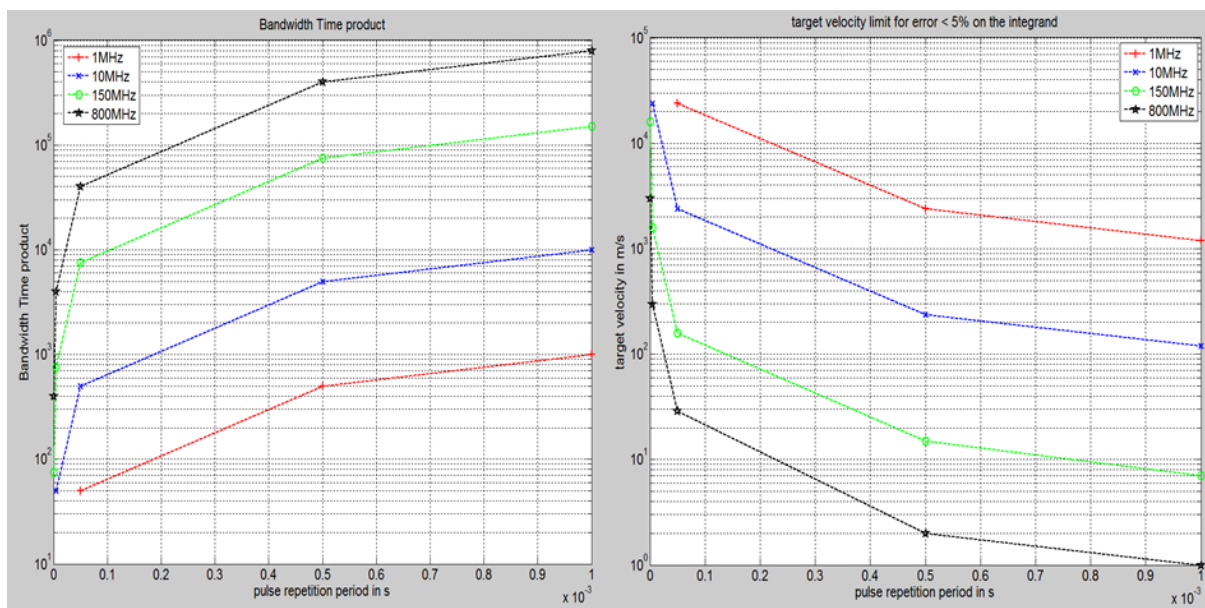


Figure 37: domain of validity of each signal configuration

The maximum velocities during the experimentation have been estimated at 7m/s for a bicycle, given the size of the experimental scene. Thus the error in the NB ambiguity function approximation for signals with 800MHz bandwidth can reach 11.73% for a PRP of 500µs and 23.46% for a PRP of 1ms. For these two signals, the NB approximation is clearly violated. However, the NB ambiguity function approximation will be applied since both waveforms are identically affected by the phase error. The NB ambiguity function doesn't change anything on pulse compression at zero-Doppler, and the Doppler experiment that was finally chosen (refer to Chapter 6.B.4.c) emulates Doppler by modulating the incoming signal with a square wave. This results in a Doppler shift, and in that case the NB ambiguity function approximation is correct.

The simulated ambiguity function used for this study was validated using the analytical NB ambiguity function equation for Chirp vs the simulated result with the algorithm presented in Chapter 4.B.1. The details on validation are referenced in Appendix Chapter 9.H.

Why choosing pulse compression and Ambiguity Function?

The pulse compression and ambiguity function are the reference tools in the radar community to evaluate waveform performances based on optimum match filtering to maximize SNR in additive white Gaussian noise.

The characteristics that most interest us for this study are the spatial resolution and the contrast. These are measured with the characteristics of the main lobe at -3dB, -6dB and -10dB, the secondary sidelobes will be measured as shown in Figure 38 in distance and Doppler dimensions.

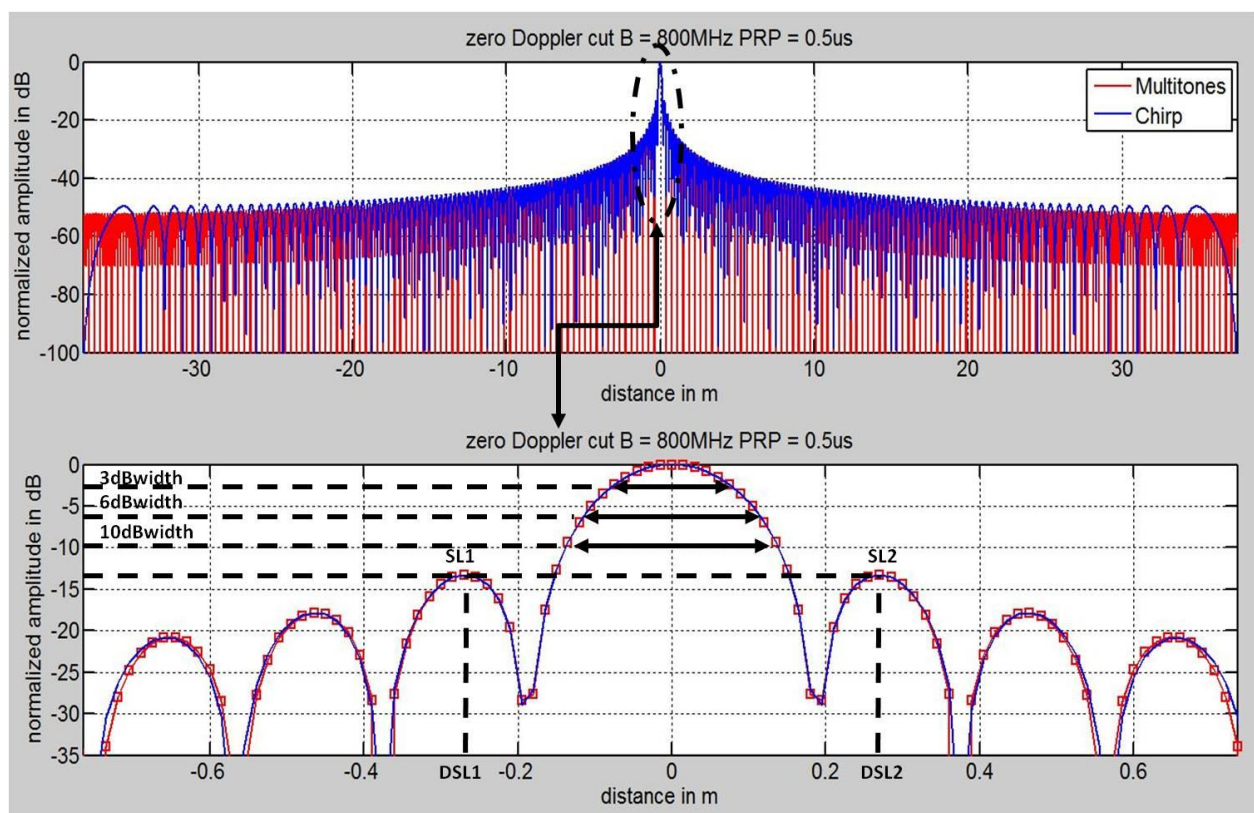


Figure 38: pulse compression measurements in distance for multitones and chirp when PRP = 500ns and B = 800MHz

The main lobe 3dB width corresponds to the spatial resolution. The 3dB width is inversely proportional to signal bandwidth; hence a variation in the main lobe width will match a variation in the signal bandwidth. The 6dB and 10dB width are used to verify the growth of the main lobe, and should be respectively the 3dB width widened by 33% and 66% respectively.

The sidelobe levels (SL1 – SL2) are a measure of the maximum RCS contrast between a big target and a small target. If the difference in RCS is greater than this value, the big target will mask the nearby smaller target. For a rectangular window, the sidelobes' amplitude should be symmetrical and about 13dB lower than the peak impulse response. Their positions should be equally apart from the mainlobe and about equal to the 10dB width of the mainlobe.

3. Synthesis of performance criteria

These parameters will allow determining the respective performances of both waveforms. PMEPR, power efficiency and ambiguity function will determine the maximum detection range, the detection capabilities and the consumption for each waveform. They'll be assessed against the number of quantization bits and saturation levels. Those are the basic criteria for assessing performances. Others could be used to get a more accurate picture of the performances. Nonetheless, these criteria are sufficient for a first performance evaluation.

The minimum number of useful bits required to reach near nominal theoretical values wrt PMEPR, power efficiency and pulse compression performances will be assessed in order to evaluate the ADC characteristics required to maximize the radar system potential in terms of range, detection and consumption.

The saturation will allow determining the best trade-off between PMEPR, power efficiency and pulse compression for non-linear amplification, and thus find the best amplifier operating point to increase range, detection and power consumption.

The simulations for quantization and saturation are kept **simple** to evaluate their effects on performances without noise or other perturbative effects. One can argue that they aren't realistic; however it has the advantage of faster implementation and shorter delays to carry out the task of experimental evaluation afterwards.

C. Simulated PMEPR

The effects of quantization and saturation processes on the nominal value of PMEPR are now evaluated through simulations. Figure 39 displays the nominal values of PMEPRs of all configurations (Bandwidth,Time) of Chirps and multitones under test.

The Chirp's PMEPR increases along with bandwidth, starting at 3.01dB @ 1MHz and going up to 4.22dB @ 800MHz. The increase in PMEPR for wideband chirp (800MHz) is explained by the filter used to ensure a 1GHz receiver bandwidth, cutting off the edges of the infinite chirp spectrum. This effectively increases the chirp's PMEPR by creating peaks in time domain.

The PMEPR for multitones are in the range 5.44dB to 5.65dB which matches the expected PMEPR reduction for Newman phase codes. Comparing both Chirp and multitones, their difference in PMEPR ($MT - Chirp$) reduces as bandwidth increases. The difference ranges

from 1.5dB @800MHz to 2.5dB @1MHz. As the signal bandwidth reaches the order of the receiver bandwidth, the difference between PMEPRs reduces. Using the radar equation, the maximum detection range for Chirp wrt multitones will be up to 15% greater in narrowband and up to 9% greater in wideband.

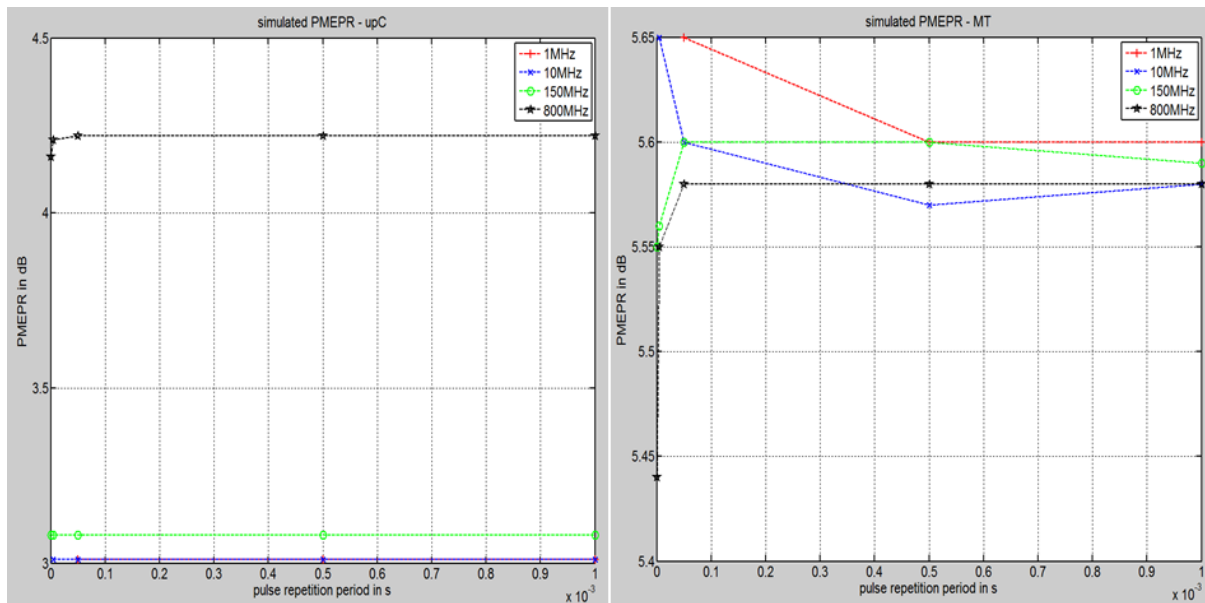


Figure 39: nominal PMEPR values in dB of the tested signals: left) Chirp right) multitones

1. Effect of the number of quantization bits on PMEPR

From Figure 40, the simulation results show that from 4 bits, the PMEPRs are at most 0.1dB away from their nominal values which is negligible. Thus wrt to PMEPR, the minimum resolution required is 4 bits.

2. Effect of saturation on PMEPR

From the simulation results shown in Figure 41, the chirp's PMEPR is only affected by 0.02dB by the saturation process, which is negligible. However, the multitones' PMEPR decreases by 0.2dB to 0.3dB at P1dB and from 1dB to 1.4dB over the full range of saturation. With respect to PMEPR, the saturation point does not impact the chirp average power, however it improves the average power of multitones. The improvement for multitones is negligible up to IP1dB but allows decreasing PMEPR by at least 1dB with further saturation.

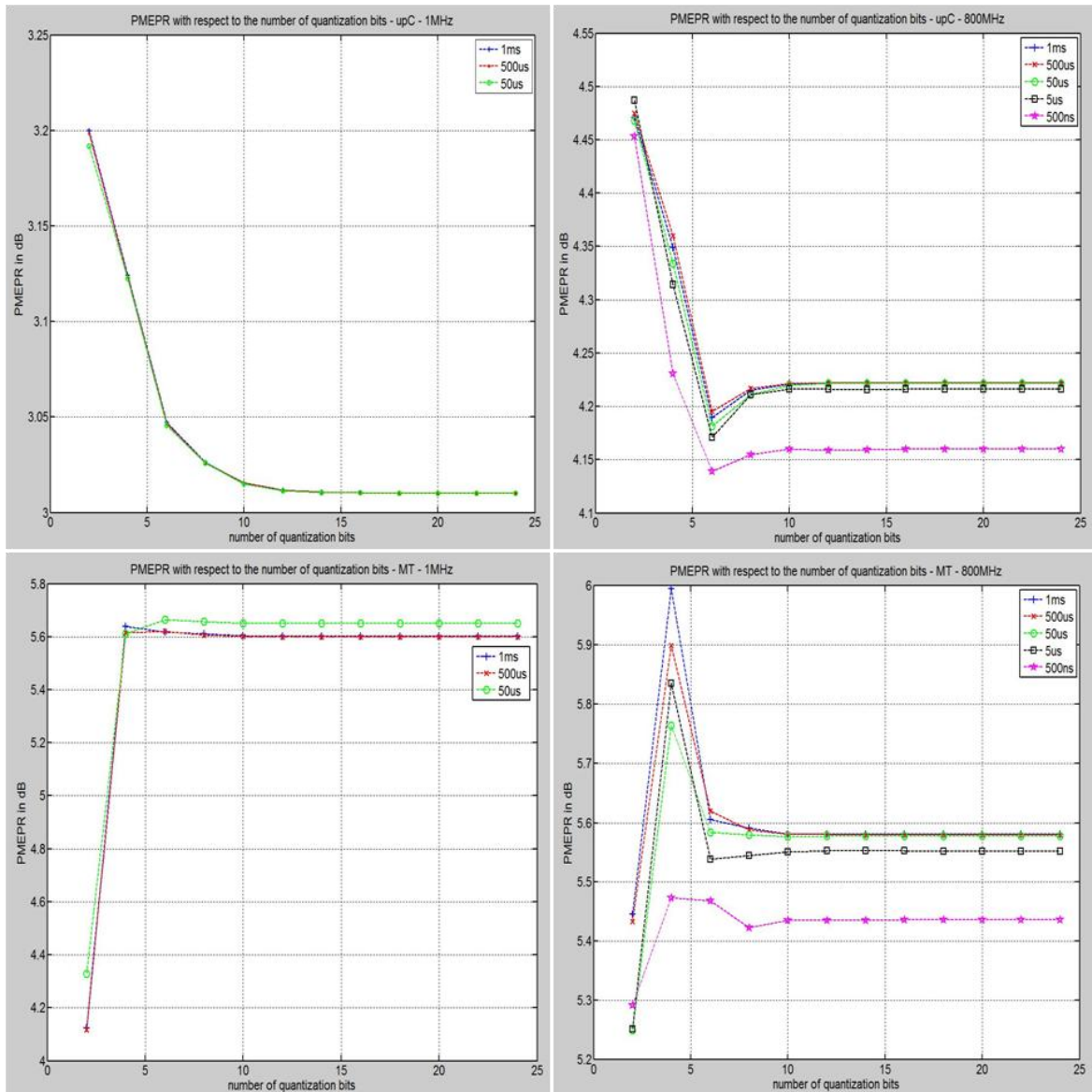


Figure 40: simulated PMEPR of Chirp and multitones with $B = [1\text{MHz (left)}, 800\text{MHz (right)}]$ wrt number of quantization bits. Top: Chirp, Bottom: multitones

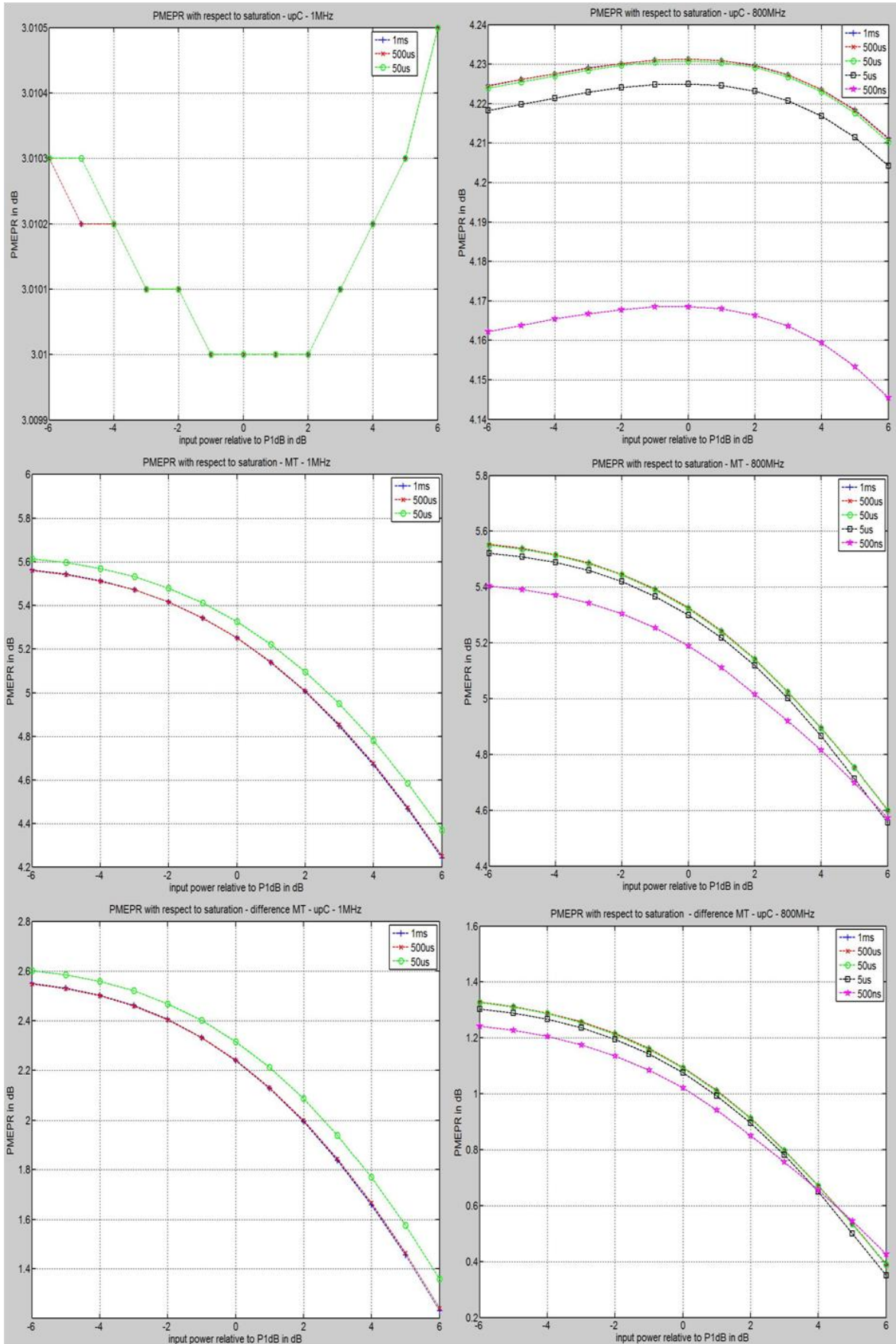


Figure 41: simulated PMEPR of Chirp and multitones with $B = [1\text{MHz (left), } 800\text{MHz (right)]$ wrt saturation. Top: upC, Mid: multitones and Bottom: difference

D. Simulated Power Efficiency simulations

The effects of the quantization and saturation process on the nominal value of power efficiency are now evaluated through simulations. Figure 42 displays the Power efficiencies of each Chirp and multitone signals under test. The power efficiencies of both waveforms increase as the bandwidth-time product increases³.

The relative error on power efficiencies between both chirp and multitones decreases as the bandwidth-time product increases. Multitones have higher power efficiency than Chirp but the error is lower than 2%⁴ which is negligible. Thus both waveforms are equivalent regarding power efficiencies

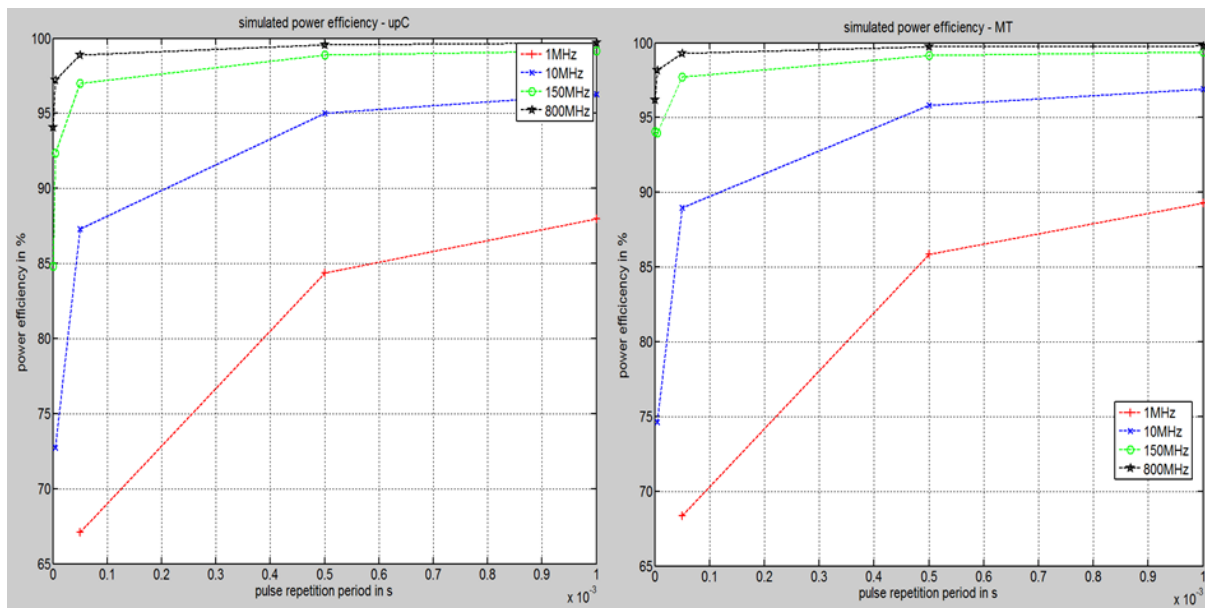


Figure 42: nominal power efficiency values in % of the tested signals

1. Effect of the number of quantization bits on Power Efficiency

From Figure 43; a minimum of 10 bits in narrowband and 8 bits in wideband is necessary to get within 5% of the nominal power efficiencies for every signal configuration⁵. Up to 8 bits in narrowband and 6 bits in wideband, chirp is more power efficient than multitones and the error on power efficiencies is lower than 12% in NB, and lower than 2.5% in wideband. The

³ Since the receiver bandwidth is fixed, the noise bandwidth is the same for every signal configuration, hence when the signal bandwidth increases, the power efficiency increases. The time or pulse repetition period has an effect on the sharpness of the spectrum roll-off and noise level. As time increases, the spectral roll-off becomes sharper, thus more power is concentrated in the useful bandwidth. The second effect of the increase is the reduction of noise power level because of the integration in the FFT.

⁴ However a discrepancy occurs at bandwidth-time product equal to 75 (B 150MHz and T 500ns) where the error is over 10%. The bandwidth-time product being lower than 100 is of no use, hence this discrepancy will be ignored.

⁵ The power efficiencies in narrowband keep increasing over 10 bits since the ratio of in-band versus out of band power is larger. It can also be observed that the power efficiencies increase with bit resolutions. This effect results from non-linearities inherent to coarse quantization, but these non-linearities effects decrease as the bit resolutions get finer.

latter is negligible but in case of low bandwidth-time product and low bit-resolution, chirp has a higher efficiency by up to 8 to 12% @ 4bits and 3-7% @ 6bits.

2. Effect of saturation on Power Efficiency

From Figure 44, it can be observed that Chirp signals barely experience any drop in efficiency ($<0.1\%$). Multitones experience almost no loss up to the 1dB compression point (IP1dB), and no more than 2% for higher input power.

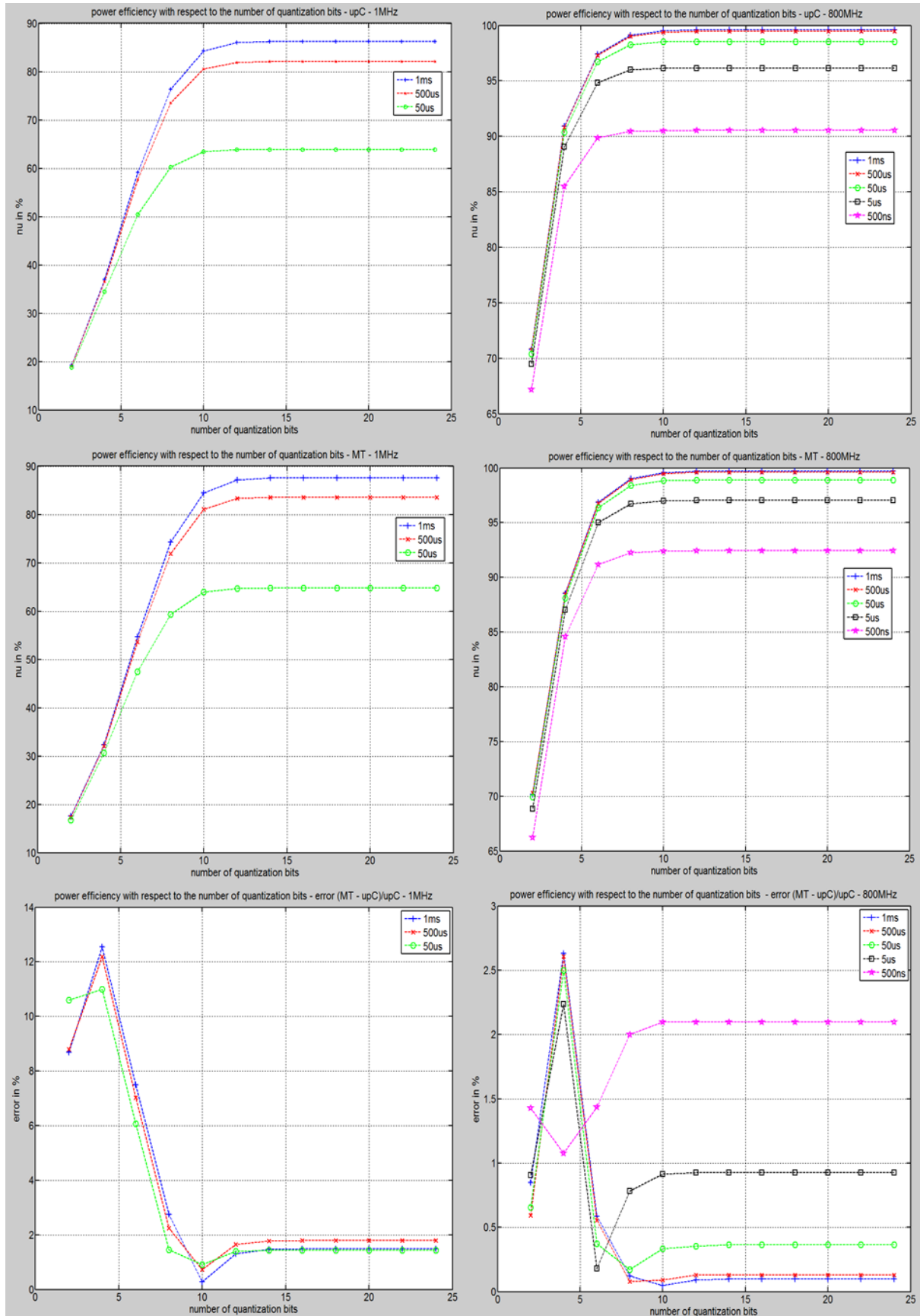


Figure 43: simulated power efficiency of Chirp and multitones with B = [1MHz (left), 800MHz (right)] wrt number of quantization bits. Top: upC, Mid: multitones and Bottom: relative error on power efficiencies between waveforms

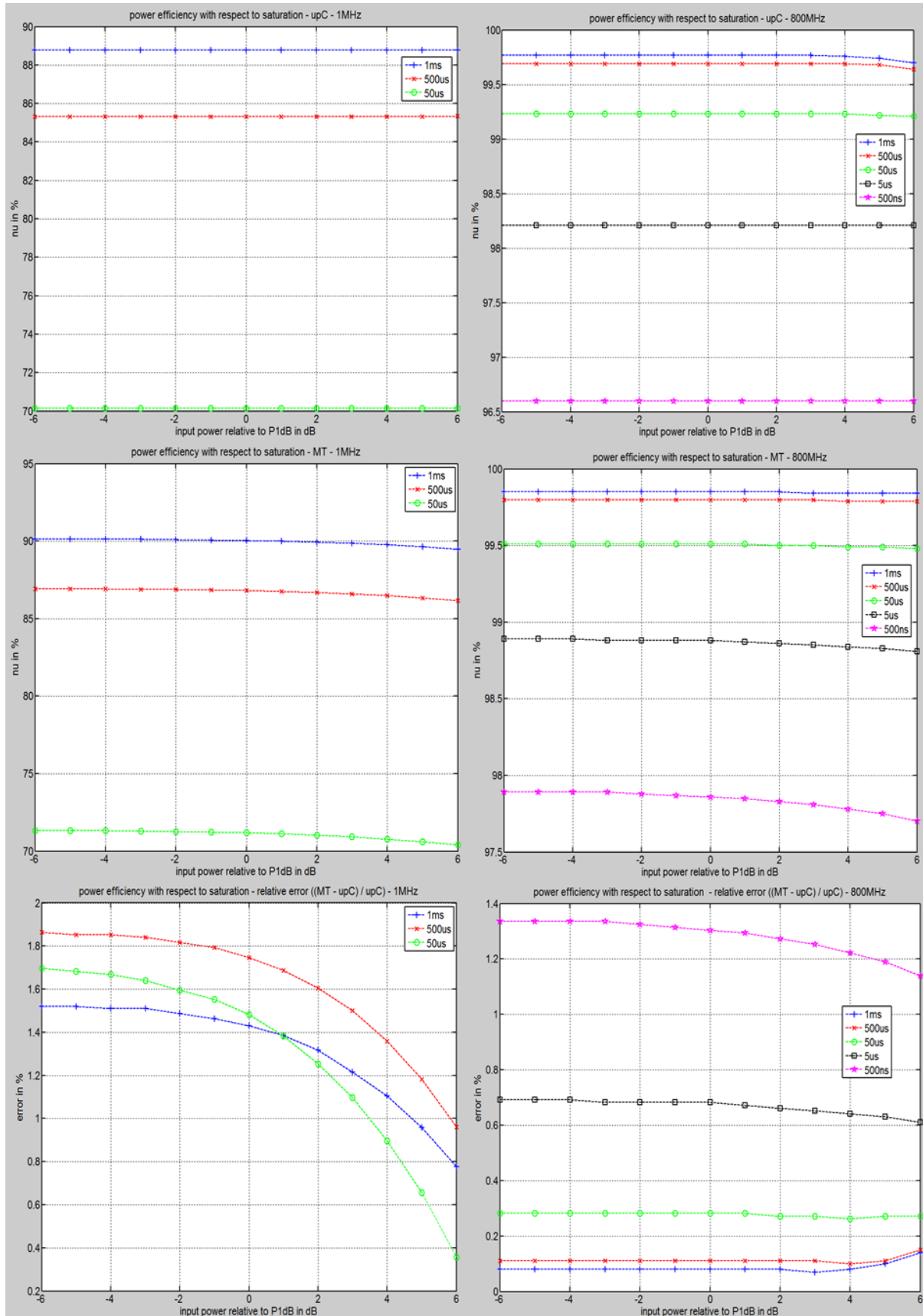


Figure 44: simulated power efficiency of Chirp and multitones with B = [1MHz (left), 800MHz (right)] wrt saturation. Top: upC, Mid: multitones and Bottom: relative error between on power efficiencies between waveforms

E. Simulated Ambiguity Function

The simulated ambiguity functions of Chirp and multitones will be presented. A theoretical equation for the Chirp's ambiguity function already exists but none for the multitone signals. A model is proposed to establish the basic characteristics of the multitones' ambiguity function. In the next subsections, the effect of quantization will be studied and finally the effect of saturation. The main characteristics of the distance compression are listed in Table 17. The simulated ambiguity function for the multitones and the chirp will be compared, first with raw data, and then with a Hamming window applied in time domain before compression.

Bandwidth	1MHz	10MHz	150MHz	800MHz
Mainlobe 3dB width	133m	13.27m	0.88m	0.165m
Sidelobe amplitudes	-13.27dB	-13.27dB	-13.27dB	-13.27dB
Sidelobe positions	$\pm 214.8\text{m}$	$\pm 21.4\text{m}$	$\pm 1.425\text{m}$	$\pm 0.27\text{m}$

Table 17: main characteristics of the distance compression – raw data

1. Simulated Ambiguity Function of Chirp and Multitones

From the chirp ambiguity function shown in Figure 45, the shearing effect, typical for LFM, has a slope equal to B/Tf_0 , where B is the bandwidth, c is the speed of light, T is the pulse time and f_0 is the central frequency. For bandwidth-time product greater than 100^6 , the same ridge can be observed for the multitones in the ambiguity function with raw data, and for the ambiguity function with Hamming windowed data in Figure 45 and Figure 46. The presence of this ridge shows that the Multitones under study also suffer from Doppler-range coupling as does chirp. In Figure 47, the levels around the main peak are very similar, with respect to 3dB, 6dB and 10dB width and sidelobes amplitudes and positions, both for raw and Hamming windowed data. Note that the difference between multitones and Chirp in Figure 47 displays a higher pedestal for multitones, meaning that chirp offers a better contrast. With Chirp it will be possible to detect smaller targets.

Two phenomena caused by sampling and processing are explained briefly in Appendix Chapter 9.H for clarity: effect of sampling time (sampling speck) and effect of Hamming window (apodization).

⁶ For bandwidth-time products lower than 100, multitone signals are distorted in time domain, causing imbalances in the impulse response, and distortions in the Doppler domain. Using windowing accentuates the distortions, thus diminishing the detection capabilities. Thus, using chirp for bandwidth-time product lower than 100 is recommended, even if the mainlobe is larger and the sidelobes slightly further than it should. Doppler processing and detection are not impaired at all. Note that signals with bandwidth time product lower than 100 are rarely exploited in radar.

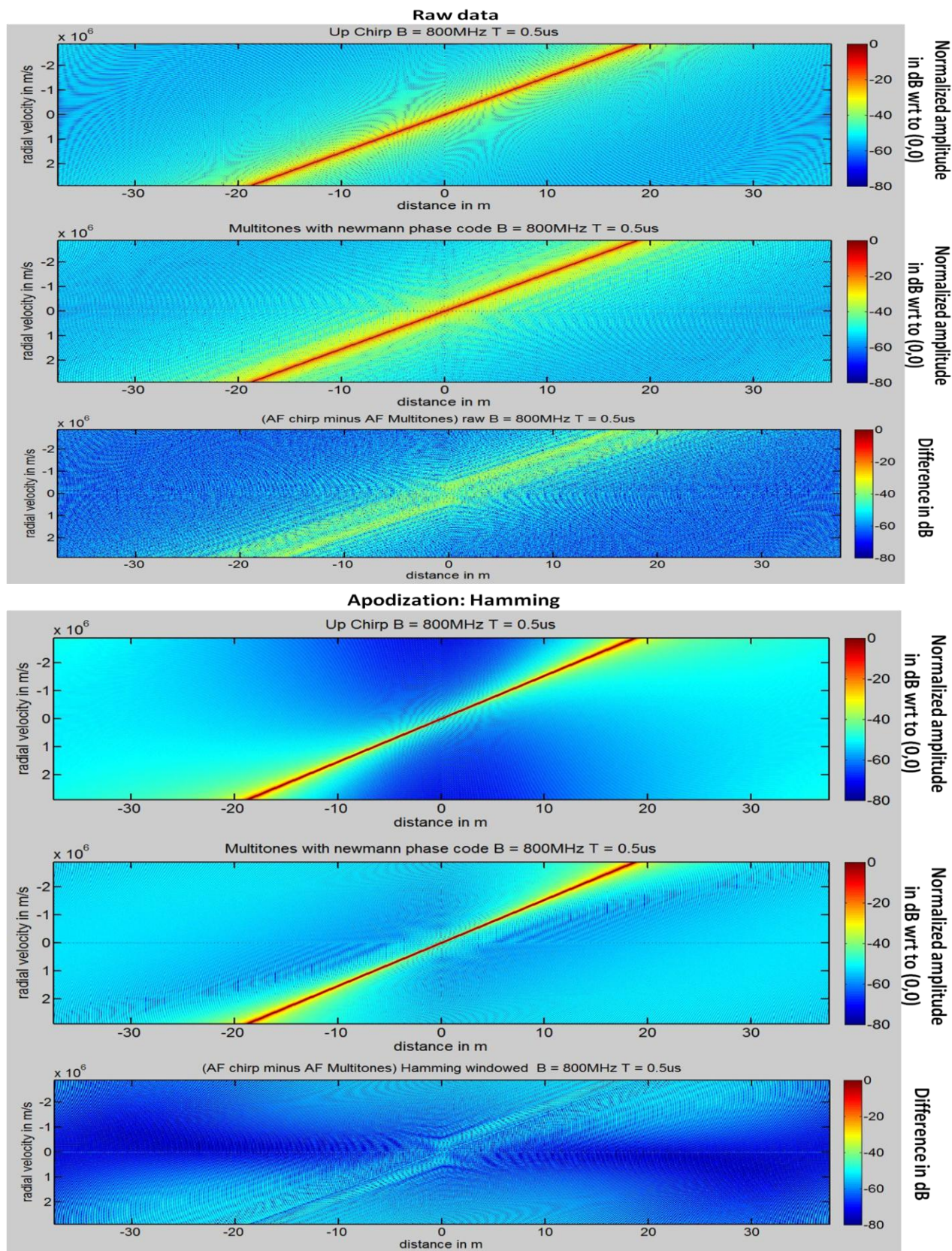


Figure 45: Simulated ambiguity function for Chirp and Multitones (B = 800MHz, PRP = 500ns, radial velocity @ 10.4GHz) (top) Chirp (middle) Multitones (bottom) ambiguity function difference for multitones and chirp with bandwidth time product equal to 400 (B 800MHz; T 500ns; velocity validity 2984m/s)

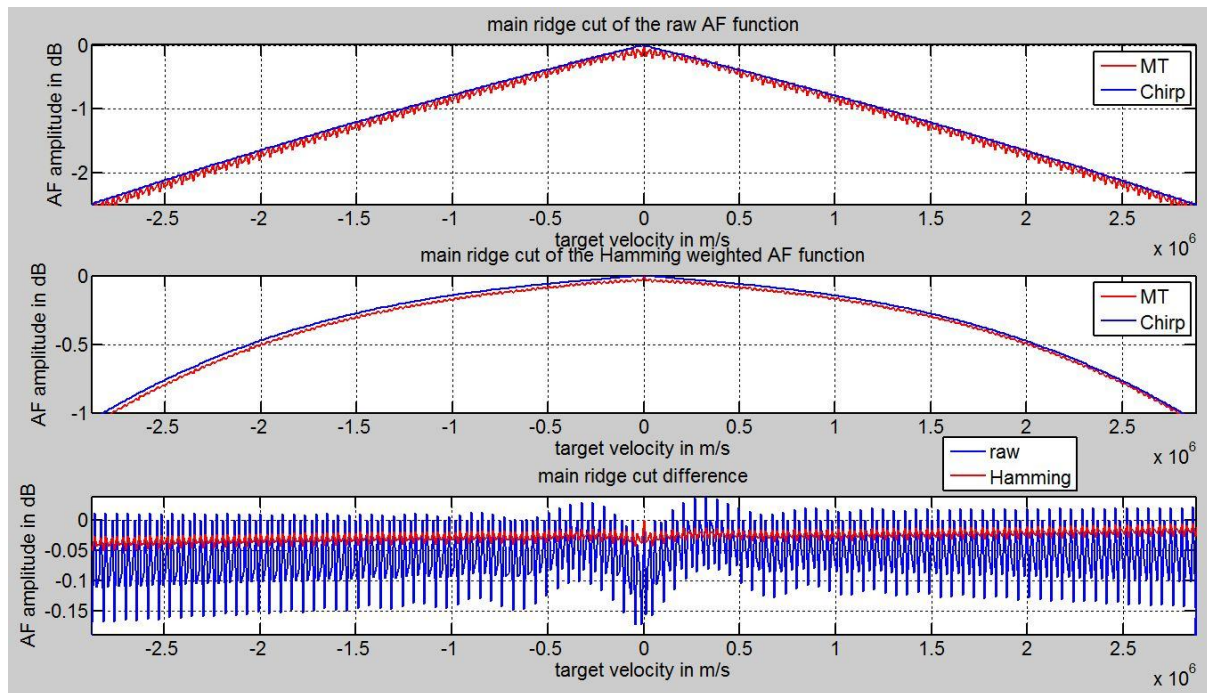


Figure 46: main ridge cut of multitones and chirp signals for raw and Hamming windowed data and their differences for multitones and chirp with bandwidth time product equal to 400 (B800MHz; T500ns; velocity validity 2984m/s)

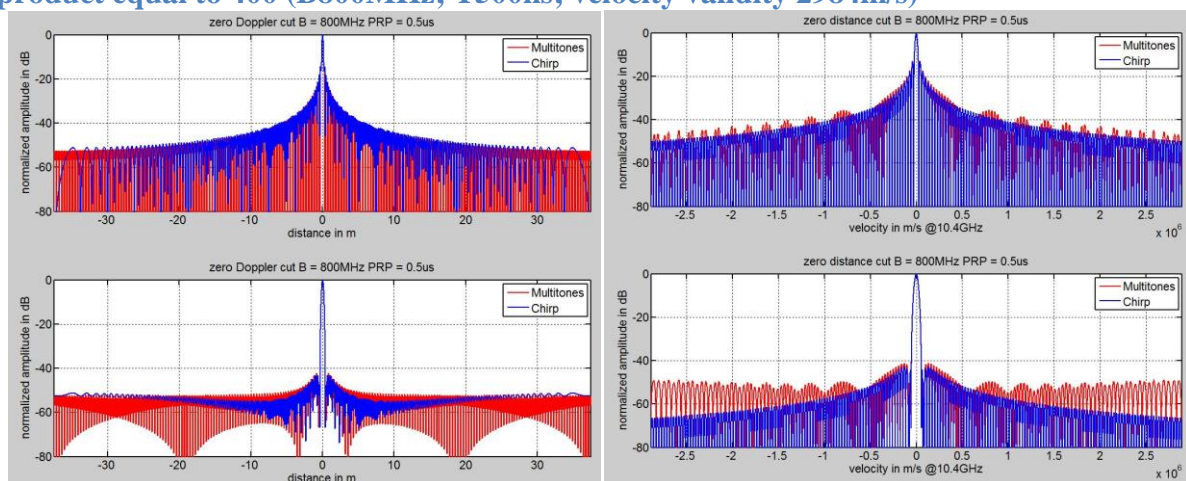


Figure 47: (left) ambiguity function zero-Doppler cut (top) raw (bottom) Hamming window (right) zero-distance cut (top) raw (bottom) Hamming window for multitones and chirp with bandwidth time product equal to 400 (B800MHz; T500ns; velocity validity 2984m/s)

2. Effect of the number of quantization bits on Distance Compression

This study on quantization will allow dimensioning the system DAC for single target compression and ADC multiple targets compression. The effect of limiting the number of bits at the DAC level with multiple targets isn't considered.

If the bit resolution is not sufficient, the pedestal level of the pulse compression increases, although the characteristics of the main lobe and second sidelobes are not affected, as shown in Figure 48. In order to dimension the digital radar DA/AD converters in single target scenarios, the highest bandwidth-time product should be set, in order to determine the required number of bits to obtain a pulse compression close to the nominal value.

Figure 48 illustrates the effect of quantization on the compression of Chirp and Multitones for $B = 800\text{MHz}$ and $\text{PRP} = 50\mu\text{s}$, thus $BT = 40000$. Both figures display a quasi-linear evolution of the error with a 6dB/bit slope. This tendency is confirmed with the Figure 49 D. It illustrates the evolution, in mean error on phase and magnitude, of pulse compression for bandwidth-time products within the range $[1000, 800000]$. The maximum achievable signal to noise ratio for sine wave at full scale is $\text{SNR}_{\text{dB}} = 6 \times \text{number of bits} + 1.76$. Thus the quantization noise for any waveforms decreases by 6dB for every extra bit of resolution.

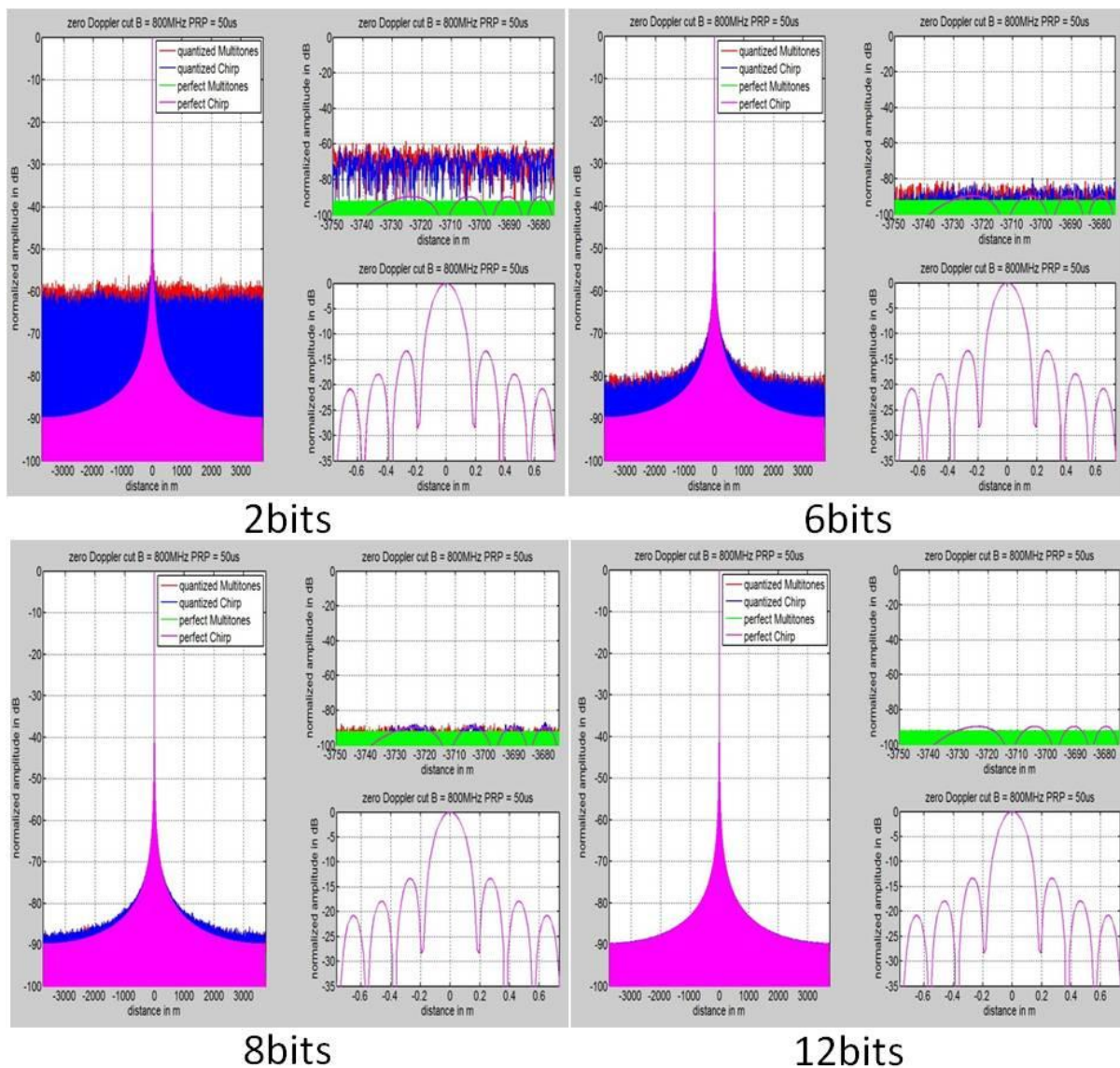


Figure 48: effect of quantization on Chirp and Multitones for $B = 800\text{MHz}$ and $\text{PRP} = 50\mu\text{s} \rightarrow BT = 40000$

Setting the acceptable relative mean error to -40dB, the number of bits required to obtain that precision is shown in Figure 49 A for both chirp and multitones. Figure 49 B and C show respectively the mean and max error, according to the number of bits obtained in A, for different bandwidth-time products for both chirp and multitones.

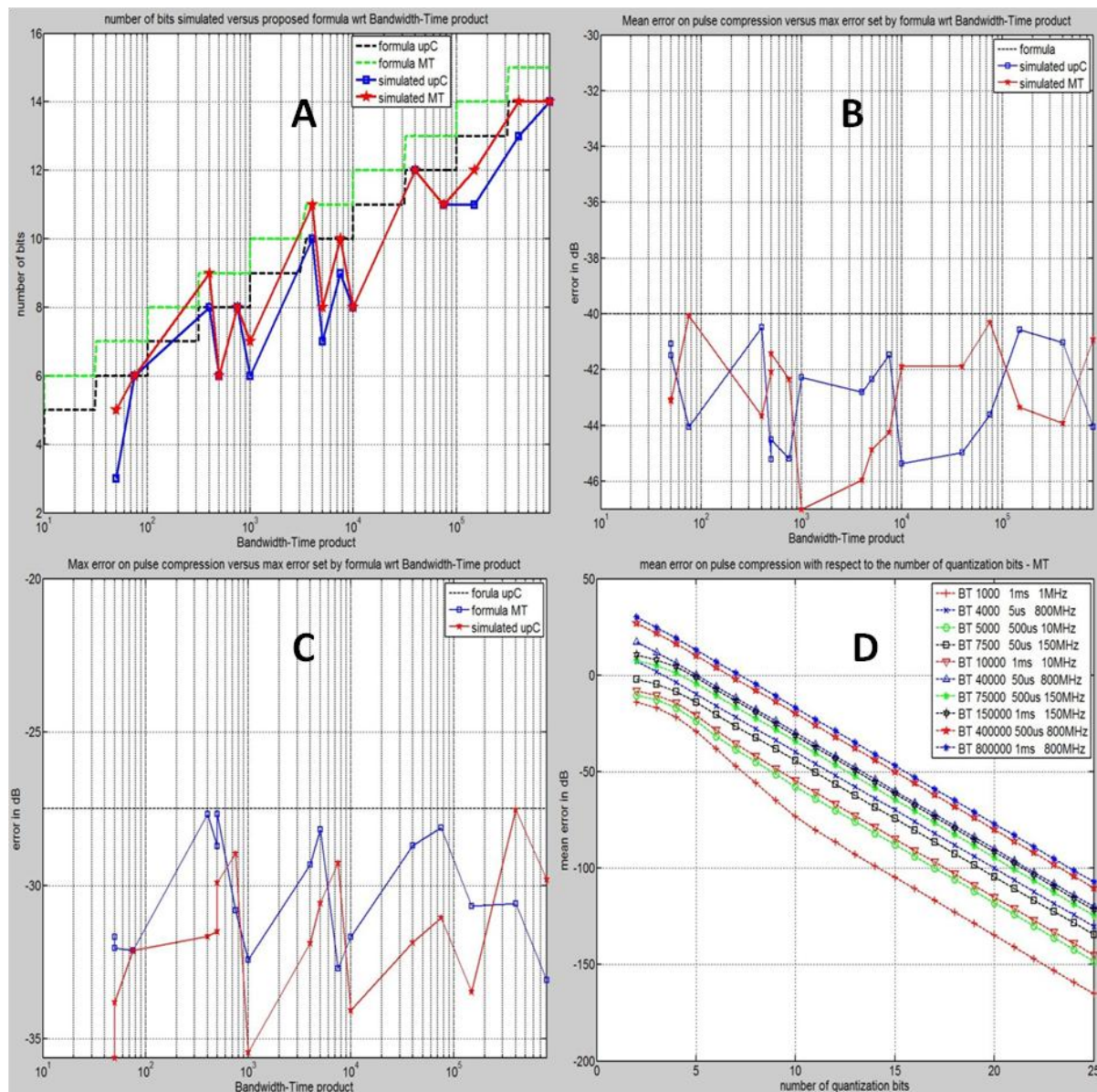


Figure 49: Equation 20 vs simulated data: A) minimum number of bits, B) mean error, C) max error on pulse compression and D) mean error on pulse compression vs number of quantization bits

From observation, it takes an extra bit for multitones with Newman phase codes to reach the -40dB mean error/27.5dB max error in amplitude and phase compared to chirp. This is related to PMEPR: the multitones are hindered compared to constant envelope signals, explaining the need for an extra bit to reach the set mean error. Equation 20 sets a rule of thumb to define the system bit-resolution, given the maximum bandwidth-time product for both chirp and multitones.

Equation 20: minimum number of useful bits necessary to digitize a signal with a given bandwidth-time product for pulse compression

for $\epsilon_{mean} < -40\text{dB}$ and $\epsilon_{min} < -27.5\text{dB}$

Chirp: min number of bits = $\lceil 2 \cdot \log_{10}(B \cdot T) \rceil + 2$, valid for $B \cdot T \geq 50$

multitones: min number of bits = $\lceil 2 \cdot \log_{10}(B \cdot T) \rceil + 3$, valid for $B \cdot T \geq 50$

For a bandwidth-time product of 40000, Equation 20 sets a resolution of at least 12bits for chirp and 13bits for multitones. The pedestal of the pulse compression or of the impulse response offers a reduced contrast when the number of bits isn't sufficient. Increasing the number of bits further than the minimum requirements reduces the noise on the curve; the distance compression pedestal remains unchanged. If the user decides to use a measured reference, the noise floor will be raised by 6dB if the minimum number of bits isn't respected. However, the transfer function is corrected since the signal comes from the radar system.

3. Effect of saturation in an amplifier on Distance Compression

The effects of saturation on distance compression characteristics (3dB main lobe width, sidelobes' amplitudes and positions) are negligible. In narrowband, the pedestal level is barely affected by saturation. In wideband, the pedestal presented oddities that are explained in the next section (Chapter 5.F) and these results on pedestal will be ignored. Extrapolating results from narrowband to wideband, the pulse compression in distance remains almost unaffected by the saturation process overall.

F. Discussion on simulations

The simulation results presented for wideband signals have to be carefully considered. The sampling frequency is the weakness of the simulation process. Indeed, the chosen sampling frequency may affect the performance results (PMEPR, Power efficiency and Pulse compression). A sampling frequency chosen too close to the Shannon-Nyquist law (e.g 2GS/s) would result in invalid results on PMEPR, power efficiency and the pedestal of pulse compression as shown in Figure 50. Increasing the sampling frequency (e.g 10GS/s) would reduce these effects.

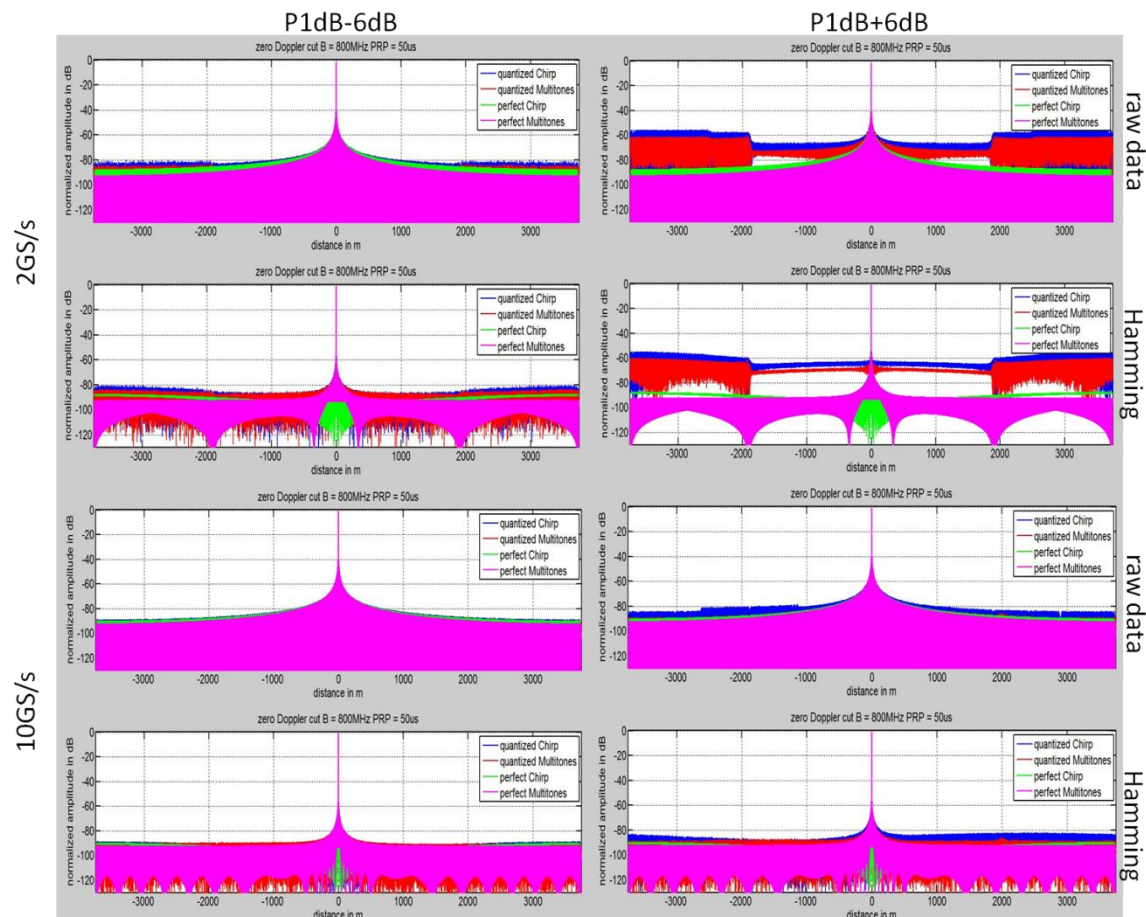


Figure 50: impulse responses wrt saturation and sampling frequency for signals with $B = 800\text{MHz}$ and $\text{PRP} = 50\mu\text{s}$

These distortions are caused by intermodulations folded into the first Nyquist band. For NB signals, if the folded intermodulations fall outside the receiver bandwidth from 1GHz to 2GHz, they can be filtered. However, for WB signals, the intermodulations fall inside the useful bandwidth, even with a high sampling frequency.

In Figure 51, the saturation effects are illustrated for both chirp and multitone signals. Observing the strongest intermodulation products orders 3,5,7,9, their positions in an analog spectrum should be respectively centered at 4.5GHz in the 1st Nyquist Band, 7.5GHz and 10.5GHz in the 2nd Nyquist band and 13.5GHz in the 3rd Nyquist band. Figure 51 displays the simulated spectra of a chirp generated @ 10GS/s after amplification at P1dB-6dB. The 3rd order intermodulations are at the correct positions. However the higher orders are all folded inside the first Nyquist band. The intermodulations of 5th, 7th and 9th order are now respectively located at 2.5GHz, 500MHz and 3.5GHz.

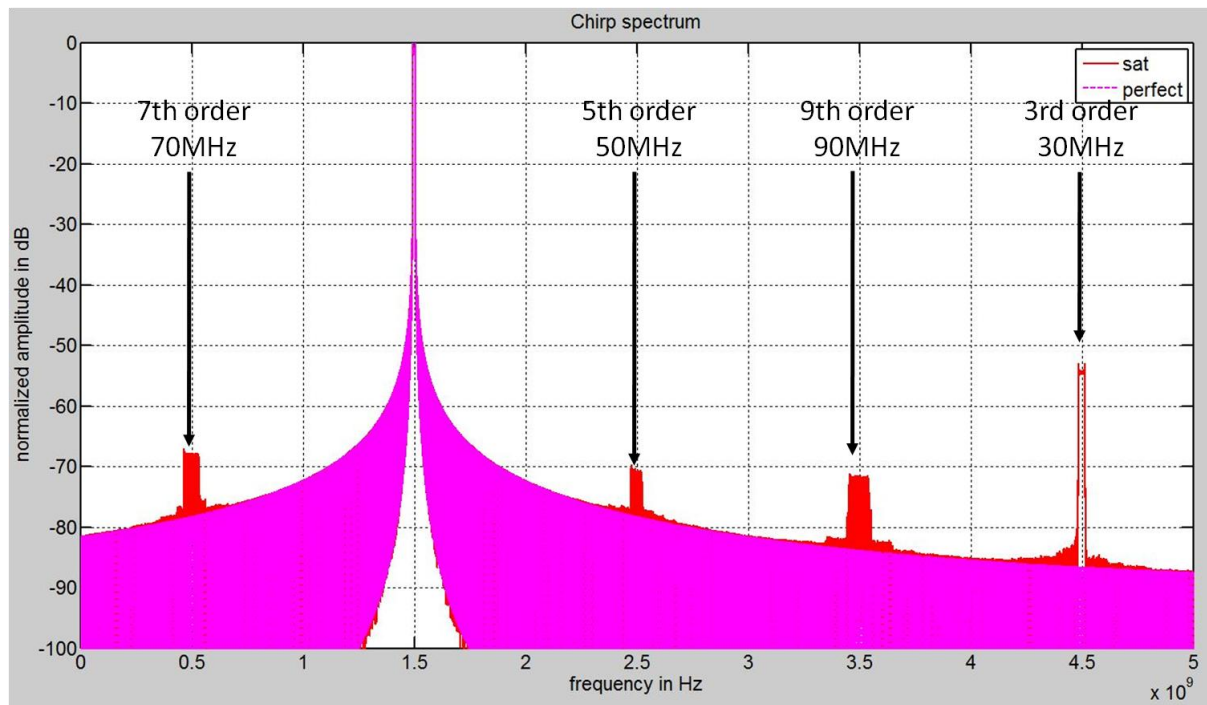


Figure 51: spectra at P1dB-6dB of chirp for $B = 10\text{MHz}$, $\text{PRP} = 50\mu\text{s}$ - positions and bandwidths of the strongest odd order intermodulations

If the sampling frequency is reduced to 2GS/s the intermodulations folds onto the useful frequency as shown in Figure 52 for chirp. When using a sampling frequency of 10GS/s, the folded intermodulations can't be removed but their contributions to distortions are lessened. The simulation has its limits when it comes to wide bandwidth, even with high sampling frequencies. The solution would be to choose an even higher sampling frequency, but there is a limit to the processing power.

This means that the results on the pedestal of the impulse response can't be used for wideband simulations, but the results on the main peak and sidelobes characteristic remain valid, since the useful bandwidth remains dominant in the simulations. Thus, the PMEPR and power efficiency for WB signals (150MHz and 800MHz) is an indication of the general behavior of these characteristics.

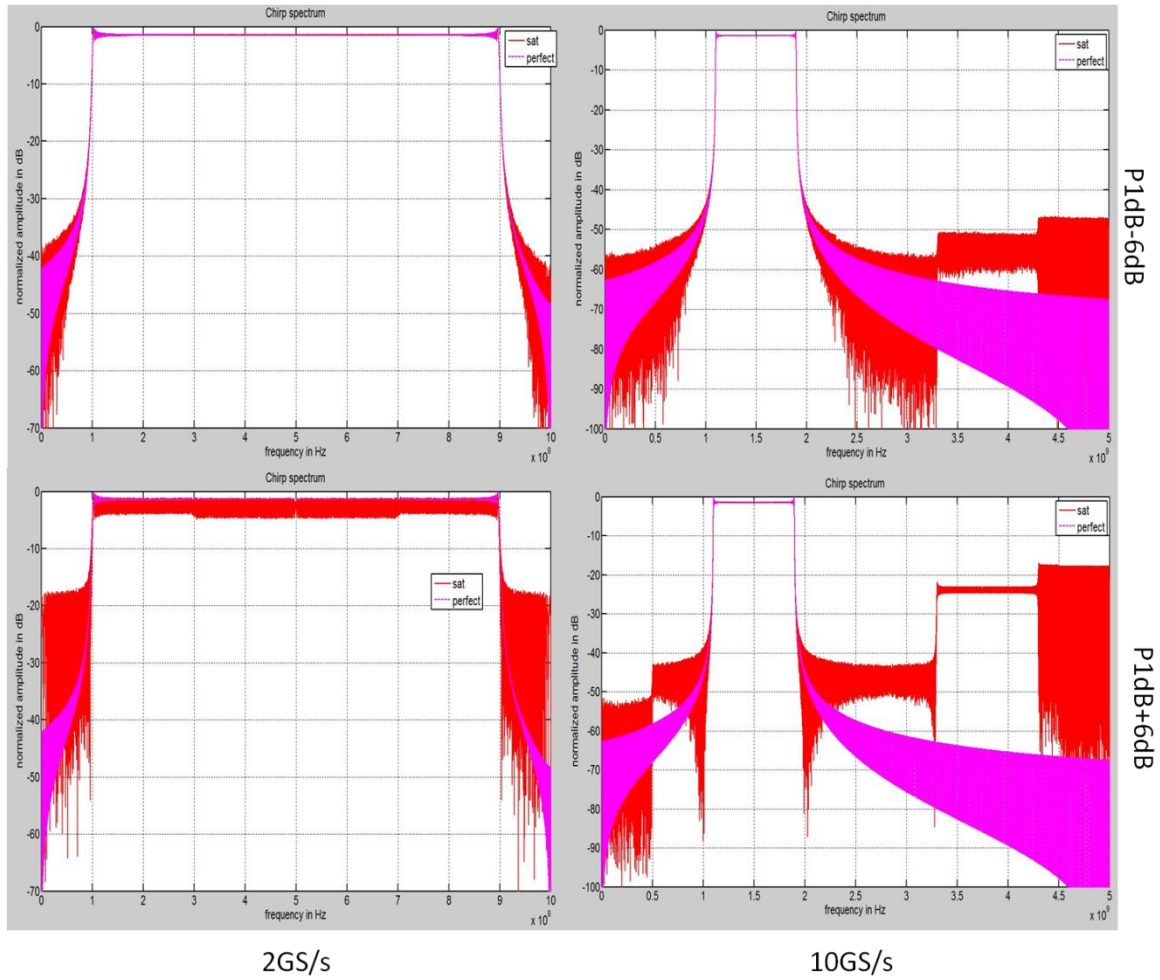


Figure 52: spectra of chirp with PRP = 500us wrt saturation and sampling frequency

G. System level performances

The average power in the useful bandwidth is determined by combining the results of PMEPR and power efficiency from the simulations @10bits for quantization, and @ IP1dB for saturation. The results are shown in the maximum detection range that was calculated using the radar equation

	Quantization @ 10 bits	Saturation @ IP1dB
Average power difference (upC-MT)	1.18dB to 2.55dB	1dB to 2.2dB
max detection range error	7% to 16%	6% to 14%

Table 18: system level performances from simulation of quantization @ 10bits and saturation @ IP1dB

The difference in average power shows that Chirp will have 6% to 16% higher detection range compared to multitones. The difference reduces by 0.2dB @IP1dB compared to the linear region, thus little improvement compared to Chirp has to be expected. If the input power is brought to IP1dB, then the detection range will be extended as the amplifier output power will increase. In terms of consumption, the chirp should be more efficient than multitone signals at the amplifier and ADC level. Especially if the system has a low bit-resolution and is narrowband, Chirp should be favored over multitones.

In terms of SNR at the reception wrt quantization and saturation, it is not possible to predict the SNR based on the original PMEPR and power efficiency, because when the signal is reflected on a target, it is not possible to predict the effect on amplitudes or phases. However, considering no distortion occurs during the propagation and reflection, the maximum achievable chirp SNR should also be [1dB-2.55dB] higher than maximum achievable multitones SNR. This means that in cluttered area, the chirp should detect targets buried [1dB-2.55dB] deeper in clutter than multitones.

Concerning pulse compression wrt quantization and saturation, multitones and Chirp have the same characteristics in compression for bandwidth-time products greater than 100.

H. Synthesis and Conclusion

The chirp and multitone waveforms were tested with bandwidth from 1MHz up to 800MHz and pulse repetition period from 500ns up to 1ms. The result of this analysis shows that the performances of multitones are close to those of Chirp in terms of PMEPR, power efficiency and ambiguity function. On the ambiguity function, chirp displays a better contrast than multitones, but the difference is of the order of a couple of dBs.

On the difference in average power between both waveforms, the result showed that as the signal bandwidth reached the order of the receiver bandwidth, the gap in power was reduced. Note that the simulations were realized with a constant receiver bandwidth of 1 GHz for all bandwidth configurations. On operational radar systems, the receiver bandwidth should be matched with the signal bandwidth to reduce noise power and avoid interferers to maximize the SNR. Extrapolating from the results @ 800MHz, with a receiver bandwidth matched to the signal bandwidth, the difference in average power would be around 1dB between chirp and multitones, resulting in detection range difference around 7%.

The analysis revealed that given 10bit resolution, any waveform reached their nominal values in terms of PMEPR and power efficiencies. Manufacturers of state of the art converters announce DAC AWG7122C (86) @24GS/s with 10bit resolution and ADC Proteus V5 (74) @5GS/s with 10bit resolution. This means that direct synthesis of signals up to X band and digitization of signals up to S band and part of C band is possible with nominal values of PMEPR and power efficiencies.

The error on pulse compression depends on the bandwidth-time product. For a set error on compression, multitones need an extra bit in resolution to reach the set value. Depending on the chosen emission band, requiring an extra bit resolution on state of the art AD/DA converters will either result in increased AD/DA converter consumption or in a reduced sampling frequency.

The saturation process showed little influence on the performance criteria over the studied range, and no degradation of signal performances up to IP1dB. Our simulations assumed no phase distortions or amplitude distortions in the saturation process; this might explain that little influence has been registered on performances.

The simulations were indeed basic using perfect quantization process and a model of saturation without phase or amplitude distortion. The simulations were performed without any noise, jitter or any complex models. This allowed determining a base for the experimental tests. If the experimental results are not satisfactory, then the simulations will go through more complex modeling to approach realistic conditions. However, simple simulations were chosen to reduce time to experiment and get a feel of the processes at work.

Chapter 6. Radar Implementation and Experiment Design

In this chapter, the radar implementation will be dealt first. In the first section, the constraints will be first presented. It will determine the boundaries for the frequency planning. Then a radar system overview will be presented. Finally, the radar basic performances will be evaluated using theoretical formulae.

The second section will deal with experiment design for waveform comparison. In that section, the radar evolution and tweaks will be explained through experimentations. In second, the measured radar basic capabilities will be presented. Then the design of experiments to compare the waveforms will be explained. Four experiments were devised to test the impact of hardware on the radar performances, test the radar stability, test the effect of Doppler on the signal performances, and finally test the effects of saturation on radar performances.

A. Radar Implementation

In this section, both hardware and design constraints inherent to RF system design and thus radar will be presented. Then, based on the boundaries set by the constraints, the radar frequency planning will be designed according to the available components. The third part will give an overview of the complete radar system. And finally, the radar characteristics will be evaluated using theoretical formulae and the components' characteristics.

1. Hardware and Design Constraints

The radar must support any waveforms in order to compare them, using the same platform with no hardware modification from one waveform to the other. Thus, it should be easily reconfigurable and emit in continuous wave mode. For calibration purposes, a reference channel has to be designed, allowing the measurement of a signal replica. Also, the radar must be as wide band as possible in order to collect information on wideband system issues. At Onera, two devices were available for the implementation of the radar system digital core. It is composed of the arbitrary waveform generator AWG 7102 from Tektronix (86) and the digitizer Neptune VXS II from Tekmicro (74). Their characteristics are shown in Table 19. The digital core interfaces the soft processing with the RF equipment.

	DAC – AWG7102	ADC – Neptune VXS 2
Maximum Sampling Frequency	10GS/s	2GS/s
Analog Bandwidth	DC - 5.8GHz	DC - 3.3GHz
Resolution	10bits	10bits
Number of channels	2	2

Table 19: DA and AD converters main characteristics

The strongest design constraints come from the digitizer because it has a lower sampling frequency and analog bandwidth. Hence the limits for the design will be drawn from those characteristics.

In order to maximize the bandwidth, the maximum frequency of the digitizer $F_{S_digitizer} = 2GHz$ was chosen. This means that the Nyquist bands are 1GHz wide.

An anti-aliasing filter is required in order to avoid the signals present in other Nyquist bands to fold onto the desired signal upon digitization. It is extremely difficult to design a selective enough wide band filter in base band. Thus, the 2nd Nyquist band will be used, it is located

between $F_{s_digitizer}/2$ and $F_{s_digitizer}$. The digitized signal is bandpass sampled, as illustrated in Figure 53.

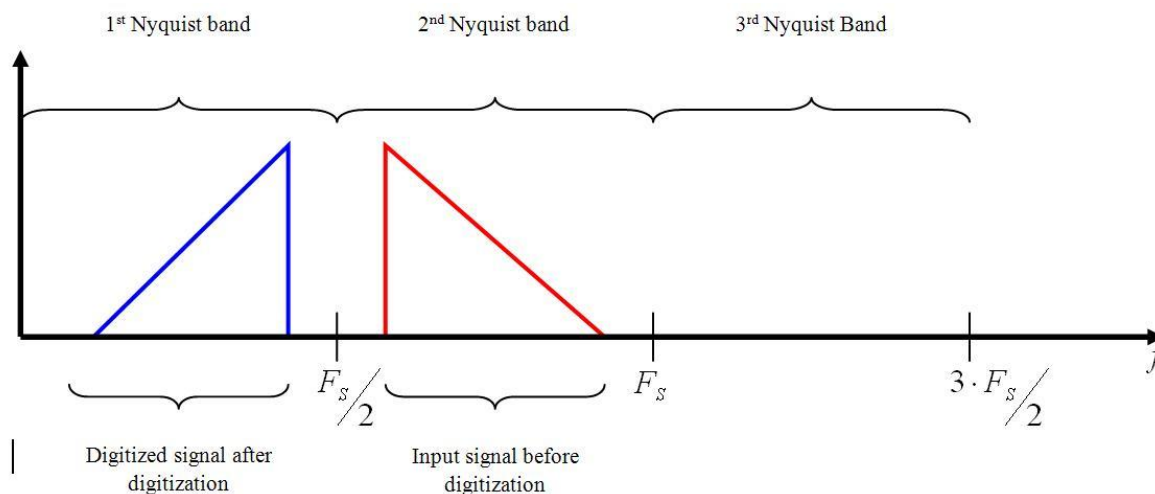


Figure 53: Bandpass sampling and Nyquist bands – $F_s = F_{s_digitizer}$

Bandpass sampling with an ADC could be compared to an analog downconversion, thus the input signal frequency range $[F_l; F_u]$ yields first order sum $[F_{s_digitizer} + F_u; F_{s_digitizer} + F_l]$ and difference $[F_{s_digitizer} - F_u; F_{s_digitizer} - F_l]$ when digitized with $F_{s_digitizer}$. The latter range is the range of interest. Note that even though the system undersamples the frequency, the information is kept intact, at the condition that it is contained within any Nyquist band, and the signal bandwidth B respects the Shannon-Nyquist condition for non-baseband signals $B < F_{s_digitizer}/2$.

The band pass signal design now will have to be taken in consideration. One design parameter of band pass filters is the 3dB percentage bandwidth which is defined in Equation 21.

Equation 21: 3dB percentage Bandwidth

$$B_{3dB\%} = \frac{3dB \text{ Bandwidth} \times 100}{Center \text{ Frequency}}$$

The center frequency is placed at the center of the 2nd Nyquist band. Manufacturers are able to design band pass filter with up to 70% relative bandwidth. The wider the relative bandwidth, the more ripple in the pass band, the more insertion loss and the higher the number of poles to get a strong rejection.

With a constraint of 40dB rejection at $F_{s_digitizer}/2$ and $F_{s_digitizer} = 2GHz$, at FILTEK (87), customizers can design filters with 3dB insertion loss around, a relative bandwidth of 53.33% or 800MHz centered at $F_c = 1.5GHz$ and 1.5dB in band ripple. This leaves 100MHz guard bands on both sides of the bandwidth. Thus, the intermediate frequencies for digitization will be within the range $[F_l = 1.1GHz; F_u = 1.9GHz]$. That means we have 800MHz instantaneous bandwidth available per channel.

The transmission frequency into the X band was chosen based on the available equipment. Thus, the bandwidth position within the range $[8GHz; 12,4GHz]$ has to be defined. This

means that at least one up-converter is required in the transmitter and at least one down-converter in the receiver.

2. Frequency planning

The Arbitrary Waveform Generator has a sampling frequency $F_{s_generator}$ of 10GHz. Thus, signal frequencies can only be defined from DC to 5GHz, and the image frequencies appear mirrored from 5GHz to 10GHz. The signal will be directly synthesized between Lower frequency $F_l = 1.1GHz$ and Upper frequency $F_u = 1.9GHz$. The mirrored image of F_u is $F_{l_mirrored} = 8.1GHz$ and F_l is transformed into $F_{u_mirrored} = 8.9GHz$. A simple low pass filter after signal generation will remove this image, see Figure 54.

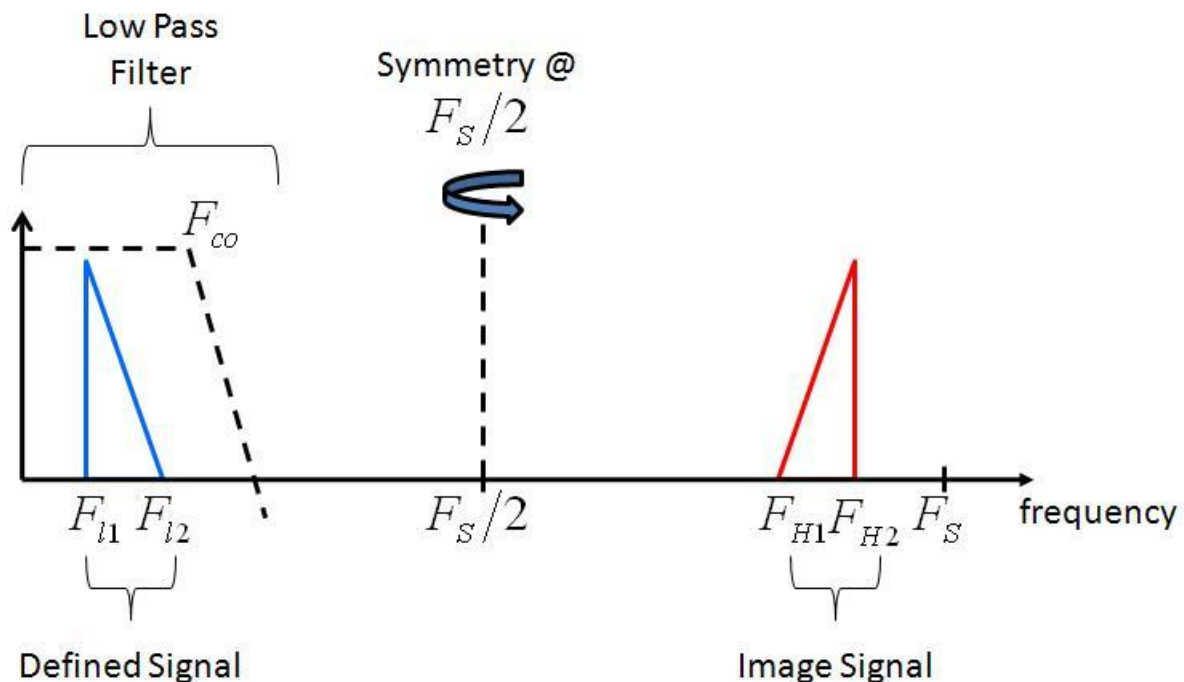


Figure 54: Signal generation with DAC - defined signal and its mirrored image around $F_s/2 - F_{s_generator} = F_s$

 Note that the low pass filter characteristics have to be checked because the filter may have regrowth in its pass band further than its specified cutoff frequency.

The signal is up-converted and down-converted with the same local oscillator frequency in order to reduce the number of components and the design complexity. Thus the IF ranges [1.1GHz, 1.9GHz] in the transmitter and the receiver are identical. Given that in our case, the bandwidth is smaller than one octave with respect to the IF frequency lower bound, the system will not be perturbed by even order intermodulation products (2^{nd} , 4^{th} , ..., $2n^{th}$). Thus, the condition $F_{l1} < F_{l2} < F_{LO} < F_{H1} < F_{H2} < 2F_{LO}$ must be respected for up and down conversions. In order to get high signal purity, the system should be free of 3^{rd} order intermodulation products at least. This system will avoid intermodulation products up to the fifth order. It'll be assumed that the mixer operates in the linear region (3^{rd} order intermodulation power levels lower than the systems sensitivity see Chapter 4.D.2)

$$(n - 1)F_{l1} + (n - 1)B < F_{LO} \underset{n=5}{\implies} 7.6GHz < F_{LO}$$

$$F_{l2} < 2F_{LO}/(n + 1) \underset{n=5}{\implies} 5.7GHz < F_{LO}$$

And since the RF frequency range must be contained within the X band.

$$F_{l2} + F_{LO} < 12.4GHz \equiv F_{LO} < 10.5GHz$$

Thus in our case, the local oscillator frequency must be in the range [7.6GHz; 10.5GHz]. This implies that the RF range upper bound, given a 800MHz bandwidth, is in the range [9.5GHz; 12.4GHz].



A band pass filter is required to remove the image frequency after up and down conversions.

Table 20 shows the list of filters available in X-band. Based on the nth order intermodulation avoidance rules and the maximum system bandwidth (800MHz), the 3rd filter only offers one configuration which beats the purpose of reconfigurability. The first filter allows a RF range shift of 300MHz. The second filter allows a RF range shift of 800MHz, hence this filter was chosen to maximize the radar RF range agility. The local oscillator range is thus [8.9GHz; 9.7GHz] when using maximum bandwidth.

	Center frequency	Pass Band	SWR	Insertion loss	Rejection < 65dB
Filter 1 (Versys)	9GHz	1600MHz	1.7:1	1.5dB	7700MHz 10300MHz
Filter 2 (Filtek)	10.8GHz	1600MHz	1.5:1	0.64dB	8720MHz 12880MHz
Filter 3 (Versys)	12.4GHz	1600MHz	1.7:1	1.5dB	11100MHz 13700MHz

Table 20: Filters for image removal after upconversion

3. System Overview

The final system overview is shown in Figure 55 and Figure 56. It is color coded to identify the different subsystems detailed below. The detailed schematics of the architecture are available with design considerations in Appendix Chapter 9.I - Experimental test bench.

Notice that two frequency synthesizers were used to generate the local oscillator frequency. It was necessary because the power available at the output of the amplifier wasn't deliver enough to drive all 3 mixer local oscillator inputs @ 20dBm. So the first synthesizer was used to drive the upconverter and the test channel downconverter, and a second synthesizer to drive the reference channel downconverter. Both synthesizers have the same 10MHz external reference from the signal generator.

The 10MHz reference is generated by the signal generator and fed into a ferrite 6 way splitter. The outputs are connected to the frequency synthesizers and the digitizer if we use the high speed digitizer. The other outputs are used to synchronize measuring equipment, such as spectral analyzers and scopes.

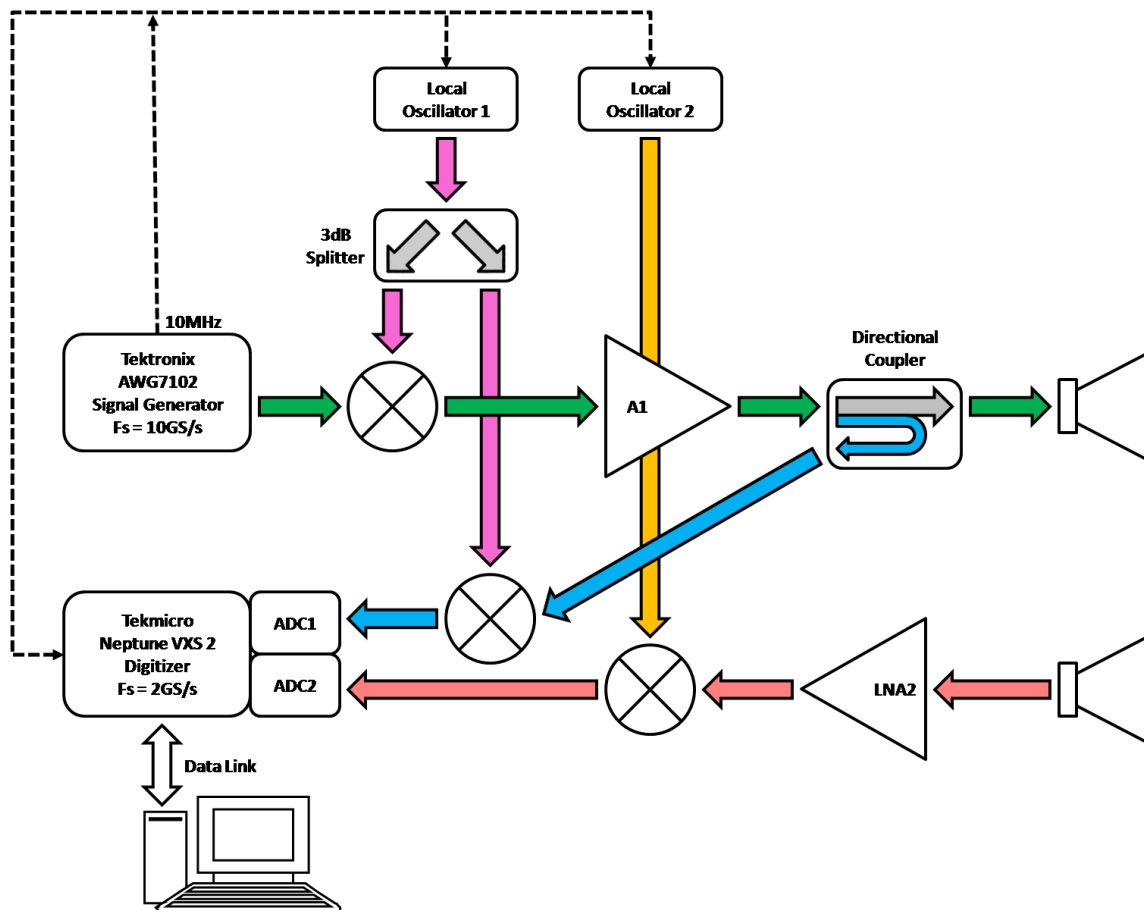


Figure 55: Experimental test bench system overview - schematic

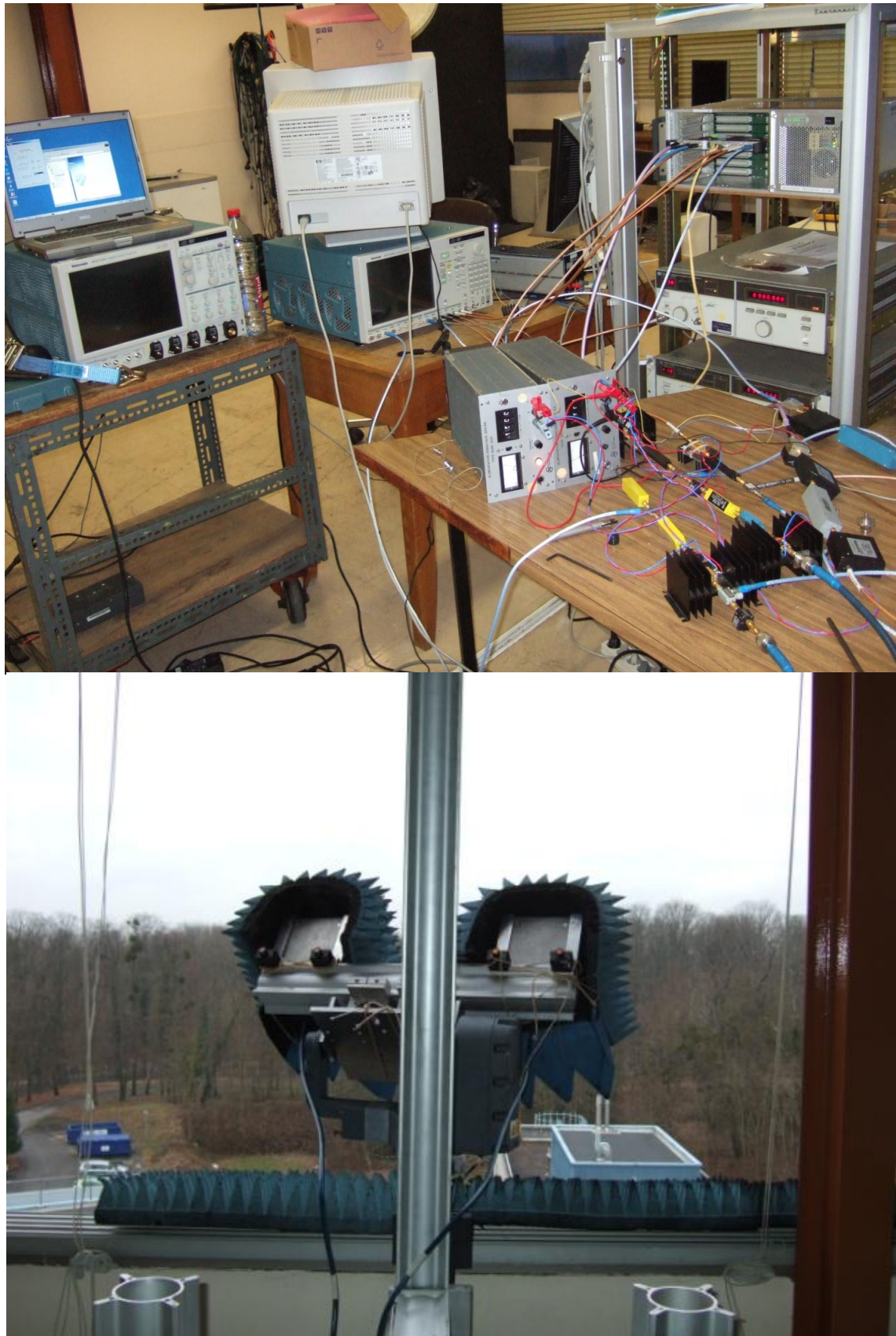


Figure 56: Experimental test bench system overview - lab experimental test bench set-up

4. Radar characteristics

In this section, the emitted power will first be evaluated. Then the RMS quantization noise floor will be studied in order to determine the maximum achievable dynamic range. Next, the noise figure and gain of the receiver channel will be determined. Finally the expected radar performances will be presented.

a) *Emitted power*

All the generated signals are normalized to fit in the DAC range, this way no signal clipping occurs upon generation. The upconverter IF signal power is about $-2dBm$. After upconversion and filtering, the signal strength is $-4dBm$. Thus after amplification, the signal power is $19dBm$ (4dB OBO) with amplification stage 1 or $26dBm$ (14dB OBO) with amplification stage 2.

b) *RMS quantization noise floor*

The quantization noise floor or maximum achievable SNR is evaluated using two methods. The first evaluates the quantization noise floor with the ENOB announced in datasheets for both digitizers. The second evaluates the quantization noise floor considering the rms jitter and the bandpass sampling losses. Both are presented in Appendix Chapter 9.K and Table 21 shows the range of maximum achievable SNR for both digitizers Neptune VXS II and DSA71254. The first digitizer is used for most experiments, the second is used for the Doppler experiments (refer to Chapter 6.B.4.c)

	ENOB+losses	RMS jitter + losses
Neptune VXS II	42.3dB	[50.5dB – 52.5dB]
DSA71254	30.26dB	41.8dB

Table 21: estimated digitizers' maximum achievable SNR

c) *Receiver Noise Figure and Gain*

The noise figure of the receiver is calculated with Friis formula for noise figure. The receiver contains 19 elements before digitization without cables.

Equation 22: Friis formula for noise figure & total gain

$$F_{total} = F_1 + \sum_{a=2}^N \frac{F_a - 1}{\prod_{b=1}^{a-1} G_b} \quad \& \quad G_{total} = \prod_{a=1}^N G_a$$

where F_{total} is the total noise figure of the receiver channel, $F_{1,2,...N}$ are individual noise figure of the components in the receiver channel, G_{total} is the total gain of the receiver channel, $G_{1,2,...N}$ are individual gain of the components in the receiver channel.

The radar receiver has a noise figure equal to $17.14dB$ and a total gain of $21.3dB$. the receiver bandwidth is $1.1GHz$ which matches the antialiasing filter bandwidth. These elements are used to calculate the noise power in the receiver.

Equation 23: Noise power

$$N_{power} = 10 \times \log_{10}(k T B) + F_{total} + G_{total} + 30 = -45dBm$$

5. Expected radar performances

The reconfigurable radar platform was designed with 800MHz instantaneous bandwidth per channel and 1.6GHz agility. This platform supports any kind of waveforms, which enables unbiased analysis of various waveforms. The reconfiguration of waveforms or frequency range can be controlled digitally and no hardware reconfiguration is required. The parallel architecture offers a reference channel to measure the signal at the power amplifier output, in order to produce a more accurate match filter for tested signal compression. The major characteristics of the radar are shown in Table 22.

Radar	
IF frequency range	[1.1GHz-1.9GHz]
Agility / RF tuning range	1.6GHz / [10GHz-11.6GHz]
Instantaneous Receiver Bandwidth	800MHz per channel
Spatial resolution	15cm
Transmitter	
Radar output power	19dBm/26dBm
Receiver	
Receiver Total Gain	21.3dB
Receiver Total Noise Figure	17.14dB
Noise power	-45dBm
Digitizer Neptune VXS2	
ENOB	7.4bits
Maximum SNR	46.3dBFS
Jitter	[160fs-200fs]
SNR limitation	[42.3dBFS-52.5dBFS]
Digitizer DSA 71254	
ENOB	5.4bits
Maximum SNR	34.26dBFS
Jitter	450fs
SNR limitation	[30.26dBFS-41.8dBFS]

Table 22: radar characteristics

B. Experiment design for waveform comparison

Many experiments were conducted in order to obtain the final system that was presented in the previous. The first section will explain the evolution and tweaks that were made to the radar through experimentations. The second part presents the measured radar capabilities. The third part describes the experiment design for waveform comparison. Four experiments will be presented. First a closed-loop DAC-filter-ADC experiment to determine the impact of RF equipment. Then, an experiment on static targets will be presented to determine the equipment stability. The third experiment will be designed to test the effect of Doppler on the performances of the tested waveforms. And the last experiment will be designed to test the effect of saturations.

1. Description of the experimentation environment

Figure 57 presents the testing environment. It shows the radar set-up, the antenna set-up, the experimentation area and targets that were used during experimentations such as a triangle corner reflector and a rotating fan.

The advantage of using a triangle corner reflector is that its reflective pattern is much wider than regular reflectors $\pm 60^\circ$. This relieves the positioning constraints; therefore the reflector can be placed with good accuracy by hand. The antennas will be static during the experimentations, thus the corner reflector is placed in the direct line of sight of the antennas. The triangle corner reflector was used as a reference to set the phase origin of the impulse responses. The reference radial distance is 25.75m. This way, knowing the distance between the radar and the reference position of the triangle corner reflector, the relative position of the target can be determined with respect to this reference position.

In Figure 57, three graduated lines can be seen traced on the parking lot. These lines indicate the directions relative to the antennas. The first line at 0° , points in the direction of the antennas line of sight and measures 14m. the second at 90° with respect to line of sight measures 16m and the third at 45° with respect to line of sight measures 18m. These lines were used as guidelines for the experiments with moving targets and also to point the static targets.

Observing the antenna set-up in Figure 57, you will notice that the window frame had to be covered below the antenna with radiation absorbent material. Indeed the frame is made of metal which would cause strong reflections. With the radiation absorbent material, the reflections dropped by 25dB compared to previous measurements.

Notice that radiation absorbent material was placed over the reflector stand because its shape formed another corner reflector, creating a second point scatterer.

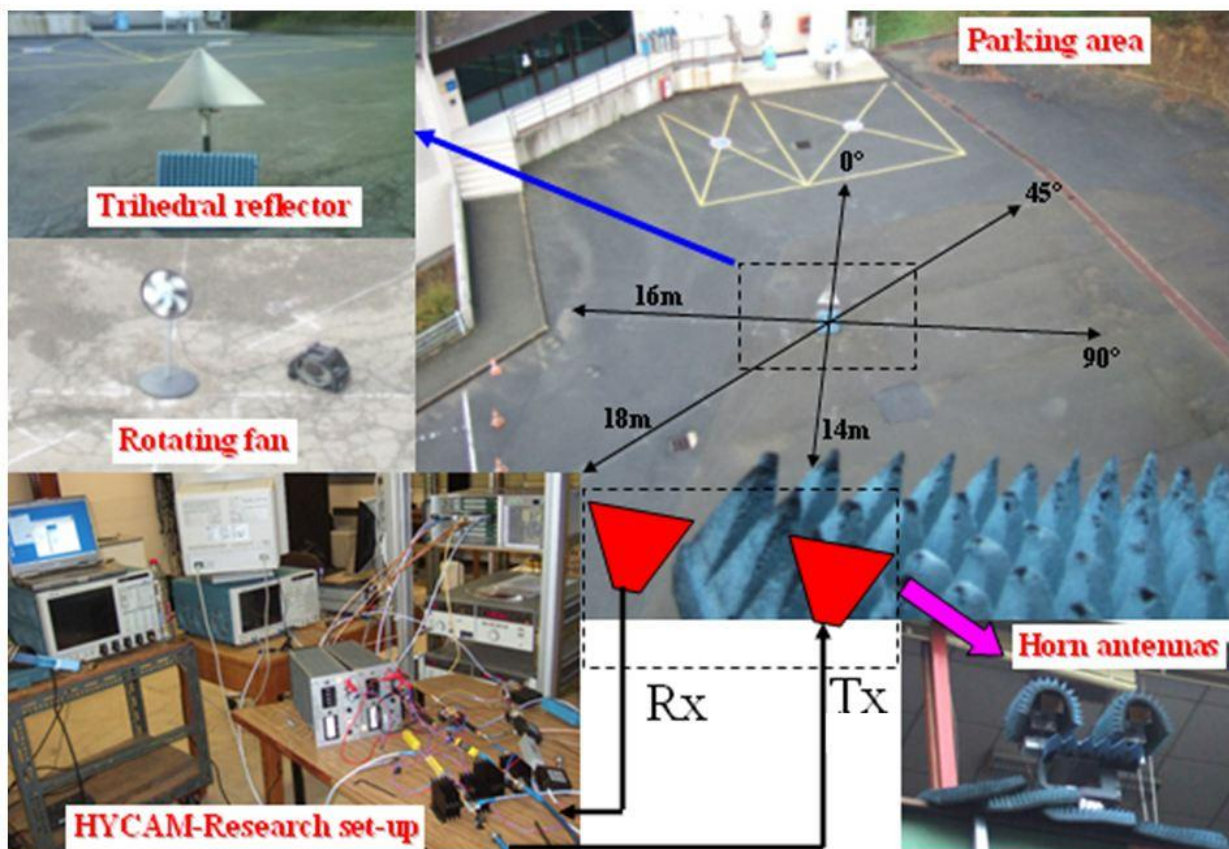


Figure 57: parking experiment (top) schematic and dimensions (bottom) lab and parking set-up

In the experimentations, the signals are normalized before generation through the DAC. Multitones will have a power handicap compared to Chirp equal to 2.5dB in average. Experimentations on static and moving targets were conducted in order to tune the radar and also to supply experimental data on micro-Doppler for Antoine Ghaleb’s thesis work (88). This work gave rise to two communications (89) (90). The targets in Table 23 were all used during the experiments.

Target	Typical RCS in dBsqm	Dimension in m $H \times W \times D$	Max Velocity in m/s
Cat	-20	$0.25 \times 0.12 \times 0.5$	11
Pedestrian	[-10 ; 0]	$1.75 \times 60 \times 15$	10
Bike + Pedestrian	[0 ; 3]	$1.75 \times 60 \times 1.75$	28
Car	[6 ; 8]	$1.4 \times 1.4 \times 4$	90
Triangle corner reflector	30.5	$0.7 \times 0.7 \times 0.7$	0
VEGA Modulator transponder	1	2x Horn Antennas 0.1×0.1	modulation [DC – 10MHz]
Rotating fan	[-40;-30]	0.2m radius fan	[0-9]

Table 23: measured targets for micro-Doppler experiments

This experimental work allowed the evolution of the radar from 2006 to 2008. The next section presents the evolution of the radar between the first and final prototypes.

2. Radar Evolution

Setup	First prototype	Final prototype
Sampling frequency	2GS/s	2GS/s
Pulsed Mode - Pulse Repetition Period - Doppler ambiguity	$500\mu\text{s} / 2\text{kHz} \equiv 29\text{m/s}$	$200\mu\text{s} / 5\text{kHz} = 72\text{m/s}$
Architecture	Frequency-Interleaved	Parallel
Bandwidth/distance resolution	$800\text{MHz} / 0.1875\text{m}$	$800\text{MHz} / 0.1875\text{m}$
Carrier Frequency	10.4GHz	10.4GHz
Acquisition in Trigger mode	2048samples/trigger	1024samples/trigger
Integration time/Doppler resolution	$0.25\text{s} / 4\text{Hz} \equiv 0.057\text{m/s}$	$0.2\text{s} / 5\text{Hz} \equiv 0.072\text{m/s}$
Distance ambiguity/frequency spacing	$75\text{m}/2\text{MHz}$	$75\text{m}/2\text{MHz}$
Theoretical Processing gain	30dB	30dB

Table 24: radar settings for micro-Doppler experiments – first try and final stage

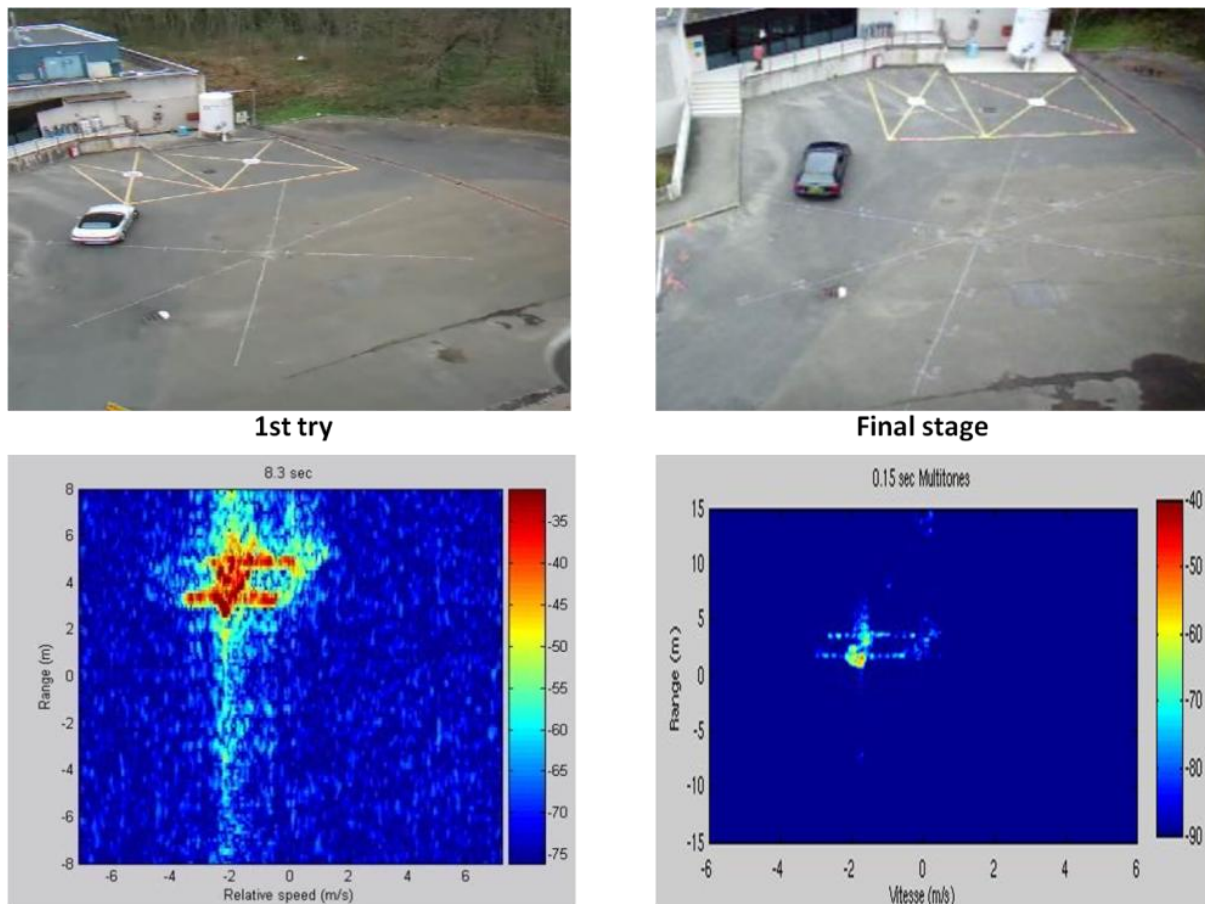


Figure 58: evolution of the radar view (top) optical camera view (bottom) radar view (left) first try (right) final stage

Figure 58 and Table 24 illustrate the evolution of the radar view quality between the first and the final stages of the radar system. On the first try, the Doppler ambiguity was too small compared to the relative micro-Doppler. Hence the trigger frequency was increased from 2 kHz to 5 kHz. Also the radar image on the left presents smudges above and below the car which means the compression is not clean and there are reflections at the circuit level. After thorough searches and circuit tweaks, the radar image seen on the right is cleaner, smudges can still be distinguished but it doesn't compare to the first image. The reflection power level compared to the triangle corner reflector is 10dB lower than in the previous image. Between the two measurements, the antennas changed position in the lab to get a better radar view of the scene; this explains the power variation since the angle wasn't the same. Furthermore the car wasn't the same. The antennas direct line of sight in the first try was located 30° clockwise with respect to the final stage antenna line of sight. Tuning the radar system allowed a 20dB gain in contrast, it was about 30dB before and now about 50dB. More details on micro-Doppler are available in Appendix Chapter 9.L.

3. Radar basic capabilities

This series of experiments allowed determining two characteristics of the radar. The smallest available target was measured first, a cat with -20dBsm attached at the center of the scene, as shown in Figure 59. The level is -50dB which is coherent with the information in Table 23. Then, the lowest measured speed was 0.14m/s (88), with a pedestrian standing still at the center of the scene while swinging his arm very slowly, as shown in Figure 60.

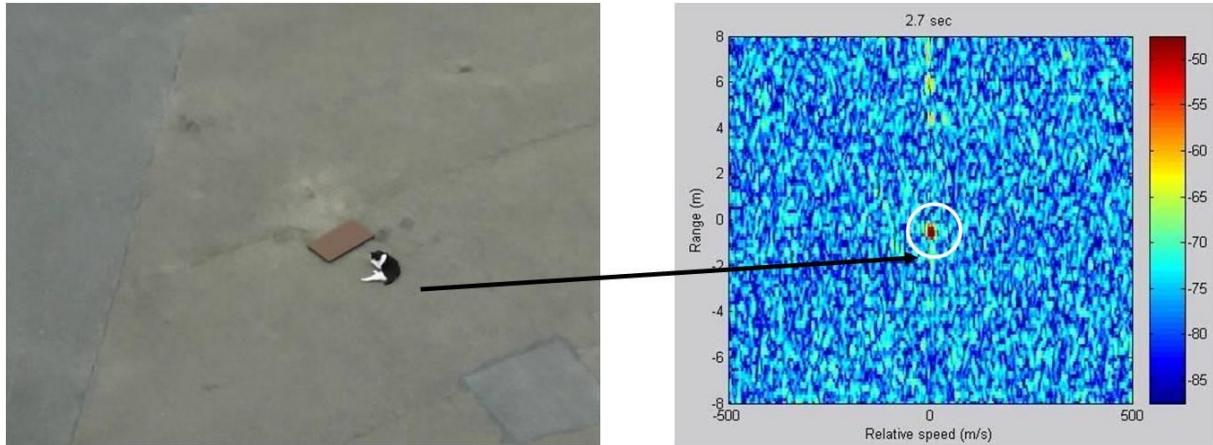


Figure 59: cat lying in the center of the scene (left) optical camera view (right) radar view

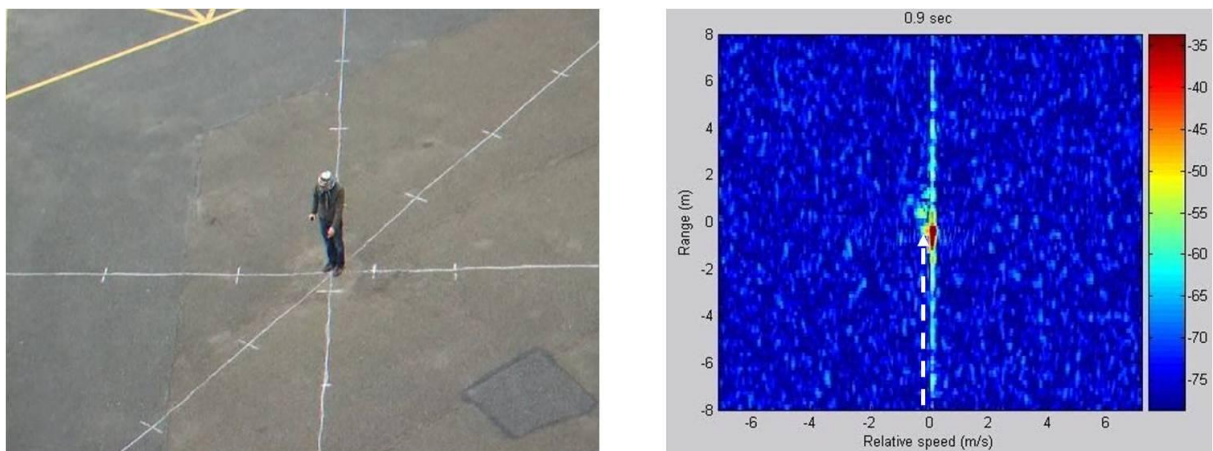


Figure 60: pedestrian standing still while swinging his left arm slowly (left) optical camera view (right) radar view

4. Experiment Design for Waveform Comparison

These experiments aim at comparing different waveforms using exactly the same parallel architecture and the generic signal processing algorithm presented in section Chapter 4.B. Four experiments were conducted in order to compare both Chirp and multitone signals.

The first experiment is a Closed-loop DAC-Filter-ADC measurement. This experiment will allow the evaluation of the waveforms' characteristics with the least distortions. The second experiment goes further, in using the full test bench to test for each waveform, the pulse compression on a triangle corner reflector, and also to evaluate the radar stability. The experiments on Doppler are used to evaluate its effects on the waveforms compression and thus test their resistance to target velocity. Finally, the saturation will be studied in order to determine the best Input Back-Off for the power amplifier.

It wasn't possible to simultaneously measure the different signals, so the experiments had to be reproducible to allow a valid comparison of successive measurements.

a) Experiments on Closed-loop DAC-Filter-ADC

The objective of the experiment shown in Figure 61 is to evaluate the characteristics of the various waveforms with minimum distortion.

Since this experiment is conducted in closed-loop, there are no problems concerning the reproducibility of the experiment apart from temperature variations during the day.

Direct DAC-filter-ADC measurements were performed. The signals are generated by the AWG7102 from Tektronix at 10GS/s with 10 bits resolution and normalized to use the DAC full scale. The signals go through a first isolator to isolate the DAC output from the filter’s impedance. The signals are then filtered by an SMT1020 filter with a center frequency at 1.5GHz and 1.1GHz bandwidth. This filter is used for antialiasing. Another isolator is used to isolate the filter’s impedance from the ADC input.

To avoid clock drift, the ADC clock is directly generated by the Arbitrary Waveform Generator, thus if the DAC clock drifts, the ADC clock does as well in the same direction. The DAC generates a 2GHz sine wave for the ADC clock input. This signal is amplified and filtered to remove the 2nd order harmonic. This insures clock signal purity, otherwise the signal would get additional jitter caused by the harmonic. The Arbitrary Waveform Generator markers are used as ADC triggers. Both cables have exactly the same length. The complementary pulses from the markers were tested with the DSA71254 to assess the time difference, it was a complete match. So the trigger mechanism is perfectly calibrated. The trigger duration is 0.5ns which is equivalent to 1 clock period. A longer or shorter trigger caused errors when data was recorded.

All the signals are generated with 1.5GHz carrier frequency with bandwidth from 1MHz to 800MHz. Since the digitizer’s sampling frequency is set at 2GS/s, the signals are within the 2nd Nyquist band. Upon generation, all the signals are normalized to fit the DAC full dynamic range. And no change occurs in the circuit when changing the signal only the DAC input data is changed. This way, the signals are evaluated for a given circuit set-up and determine which one exploits the RF equipment to its fullest.

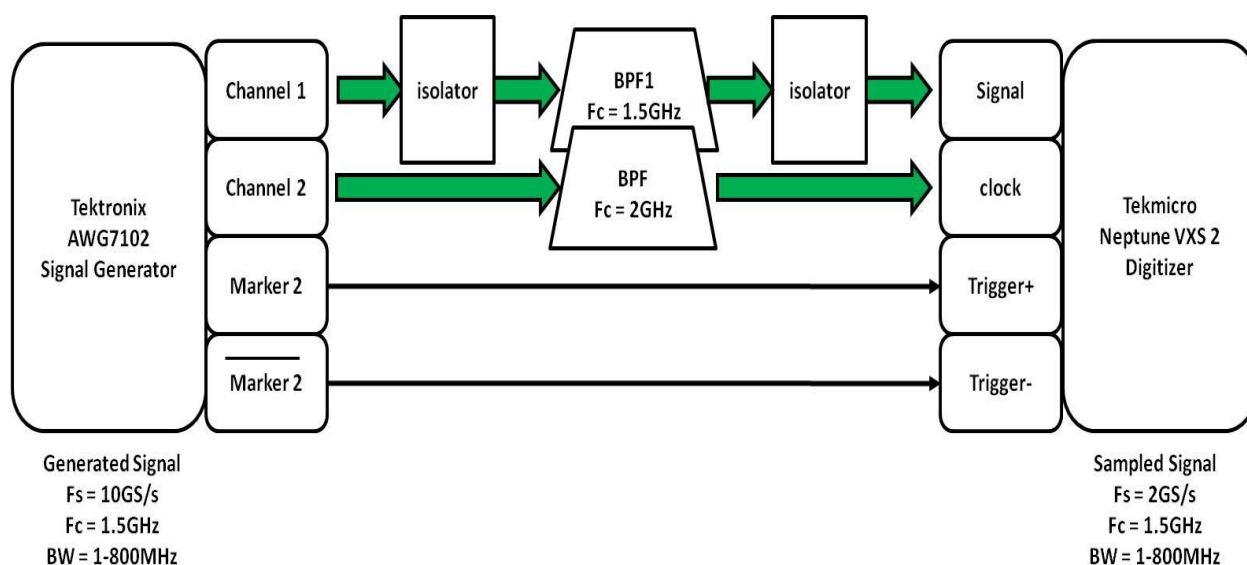


Figure 61: direct measurement DAC filter ADC for waveform evaluation

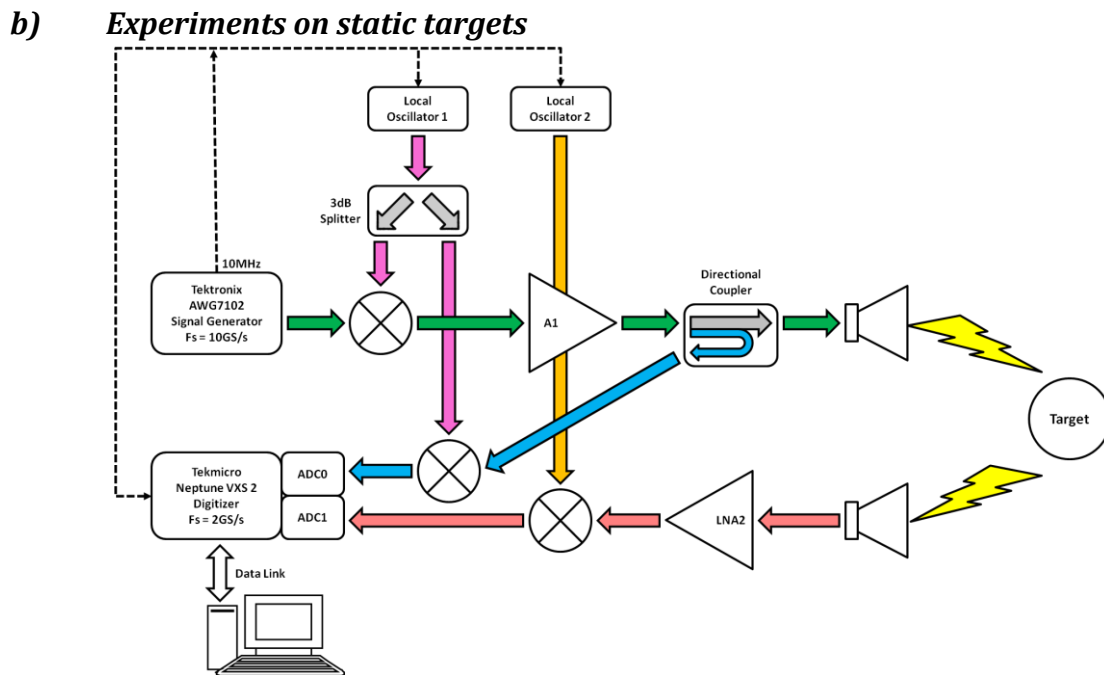


Figure 62: experimental set-up for waveform experiments

The objective of this experiment is to evaluate the radar stability. For this experiment, the radar to target set-up is shown in Figure 62 and the target positions are shown in Figure 63.

For the static measurement, the reproducibility was insured by fixing the triangle corner reflector with screws on a heavy and stable stand. Two panels of radiation absorbent material were put in front of the stand to suppress the secondary target created by the stand's shape. This was important to have a point target as phase reference. Multiple targets as reference would alter the accuracy of the measurements. The target is placed at 25.75m (radial) from the antenna for calibration which is the center of the markings on the scene. For the second measurement, the triangle corner reflector was placed -5.197m from the reference position, on the 0° axis as shown in Figure 63.



Figure 63: static targets (left) calibrator position (right) calibrator placed at 5.197meter from the calibrator on the 0° axis

One measurement is executed for compression purposes only, a few signal periods are recorded. A second measurement is executed with the full memory depth of the Neptune VXS II, which means $2^{25} = 33554432$ samples. At 2GS/s, it gives a continuous record length of 16.8ms.

The pulse compression will be calculated using the generic signal processing algorithm as described in Chapter 4.B, and the stability will be evaluated as shown in Figure 64. The stability is tested over a few values of integration depending on the signal period. Then the first impulse response is stored as fixed reference. It will be subtracted to all the following impulse responses. The peak response location is chosen to follow the evolution of the stability over time. This is shown in Figure 64.

The next step is to devise experiments to test the waveforms with moving targets.

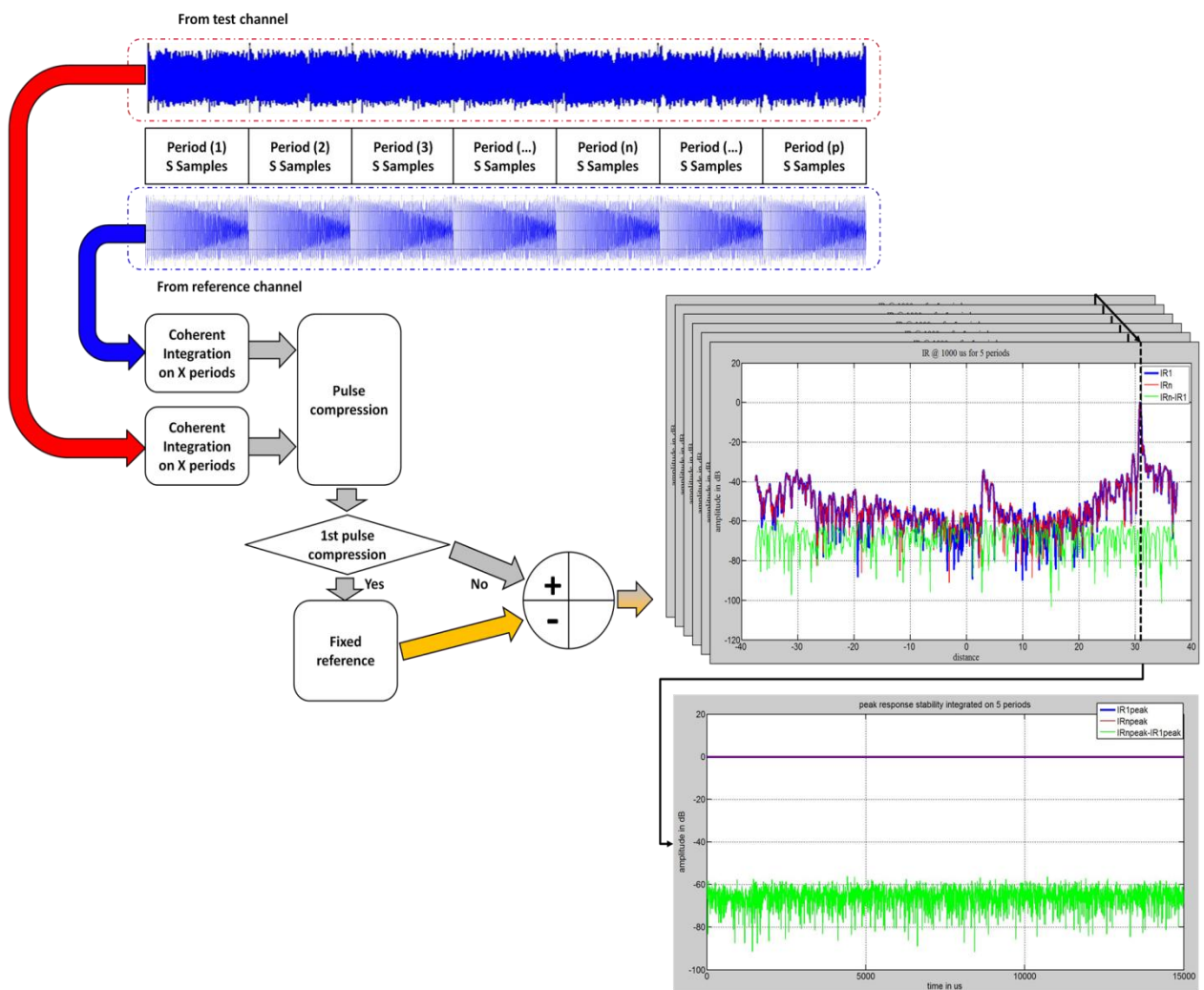


Figure 64: stability measurement protocol

c) Doppler Experiments

The objective is to compare the waveforms responses to Doppler effects and observe how it affects the waveforms. The comparison will be made on the responses in the velocity dimension. Hence the full algorithm exposed in (section Chapter 4.B) will be used. Only the integration limit has to be determined to avoid range walk. On the available surface, even with a car, the target's maximum speed is of the order of 10m/s. Thus range walk will occur if the signal is integrated over 18.75ms with 800MHz. However, to observe micro Doppler, this rule has to be breached and the integration time is set to 0.15s. The PRP was set to $0.5\mu\text{s}$ to allow longer acquisitions up to 6.5seconds with burst acquisition at 5 kHz.

Reproducible experiments on moving targets outdoor are not feasible with the equipment available and also the human factor is a problem. Further details on Doppler experiments with moving targets can be found in Appendix Chapter 9.L.

The solution devised was to use an active transponder to emulate Narrowband Doppler in an anechoic chamber. When the transponder shown in Figure 65 receives a signal, the signal goes through a power splitter connected to a direct path and a path with modulation. The modulation is performed via a mixer. The received signal goes in the local oscillator input of the mixer, the modulation in the IF input and the RF output is connected to a power combiner. The modulation is a square signal with $\pm 0.8\text{V}$ amplitude and 20kHz frequency. The other input of the power combiner is fed by the direct path. The combined signal, which is the sum of the received signal and the modulated signal, is then amplified and sent back in through the transmitting antenna in the same direction. Thus this target creates two fixed echoes due to the primary reflection on the antennas, and a delayed response with amplified sum of the received signal and its modulation. The advantage with this device is that no synchronization is required and the modulation is always the same. The signal returns always occur at the same time after the radar starts emitting. The result is shown in Figure 65. Thus this experiment is perfect for the comparison. However, there is a downside to it: this is a modulation emulating narrowband Doppler not actual Doppler. Thus the conclusions drawn from those experiments will be valid for narrowband only.

For this experiment; the digitizer has changed to a DSA71254 high speed digitizer because the Neptune VXS2 was out of order. This new digitizer's basic sampling frequency is 50GS/s and can only be divided by an even number. Given the sampling frequency subset, two qualified as valid candidates 3.125GS/s and 6.25GS/s. The first was eliminated because the useful signal bandwidth crosses over two Nyquist bands, which would cause aliasing. Thus with 6.25GS/s, there is no baseband sampling. However the digitizer has only 8bits resolution. The anechoic chamber, named CAMERA, is located at Onera in Palaiseau. Its dimensions are 12m deep, 6m wide and 6.4m high. It is designed for measurements from 0.6GHz up to 40GHz. The measuring pole where the targets are placed is made of polystyrene and is completely invisible to radar signals. In this configuration the targets on the measuring pole is in the direct line of sight of the radar system. Since the setup is located in an anechoic chamber and the range is reduced, no simulations were required to estimate the clutter level and the power budget.

In Figure 65, the transponder was measured using signals with 800MHz bandwidth and a PRP equal to $0.5\mu\text{s}$ in continuous acquisition.

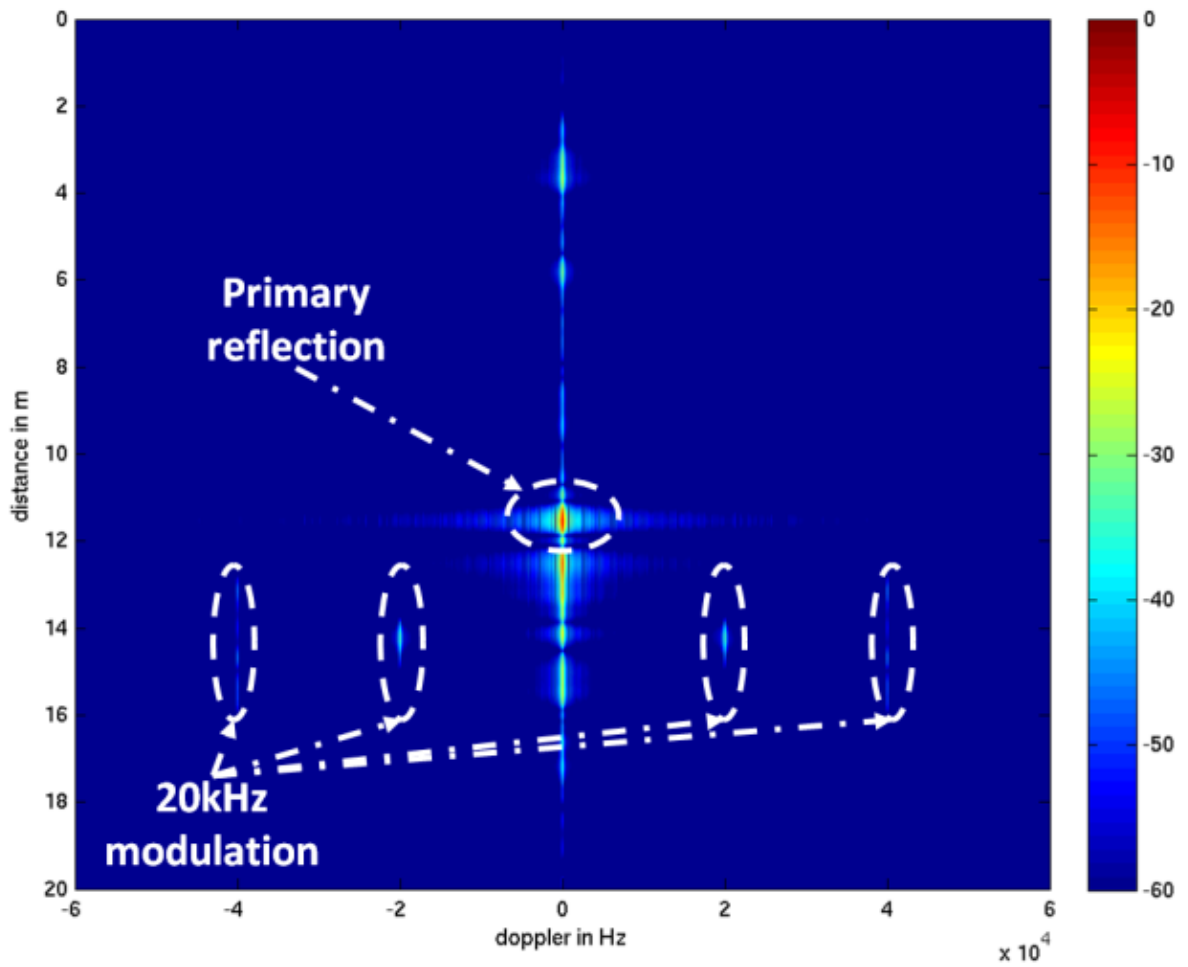
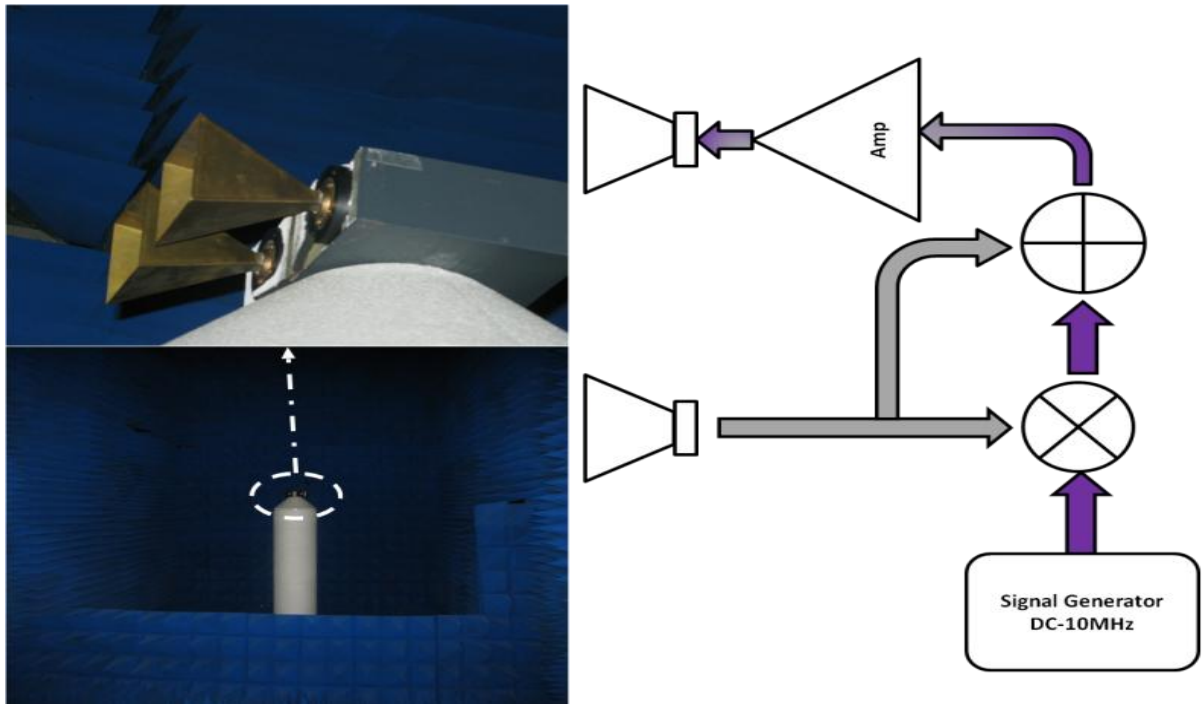


Figure 65: set up inside the anechoic chamber (top) optical view (bottom) radar view

After checking the static target case and the Doppler case, it was decided to experimentally determine the transmitting amplifier’s optimum input back off.

d) Experiment on Saturation with static targets

The objective of the experiment shown in Figure 66, is to evaluate the waveform optimum operating point for a given amplifier. To do so, the signals are injected in the solid state power amplifiers at various power levels, from about 6dB below IP1dB up to saturation levels. For the power amplifier PA-95105-4050, the input power range range should be $-17dBm \pm 6dB$, as demonstrated in Appendix Chapter 9.M. The experiment measures a reference and the reflected signal from a triangle corner reflector @ 46m. Thus the pulse compression can be performed either with the measured reference or a simulated reference. In this experiment the signals are digitized in IF @ 2GS/s.

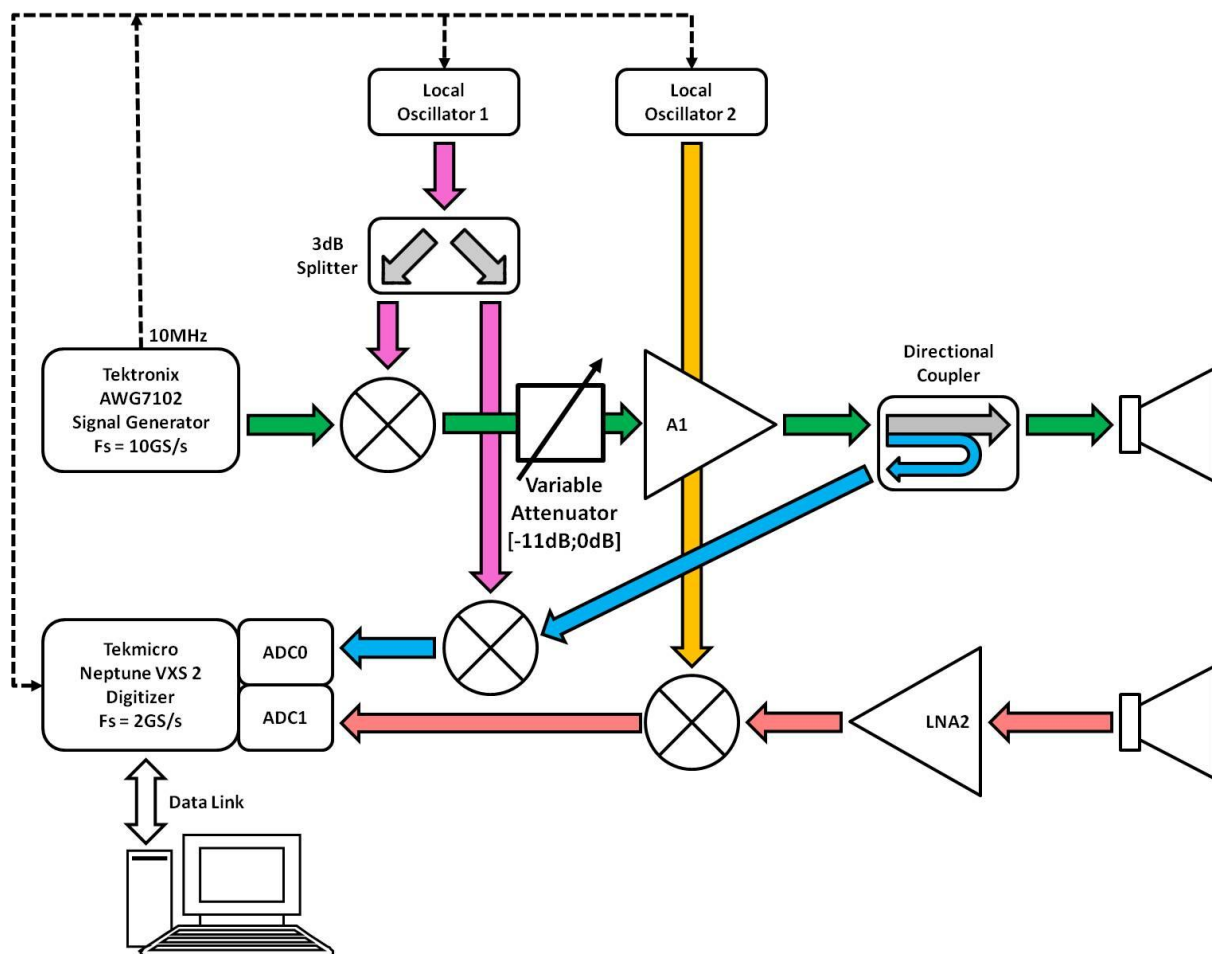


Figure 66: saturation experiment synoptic

C. Conclusions

A reconfigurable radar test bench was implemented; its characteristics in orange are compared in Table 25 to the RF platforms that were studied in the literature review. This platform's performances match the state of the art from 2006. Indeed the digitizer Neptune VXS 2 (74) was at the time the digitizer with the largest instantaneous bandwidth 3.3GHz, highest sampling frequency 2GS/s for 10bit resolution ADCs. The characteristics of this platform match or outperform the studied platforms in term of instantaneous bandwidth, frequency tuning range, tested range, sampling frequency, bit resolution and waveform testing capabilities.

Platform	PANDORA APAR	HYCAM	Garmatyuk et al.	IDROMel	UWB Software defined radar HYCAM v2
Instantaneous Bandwidth	384MHz 776MHz with guard bands	800MHz	500MHz	20MHz	800MHz Up to 1.6GHz
Experimental range resolution	0.39m 0.19m	X	0.3m	X	0.1875m
Tested range	X	10m	1.5m – 5m	X	60m
Sampling scheme	Shannon	Sub-Nyquist Bandpass	Shannon	Shannon	Bandpass Sub-Nyquist
Sampling frequency	X	1.35GS/s	1GS/s	X	2GS/s
resolution	X	10bits	8bits	X	10bits
Frequency Tuning range	8-12GHz	10-11.6GHz	7-8GHz	400MHz-7.5GHz	10-11.6GHz
Max Tx Power	X	10dBm	14dBm	15dBm 21dBm	19dBm 26dBm
architecture	Super-heterodyne Stretch-Processing	Super-heterodyne Frequency-interleaving	Super-heterodyne	Super-heterodyne 4x4 MIMO I/Q channels	Super-heterodyne parallel
waveforms	Stepped-Multitones, Multiband-FMCW	Phase-Coded Multitones	Phase-coded OFDM	UMTS, GSM, IEEE.802.11/16	Any
Pulse width	3.125ms per step	100ns-200ns	128ns-513ns	Dependent on standard	Depend on waveform

Table 25: comparison of the experimental UWB reconfigurable radar HYCAM v2 to the RF platforms from the literature review

Concerning the receiver characteristics in terms of gain, NF and Noise power, the receiver gain is low. However, the experimental ground covers ranges up to 60m, thus it is sufficient. The NF is elevated because of the numerous components that compose the receiver channel. For operational radar, this particular figure should be kept to the minimum by carefully selecting components or by designing a custom radar circuit using lithography and MMIC components for optimum performances.

In this reconfigurable radar, a dedicated channel was used to measure a reference in order to have a more accurate match filter. From experience, it was determined that the match filter could be generated from a digital reference. Using a dedicated reference channel is costly, so comparing measurement results using a measure reference and a digital replica should give some insight on the importance of a reference channel. Indeed the expected advantage is the correction of the circuit transfer function, but at the cost using only 50% of the reachable instantaneous bandwidth if both ADC channels were used together with sub-Nyquist sampling. This could also simply mean at equal instantaneous bandwidth that the reference channel should be removed completely, thus reducing hardware complexity and saving the cost of an extra ADC.

This platform also incorporated off-line data processing for distance-Doppler analysis. The algorithm uses radix-2 FFT to reduce the MACS. Considering state of the art digitizer (Proteus V5 (74) @5GS/s and 10bits resolution) and the increase in required processing power, FPGA families Altera Stratix V (75) and Xilinx Virtex 6 (76) are announcing over 1TMACS each . Thus processing power for real time signal processing is achievable. The real bottleneck is data throughput and storage. In this case, recording data continuously required a throughput of 10GB/s per channel. No commercially available bus exists that announces throughputs of this order: National Instruments NI-PXIE-1075 (77) announces up to 4GB/s. For data storage, the problem is more complicated, since the recording speeds with the latest NI-HDD-8264 (77) go up to 600MB/s. This shows that the bottleneck is in the middleware where with increasing sampling frequencies and the race for higher resolution, the data throughput will keep increasing. Thus, real time signal processing will require much work to size down the raw data for bus communication and data storage.

The parking experiments allowed working out the radar final design by fixing the problems experimentally. Two minimum radar capabilities were extracted: the minimum measured radar cross section -20dBsqm for a cat and the minimum measured speed 0.14m/s with a pedestrian swinging his arm both 27m away from the radar. These two parameters indicate the good quality in terms of detection of the radar platform.

Four experiments were designed to compare the multitones with the chirp. The objective was to design reproducible experiments to allow the comparison of consecutively measured waveforms. Experience shows that reproducible experiments outdoor are extremely hard to perform, even on static targets. The experimenting ground had at times uncontrollable elements that perturbed the experiments: wind, rain, cars, people, parasite transmissions... Indoor or even in an anechoic chamber would be a more controllable environment, but nothing beats live experiments to test waveforms. This allows taking in all parameters for operational radar system, predictable or unpredictable.

The results from those experiments will now be analyzed in the next chapter.

Chapter 7. Experimental Results

In this chapter, the experimental results extracted from the measurements on four different setups will be analyzed and compared to the simulated results. It will be organized as in Chapter 6.B.4 going from least to most distortions in the waveform. First, the results of the Closed-loop DAC-Filter-ADC measurement will be presented to verify the effect of quantization on performances. Then, using the full test bench, the stability of the pulse compression peak response on a triangle corner reflector results will be analyzed. In third, the Doppler effects on waveform performances will be studied and thus test their resistance to target velocity. Finally, the saturation will be studied in order to determine the best Input Back-Off for the power amplifier.

A. Closed-loop DAC-Filter-ADC

The DAC-Filter-ADC experimental measurements described in section Chapter 6.B.4.a) are now analyzed in the following subsections. It will start with a PMEPR analysis followed by a power efficiency analysis and finally by the pulse compression analysis.

1. PMEPR

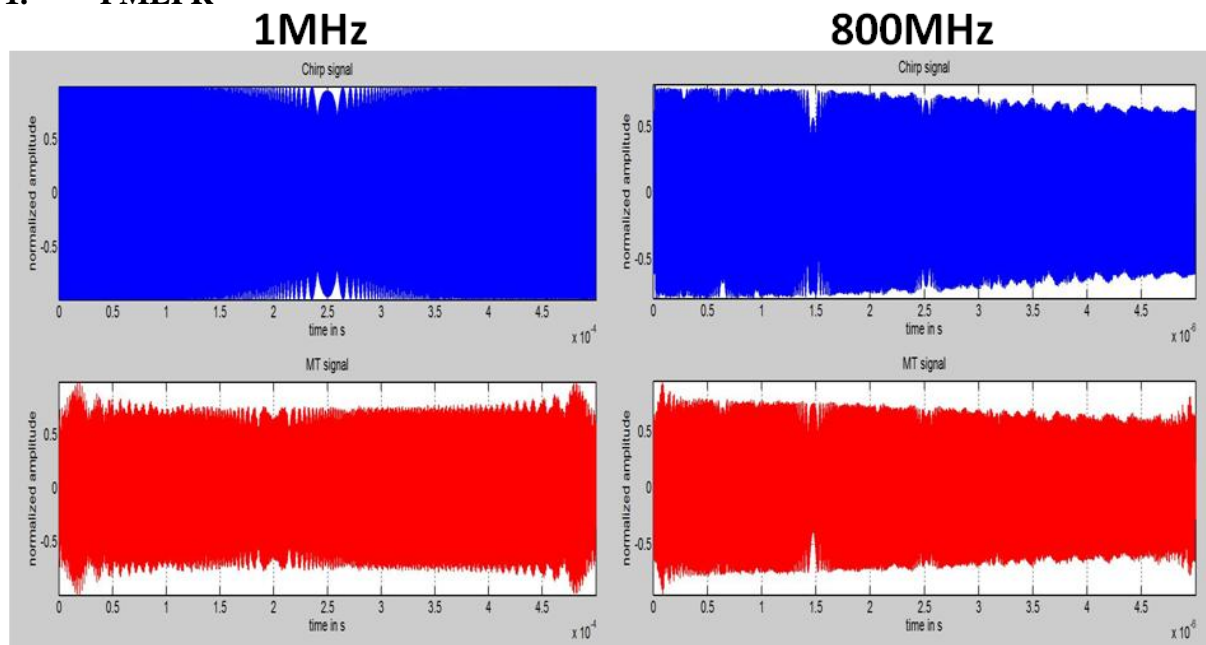


Figure 67: measured chirp and Multitones signals at 1MHz and 800MHz

From Figure 68, the measured PMEPR for multitones and Chirp are consistent with simulations on the closed-loop DAC-filter-ADC experiment, with a difference between measured and simulated values ranging from -0.19dB to 0.8dB. The PMEPR for multitones is in the range [5dB; 6dB]. As for Chirp, PMEPR increases as the signal bandwidth grows closer to the receiver instantaneous bandwidth. The differences in PMEPR between both waveforms are within the range [1.5dB; 2.5dB].

From simulation results, it was determined that 4 bits were sufficient to reach the nominal value of PMEPR. On this experiment, upgrading the resolution from 8 to 10bits only affected the result on PMEPR by 0.15dB, which is negligible. This confirms the hypothesis on bit resolution for PMEPR.

In the experiment description in Chapter 6.B.4.a), it was specified that the anti-aliasing filter was too wide, and some of the frequency contents from the 1st and 3rd Nyquist Band leak into

the 2nd Nyquist band, thus the recorded signals can be distorted. Also, the gain isn't flat over the full bandwidth, as illustrated in Figure 67. This might have contributed to the PMEPR degradation. However, the simulated and measured results on PMEPR match, and this wasn't predictable a priori.

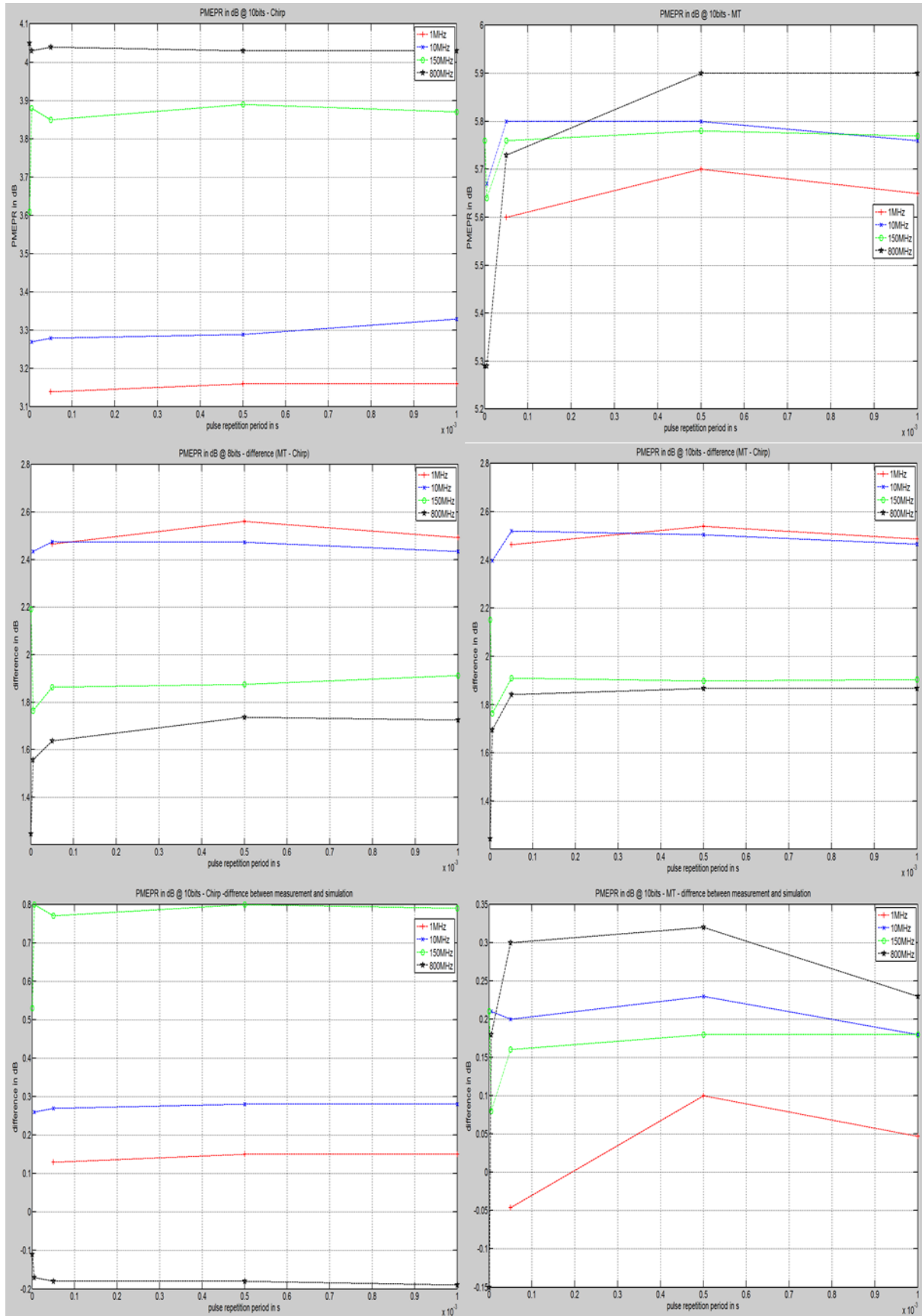


Figure 68: top: PMEPR @ 10 bits for chirp and multitones, middle: difference between multitones and Chirp @ 8 and 10bits, bottom: difference between measurement and simulation @ 10 bits for chirp and multitones

2. Power efficiency

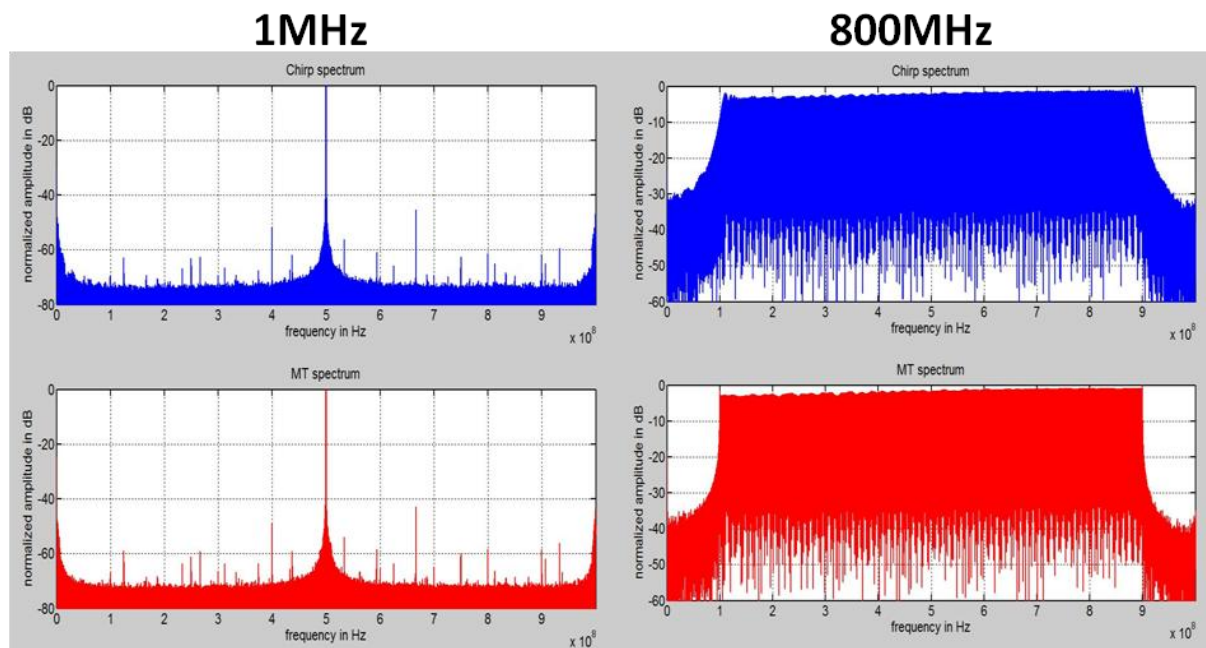


Figure 69: Measured spectrum of chirp and Multitones at 1MHz and 800MHz

From Figure 70, the measured power efficiency is within 10% of the expected value and its general behavior is consistent with simulations. Also, the difference between 8 and 10 bits resolutions is at most 0.62%, against 10% in simulation. So, this indicates that changing the DAC resolution from 8 to 10bits for this experiment has little impact on this feature This confirms the idea that 8 to 10bit resolution is sufficient to get near nominal values for power efficiency.

Figure 69 displays the measured spectrum of chirp and multitones for 1MHz and 800MHz. It illustrates in the frequency domain the unevenness of the gain response of the closed loop DAC-filter-ADC experiment. Some unwanted signals are visible in the narrowband case, which reduces the power efficiency of the narrowband signals, explaining the error. However, these are also present in WB case, but since they are buried in the useful bandwidth, they don't affect power efficiency.

Since we are in closed loop, the unwanted signals come from the test bench. This means that with a radar platform with a receiver bandwidth adapted and a fine tuning to have a clean spectrum, the power efficiencies in narrowband would match the simulated values. Thus, extrapolating from the wideband case on this performance criterion, the measurement results are coherent with expected values, and this wasn't foreseeable before experimental testing.

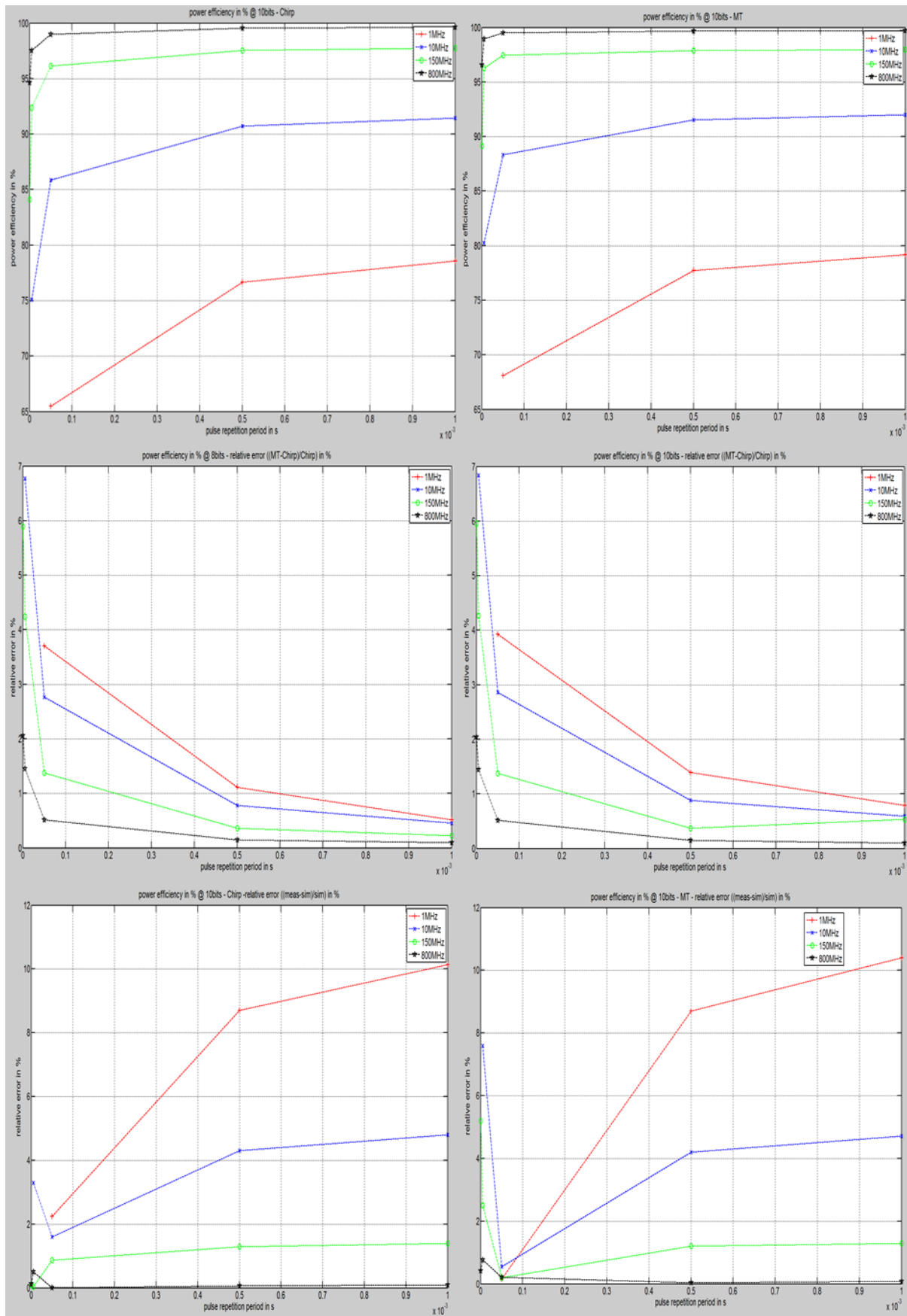


Figure 70: top: power efficiency @ 10 bits for chirp and multitones, middle: relative error between multitones and Chirp @ 8 and 10bits, bottom: relative error between measurement and simulation @ 10 bits for chirp and multitones

3. Pulse compression DAC-ADC measurements

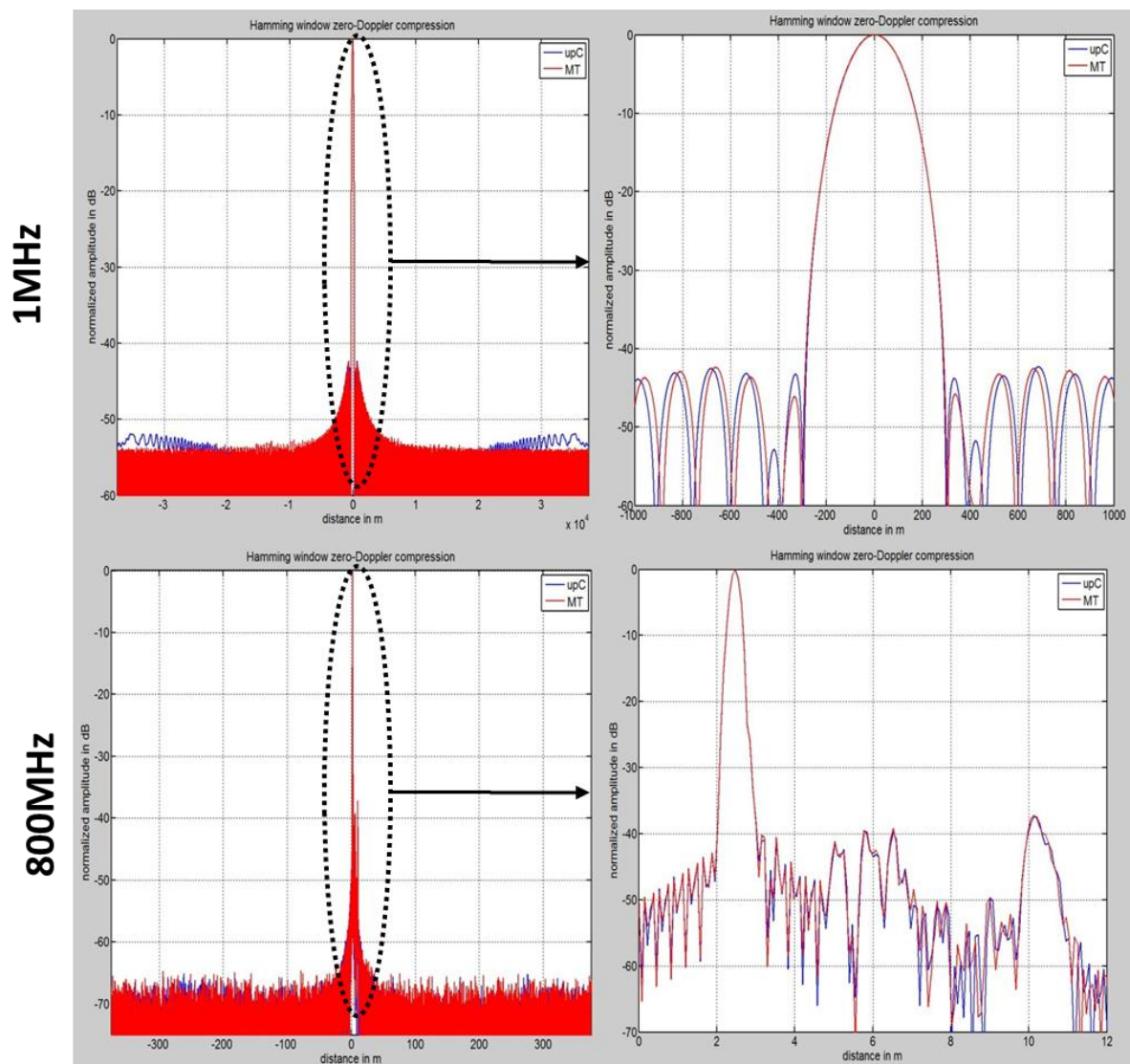


Figure 71: Compression in Distance of Chirp and multitones with (B 1MHz, PRP 500us) and (B 800MHz, PRP 5us) with Hamming window

The pulse compression was performed with a digital replica of the tested signals. The digital replica is a bandpass sampled version of the generated waveform. This generated waveform is sampled @ 10GHz and the digital replica @ 2GHz. The right hand side of the pulse compression presents reflections that are buried when the data is raw, but appear clearer when Hamming windowing is applied. The higher the bandwidth is, the more visible the circuit imperfections are, as shown in Figure 71. Indeed, problems with standing wave ratios cause uneven second sidelobes @ 800MHz, thus the second sidelobes' characteristics will be exploited only for signal bandwidth, from 1MHz to 150MHz.

Table 26, Table 27 and Figure 27 show the measured distance compressions: main characteristics and differences/errors between measurements and simulations.

Bandwidth	1MHz	10MHz	150MHz	800MHz
Mainlobe 3dB width	133m	13.3m	0.9m	0.15/0.225m
Sidelobe amplitudes	-13.3dB	-13.2dB	-13.3dB	-19.9dB/-10dB
Sidelobe positions	±215m	±21.5m	±1.425m	±0.3m

Table 26: Main characteristics of the pulse compression wrt bandwidth

Bandwidth	1MHz	10MHz	150MHz	800MHz
Mainlobe 3dB width error	<1.9%	<1.8%	<2.3%	<37%
Sidelobe amplitudes difference	<0.3dB	<0.3dB	<0.3dB	-7dB / 3dB
Sidelobe positions	<0.7%	<1.7%	<3.1%	<67%

Table 27: relative error on 3dB mainlobe width, sidelobes' positions and difference in sidelobes' amplitudes between measurements and simulations

In Table 27, the large errors for 3dB mainlobe width and sidelobes positions @ 800MHz are caused by sample speck and perturbations induced by standing wave ratios in the circuit. Otherwise, the other signals from 1MHz to 150MHz are within 3.1% of expected values, for 3dB mainlobe width and sidelobe positions, and the difference in sidelobes amplitudes are lower than 0.3dB. Also both waveforms are equivalent on pulse compression. These results are really close to the expected values and the matching performances indicate good quality regarding the test bench.

The pulse compression displays large errors @ 800MHz caused by reflections in the circuit. From the results obtained for the other signals, reducing the standing wave ratios in the circuit would result in a good match between expected and measured performances @800MHz. In other words, imperfections in the circuit can be overlooked for narrowband systems as it only affects the pulse compression by fractions of dBs. As the bandwidth increases, the imperfections cause impairments and are visible in the distance compression. For radar systems, these reflection levels need to be reduced below target detection thresholds to avoid causing false alarms. Also, in presence of two targets close from one another, one big target and one small, the reflection level may mask the smaller target, thus they should be kept below the desired contrast.

Furthermore, increasing the bandwidth allows locating smaller targets; however, a greater care has to be put to system reflections, as the sources of those reflections appear in the pulse compression. The upside is that with a high bandwidth, the sources of reflections can be more accurately located in the circuit.

Concerning Equation 20: minimum number of useful bits necessary to digitize a signal with a given bandwidth-time product for pulse compression, the reflections in the circuit create secondary peaks that change the results on the error. Thus, this formula won't be experimentally validated.

4. Synthesis

The closed-loop DAC-filter-ADC measurements were remarkably close to the performance criteria's expected values. This allowed confirming the stability of PMEPR and power

efficiency with bit resolution of 8 to 10bits. This proves that the equipment used to perform the closed-loop experiment closely matches the simulation results obtained using perfect quantization process. These experiments showed that the digitizer technology was mature and that jitter is negligible. Thus simulation for high performance digitizers need not model the jitter. With state of the art digitizers, the expected performances in simulations will be the obtained performances in measurement.

B. Experiment on static targets: Stability measurements

The experiment presented in section Chapter 6.B.4.b) allowed determining the stability on the peak response of the compression in amplitude and phase over one pulse. The worst case results are displayed in Table 28, and the evolution of stability over 16ms is shown in Figure 72, for chirp and multitones with 1MHz bandwidth. The details of the measured stability are shown in Appendix 0.

The measurements on stability were obtained using a digital replica and a measured replica. The difference in stability between the two methods is lower than 0.7dB on the mean and minimum stability wrt relative error, thus both methods are equivalent.

Overall, the relative error in amplitude and phase is about -40dB in mean value and -30dB in minimum value. Both waveforms perform with equivalent performances wrt stability. Thus, stability depends mostly on hardware rather than waveform.

This measurement of -40dB in stability, shows the robustness of the system to clock drift. Note that stability measurements usually remain stable for a set period of time and then degrades with clock drift. Here two hypotheses can be considered: either the set time hasn't been reached, or the clock is stable. The latter is actually the most plausible, as the sampling clock for the ADC was generated using the DAC, thus when the clock drifts in the DAC, it drifts accordingly in the ADC. Moreover the aperture jitters of the converters are lower than 200fs, compared to a 500ns sampling period which is excellent. Finally the mean value found in measurement is of the order of the predicted -42.3dB in RMS quantization noise floor, established in Table 21 for the Neptune VXS2, with a sine wave @ 0dBFS based on ENOB + losses.

Relative error		1MHz	10MHz	150MHz	800MHz
Raw	Mean	-41.6dB	-40.1dB	-38.6	-39
	Min	-32.11dB	-27dB	-28.8	-27.9

Table 28: worst case relative error on stability wrt bandwidth with digital replica

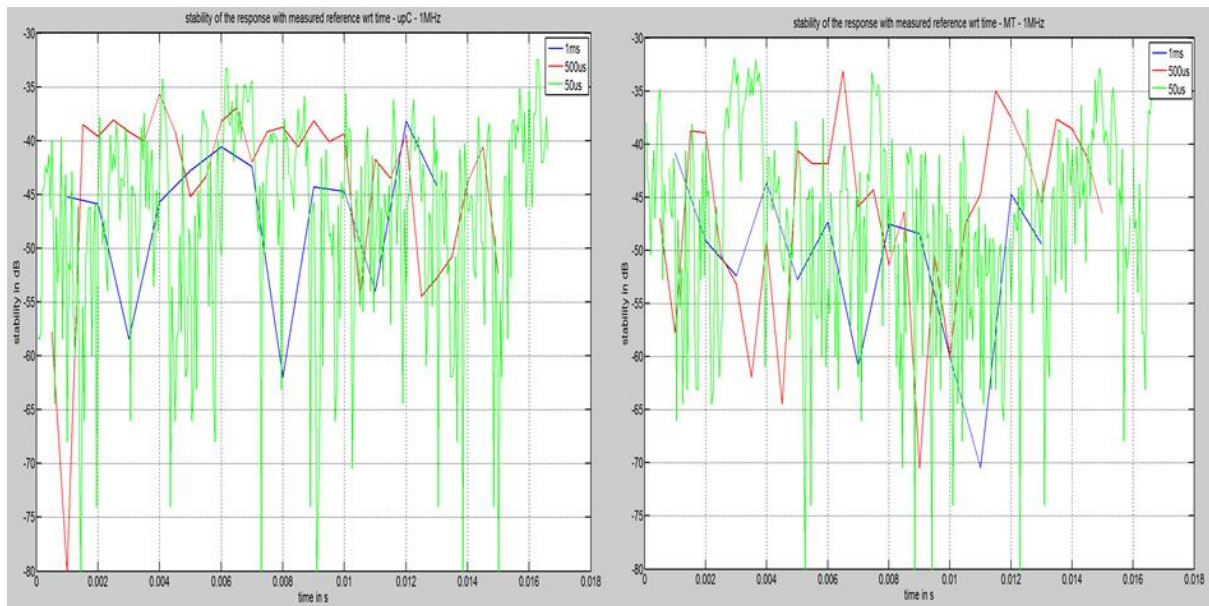


Figure 72: stability on the peak response of the pulse compression of a trihedral reflector placed @ 27m from the antenna for chirp (right) and multitones (left) @ 1MHz over 16ms with digital replica

C. Doppler Experiments

Figure 73 illustrates the results from the measurements obtained with the experiment with the active transponder, as described in section Chapter 6.B.4.c). The top half image represents the Doppler-distance obtained for both Chirp (left) and multitones (right) with 800MHz bandwidth and 500ns PRP. The bottom half represents the zero-Doppler cuts (left) and distance cuts (right). The distance cuts correspond to the modulated signal positions.

Figure 74 shows the amplitudes and Doppler shifts of the modulated signal in the distance cuts for both Chirp (left) and multitones (right) 1MHz and 800MHz bandwidths and their differences. The tendency shows that multitones perform better with modulation than Chirp on average between 0.5dB and 3dB. This differs from simulations, where both waveforms performed identically wrt modulation. The difference between measured and simulated results can't be explained directly. In (9), the multitones are used to improve time-varying target imaging. The multitones would improve imaging of target's creating signal modulation especially. Further experiments and analysis would be necessary to confirm the results on Doppler.



Note that the results on Doppler are emulated by a square wave modulation on the emitted signal, as described in Chapter 6.B.4.c). The effect of time-varying targets on the multitones phase and orthogonality has yet to be investigated. In effect, the phase variations caused by the moving target would first change the PMEPR, as the phase arrangement to insure low PMEPR would be broken, and the effect on compression is not known and would need to be quantified.

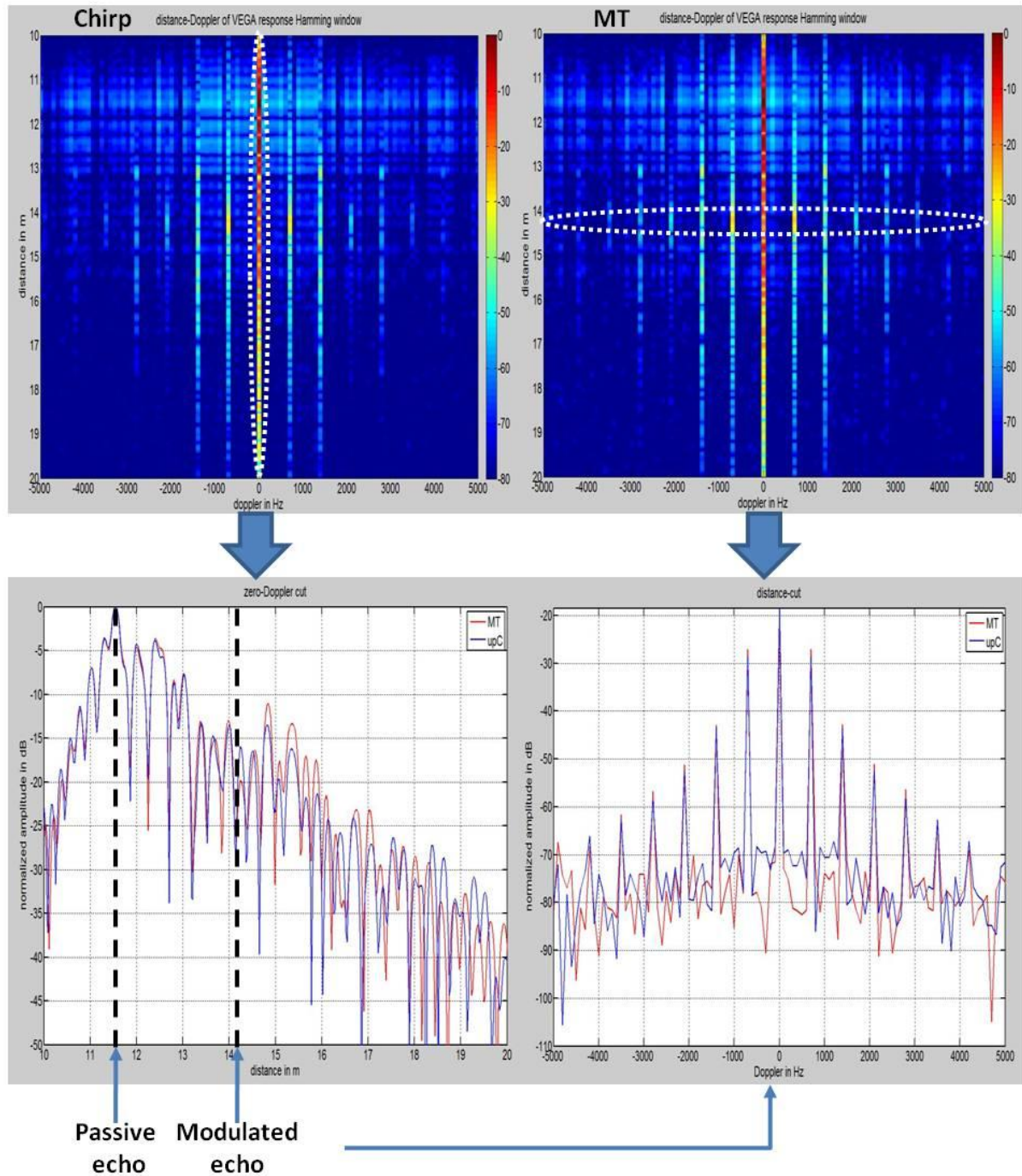


Figure 73: Doppler-distance images of the Doppler experiment top) Doppler-distance images bottom-left) zero-Doppler cut bottom-right) distance-cut

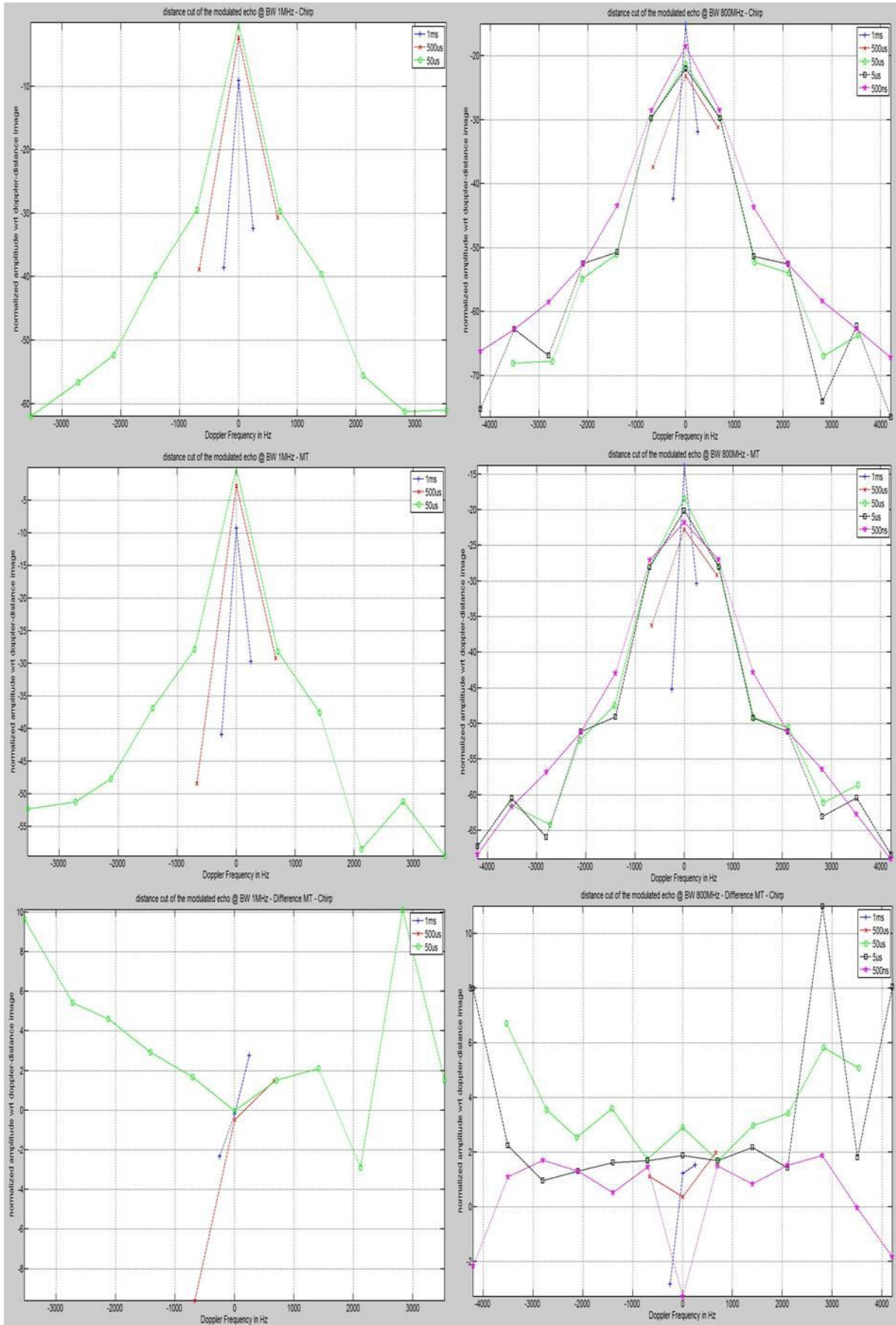


Figure 74: Amplitude of the modulation peaks of a 700Hz square-wave in the distance cuts @ BW 1MHz & 800MHz

D. Experiments on Saturation

The following results were obtained with the experimental set-up proposed in section Chapter 6.B.4.d) to study the saturation effects on performances. The first section will present an algorithm that allows recovering the main contribution of the test channel, in order to study its characteristics. In other words, the signal corresponding to the return from the strongest reflector, aka triangle corner reflector is recovered for study. Then the PMEPR of both reference and processed test channels will be analyzed for both chirp and multitones, followed by their power efficiencies. Finally, the pulse compression of both Chirp and multitones will be studied against saturation in two different configurations: first using a digital replica, and then using a measured replica.

1. Test channel recovery algorithm

In order to compare the performances criteria measured from the reference channel, an algorithm was implemented, as shown in Figure 75, to recover the echo from the triangle corner reflector. This algorithm introduces distortions in the spectrum and the PMEPR of the recovered echo. However, the objective isn't to get absolute values, but rather tendencies in PMEPR and power efficiency behaviors to fill the blanks in the reference channel data. The presence of other reflectors close to the main target may cause some strong variations in the recovered data⁷.

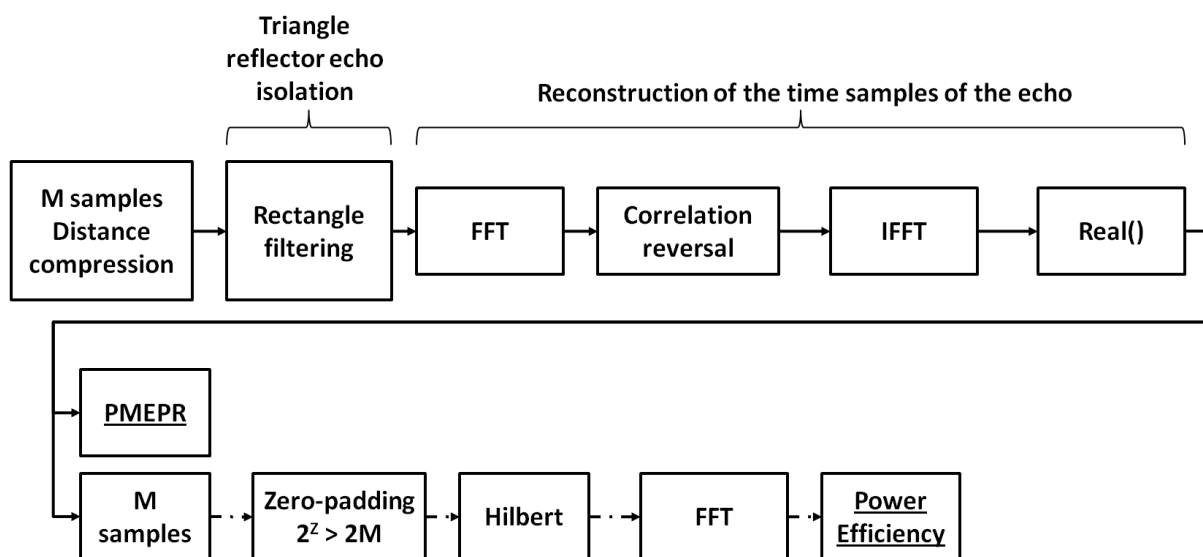


Figure 75: echo reconstruction algorithm from distance compression

Figure 76 shows the effect of the algorithm on data measured on the test channel, for multitones with 800MHz bandwidth and pulse repetition period of 500ns and 5us. The sum of all signal returns from the environment, result in a PMEPR between 8 and 12dB. Using the recovery algorithm reduces the PMEPR down to the range 4 to 5dB, but is lower than the multitones nominal PMEPR values and higher than the Chip nominal PMEPR. The rectangle filter applied to recover the echo distorts the signal resulting in lower PMEPR for multitones and higher PMEPR for chirp. The other side effect is the attenuation of the energy outside the useful signal bandwidth, thus improving power efficiency compared to the reference channel. Indeed, filtering effectively reduces the receiver bandwidth digitally, and so reduces the noise

⁷ A CLEAN algorithm, first introduced in (114), would normally be required to recover the main contributor from a “dirty” signal but it would be too long to implement.

power. Finally the recovery algorithm is sensitive to echoes close to reflector's echo, so odd values may appear in the recovered performance criteria.

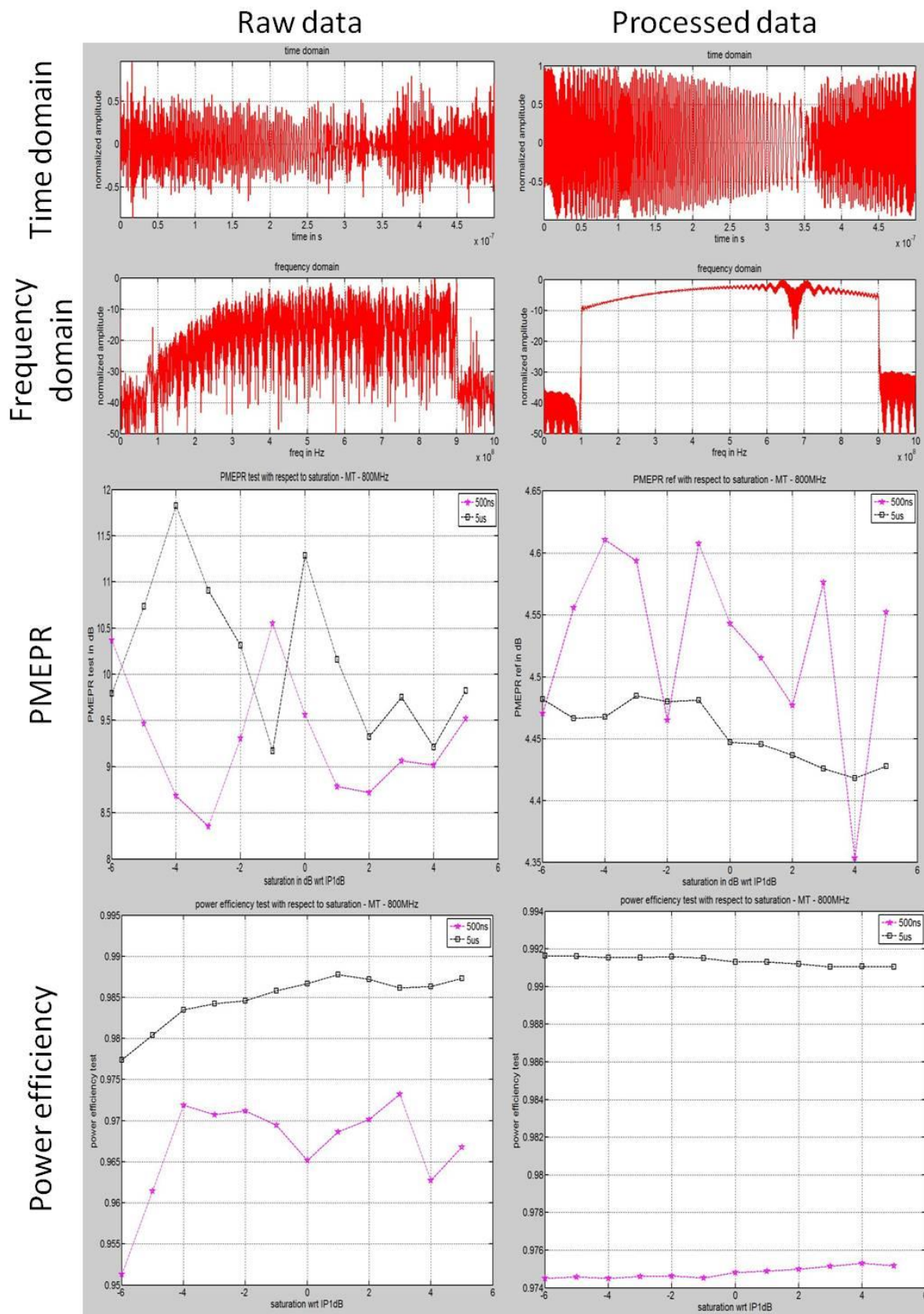


Figure 76: reversal algorithm effect on signal time and frequency domain, PMEPR and power efficiency for multitones with 800MHz bandwidth and 500ns PRP

2. PMEPR

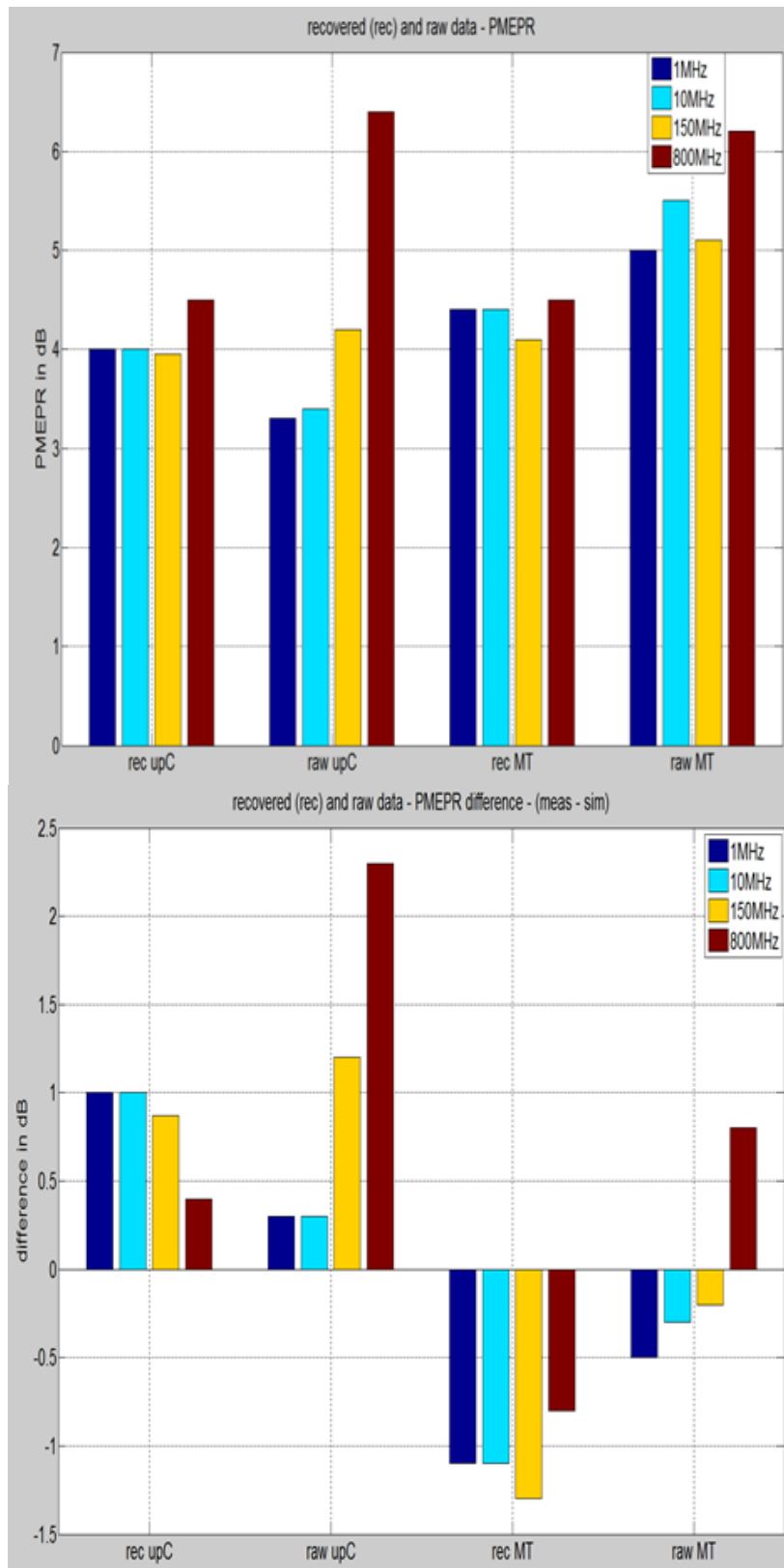


Figure 77: measured PMEPR from saturation experiment and difference between measured and simulated data

Figure 77 shows the average PMEPR measured over the range -6dB to 0dB, wrt 1dB compression point. The details of the measurement can be found in Appendix Chapter 9.O.1. From Figure 77, the effect of the recovery algorithm on chirps' PMEPR is visible: in narrowband, chirp PMEPR is elevated (4dB) compared to the raw data [3.3dB; 3.4dB]. In the wideband case, the raw data presents larger PMEPRs [4.2dB; 6.4dB] and is attenuated by the recovery algorithm [3.95dB; 4.95dB]. Multitones PEMPRs are within [5dB; 6.2dB] for raw data and lower values between [4.1dB; 4.5dB], using the recovery algorithm. These values indicate that the reference channel presents stronger distortions than those observed in the previous experiments.

For this experiment a different power amplifier PA-95105-4050 was used to improve transmitted power. It involved adding extra component in the reference channel to measure the reference at the amplifier output. These added components probably cause further standing waves in the reference channel. Also the amplifier band pass starts dropping from 10.5GHz, thus signals with 150MHz bandwidth ranging from 10.325MHz to 10.475MHz, and 800MHz bandwidth ranging from 10GHz to 10.8GHz are affected by the gain loss problems, especially chirp as its spectrum is clipped. This means that the information gathered from this experiment will concern signal bandwidth up to 150MHz.

The fact that multitones is unaffected by the gain loss @10.5GHz shows its robustness. When the allocated bandwidth is limited, multitones can use larger bandwidth than chirp without being affected. This confirms the conclusion on receiver bandwidth drawn in the close-loop experiment that the closer the signal bandwidth gets to the receiver bandwidth, the smaller the gap between chirp and multitones is. This concept can be generalized to component bandwidth as well.

In Figure 77, the difference between measured and simulated PEMPR is no more than 0.5dB except for Chirp @ 150MHz with a difference of 1dB because of the amplifier cut off frequency. This means that the values for PMEPR are pretty close to the expected values in the saturation experiment.

The difference in PEMPR between both waveforms ranges from 0.52dB to 2.37dB. Chirp would have a detection range from 3% to 14% greater than multitones, the gap reduces as bandwidth increases.

3. Power Efficiency

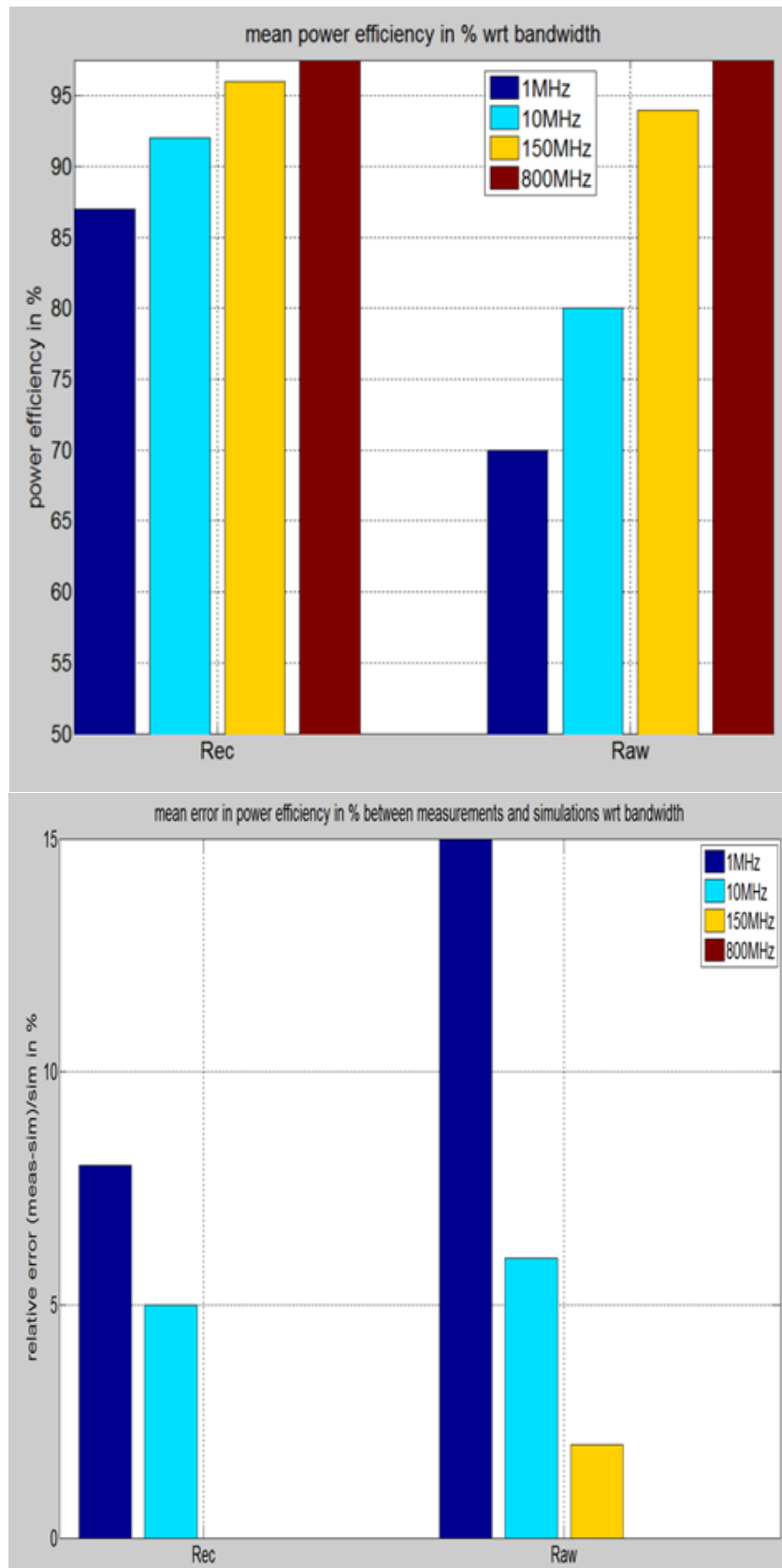


Figure 78: measured power efficiency from saturation experiment and error between measured and simulated data for multitones

Figure 78 presents the measured results for power efficiency or raw and recovered data. The details of the measurements are available in Appendix Chapter 9.O.2. Multitones and Chirp performances do not differ much, only the power efficiency of multitones are presented in Figure 78.

From 1MHz to 150MHz both waveforms are equivalent in power efficiency. From Figure 78, performances are lower than expected values in saturation, and the error between measurements and simulations goes up to 15%. The power amplifier PA-95105-4050 has a larger noise figure than the previous amplifier, and the extra components in the reference channel increase the noise power in the receiver bandwidth, therefore reducing the power efficiency. Also, the experiment was realized using the amplifier output power level @ IP1dB+6dB as the ADC full scale. Over the studied range the signal power varied at the ADC output, but the noise power remained constant. This reduces power efficiency in the linear region of amplification.

All these reasons explain the reduction in power efficiency compared to expected values. Looking at the recovered power efficiencies, they are greater than the expected values, because the data was filtered therefore reducing noise power level. The error on recovered data goes up to 8%.

Observing the results on power efficiency shows a perfect match between simulated and measured values @ 800MHz in both cases. This means that even though there is a power drop at the edge of the bandwidth, most of the energy is concentrated there. It also implies that this evaluation tool is not complete concerning spectral efficiency, and that new performance criteria should be measured to complete the analysis such as amplitude and phase distortion analysis, adjacent channel power ratio and noise power ratio⁸.

4. Compression

In this section, two methods of compression were tested to evaluate the need to implement a reference channel in the radar system: compression with a digital replica, and compression with a measured replica.

The expected advantage of a measured replica is a more accurate matched filter, compensating the transmitter transfer function (see section Chapter 4.C.3). This would result in a more accurate pulse response, however as the amplifier gets closer to saturation levels, a ringing appears on the curves which gets more pronounced as the input power increases. This is probably caused by increasing noise in the reference signal due to saturation.

On the other hand, the pulse compression realized with a digital reference is very close to what is obtained using a measured reference. Also the ringing phenomenon is not present as the digital replica is “perfect”. Note that the compression still works with saturated signals using a digital replica.

Figure 79 shows the pulse compression of the same signal using measured and simulated reference signal. The performances are similar which illustrates the ringing phenomenon with a measured reference, for an input power of IP1dB. A study on stability would reveal if this

⁸ The noise power ratio is measured using a notch of 10% of the total signal bandwidth at its center to evaluate noise power and in band intermodulation power during amplification.

ringing in the pedestal hinders the measurement or not and to what extent. Other than that, both methods display equivalent performances.

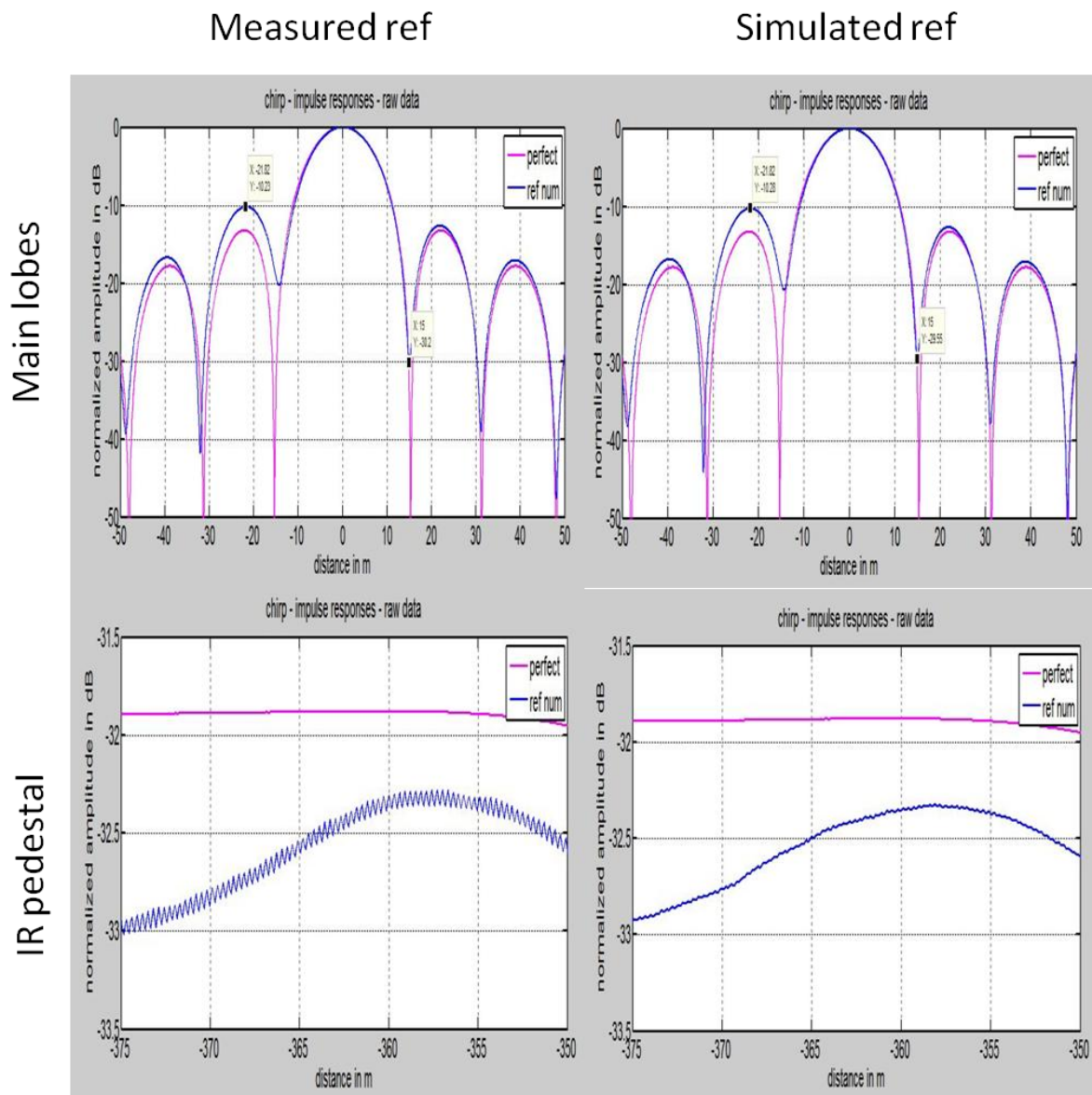


Figure 79: impulse response of a chirp with 10MHz bandwidth and PRP 5us @ IP1dB

The main characteristics of the pulse compression are shown in Table 29 and Figure 80. The detailed measurements are available in Appendix Chapter 9.O.3 through 5. The performances of multitones and chirp were quite similar, so only the multitones’ performances are presented in Figure 80.

Bandwidth	1MHz	10MHz	150MHz	800MHz
Mainlobe 3dB width	133m	14m	0.9m	0.3m
Sidelobe amplitudes				
• Left	-13dB	-10.5dB	-14dB	-21dB
• Right upC/MT	-13dB	-13.5dB	-11.5dB	[-9;-5dB]/[-15;-8]dB
Sidelobe positions	±215m	±21m	±1.35m	±0.3m

Table 29: measured compression characteristics from saturation experiment

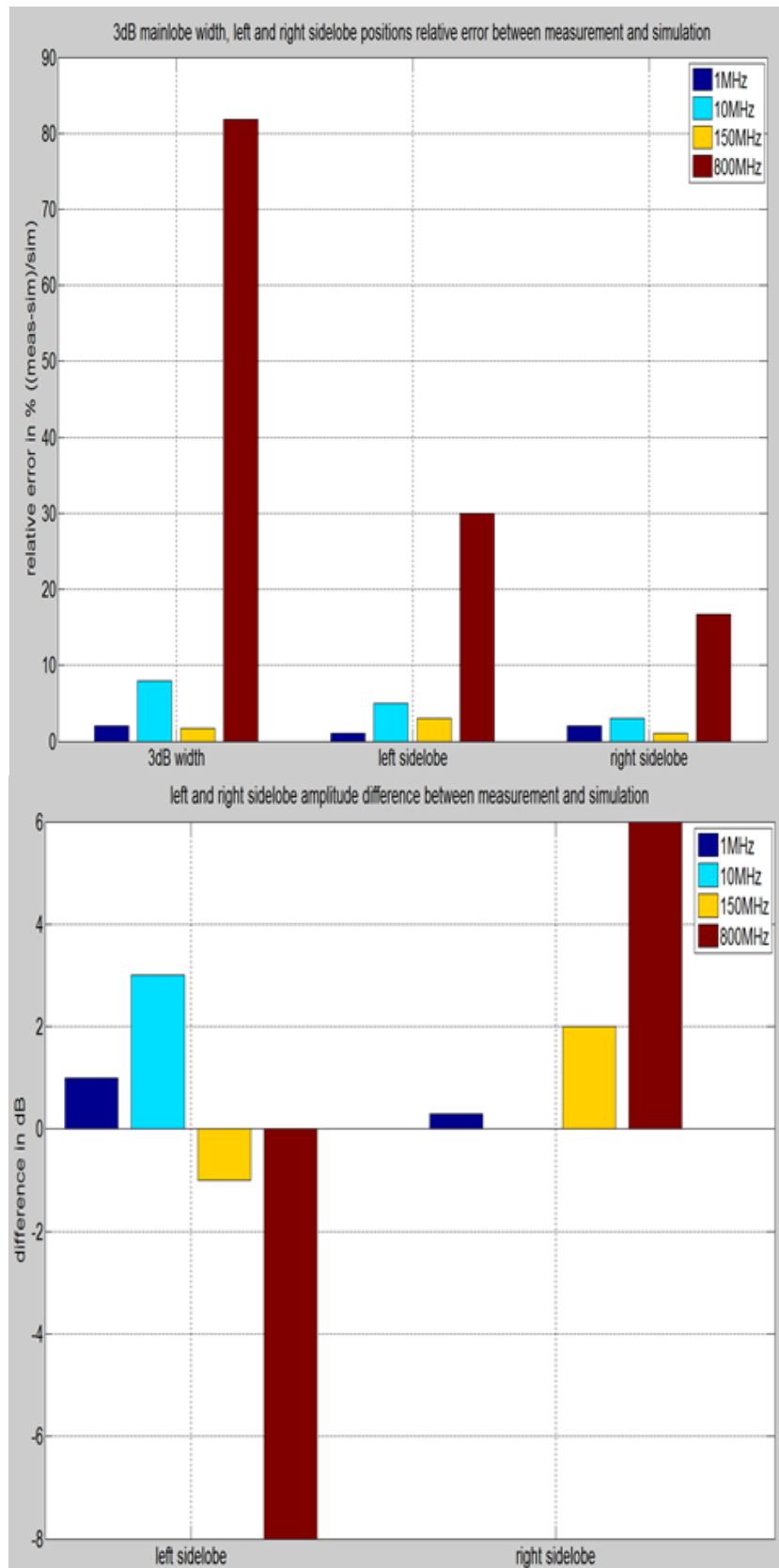


Figure 80: relative error and differences between measurement and simulation of the impulse response characteristics for multitones

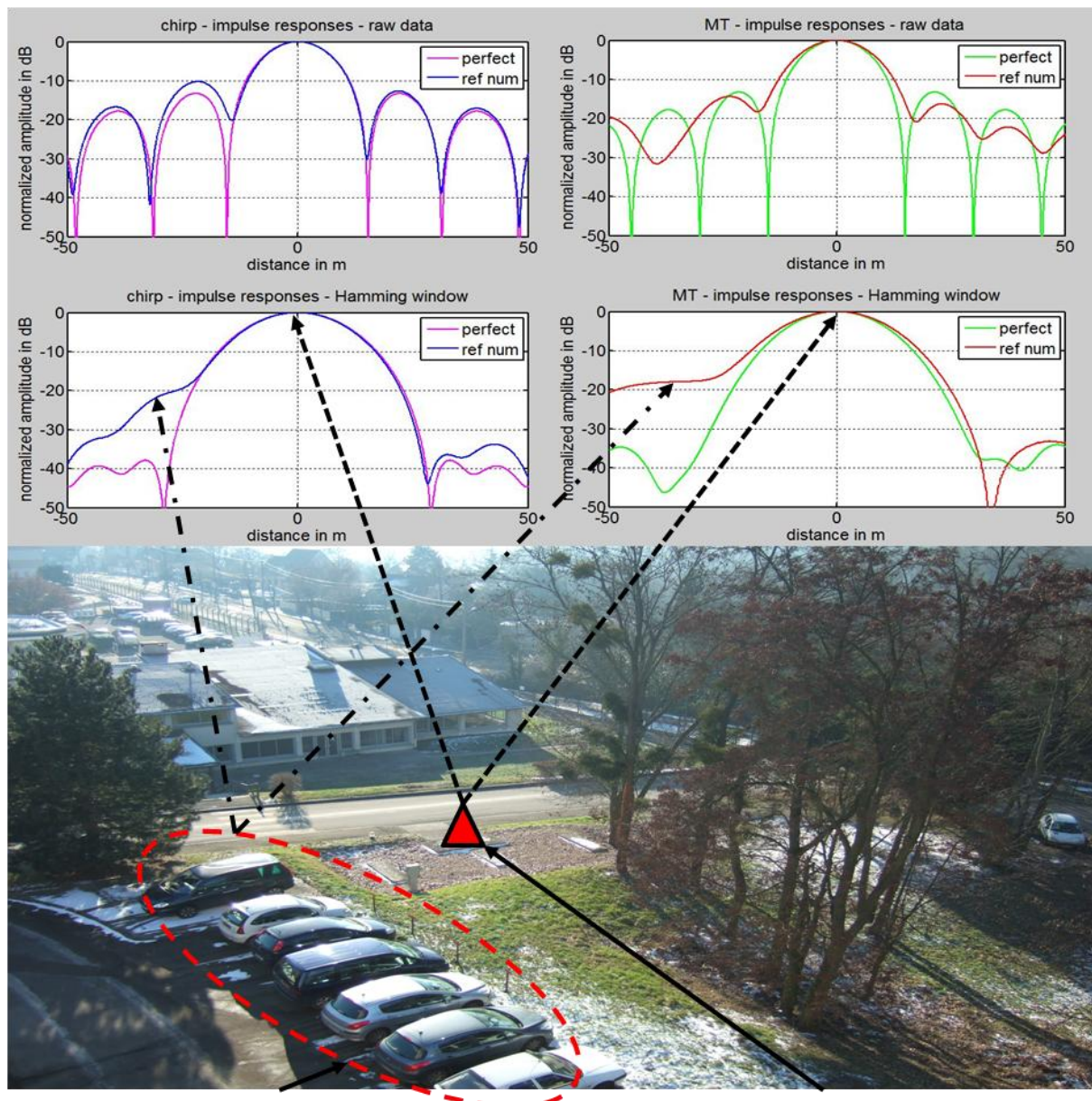
The results in Table 29 show that the values for 3dB bandwidth and sidelobe positions match the expected values with error lower than 10% up to 150MHz. For 800MHz bandwidth, the signal is distorted and sample speck error amplifies the problem, resulting in an error of 80%. The sidelobes' positions are also affected, with an error on position up to 45%.

On the other hand; the sidelobes' amplitudes do not display results close to the simulations. Only the compressions with 1MHz bandwidth match simulations. This configuration has the coarsest spatial resolution (150m), thus the experimentation ground holds in one distance cell. For the other bandwidth configurations, as the spatial resolution is refined, the impairment in sidelobes' amplitudes increases. The multiple returns from the experimentation ground result in several peak responses, some very close to the reflector's peak. Also, using a variable attenuator has a side effect on pulse compression. Indeed, the standing wave ratio of the transmitter channel ahead of the amplifier changes when the attenuation is changed. Thus, the reflections near the peak response increase as attenuation decreases. All these distort the main contributor response, thus the sidelobes' amplitudes for bandwidth from 10MHz to 800MHz will be ignored.

The performances of both waveforms, Chirp and Multitones, are comparable in terms of 3dB mainlobe width and sidelobes' positions, but not on the sidelobes' amplitudes, except with 1MHz bandwidth. This is mainly explained by the various changes in the environment during the measurements, resulting in strong discrepancies in measured sidelobe levels. Further details on the changes in the environment are given in the following section.

a) Discussion on saturation measurements

Figure 81 illustrates the scene where the saturation measurements were performed. The red triangle shows the position of the trihedral reflector, and the red ovoid shows targets in the line of sight. The discrepancies between Chirp and multitone side lobes in amplitude, and 3dB main lobe width, are partially caused by the change in the targets in the radar line of sight. Indeed, the measurements were not simultaneously performed, thus the scene changed over time. In other words, the number of cars varied over the time span of the measurement. This is valid for both NB and WB measurements. In Figure 81, the impulse responses clearly show a strong return on the left of the main lobe for multitones but not for Chirp, showing the presence of cars in the multitone impulse response but not in the Chirp impulse response. However, in WB another factor comes into play. The reflections in the circuit are increasing as the attenuation ahead of the amplifier reduces, thus creating another imbalance in amplitudes.



Targets in the LOS

Trihedral corner reflector

Figure 81: Difference between multitones and Chirp impulse response on the saturation experiment

5. Synthesis on saturation

The saturation experiment wasn't as fruitful as expected, but further validations on the signal behavior were drawn, and some of the simulation results with saturation were verified.

The measurement results were coherent with the simulations for narrowband signals especially. The discrepancies on PMEPR, power efficiencies were mainly caused by the setup, which presented mismatched components, introducing distortions and added noise power. So choosing components matched to our requirements would improve the quality of the measurement. Also, it is important to mention that the ADC dynamic range was set to the maximum amplifier output power. Hence, when the input power was increased from -6dB to 6dB wrt IP1dB, the amplifier output level presented at the ADC input was not measured @

full scale over the entire input power range. A more accurate set-up would need to adapt the ADC dynamic range to the amplifier output over the full studied input range. Respecting those two requirements would produce better results.

The difference between multitones and Chirp drops down to about 1dB when the signal bandwidth draws near the component instantaneous bandwidth. On operational radar systems, all component bandwidth match the receiver bandwidth for optimum performances, thus the difference between Chirp and multitones average powers should be about 1dB. This difference in average power would result in an extra 6% in detection range for chirp. Considering the saturation level up to 1dB, the multitones average power difference could drop to 0.5dB, thus reducing the extra range between chirp and multitone to 3%.

Also this experiment showed that the compression of a saturated pulse with a perfect digital replica was possible, and resulted in a close match to the pulse compression with a measured replica. However, when strong standing wave ratios were present, the measured replica allowed compensating for the reflections better than the perfect replica. This means that digital radar, with well-tuned circuitry with low standing wave ratios, could operate without implementing a reference channel. This would mean for this test bench that the receiver bandwidth would be doubled by removing the dedicated reference channel, and using both ADCs in sub-Nyquist sampling in the test channel. It could also mean that the number of required channels would be halved, compared to an architecture with reference channels, thus reducing hardware cost and complexity.

E. Conclusions

The experiments proved that the measurements matched the results obtained using perfect quantization. This indicates the degree of accuracy of the AD/DA converters (AWG7102 (86) and Neptune VXS 2 (74)) used in this experiment, which had aperture jitters lower than 200fs. This accuracy is confirmed from the stability measurements, with a mean relative error on peak response subtraction of -40dB. With state of the art converters from 2006, the simple simulation results allowed accurate predictions of the PMEPR, power and efficiency and compression performances. Future converters will have improved performances compared to that. This means that more complex modeling of jitter effect is unnecessary in that case. The requirements on bit resolution for radar systems could be dimensioned using this simple simulation process, rather than complex modeling.

The results from the experiments on saturation are mitigated, considering the discrepancies between measured and simulated values. Even though, the measurements are coherent with simulations and display similar traits. This showed that the experimental set-up didn't match the simulation process. This was explained by mismatched components and variable power level wrt to ADC's full dynamic range. The results are indeed mitigated, but the simple simulation that was performed yielded coherent results. Thus, assuming a more adequate experimental set-up, the measured results would be closer to the expected values.

Throughout the experimental results, there was a recurrent theme about signal bandwidth compared to receiver bandwidth. In radar systems, the receiver bandwidth is matched to the signal bandwidth. This cuts off some of the Chirp spectrum, thus raising its PMEPR, and effectively reduces the gap in average power between both waveforms. Given unbound spectrum and linear properties, the average power difference between Chirp and Multitones is about 2.5dB. When considering the receiver bandwidth matched to the signal bandwidth, this

difference drops to about 1dB. It is common in a radar system using Chirp to widen the receiver bandwidth to keep good signal properties and avoid spectrum clipping. Multitones could actually allow slightly reducing receiver bandwidth to slightly improve the SNR level, or use the full receiver bandwidth to slightly improve the spatial resolution. In any case, the conclusion of these measurements is that Chirp and Multitones have equivalent performances. The chirp's maximum detection range is extended by 6% wrt multitones maximum detection range. Also the maximum achievable SNR using the full ADC dynamic range would be 1dB higher for Chirp than for multitones, thus improving a little detection performances and consumption at the ADC and amplifier stages.

The Doppler experimental results demonstrated that multitones outperforms chirp when measuring a squarewave modulation. The difference in modulation response could go as high as 3dB on the modulation peaks in the Doppler-distance image. This indicates that multitones may have better detection capabilities on scintillating targets than Chirp. This matter should be further investigated using live targets to ensure the validity of these results

Chapter 8. Conclusion

In this section, the results on all three objectives: RF architecture, effect of RF components on performances, and the comparison between multitones and chirp performances are gathered. Here the conclusions of the study are presented and commented. Also further developments and perspectives are proposed to complete the study and work towards the software defined radar. Finally the communications in conferences that were published during this thesis are listed.

A. Conclusions

The three objectives that were set at the beginning of this work were:

- To develop a ultra wide band reconfigurable platform able to support any kind of waveforms
- To determine the effect of RF equipment on radar performances
- To compare the performances of multitones and chirp

The first objective led to the implementation of a reconfigurable radar platform which has an instantaneous bandwidth of 800MHz and a frequency tuning range in X band of 1.6GHz. The RF architecture was designed to support any kind of waveforms.

To relieve constraints on both converters and DSPs, super heterodyne structures are used to bring the IF frequency range up to the desired RF frequency range. This obviously comes with a price: degraded signal purity. To insure that intermodulation products don't fall in band for up and down conversion, the design rules from Table 13 and Table 14 should be respected. Several intermediate up and down conversion stages might be required to insure signal purity for large frequency tuning range e.g 2-18GHz. However, the number of stages should be kept to the minimum, as a larger number of intermediate stages would result in a higher noise figure.

The second objective was to study the impact of RF equipment on performances. This thesis focused on AD/DA converters and power amplifiers.

The converters are sufficiently reliable to reach expected radar performances. This displays the degree of maturity of the converters, since their aperture jitter can be overlooked in the simulations to dimension the radar. However low cost converters do not have such a degree of accuracy in aperture jitter. So measured performances from low cost converters might differ from simulation results with perfect quantization.

It was determined that a minimum of 10bit resolution is required to get nominal performances for PMEPR, power efficiency and the main response (3dB mainlobe width and second sidelobe characteristics) of pulse compression. Nevertheless, higher resolution will reduce the pedestal error in the compression. Furthermore, the simulations with perfect quantization are sufficiently accurate to determine experimental radar performances.

Since it was found that the simulated performances matched the measured performances, the issue of experimentation could be raised. Indeed looking at the results a posteriori, the simulations alone would be sufficient. But this was actually not predictable beforehand. Experimental validation is always interesting to ascertain the findings in simulation and take into account circuit imperfections. This means that system performances could be determined

using simple simulations, before purchasing expensive equipment to validate a concept. The designer could make sure the expected performances meet the requirements using simple simulations, rather than complex models that are awkward to tune properly.

The saturation does not degrade neither PMEPR, nor power efficiency, nor the main response of the pulse compression. The saturation process barely affects the compression pedestal. Hence the maximum detection will be obtained at the amplifier 1dB compression point.

The third objective was to compare the performances of multitones wrt those of chirp. Based on the performance criteria chosen multitones is almost as good as chirp. Overall the difference in maximum detection range is lower than 6% and the difference in SNR is lower than 1dB.

Furthermore, the first results on modulation showed that multitones had improved detection capabilities compared to chirp. If this waveform is already neck and neck with chirp, and if these performances on modulation were confirmed, then multitones would offer improved performances in the detection of scintillating targets.

This study showed that multitones are suited for software defined radar. Multitones are neck and neck with chirp and are easily reconfigurable. The evolution of digital technologies and their proven reliability and robustness, now opens the way to develop software defined radar. Further evolutions though are required in the RF front end to replace banks of components or multiple stages by adaptive circuitry.

B. Perspectives

Building on the obtained results, this subsection will present several propositions and perspectives to further this study.

In order to complete the comparison between both waveforms, the Doppler should be studied in real conditions, using a synchronization technique combined with a moving target that can reproduce the same motion over and over. In this thesis, the processing algorithm allowed distance-Doppler compression. The next logical step to continue the comparison of waveforms would be to implement detection algorithms to evaluate the SNR required by each waveform for a given alarm rate ($<10^{-3}$).

The chosen performance criteria showed little degradation with saturation, especially with efficiency. But the power efficiency doesn't give a full picture of the saturation process, indeed there is amplitude and phase distortions, in-band and out-of-band intermodulation power levels. The signal should be measured over the full amplifier bandwidth to get the full picture. Obviously, a different set of performance criteria might yield different results for the optimal operating point. This should be investigated to refine our findings

It was mentioned in the introduction the future development of software defined radar. Software defined radar is a platform that can adaptively switch between various radar modes such as surveillance, tracking, terrain mapping, etc... This requires modifications of both the waveform and signal processing tasks to match the new radar mode. These reconfigurations have to be performed dynamically. This also implies that a certain level of intelligence is implemented to manage the resources, and adapt the radar mode according to its environment.

Being able to dynamically reconfigure the emitted signal is a key feature for a software defined radar that has to switch between different radar modes. Software defined radar are able to sense their environment and adapt the radar mode accordingly. This enables interferers' identification and adapting the radar emission and reception to avoid these interferers by switching off frequencies. This feature could also be used in a context of spectrum insertion, where the software defined radar would have to respect regulations. Including notches in a signal have consequences, and the effects should be studied on compression mostly.

It was established that multitones perform almost as well as chirp for basic radar. So why use multitones? Multitones for the software defined radar presents a very interesting feature for dynamic reconfiguration. Indeed, this waveform is purely digital, so tones can be turned on and off at will. This only requires changing the values from 0 to 1 in the vector defining the tones amplitudes.

Working towards operational software defined radar requires to overcome a few technological limitations. The AD/DA converters still need to improve their bit-resolutions, instantaneous bandwidth and sampling frequencies to allow for direct synthesis and digitization higher in the spectrum. This also calls for improvements in processing power of DSPs and FPGAs, higher bus throughputs and finding means to size down the flow of raw data.

Performing adaptive signal processing would require further developments in digital architecture management and reconfiguration.

Concerning the RF architectures, adaptive RF blocks especially filters need to be developed to adapt the component characteristics to match the bandwidth of operation and thus maximize detection capabilities. The choice of sampling scheme (direct, bandpass, subnyquist) should be taken in account when developing the platform.

In conclusion, for software defined radar to be operational several technological breakthroughs are required and multitones offers the qualities required for adaptive reconfiguration, both in the transmitted signal and the processing algorithms.

C. Publications & Communications

Communications

Julien Le Kernec, Philippe Dreuillet, Gérard Bobillot, Juan-Carlos Castelli, Patrick Garda, Olivier Romain, Julien Denoulet, “Case study analysis of linear Chirp and multi-tones radar signals through simulations and measurement with HYCAM-Research Test Bench”, national conference GDR SOC-SIP (Research Group on System on Chip – System in Package), Orsay, France, 10-12 June 2009

L. Vignaud, J.-M. Nicolas, J. Le Kernec, “Radar high resolution range and micro-Doppler analysis of human motion”, Radar Conference - Surveillance for a Safer World, 2009. RADAR. International, IEEE, pp 1-6, Bordeaux, France, 12-16 october 2009, ISBN 978-2-912328-55-7

Julien Le Kernec, Philippe Dreuillet, Gérard Bobillot, Juan-Carlos Castelli, Patrick Garda, Olivier Romain, Julien Denoulet, “Case study analysis of linear Chirp and multi-tones radar signals through simulations and measurement with HYCAM-Research Test Bench”, Radar Conference - Surveillance for a Safer World, 2009. RADAR. International, IEEE, pp 1-5, Bordeaux, France, 12-16 october 2009,

Julien Le Kernec, Martin Klepal, Vratislav Sokol, “3D Directional Coupler for Impulse UWB - 3D Electromagnetic Simulation and Prototyping”, Interdisciplinary conference on instrumentation C2I'2010, HERMES, pp 1-8, Le Mans, France, 26-27 January 2010

Chapter 9. Appendix

A. Multicarrier advantages and drawbacks

Resistance to frequency selective fading

Multitone transmission is carried out in parallel on the different frequencies. This technique is desirable for the transmission of the digital data through the multipath fading channels. Indeed, the deleterious effect of fading is spread over many bits; therefore, instead of a few adjacent bits completely destroyed by the fading, it is more likely that several bits will only be slightly affected by the channel. (91)

Efficient bandwidth usage

The other advantage of this technique is its spectral efficiency. In the multicarrier method, the spectra of sub-channels overlap each other while satisfying orthogonality, giving rise to the spectral efficiency. Because of the parallel transmission in the multitone Technique, the symbol duration is increased. This has the added advantage to work in channels with impulsive noise characteristics. (91)

Immunity to delay spread and multipath

The guard interval principle illustrated in Figure 82 allows the Coded OFDM (COFDM) to support superposition of different paths “without troubles” (5). The guard interval of length N , is an overhead that results in a power and bandwidth penalty, since it consists of redundant symbols. (31) This is irrelevant for radar systems with no communications.

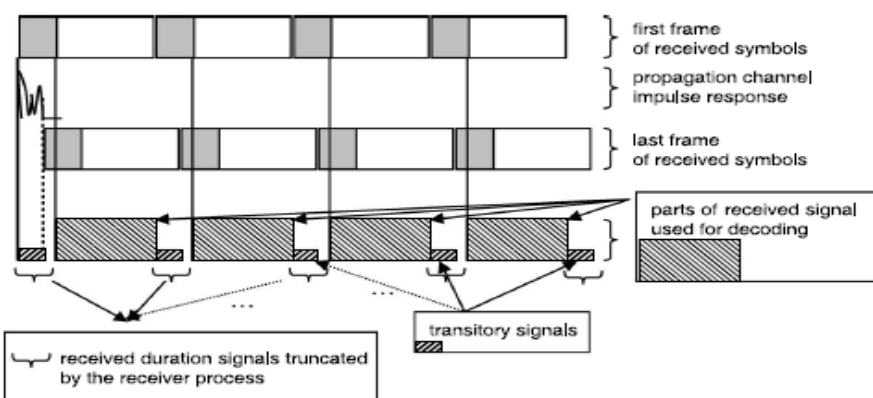


Figure 82: guard interval principle (5)

Simple equalization

Ease of equalization is often touted as the primary advantage of OFDM. However, the advantage is not exclusive to OFDM, similar equalization techniques can be applied to single-carrier systems as well (31).

Sub-band independence

Each sub-band in OFDM signal can be independently generated and processed, conceptually making it a “discrete linear-frequency modulated (LFM)” signal with selectable frequencies. In contrast to LFM, OFDM signal can be generated by purely digital means, without the need to continuously change the transmitted signal frequency (40).

Synchronization

An OFDM receiver operating in the acquisition mode must perform time synchronization, RF and sample clock frequency offset estimation and correction, and initial channel estimation. (31) This synchronization is not required for a mono-static radar system since both transmitter and receiver are in the same RF platforms thus all the clocks and local oscillators are already synchronized.

B. PMEPR reduction techniques

- Amplitude clipping and filtering

The operation consists in hard limiting the multitone signal peaks (92). The clipping causes in and out-of-band distortions. Filtering after clipping reduces out-of-band distortions but may also cause some peak regrowth (93) (94) . Hence an iterative algorithm is required to attain the desired amplitude level and a trade-off between the number of iteration and performances has to be determined.

- Coding

This scheme consists in phase coding each subcarrier in order to reduce the PMEPR. The codewords code with e.g binary phase shift keying, QPSK and MPSK with minimum PMEPR are chosen for transmission. The use of Reed-Muller with Golay complementary sequence (95) , reported by J.A. Davis and J. Jedwab (96), allows a PMEPR reduction down to 3dB for signals composed of $N = 2^M$ subcarriers. Further improvements and extensions to this approach can be found in (97) (98) (99). However, their use is limited and become intractable with large N. (100).

Using polyphase codes e.g. P3 and P4 codes (36) allows yielding at PMEPR of the order of 5dB (12). There is much less computation required but no data can be encoded.

- Other techniques also exist

Partial Transmit Sequence (PTS), (101) (102) (103) (104) (105), Selected Mapping (SLM), (106) (107) (108), Interleaving (109) (110) (111), Tone Reservation (TR) and Tone Injection (TI) (112) and Active Constellation Extension (113).

The effects of these schemes are summed up in Table 30 (32).

	Distortionless	Power Increase	Data Rate Loss	Requires processing at transmitter (Tx) and receiver (Rx)
Clipping and filtering	No	No	No	Tx: Amplitude clipping, filtering Rx: None
Coding	Yes	No	Yes	Tx: Encoding or table search Rx: Decoding or table search
PTS	Yes	No	Yes	Tx: M IDFTs, W^{M-1} vector sums Rx: Side information extraction, inverse PTS
SLM	Yes	No	Yes	Tx: U IDFTs Rx: Side information extraction, inverse SLM
Interleaving	Yes	No	Yes	Tx: K IDFTs, (K-1) interleavings Rx: Side information extraction, inverse interleaving
TR	Yes	Yes	Yes	Tx: IDFTs, find value of PRCs Rx: Ignore non-data-bearing subcarriers
TI	Yes	Yes	No	Tx: IDFTs, search for maximum point in time, tones to be modified, value of p and q Rx: Modulo-D operation
ACE	Yes	Yes	No	Tx: IDFTs, projection onto extended constellation Rx: None

Table 30: Comparison of PMEPR reduction techniques

These techniques developed for telecommunications show either increased hardware or software complexity with limited performance improvement compared to the added computational or hardware cost. The techniques for telecommunications require a specific number of carriers and an exhaustive search to get the codewords with the lowest PMEPR to about 3dB (32).

C. IDROMel

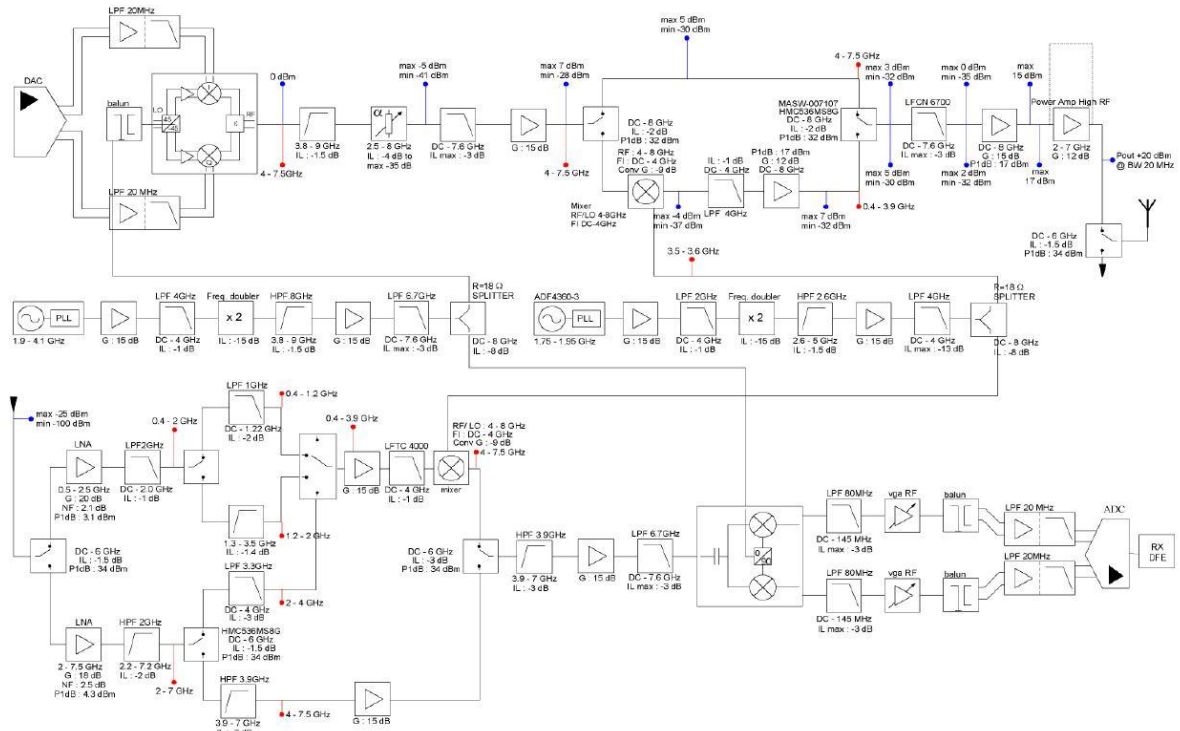


Figure 83: schematic of the IDROMEL architecture (46)

D. Processing Power calculations

1. Frequency Interleaved Architecture

If the frequency-interleaved architecture interleaves $2n$ signals, the received signal orthogonal time becomes $2nT_{orth}$ and the new vector length is $2nM$. After Hilbert Transform, the new vector size is $2nM$. Interleaving the channels in the frequency domain implies an extraction after digitization; hence the vector can't be zero-padded up to the next power of 2. Two cases are identified case 1 when $2nM \neq 2^Z$ and case 2 when $2nM = 2^Z$.

a) Case 1 $\rightarrow 2nM \neq 2^Z$

The DFT is used, if M is the vector length, hence M^2 complex multiplications and $M(M - 1)$ complex additions are required to perform a DFT. Thus the number of operations to get one impulse response is shown in Table 31.

	Cplx mult	Cplx add	Real mult	Real add
Hilbert transform				
► DFT	$(2nM)^2$	$(2nM)(2nM - 1)$	$(4nM)^2$	$4nM(4nM - 1)$
► Cplx mult $-j$	$2nM$	\emptyset	$8nM$	$4nM$
► IDFT	$(2nM)^2$	$(2nM)(2nM - 1)$	$(4nM)^2$	$4nM(4nM - 1)$
► Cplx add	\emptyset	$2nM$	\emptyset	$4nM$
Downconversion	$2nM$	\emptyset	$8nM$	$4nM$
DFT 1	$(2nM)^2$	$(2nM)(2nM - 1)$	$(4nM)^2$	$4nM(4nM - 1)$
Extraction	Memory access	Memory access	Memory access	Memory access
IDFT	$(nM)^2$	$(nM)(nM - 1)$	$(2nM)^2$	$(2nM)(2nM - 1)$
Downconversion	nM	\emptyset	$4nM$	$2nM$
Apodization	nM	\emptyset	$4nM$	$2nM$
DFT	$(nM)^2$	$(nM)(nM - 1)$	$(2nM)^2$	$(2nM)(2nM - 1)$
conjugate	\emptyset	\emptyset	\emptyset	nM
correlation	nM	\emptyset	$4nM$	$2nM$
IDFT	$(nM)^2$	$(nM)(nM - 1)$	$(2nM)^2$	$(2nM)(2nM - 1)$
Operations/impulse response	$nM(15nM + 4)$	$nM(15nM - 7)$	$4nM(15nM + 4)$	$6nM(10nM - 1)$
Operations/second	$\frac{M(15nM + 4)}{2T_{orth}}$	$\frac{M(15nM - 7)}{2T_{orth}}$	$\frac{2M(15nM + 4)}{T_{orth}}$	$\frac{3M(10nM - 1)}{T_{orth}}$

Table 31: number of operations per second for frequency interleaved architecture for DFT

b) Case 2 $\rightarrow 4nM = 2^Z$

The FFT radix-2 is used, if $M = 2^Z$ is the vector length, hence The number of complex operations to obtain one impulse response is shown in Table 32.

	Cplx mult	Cplx add	Real mult	Real add
Hilbert transform				
▶ FFT	$2^{Z-1}Z$	$2^Z Z$	$2^{Z+1}Z$	$3 \times 2^Z Z$
▶ Cplx mult $-j$	2^Z	\emptyset	2^{Z+2}	2^{Z+1}
▶ IFFT	$2^{Z-1}Z$	$2^Z Z$	$2^{Z+1}Z$	$3 \times 2^Z Z$
▶ Cplx add	\emptyset	2^Z	\emptyset	2^{Z+1}
Downconversion	2^Z	\emptyset	2^{Z+2}	2^{Z+1}
FFT 1	$2^{Z-1}Z$	$2^Z Z$	$2^{Z+1}Z$	$3 \times 2^Z Z$
Extraction	Memory access	Memory access	Memory access	Memory access
IFFT	$2^{Z-2}(Z-1)$	$2^{Z-1}(Z-1)$	$2^Z(Z-1)$	$3 \times 2^{Z-1}(Z-1)$
Downconversion	2^{Z-1}	\emptyset	2^{Z+1}	2^Z
Apodization	2^{Z-1}	\emptyset	2^{Z+1}	2^Z
FFT	$2^{Z-2}(Z-1)$	$2^{Z-1}(Z-1)$	$2^Z(Z-1)$	$3 \times 2^{Z-1}(Z-1)$
conjugate	\emptyset	\emptyset	\emptyset	2^{Z-1}
correlation	2^{Z-1}	\emptyset	2^{Z+1}	2^Z
IFFT	$2^{Z-2}(Z-1)$	$2^{Z-1}(Z-1)$	$2^Z(Z-1)$	$3 \times 2^{Z-1}(Z-1)$
Operations/impulse response	$2^{Z-2}(9Z+11)$	$2^{Z-1}(9Z-1)$	$2^Z(9Z+11)$	$2^{Z-1}(27Z+9)$
Operations/second	$\frac{2^{Z-3}(9Z+11)}{nT_{orth}}$	$\frac{2^{Z-2}(9Z-1)}{nT_{orth}}$	$\frac{2^{Z-1}(9Z+11)}{nT_{orth}}$	$\frac{2^{Z-2}(27Z+9)}{nT_{orth}}$

Table 32: number of operations per second for frequency interleaved architecture for FFT

2. Parallel Architecture

The parallel architecture has $2n$ channels and the received signal orthogonal time is T_{orth} on each channel. Two sliding window sizes are implemented. On the reference channels, the window size is M and $3M$ on the test channels. the vector can be zero-padded up to the next power of 2, thus the vector size is 2^Y for $4M \leq 2^Y$. Thus the total number of operations required to obtain an impulse response is shown in Table 33.

	Cplx mult	Cplx add	Real mult	Real add
Hilbert trans				
▶ FFT	$2^Y nY$	$2^{Y+1} nY$	$2^{Y+2} nY$	$3 \times 2^{Y+1} nY$
▶ mult $-j$	$2^{Y+1} n$	\emptyset	$2^{Y+3} n$	$2^{Y+2} n$
▶ IFFT	$2^Y nY$	$2^{Y+1} nY$	$2^{Y+2} nY$	$3 \times 2^{Y+1} nY$
▶ Cplx add	\emptyset	$2^{Y+1} n$	\emptyset	$2^{Y+2} n$
Down-conversion	$2^{Y+1} n$	\emptyset	$2^{Y+3} n$	$2^{Y+2} n$
Apodization	M	\emptyset	$4M$	$2M$
FFT 1	$2^Y nY$	$2^{Y+1} nY$	$2^{Y+2} nY$	$3 \times 2^{Y+1} nY$
conjugate	\emptyset	\emptyset	\emptyset	$2^Y n$
correlation	$2^Y n$	\emptyset	$2^{Y+2} n$	$2^{Y+1} n$
IFFT	$2^{Y-1} nY$	$2^Y nY$	$2^{Y+1} nY$	$3 \times 2^Y nY$
Operations/im pulse response	$M + 2^{Y-1} n(7Y + 10)$	$2^Y n(7Y + 2)$	$4M + 2^{Y+1} n(7Y + 10)$	$2M + 2^Y n(21Y + 15)$
Operations/s	$\frac{M + 2^{Y-1} n(7Y + 10)}{T_{orth}}$	$\frac{2^Y n(7Y + 2)}{T_{orth}}$	$\frac{4M + 2^{Y+1} n(7Y + 10)}{T_{orth}}$	$\frac{2M + 2^Y n(21Y + 15)}{T_{orth}}$

Table 33: number of operations per second for frequency parallel architecture

3. Time Interleaved Architecture

The number of channels is halved for time interleaving compared to the parallel architecture. A new parameter is also involved the reference refresh rate. Otherwise the algorithm is similar to the previous one. The required processing power is presented in Table 34

	Cplx mult	Cplx add	Real mult	Real add
Hilbert trans				
▶ FFT	$2^{Y-1}nY$	$2^Y nY$	$2^{Y+1}nY$	$3 \times 2^Y nY$
▶ mult -j	$2^Y n$	\emptyset	$2^{Y+2}n$	$2^{Y+1}n$
▶ IFFT	$2^{Y-1}nY$	$2^Y nY$	$2^{Y+1}nY$	$3 \times 2^Y nY$
▶ Cplx add	\emptyset	$2^Y n$	\emptyset	$2^{Y+1}n$
Down-conversion	$2^Y n$	\emptyset	$2^{Y+2}n$	$2^{Y+1}n$
Refresh- rate	r	r	r	r
Apodization	M	\emptyset	$4M$	$2M$
FFT 1	$2^{Y-1}nY$	$2^Y nY$	$2^{Y+1}nY$	$3 \times 2^Y nY$
conjugate	\emptyset	\emptyset	\emptyset	$2^Y n$
correlation	$2^Y n$	\emptyset	$2^{Y+2}n$	$2^{Y+1}n$
IFFT	$2^{Y-1}nY$	$2^Y nY$	$2^{Y+1}nY$	$3 \times 2^Y nY$
Operations/i mpulse response	$2^Y n(2Y + 3) + rT_{orth}M$	$2^Y n(4Y + 1)$	$2^{Y+2}(2Y + 3) + 4rT_{orth}M$	$2^{Y+2}n(3Y + 2) + rT_{orth}(2M + 2^Y n)$
Operations/s	$\frac{2^Y n(2Y + 3)}{T_{orth}} + rM$	$\frac{2^Y n(4Y + 1)}{T_{orth}}$	$\frac{2^{Y+2}(2Y + 3)}{T_{orth}} + 4rM$	$\frac{2^{Y+2}n(3Y + 2)}{T_{orth}} + r(2M + 2^Y n)$

Table 34: number of operations per second for frequency time-interleaved architecture

E. Transfer Function Compensation

Throughout this demonstration, we will remain in the frequency domain and add the various transfer functions effects to the original signal frequency and phase. We will demonstrate here the transfer function compensation capabilities for the different architectures. The radar operates in continuous wave mode. All the architectures presented in this thesis have the same circuit at the transmitter up to the amplifier output.

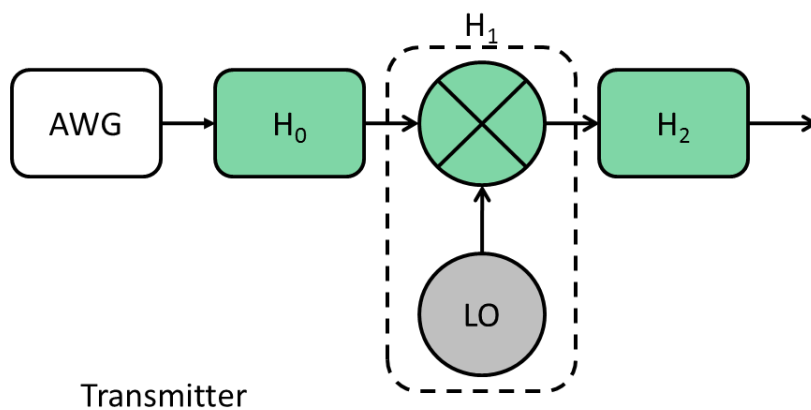


Figure 84: Common Transmitter transfer function block diagram

The three parameters considered in the transfer function are the amplitude Here the signal $S(1, f, \varphi)$ is generated by the Arbitrary Waveform Generator, travels through cables, filters and attenuators that corresponds to $H_0(A_0, f, \varphi_0)$. Then the resulting is upconverted $H_1(A_1, f_{LO} \pm f, \varphi_1)$ and then a filter selects the sum upconverted signal that is amplified $H_2(A_2, f_{LO} + f, \varphi_2)$. The resulting signal is S_{Tx} .

$$S_{Tx}(A_{Tx}, f_{Tx}, \varphi_{Tx}) = S(A_0 A_1 A_2, f + f_{LO}, \varphi_0 + \varphi_1 + \varphi_2)$$

This signal then follows different paths depending on the architecture

1. Frequency-interleaved

Two paths are present the reference in blue and the test channel in red travelling into free space. The reference is taken on the coupled output of the directional coupler $H_{dir2}(A_{dir2}, f_{Tx}, \varphi_{dir2})$. It then goes towards downconversion $H_{down1}(A_{down1}, f_{Tx} \pm f_{LO1}, \varphi_{down1})$ through cables, filters and attenuators $H_{ref}(A_{ref}, f_{Tx}, \varphi_{ref})$. The signal is downconverted with $f_{LO1} = f_{LO} + \Delta f/2$ where $1/\Delta f = T$ is the signal period. The downconverted signal goes through another set of cables, filters and attenuators $H_{s1}(A_{s1}, f + \Delta f/2, \varphi_{s1})$ as the upper IF product is filtered out. This signal then goes into the first input of the power combiner. Thus signal from the reference path is:

$$\begin{aligned} S_{PC1}(A_{PC1}, f + \Delta f/2, \varphi_{PC1}) \\ = S_{Tx}(A_{Tx} A_{dir2} A_{ref} A_{down1} A_{s1}, f_{Tx} - f_{LO1}, \varphi_{Tx} + \varphi_{dir2} + \varphi_{ref} + \varphi_{down1} + \varphi_{s1}) \end{aligned}$$

The test channel goes through the directional couple direct path $H_{dir1}(A_{dir1}, f_{Tx}, \varphi_{dir1})$. The signal then propagates into free space $H_{ch}(A_{ch}, f_{Tx}, \varphi_{ch})$. The signal returns are received amplified and filtered $H_{rx}(A_{rx}, f_{Tx}, \varphi_{rx})$ before downconversion $H_{down2}(A_{down2}, f_{Tx} \pm f_{LO}, \varphi_{down2})$. The downconverted signal goes through another set of cables, filters and attenuators $H_{s2}(A_{s2}, f, \varphi_{s2})$ as the upper IF product is filtered out. This signal then goes into the second input of the power combiner. Thus the signal from the test channel is:

$$\begin{aligned} S_{PC2}(A_{PC2}, f, \varphi_{PC2}) \\ = S_{Tx}(A_{Tx} A_{dir1} A_{ch} A_{rx} A_{down2} A_{s2}, f_{Tx} - f_{LO}, \varphi_{Tx} \\ + \varphi_{dir1} + \varphi_{ch} + \varphi_{rx} + \varphi_{down2} + \varphi_{s2}) \end{aligned}$$

At the power combiner output, the signal is the sum of S_{PC1} and S_{PC2} . This signal goes through the IF stage right before being digitized $H_{IF}(A_{IF}, f, \varphi_{IF})$. The signal before digitization is:

$$S_{ADC} = S_{PC1}(A_{PC1} A_{IF1}, f + \Delta f/2, \varphi_{PC1} + \varphi_{IF1}) + S_{PC2}(A_{PC2} A_{IF2}, f, \varphi_{PC2} + \varphi_{IF2})$$

So first of all; the reference channel compared to the test channel is modulated by $\Delta f/2$. In order to process it and determine the compensation that can accomplished with the reference. The signal's complex form is rebuild via a Hilbert transform. After extraction of the coefficients from both channels, the reference channel needs to be down-converted by $\Delta f/2$. This means that after extraction of both signals in order to perform compensation, the reference channel needs to be down-converted by $e^{i\Delta f/2}$. This results in two sets of complex coefficients that can now be expanded for comparison. The frequency components will be removed since we compare the coefficients at equal frequencies.

$$S_{PC1}(A_{PC1}A_{IF1}, \varphi_{PC1} + \varphi_{IF1}) = S_{Tx}(A_{Tx}A_{dir2}A_{ref}A_{down1}A_{s1}A_{IF1}, \varphi_{Tx} + \varphi_{dir2} + \varphi_{ref} + \varphi_{down1} + \varphi_{s1} + \varphi_{IF1})$$

$$S_{PC2}(A_{PC2}A_{IF2}, \varphi_{PC2} + \varphi_{IF2}) = S_{Tx}(A_{Tx}A_{dir1}A_{ch}A_{rx}A_{down2}A_{s2}A_{IF2}, \varphi_{Tx} + \varphi_{dir1} + \varphi_{ch} + \varphi_{rx} + \varphi_{down2} + \varphi_{s2} + \varphi_{IF2})$$

$$\frac{S_{PC2}(A_{PC2}A_{IF2}, \varphi_{PC2} + \varphi_{IF2})}{S_{PC1}(A_{PC1}A_{IF1}, \varphi_{PC1} + \varphi_{IF1})} = \frac{S_{Tx}(A_{Tx}A_{dir1}A_{ch}A_{rx}A_{down2}A_{s2}A_{IF2}, \varphi_{Tx} + \varphi_{dir1} + \varphi_{ch} + \varphi_{rx} + \varphi_{down2} + \varphi_{s2} + \varphi_{IF2})}{S_{Tx}(A_{Tx}A_{dir2}A_{ref}A_{down1}A_{s1}A_{IF1}, \varphi_{Tx} + \varphi_{dir2} + \varphi_{ref} + \varphi_{down1} + \varphi_{s1} + \varphi_{IF1})}$$

So here we can see that the transfer function of the transmitter is cancelled out. Also assuming that the amplitude and phase variables in the IF stage do not vary much over $\Delta f/2$; then the IF stage transfer function is also cancelled out.

$$\frac{S_{PC2}(A_{PC2}A_{IF2}, \varphi_{PC2} + \varphi_{IF2})}{S_{PC1}(A_{PC1}A_{IF1}, \varphi_{PC1} + \varphi_{IF1})} = \frac{S_{Tx}(A_{dir1}A_{ch}A_{rx}A_{down2}A_{s2}, \varphi_{dir1} + \varphi_{ch} + \varphi_{rx} + \varphi_{down2} + \varphi_{s2})}{S_{Tx}(A_{dir2}A_{ref}A_{down1}A_{s1}, \varphi_{dir2} + \varphi_{ref} + \varphi_{down1} + \varphi_{s1})}$$

In order to increase the compensation capability, the designer has to select identical components in the circuit portions that allow it (H_{s1} & H_{s2} and H_{down1} & H_{down2}). Also we assume that the power combiner inputs are equivalent. And assuming that the gain and phase variations are negligible over $\Delta f/2$. The transfer functions are cancelled except for the Local Oscillators phase components φ_{down1} and φ_{down2} because of the difference in local oscillator frequencies there will be a phase that can't be compensated and we'll call it $\Delta\varphi_{LO}$. Thus

$$\frac{S_{PC2}(A_{PC2}A_{IF2}, \varphi_{PC2} + \varphi_{IF2})}{S_{PC1}(A_{PC1}A_{IF1}, \varphi_{PC1} + \varphi_{IF1})} = \frac{S_{Tx}(A_{dir1}A_{ch}A_{rx}, \varphi_{dir1} + \varphi_{ch} + \varphi_{rx})}{S_{Tx}(A_{dir2}A_{ref}, \varphi_{dir2} + \varphi_{ref} + \Delta\varphi_{LO})}$$

Thus for the frequency interleaved architecture, the transmitter transfer function can be compensated fully. The IF stage transfer function is cancelled out if the amplitude and phase variations over $\Delta f/2$. If the components are matched, further compensation on gain can be accomplished for downconverters stages and the paths linking the downconverters to the power combiner. However because of the phase difference between the two local oscillator frequencies there is a phase component that can't be cancelled out.

This architecture also requires extra calculations in order first to extract the complex coefficient of both channels from the frequency interleaved signal. Then the reference signal must be downconverted digitally to compensate for the frequency modulation $\Delta f/2$.

This analysis shows also that from the power combiner the signals from the reference path and the test channel are summed. This means that if any interferences appearing in either channels are combined with the other one, thus corrupting it. So this limits the use of such an architecture to short ranges or environments with low interference levels such as an anechoic chamber.

2. Parallel

Two paths can be identified the reference path and test path. For the reference path in blue, the signal from the transmitter comes out the directional coupler coupled output $H_{dir2}(A_{dir2}, f_{Tx}, \varphi_{dir2})$ and then goes through cables filters and attenuators $H_{ref}(A_{ref}, f_{Tx}, \varphi_{ref})$. The signal is then downconverted with the same local oscillator used for upconversion $H_{down1}(A_{down1}, f_{LO} \pm f_{Tx}, \varphi_{down1})$. The IF stage selects the useful signal and amplifies it $H_{IF1}(A_{IF1}, f_{LO} - f_{Tx}, \varphi_{IF1})$ before digitization.

$$S_{ADC1} = S_{Tx}(A_{Tx}A_{dir2}A_{ref}A_{down1}A_{IF1}, f, \varphi_{Tx} + \varphi_{dir2} + \varphi_{ref} + \varphi_{down1} + \varphi_{IF1})$$

The test channel in red goes through the directional coupler direct path $H_{dir1}(A_{dir1}, f_{Tx}, \varphi_{dir1})$. the signal propagates into free space $H_{ch}(A_{ch}, f_{Tx}, \varphi_{ch})$ and is picked up by the receiver front end $H_{rx}(A_{rx}, f_{Tx}, \varphi_{rx})$ before downconversion $H_{down2}(A_{down2}, f_{LO} \pm f_{Tx}, \varphi_{down2})$ with the same local oscillator used for the reference channel. The IF stage selects the useful signal and amplifies it $H_{IF2}(A_{IF2}, f_{LO} - f_{Tx}, \varphi_{IF2})$ before digitization with a second ADC.

$$S_{ADC2} = S_{Tx}(A_{Tx}A_{dir1}A_{ch}A_{rx}A_{down2}A_{IF2}, f, \varphi_{Tx} + \varphi_{dir1} + \varphi_{ch} + \varphi_{rx} + \varphi_{down2} + \varphi_{IF2})$$

In this case the reference and the test channel are demodulated by the same local oscillator frequency so if the components are matched in the IF stages and downconverters, their transfer function can potentially be compensated. And here the transmitter transfer function is compensated fully.

$$\frac{S_{ADC2}}{S_{ADC1}} = \frac{S_{Tx}(A_{Tx}A_{dir1}A_{ch}A_{rx}A_{down2}A_{IF2}, f, \varphi_{Tx} + \varphi_{dir1} + \varphi_{ch} + \varphi_{rx} + \varphi_{down2} + \varphi_{IF2})}{S_{Tx}(A_{Tx}A_{dir2}A_{ref}A_{down1}A_{IF1}, f, \varphi_{Tx} + \varphi_{dir2} + \varphi_{ref} + \varphi_{down1} + \varphi_{IF1})}$$

$$\frac{S_{ADC2}}{S_{ADC1}} = \frac{S_{Tx}(A_{dir1}A_{ch}A_{rx}, f, \varphi_{dir1} + \varphi_{ch} + \varphi_{rx})}{S_{Tx}(A_{dir2}A_{ref}, f, \varphi_{dir2} + \varphi_{ref})}$$

This analysis shows that the reference and test channels are completely decorrelated so any interference affecting one of the channels will not contaminate the other.

3. Time interleaved

Two paths can be identified the reference path in blue and the test path in red. In this case the receiver is common to the reference and test channels. The reference signal is recorded when the switches bypass the aerials $H_{SW12}(A_{SW12}, f_{Tx}, \varphi_{SW12})$ & $H_{SW22}(A_{SW22}, f_{Tx}, \varphi_{SW22})$ and goes through cables and attenuators $H_{ref}(A_{ref}, f_{Tx}, \varphi_{ref})$. The test path is enabled when the switches connect the system to the aerials $H_{SW11}(A_{SW11}, f_{Tx}, \varphi_{SW11})$ & $H_{SW21}(A_{SW21}, f_{Tx}, \varphi_{SW21})$. The signal propagates in free space and is picked up by the receiving antenna. $H_{ch}(A_{ch}, f_{Tx}, \varphi_{ch})$.

$$S_{ADCref} = S_{Tx}(A_{Tx}A_{SW12}A_{ref}A_{SW22}A_{rx}, f, \varphi_{Tx} + \varphi_{SW12} + \varphi_{ref} + \varphi_{SW22} + \varphi_{rx})$$

$$S_{ADCtest} = S_{Tx}(A_{Tx}A_{SW11}A_{ch}A_{SW21}A_{rx}, f, \varphi_{Tx} + \varphi_{SW11} + \varphi_{ch} + \varphi_{SW21} + \varphi_{rx})$$

$$\frac{S_{ADCTest}}{S_{ADCref}} = \frac{S_{Tx}(A_{Tx}A_{SW11}A_{ch}A_{SW21}A_{rx}, f, \varphi_{Tx} + \varphi_{SW11} + \varphi_{ch} + \varphi_{SW21} + \varphi_{rx})}{S_{Tx}(A_{Tx}A_{SW11}A_{ch}A_{SW21}A_{rx}, f, \varphi_{Tx} + \varphi_{SW11} + \varphi_{ch} + \varphi_{SW21} + \varphi_{rx})}$$

In this case, both signals are downconverted with the same local oscillator frequency. The transfer functions from the transmitter and receiver are cancelled out. Only remains transfer functions from the reference path and the test path. In other words, the difference in switches and between the bypass and the channel with aerials.

$$\frac{S_{ADCTest}}{S_{ADCref}} = \frac{S_{Tx}(A_{SW11}A_{ch}A_{SW21}, f, \varphi_{SW11} + \varphi_{ch} + \varphi_{SW21})}{S_{Tx}(A_{SW11}A_{ch}A_{SW21}, f, \varphi_{SW11} + \varphi_{ch} + \varphi_{SW21})}$$

Here the isolation between the channels, is as good as the isolation in the switches. Therefore the designer should take this into account when selecting the switches.

F. Spurious and Intermodulation avoidance

In Narrow Band (NB), the even spurious products are neglected because the band considered is too small to cause in interference within the upconverted bandwidth. In our case dealing with UWB signals, a limit will have to be established based on the order of intermodulation the designer wants to avoid. The 3rd order being the strongest intermodulations those will have to be avoided in any case. Then the level of avoidance will be determined by the level of signal purity wanted. The limit will be based on the most limiting dynamic range in the radar and the non-linear components quality (3rd order interception point).

1. Upconversion

For this analysis, a signal in Intermediate Frequencies (IF) range $[F_{l1}; F_{l2}]$ is considered. The input signal goes in the IF port of the mixer. The Local Oscillator is driven with a single frequency at F_{LO} . At the Radio Frequencies (RF) port, the upconversion yields two main signals of interest in the range:

Condition 1: the Local Oscillator frequency must be outside the IF frequency range thus

$$F_{l1} < F_l < F_{l2} < F_{LO}$$

Sum upconversion (case 1)

$$F_{LO} < F_{H1} < F_{H2} < 2F_{LO}$$

$$F_{H1} = F_{LO} + F_{l1}$$

$$F_{H2} = F_{LO} + F_{l2}$$

Difference upconversion (case 2)

$$F_{H1} < F_{H2} < F_{LO}$$

$$F_{H1} = F_{LO} - F_{l2}$$

$$F_{H2} = F_{LO} - F_{l1}$$

The upconversion products are defined as follow

$|aF_{LO} \pm bF_l|$ where $a = n - b$ and $b \in [0; n]$ and n is the intermodulation order

a) n^{th} order intermodulation Case 1

Basic rules regardless of the order of intermodulation avoidance

$$F_{LO} < F_{H1} < F_{H2} < 2F_{LO}$$

$$F_{H2} < F_{LO} + 2F_{l1} \rightarrow F_{l2} < 2F_{l1}$$

For $n \geq 3$ and in linear operation when the IF mixer input is driven well below 3rd order interception point, the intermodulation avoidance rules up to the n^{th} order are:

$$F_{H2} < 2F_{LO} - (n - 2)F_{l2} \rightarrow (n - 1)F_{l2} = (n - 1)F_{l1} + (n - 1)B < F_{LO}$$

$$F_{l1_max} = B_{max} = \frac{F_{LO}}{2(n - 1)}$$

For $n \geq 3$ and in saturated operation when the IF mixer input is overdriven with respect to 3rd order interception point, the pure intermodulations of order n are no longer negligible

$$nF_{l2} < F_{H1} = F_{LO} + F_{l1} \rightarrow nF_{l2} - F_{l1} = (n - 1)F_{l1} + nB < F_{LO}$$

$$F_{l1_max} = B_{max} = \frac{F_{LO}}{2n - 1}$$

b) n^{th} order intermodulation Case 2

Basic rules regardless of the order of intermodulation avoidance

$$F_{H1} < F_{H2} < F_{LO}$$

$$F_{LO} - 2F_{l1} < F_{H1} = F_{LO} - F_{l2} \rightarrow F_{l2} < 2F_{l1}$$

$$F_{l2} < F_{H1} = F_{LO} - F_{l2} \rightarrow F_{l2} < F_{LO}/2 \rightarrow F_{l1} < F_{LO}/4$$

For $n \geq 4$ and in linear operation when the IF mixer input is driven well below 3rd order interception point, the intermodulation avoidance rules up to the n^{th} order are:

$$F_{H2} < 2F_{LO} - (n - 2)F_{l2} \rightarrow (n - 2)F_{l2} - F_{l1} = (n - 3)F_{l1} + (n - 2)B < F_{LO}$$

$$F_{l1_max} = B_{max} = \frac{F_{LO}}{2n - 5}$$

For $n \geq 4$ and in saturated operation when the IF mixer input is overdriven with respect to 3rd order interception point, the pure intermodulations of order n are no longer negligible

$$nF_{l2} < F_{H1} = F_{LO} - F_{l2} \rightarrow (n+1)F_{l2} = (n+1)F_{l1} + (n+1)B < F_{LO}$$

$$F_{l1_max} = B_{max} = \frac{F_{LO}}{2(n+1)}$$

This demonstrates that to avoid high order intermodulations, the bandwidth will have to be reduced.

2. Downconversion

For this analysis, a signal in Radio Frequencies (RF) range $[F_{H1}; F_{H2}]$ is considered. The input signal goes in the RF port of the mixer. The Local Oscillator is driven with a single frequency at F_{LO} . At the Intermediate Frequencies (IF) port, the downconversion yields two main signals of interest in the range:

Condition 1: the RF frequency range $F_{H1} < F_{H2}$, the F_{LO} must be outside the RF range. Two cases have to be considered, F_{LO} is either greater than F_{H2} or smaller than F_{H1} .

Case 1

$$F_{l1} < F_{l2} < F_{LO} < F_{H1} < F_H < F_{H2} < 2F_{LO}$$

$$F_{l1} = F_{H1} - F_{LO}$$

$$F_{l2} = F_{H2} - F_{LO}$$

Case 2

$$F_{l1} < F_{l2} < F_{H1} < F_H < F_{H2} < F_{LO}$$

$$F_{l1} = F_{LO} - F_{H2}$$

$$F_{l2} = F_{LO} - F_{H1}$$

The downconversion products are defined as follow

$|aF_{LO} \pm bF_H|$ where $a = n - b$ and $b \in [0; n]$ and n is the intermodulation order (IMn)

When downconverting, the pure RF and local oscillator frequencies intermodulations of order n at nF_{LO} , nF_{H1} and nF_{H2} will not interfere since they'll be much higher than the range of interest.

a) IMn Case 1

$$F_{l1} < F_{l2} < F_{LO} < F_{H1} < F_H < F_{H2} < 2F_{LO}$$

For $n \geq 4$ and n even

$$F_{l2} < nF_{H1}/2 - nF_{LO}/2 \rightarrow F_{l2} < nF_{l1}/2 \text{ thus } F_{l2} < 2F_{l1} \text{ is sufficient}$$

For $n \geq 3$ and n odd

$$F_{l2} < (n+1)F_{LO}/2 - (n-1)F_{H2}/2 \rightarrow F_{l2} < 2F_{LO}/(n+1)$$

$$\text{for } n = 3 \rightarrow B_{max} = 2F_{LO}/(n+1)$$

$$\text{for } n \geq 5 \rightarrow F_{l1_max} = B_{max} = \frac{F_{LO}}{(n+1)}$$

b) *IMn Case 2*

$$F_{l1} < F_{l2} < F_{H1} < F_H < F_{H2} < F_{LO}$$

$$F_{l2} < F_{H1} = F_{LO} - F_{l2} \rightarrow F_{l2} < F_{LO}/2$$

For $n \geq 4$ and n even

$$F_{l2} < nF_{LO}/2 - nF_{H2}/2 \rightarrow F_{l2} < nF_{l1}/2 \text{ thus } F_{l2} < 2F_{l1} \text{ is sufficient}$$

For $n \geq 3$ and n odd

$$F_{l2} < (n+1)F_{H1}/2 - (n-1)F_{LO}/2 \rightarrow F_{l2} < 2F_{LO}/(n+3)$$

$$\text{for } n = 3 \rightarrow B_{max} = F_{LO}/2$$

$$\text{for } n \geq 5 \rightarrow F_{l1_max} = B_{max} = \frac{F_{LO}}{(n+3)}$$

This demonstrates that the higher order intermodulation avoidance results in a reduced bandwidth.

G. Model for the AFD2-010020-23P-SP

Equation 24 describes the model derived by the gain measurement of the amplifier and is shown in Figure 85.

Equation 24: AFD2-010020-23P-SP amplification model – 7th order polynomial

$$P_{outdB} = a_7z^6 + a_6z^5 + a_5z^4 + a_4z^3 + a_3z^2 + a_2z + a_1$$

$$z = \frac{P_{indB} - \mu}{\sigma}; \mu = -13.5; \sigma = 9.9582;$$

$$a_1 = 0.029128; a_2 = -0.056113; a_3 = -0.34154; a_4 = -0.29082;$$

$$a_5 = 0.019387; a_6 = -0.082181; a_7 = 27.473$$

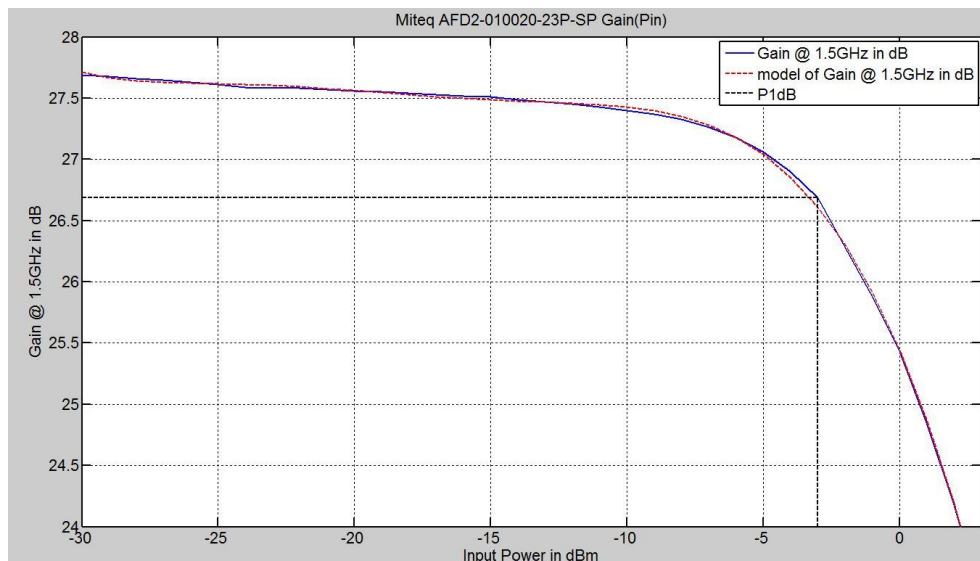


Figure 85: AFD2-010020-23P-SP gain wrt input power measurement, model and IP1dB

H. Ambiguity function algorithm validation

In (12) , an analytical formula of the NB chirp ambiguity function is given as shown in Equation 25.

Equation 25: Linear Chirp ambiguity function Analytical equation

$$|\chi(\tau, \nu)| = \left| \left(1 - \frac{|\tau|}{T}\right) \frac{\sin\left(\pi T \left(\nu \pm B \left(\frac{\tau}{T}\right)\right) \left(1 - \frac{|\tau|}{T}\right)\right)}{\pi T \left(\nu \pm B \left(\frac{\tau}{T}\right)\right) \left(1 - \frac{|\tau|}{T}\right)} \right| ; |\tau| \leq T$$

Where τ is the delay, ν is the Doppler shift, B is the bandwidth, T is the pulse length.

The algorithm used to compare the ambiguity function of both waveforms assumes a Narrow bandwidth approximation for the Doppler effect. In other words, the Doppler effect applied to the signals corresponds to a shift in frequency. The compression of the matched filter configured at zero-delay and zero-Doppler is tested against replica of the signal at various delays and Doppler shift ranging over the full bandwidth. The limits of this algorithm were determined by comparing the algorithm outputs to the analytical results for chirp.

The difference is more pronounced around the edges of the function. Indeed the theoretical formula considers an infinite spectrum where the simulated spectrum has a sampling frequency at 10GHz.

In Figure 86, the theoretical and simulated ambiguity function function for up chirp with a 800MHz bandwidth and a pulse repetition of 500ns are shown. Also the simulated ambiguity function is subtracted to the theoretical ambiguity function yielding very good agreement (no more than -55dB in this case).

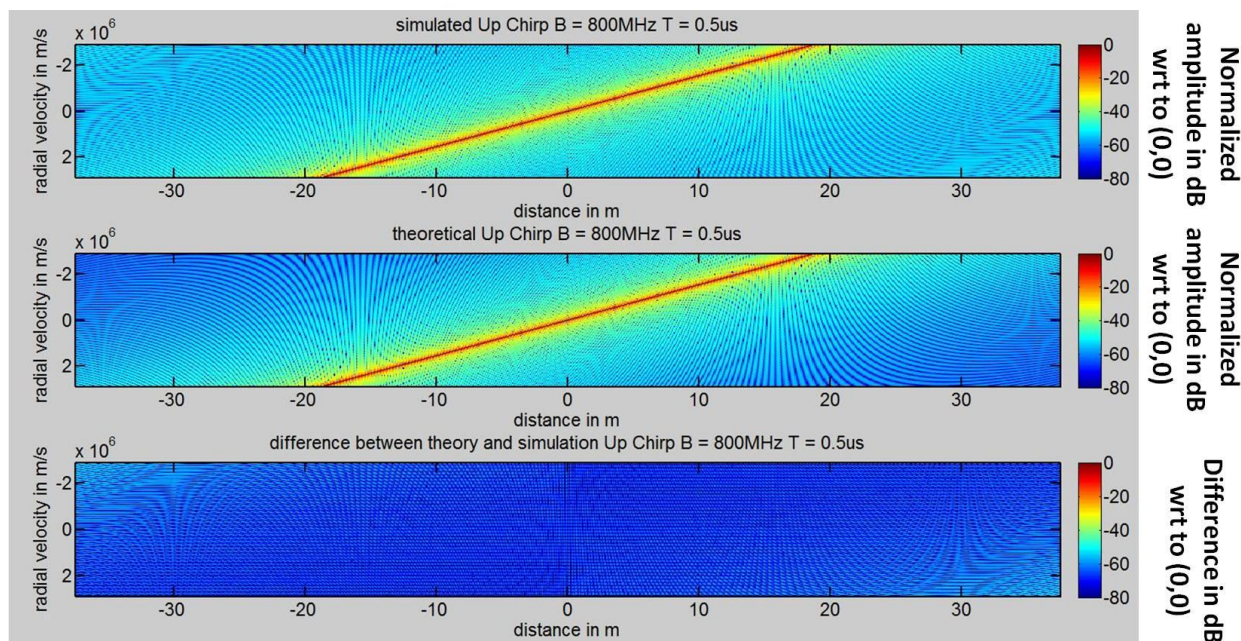


Figure 86: Comparison of the analytical versus the numerical ambiguity function for chirp (B = 800MHz, PRP = 500ns) (top) theoretical (middle) simulated (bottom) difference

Effect of Hamming Window on Ambiguity Function

From bandwidth-time products greater than 100, the Hamming window affects the ambiguity function characteristics. The main lobe width increases by a factor 1.38 @ 3dB, 1.4 @ 6dB and 1.45 @ 10dB. The sidelobe levels drop 20.5dB.

Effect of sampling time

Comparing theory and simulation, the results may differ from the expected value and some jumps in the measurement might seem odd. However it should be kept in mind that sampling the IF signal produces a regular spatial speck proportional to the IF sampling frequency as shown in Equation 26.

Equation 26: IF sampling spatial speck

$$\begin{aligned}
 \text{sampling speck} &= \frac{\text{speed of light}}{2 \cdot F_{IF \text{ sampling}}} = \frac{3 \cdot 10^8}{2 \cdot 10 \cdot 10^9} \\
 &= 0.015m @ 10GS/s \Rightarrow 0.075 @ 2GS/s
 \end{aligned}$$

This explains the discrepancies between the expected 3dBwidth with at 800MHz is 0.15m and the measured 3dBwidth on the simulation output 0.165m @ 10GS/s and 0.225m @ 2GS/s). The spatial resolution is within 10% of the expected value for all configurations, except when the speck is large compared to the resolution.

I. Experimental test bench

The color code used for different parts of the test bench in the overview of Figure 56 is used to associate rapidly the detailed schematics to their positions in the general synoptic. In green, the transmitter (Figure 87) and amplification stage 1 (Figure 88) and 2 (Figure 90). There are 2 amplifications stages: one was designed for short range the other for mid range applications. The reference channel (Figure 91) is shown in blue and the test channel (Figure 92) in red. The local oscillator subsystems are coded in purple for the 1st one (Figure 93) and orange for the 2nd one (Figure 91).

1. System Overview

Two digitizers are presented here because one of the Neptune VXS 2 channel (component 32) presented a failure. It was actually a memory access problem. The origin is hardware so it couldn't be fixed. The failure was identified the failure, it is a problem with the memory access. If the number of samples was kept below 65536, the samples were saved properly because the internal radiation absorbent material was used but exceeding this number of samples the digitizer uses the external radiation absorbent material and the memory access causes an artificial modulation inside the captured data @ $F_s/16$. For example @ 2 GHz, the reference signal presented a 125MHz modulation even with a 50Ω load at the ADC0 input. Thus a replacement had to be found to finish my measurements. The Tektronix DSA71254 was chosen for its 4 channels and its sampling frequency up to 50GS/s.

2. Transmitter

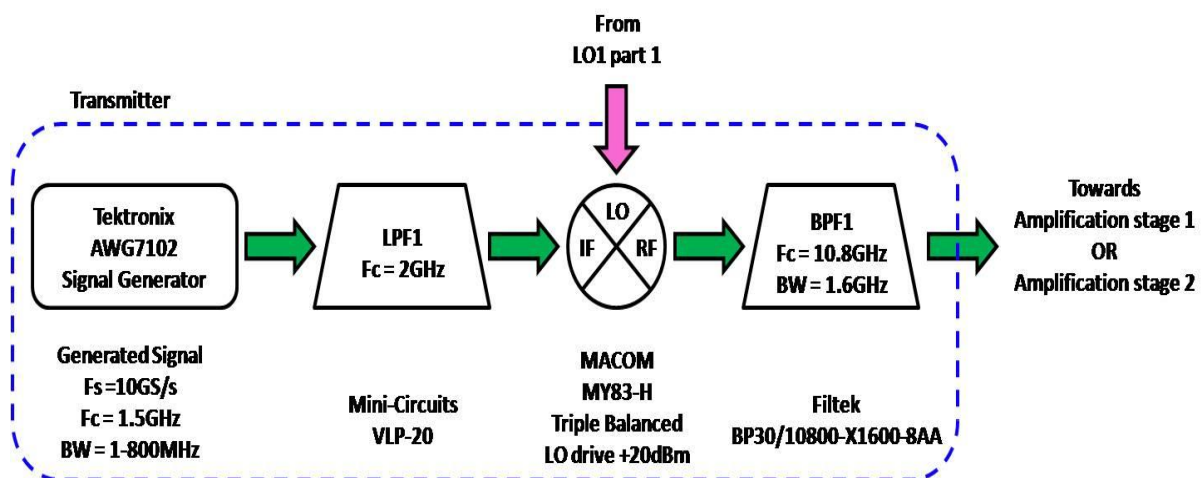


Figure 87: Detailed architecture of the transmitter

The signal generator AWG7102 (component 1) is used on channel 1 with 10bits resolution to generate the radar signal between $[1.1 - 1.9\text{GHz}]$ and on channel 2 with 8bits resolution to generate the 2GHz clock for the digitizer. The 2 remaining bits are used to generate the differential triggers plugged into ADC 0 & 1, this way both ADCs start their measurements at the same time. The signal generator sampling frequency is set to its maximum 10GHz.

The radar signal, generated by the DAC, has a mirror image with respect to half the DAC sampling frequency, thus a low pass filter (component 2) with a 3dB cut-off frequency @ 1980MHz was placed to filter out the mirror image. This will prevent any disturbances at the up-conversion.

The up-converter (component 3) is driven at the local oscillator input by the 1st local oscillator part 1 (Figure 93) output signal @ 20dBm and 8.9GHz and the IF input is driven by the filtered IF signal between [1.1 – 1.9GHz]. The upconversion results in two signals: sum @ [10 – 10.8GHz] and difference @ [7 – 7.8GHz].

The band pass filter (component 4) chosen filters out the difference upconversion with 50dB rejection @9.2GHz. Even if the signal is shifted by 800MHz, the difference would reach at most 8.6GHz, so the filter still offers a minimum rejection of 65dB. Notice that the further the sum upconversion goes over 10.8GHz, the stronger the difference upconversion gets. And notice as well that the local oscillator frequency leakage is attenuated by 60dB @8.9GHz but only by 15dB @ 9.7GHz.

Since the isolation in the upconverter is 25dB between local oscillator and RF, and the attenuation in the filter might go as low as 15dB. The signal will then be amplified, thus to respect emission regulations, the local oscillator signal might need to be filtered again or the local oscillator frequency might have to be limited to a smaller range to allow stronger attenuation.

Tektronix (www.tek.com)	AWG7102
Settings	
Sampling Frequency	$F_s = 10GS/s$
Emission Mode	Continuous
Channel 1- radar signal generation [1.1 – 1.9GHz]	
Connection	Transmitter IF
Peak-to-peak voltage	$V_{pp} = 1V$
Offset	$V_{dc} = 0V$
Resolution in bits	$Nb = 10bits$
Channel 2 – 2GHz clock signal and differential trigger signals for Neptune VXS 2	
Connection	Neptune VXS 2 Clock input
Peak-to-peak voltage	$V_{pp} = 1V$
Offset	$V_{dc} = 0V$
Resolution in bits	$Nb = 8bits$
Marker 1	Neptune VXS 2 ADC0 positive trigger input
<u>Marker 1</u>	Neptune VXS 2 ADC0 negative trigger input
Peak-to-peak voltage	$V_{pp\ marker1} = 0.7V$
Marker 2	Neptune VXS 2 ADC1 positive trigger input
<u>Marker 2</u>	Neptune VXS 2 ADC1 negative trigger input
Peak-to-peak voltage	$V_{pp\ marker2} = 0.7V$
10MHz reference out	
Connection	6-way power splitter

component 1: signal generator AWG7102

Minicircuits (minicircuits.com)	VLP-20
Characteristics	

Cutt-off frequency	$F_{CO} = 1980MHz@3dB$
Insertion Loss	$L_1 < 1dB@[DC - 1700MHz]$
Rejection 1	$R_1 > 20dB@2700MHz$
Rejection 2	$R_2 > 40dB@3300MHz - 3750MHz$
Voltage Standing Wave Ratio	1.1

component 2: filter VLP-20

MACOM (www.macomtech.com)	MY83H
Characteristics @ local oscillator drive = 20dBm - Triple balanced	
Conversion Loss	$L = 8.5dB$
Max Noise Figure	$NF = 11dB$
Isolation local oscillator/RF	25dB
Isolation local oscillator/IF	30dB
Input 1dB compression point	17dB
Input 3dB compression point	24dBm

component 3: mixer MY83H

FILTEK (www.filtekkfilters.com)	BP30/10800-X1600-8AA
Characteristics – comb line filter	
Center Frequency	$F_c = 10.8GHz$
Bandwidth	$BW = 1.6GHz$
Number of sections	8
Insertion Loss	0.65dB
VSWR	1.5
Rejection > 50dB	$F_{low} = 9.2GHz - F_{high} = 12.25GHz$

component 4: filter BP30/10800-X1600-8AA

3. Amplification stage 1

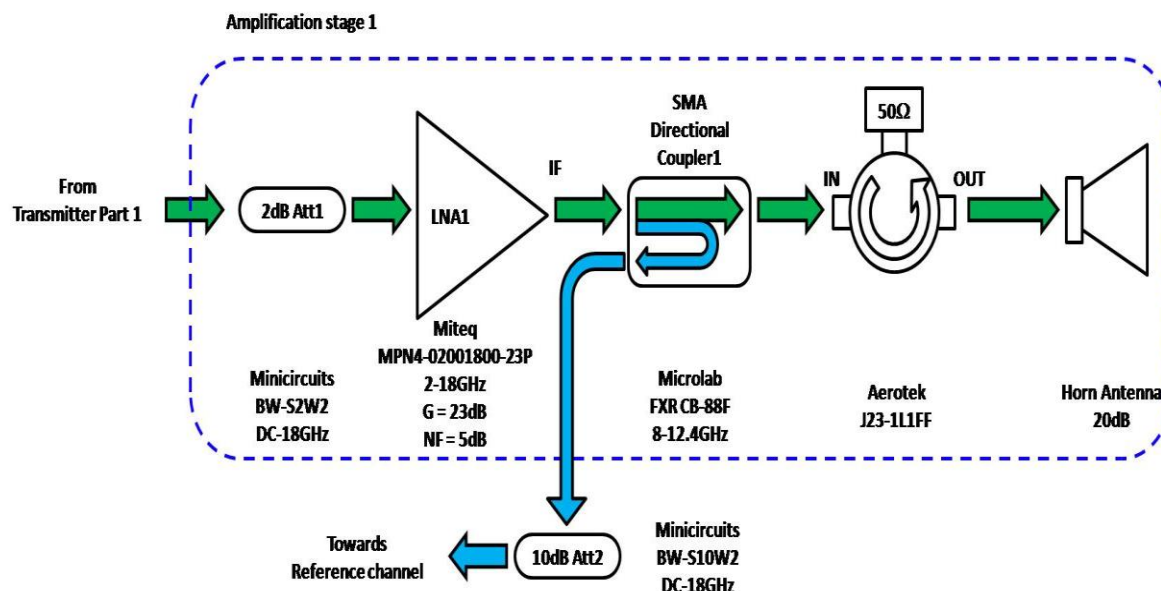


Figure 88: Detailed architecture of amplification stage 1

The first amplification stage is used for short range application i.e. $\approx 60m$. To avoid reflections between the filter (component 4) and amplifier (component 6), a 2dB attenuator (component 5) was placed. The signal is then amplified by a low noise amplifier (component

6) with 25dB gain. The signal then goes through a directional coupler (component 7). The direct path is connected to an isolator (component 8) to block antenna feedline reflections and signal returns received by the transmitter antenna (component 9). The coupled output transmits the emitted signal but only 1% of the original signal power. This goes to the reference channel after passing into a 10dB attenuator (component 10).

Minicircuits (minicircuits.com)	BW-S2W2
Characteristics	
Frequency range	<i>DC – 18GHz</i>
Attenuation	<i>2dB ± 0.4dB</i>
VSWR	1.3
Max input power	33dBm

component 5: attenuator BW-S2W2

Miteq(www.miteq.com)	MPN4-02001800-23P
Characteristics	
Frequency range	<i>[2 – 18GHz]</i>
Gain	<i>23dB</i>
Gain flatness	<i>±2.5dB</i>
VSWR _{in}	2.5
VSWR _{out}	2.2
Output power 1dB compression point	<i>23dBm</i>
Output power 3dB compression point	30dBm
Noise Figure	5dB

component 6: low noise amplifier MPN4-02001800-23P

Microlab FXR (www.microlab.fxr.com)	CB-88F
Characteristics	
Frequency range	<i>[6 – 12GHz]</i>
Coupling	<i>C = 20dB ± 1dB</i>
Gain Flatness	<i>0.5dB</i>
VSWR	1.3
Insertion Loss	<i>0.3dB</i>
Isolation	<i>17dB</i>

component 7: directional coupler CB-88F

Aerotek Thailand	J23-1L1FF
Characteristics	
Frequency range	<i>[9.7 – 12GHz]</i>
Isolation	<i>20dB</i>
Insertion Loss	<i>0.4dB</i>
VSWR	1.15

component 8: isolator J23-1L1FF

For the horn antenna, a pair of X band antenna with no data on it was collected. So theoretical equations found in (114) were derived to obtain these approximated specifications.

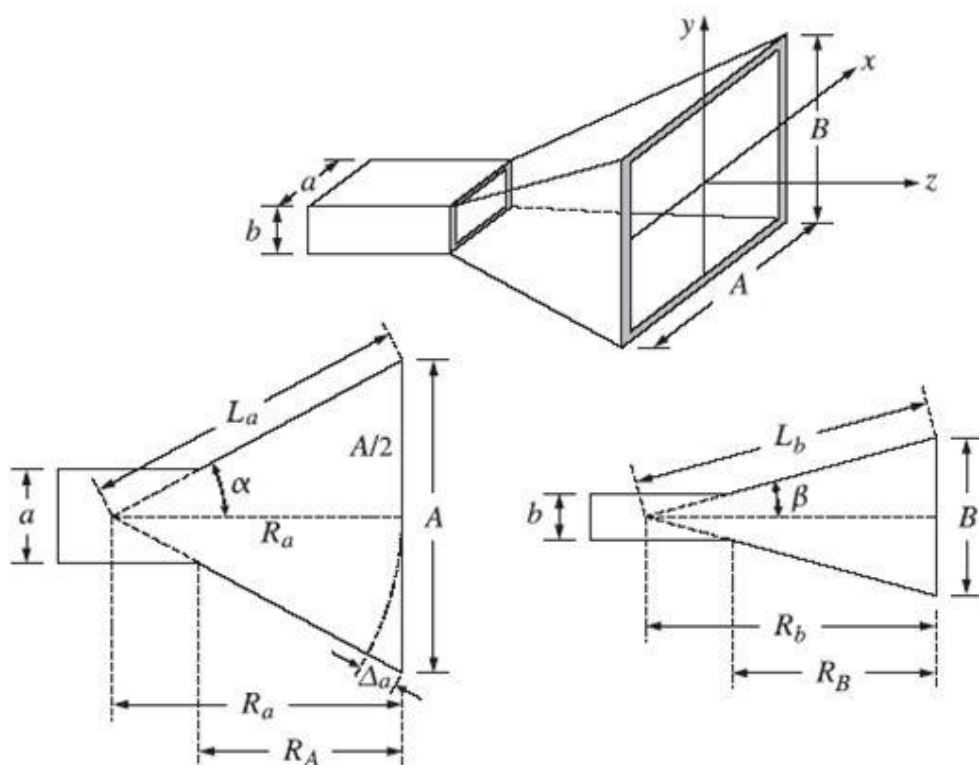


Figure 89: Horn antenna dimensions

Horn antenna	
$A = 0.136m$	$B = 0.112m$
$a = 0.025m$	$b = 0.012m$
$RA = 0.156m$	$RB = 0.156m$
$Ra = 0.191m$	$Rb = 0.174m$
Total 3dB Beamwidth azimuth	$0.265rad / 14.85^\circ$
Total 3dB Beamwidth elevation	$0.325rad / 18.04^\circ$
Gain @ [10 – 10.8GHz]	$20.5dB \pm 0.5dB$
Frequency range	8 – 12.4GHz

component 9: horn antenna

Minicircuits (minicircuits.com)	BW-S10W2
Characteristics	
Frequency range	DC – 18GHz
Attenuation	$10dB \pm 0.6dB$
VSWR	1.3
Max input power	33dBm

component 10: attenuator BW-S10W2

4. Amplification stage 2

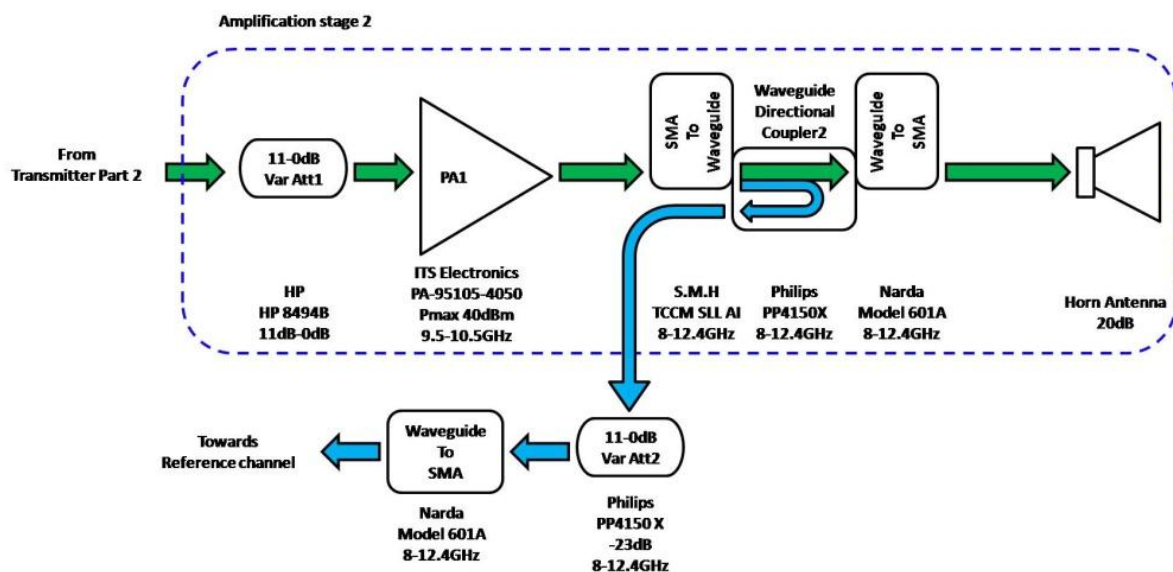


Figure 90: Detailed architecture of amplification stage 2

This amplification stage was used for saturation experiments and medium range applications i.e. 2.5km. the signal first goes through a variable attenuator (component 11). The attenuator is used to explore the input power range to drive the amplifier from linear mode to saturation mode. The signal is amplified by a Solid State Power Amplifier (component 12) with 40dBm max output power and 50dB gain. In order to handle the power increase, a waveguide directional coupler (component 14) was used since waveguides offer a reduced VSWR; also a waveguide attenuator (component 16) at the output of the coupled output was implemented. At the amplifier output, an SMA to waveguide adapter (component 13) was placed. The directional coupler direct output is connected to another adapter (component 15). The adapter output is then connected to the transmitting antenna. The coupled output transmits 10% of the transmitted power to the reference channel. The signal is attenuated by 33dB before going to the reference channel.

HP (archive HP11500B-MTA)	HP 8494B
Characteristics	
Frequency range	[DC – 18GHz]
Attenuation	[11dB – 0dB]
Step	1dB
Insertion Loss	1.5dB
VSWR	1.6
Max Power	$P_{avg} = 30dBm; P_{peak} = 50dBm$

component 11: variable attenuator HP 8494B

ITS electronics (www.itselectronics.com)	PA95105-4050
Characteristics – Solid State Power Amplifier	

Frequency range	[9.5 – 10.5GHz]
Max output power	40dBm
Gain	57dB ± 1dB
VSWRin	1.4
VSWRout	1.25
IP1dB	40dBm

component 12: power amplifier P95105-4050

S.M.H	TCCM SLL AI
Characteristics	
Frequency range	[8 – 12.4GHz]

component 13: adapter waveguide - SMA TCCM

FMI (www.flamm.com)	16132-10
Characteristics Waveguide directional coupler	
Coupling Factor	$C = 10dB \pm 0.5dB$
Frequency range	[8.2 – 12.5GHz]
Isolation	46dB
VSWRin	1.03
VSWRcoupled	1.1

component 14: directional coupler 16132-10

Narda (www.nardamicrowave.com)	601A
Characteristics	
Frequency range	[8.2 – 12.4GHz]
VSWR	1.25

component 15: adapter waveguide-SMA 601A

Philips	PP4150X
Characteristics – waveguide variable attenuator	
Attenuation	[50dB – 0dB]

component 16: variable attenuator PP4150X

5. 2nd oscillator and reference channel

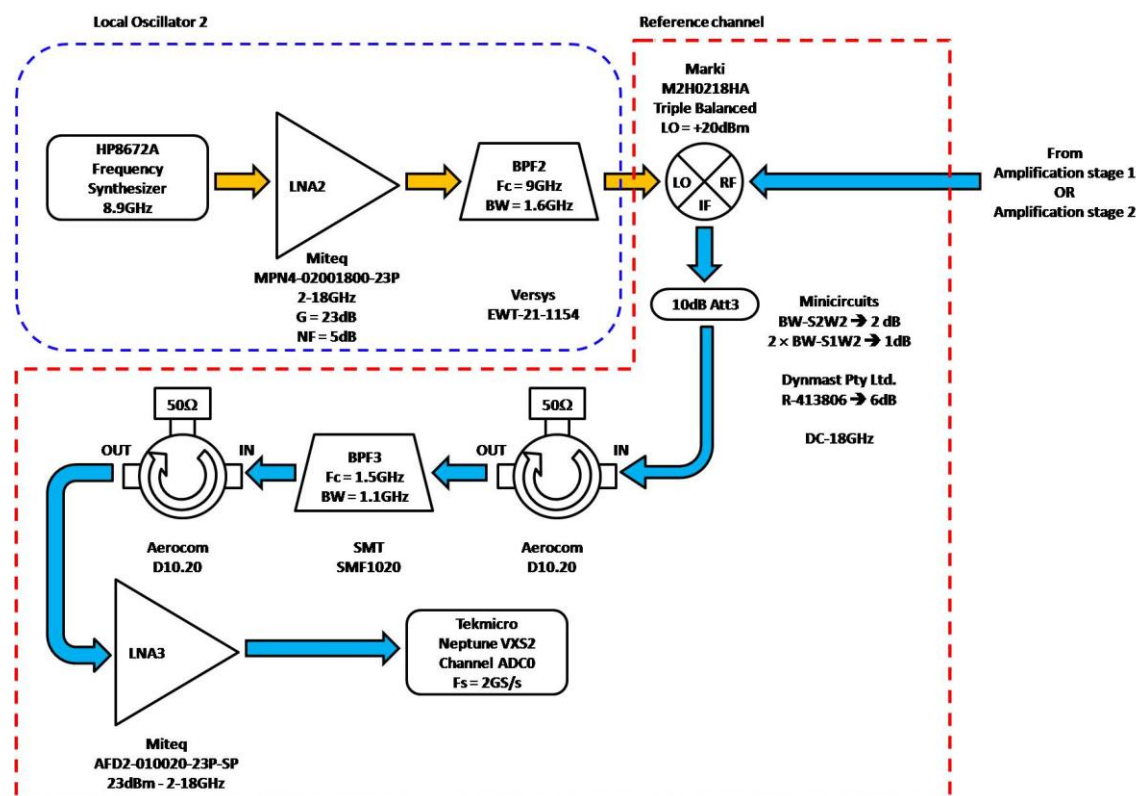


Figure 91: Detailed architecture of the 2nd local oscillator and the reference channel

a) 2nd local oscillator

The frequency synthesizer component 17 generates a 8.9GHz frequency @ -2dBm. The amplifier (component 6) is thus driven into saturation. a band pass filter (component 18) was placed to suppress the 2nd order harmonic at twice the local oscillator frequency. This filter allows the frequency agility for the specified local oscillator frequency range [8.9 – 9.7GHz].

Agilent (www.home.agilent.com)	HP8672A
Characteristics	
Frequency Setting	8.9GHz
External reference	10MHz from AWG7102
Output power setting	-3dBm (maximum available)

component 17: frequency synthesizer HP8672A

The amplifier is a MPN4-02001800-23P, for the characteristics refer to component 6 on page 9-20.

Versys (www.versys.fr)	EWT-21-1154
Characteristics	
Center frequency	9GHz
Bandwidth	1.6GHz
Insertion loss	1.5dB
VSWR	1.7
Rejection <65dB	$F_{low} = 7.7GHz$ & $F_{high} = 10.3GHz$

component 18: filter EWT-21-1154

b) Reference channel

Since a reference channel is implemented, ideally another filter at the amplifier (component 6) output would be required to prevent any harmonics to enter the reference. However because of the limited number of filters, they were placed in more critical parts e.g. in the transmitter before amplification and in the receiver after amplification.

Triple balanced mixer main advantage is their broadband IF port and RF-local oscillator ports allowing a great design flexibility. The reference channel down-converter (component 19) is driven at the RF input by the attenuated coupled output of the directional coupler, and the local oscillator is driven by the 2nd local oscillator output. The IF output is fed to a 10dB attenuator. The attenuator placed at the mixer IF output is composed of 4 attenuators: 1 × Minicircuits BW-S2W2 2dB (component 5), 2 × Minicircuits BW-S1W2 1dB (component 20) and 1 × Dynmast Pty Ltd. R-413806 6dB (component 21).

Since filters are mismatched in impedance, isolators (component 22) were placed on both sides of the filter (component 23). This way, the mixer output and amplifier input are isolated from mismatched impedances. The filter used here is not ideal, notice that the bandwidth is wider than the Nyquist band thus with more than 100MHz out of band signal in reception, the digitized signal will suffer from aliasing. Ideally a 800MHz bandwidth filter with a 1.5GHz center frequency should be used. The signal is then amplified by a low noise amplifier (component 24) in its linear amplification range before digitization on channel 0 of the digitizer (component 32 or component 33).

Marki microwave (www.markimicrowave.com)	M2H0218HA
Characteristics @ local oscillator drive = 20dBm - Triple balanced	
local oscillator-RF frequency range	[2 – 18GHz]
IF frequency range	[1 – 10GHz]
Conversion loss	$L = 8.5dB$
Noise Figure	$NF = 11dB$
Isolation local oscillator → RF	23dB
Isolation local oscillator → IF	25dB
Isolation RF → IF	20dB
Input 1dB compression point	14dBm
Input 3dB compression point	24dBm

component 19: mixer M2H0218HA

Minicircuits (minicircuits.com)	BW-S1W2
Characteristics	
Frequency range	DC – 18GHz

Attenuation	$1dB \pm 0.4dB$
VSWR	1.3
Max input power	33dBm

component 20: attenuator BW-S1W2

Dynmast Pty Ltd. (www.dynmast.com.au)	R-413806
Characteristics	
Frequency range	$[DC - 18GHz]$
Attenuation	6dB
Max Input Power	33dBm

component 21: attenuator R-413806

AEROCOMM (www.aerocommthailand.com)	D10.20
Characteristics	
Frequency range	$[1 - 2GHz]$
Isolation	17dB
Insertion loss	0.5dB
VSWR	1.5

component 22: attenuator D10.20

SMT	SMT1020
Characteristics	
Center frequency	1.53GHz
Bandwidth	1.14GH
Insertion Loss	1.8dB
VSWR	1.5
Rejection <-30dB	$F_{low} = 870MHz$ & $F_{high} = 2.165GHz$

component 23: filter SMT1020

The second isolator is also a D10.20 refer to component 22 above.

Miteq (www.miteq.com)	AFD2-010020-23P-SP
Characteristics	
Frequency range	$[1 - 2GHz]$
Gain	$25dB \pm 1.5dB$
Noise Figure	$NF = 3.5dB$
VSWRin/out	2
Output 1dB compression point	23dBm
Output 3dB compression point	33dBm

component 24: amplifier AFD2-010020-23P-SP

6. Test Channel

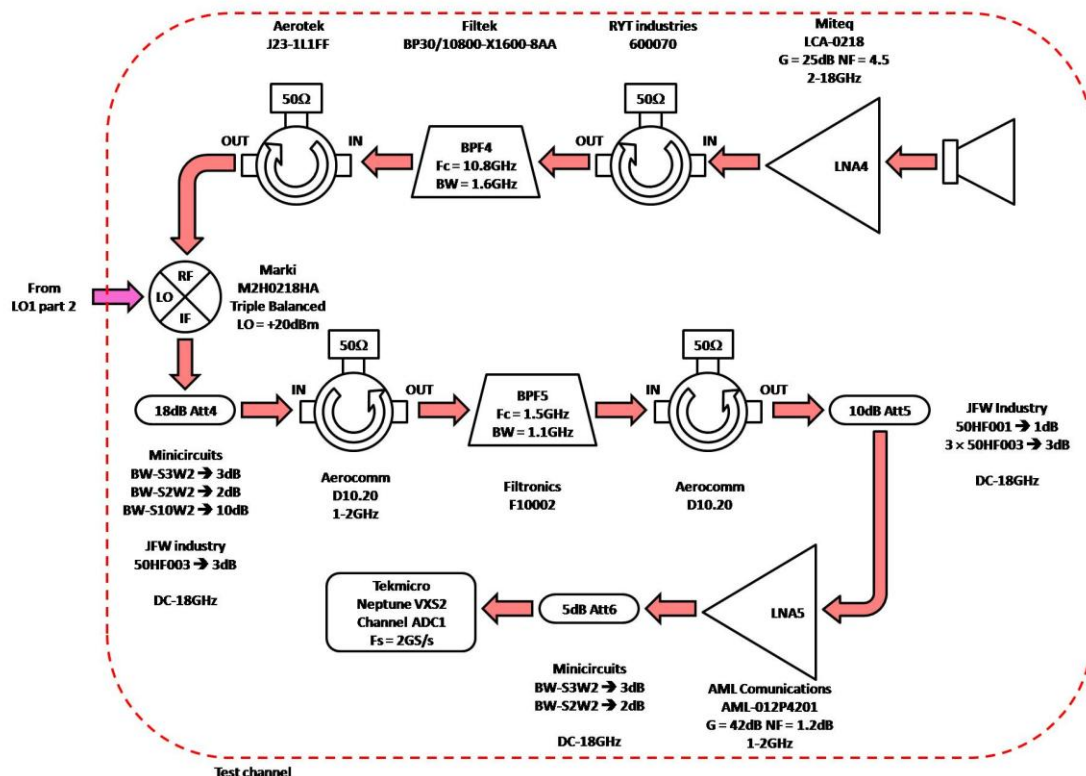


Figure 92: Detailed architecture of the test channel

The receiver horn antenna is the same as the antenna used for the transmitter (component 9). They are 1.3m apart to guarantee a good isolation.

A 72dB isolation was measured. When feeding a sine wave @ 10GHz with 20dBm input power, the received sine wave had a level of -52dBm.

The signal is then amplified by low noise amplifier (component 25). It was chosen because it presented the lowest noise figure (4.5dB) from the available amplifiers. This element is crucial for the total noise figure of the receiver, because it is the main contributor. The signal then needs to be filtered so once again the filter was isolated for the same reasons stated above. Two isolators (component 26 & component 8) and the same band pass filter (component 4) were used in reception. This signal is then fed to the test channel downconverter (component 19), identical to the mixer used in the reference channel. The mixer local oscillator input is driven by the 1st local oscillator part 2 (Figure 93). The RF output is attenuated by 18dB because the amplifier (component 31) used in this channel has a much higher gain (42dB) than the amplifier (23dB) (component 24) used in the reference channel. The 18dB attenuator is composed of is composed of 1 × Minicircuits BW-S3W2 3dB (component 27), 1 × Minicircuits BW-S2W2 2dB (component 5), 1 × Minicircuits BW-S10W2 10dB (component 10) and 1 × JFW industries 50HF003 3dB (component 28). The filter (component 23) is once again isolated from the mixer and the amplifier by a set of isolators (component 22). The filter is once again too wide and the signal in reception might suffer from aliasing if the signal in reception exceeds 100MHz out of band. After the isolator-filter-isolator combo, the signal is further attenuated by 10dB before amplification to drive the amplifier in its linear region. The 10 dB attenuator is composed of 1 × JFW industries 50HF001 1dB (component 30) and 3 × JFW industries 50HF003 3dB (component 28). The

signal is then amplified (component 31) and once more attenuated by 5dB to reduce the amplifier output power below -2dBm so avoid overdriving the digitizer. The 5dB attenuator A 5dB attenuator is placed before digitization composed of 1 × Minicircuits BW-S3W2 3dB (component 27) and 1 × Minicircuits BW-S2W2 2dB component 5. The signal is digitized on channel 1 of the digitizer (component 32 or component 33).

Miteq (www.miteq.com)	LCA-0218
Characteristics	
Frequency range	[2 – 18GHz]
Gain	25dB ± 2dB
Noise Figure	4.5dB
VSWRin/out	2.2
Output 1dB compression point	10dBm
Output 3dB compression point	20dBm

component 25: amplifier LCA-0218

RYT-industries	600070
Characteristics	
Frequency range	8-12GHz
Isolation	???
Insertion loss	???
VSWR	???

component 26: isolator 600070

The band pass filter used in the reception is the twin from the filter in the transmitter. (refer to component 4 on page 9-19)

The isolator is identical to the other one present in the transmitter. Refer to component 8 on page 9-20.

The mixer used for downconversion is the same that was used in the reference channel. Refer to component 19 on page 9-25.

Minicircuits (minicircuits.com)	BW-S3W2
Characteristics	
Frequency range	DC – 18GHz
Attenuation	3dB ± 0.4dB
VSWR	1.3
Max input power	33dBm

component 27: attenuator BW-S3W2

JFW industries (www.jfwindustries.com)	50HF003
Characteristics	
Frequency range	DC – 18GHz
Attenuation	3dB ± 0.3dB
VSWR	1.3
Max input power	33dBm

component 28: attenuator 50HF003

The isolators are D10.20 from AEROCOMM. Refer to component 22 on page 9-26.

Filtronics	F10002
Characteristics	
Center frequency	1.5GHz
Bandwidth	1.08GHz
Insertion Loss	1.75
VSWR	1.4
Rejection <-30dB	$F_{low} = 780MHz$ & $F_{high} = 2.1GHz$

component 29: filter F10002

JFW industries (www.jfwindustries.com)	50HF001
Characteristics	
Frequency range	DC – 18GHz
Attenuation	1dB ± 0.3dB
VSWR	1.3
Max input power	33dBm

component 30: attenuator 50HF001

AML communications (www.amlj.com)	AML012P4201
Characteristics	
Frequency range	[1 – 2GHz]
Gain	42dB ± 1.5dB
Noise figure	1.2dB
Output 1dB compression point	20dBm
Output 3dB compression point	33dBm
VSWRin/out	2

component 31: amplifier AML012P4201

7. Digitizer

Tekmicro (www.tekmicro.com)	Neptune VXS 2
Characteristics	
FPGA	Virtex II Pro XC2VP70

Memory	DDR2 (64bits wide data bus)
Bus maximum throughput	390MB/s
Channel 0	Reference channel
Differential trigger 0 (AN0+/-)	Marker 1 & <i>Marker 1</i>
Channel 1	Reference channel
Differential trigger 1 (AN1+/-)	Marker 2 & <i>Marker 2</i>
Clock in	AWG7102 channel 2
ADC – folding and interpolation	
Atmel	AT84AS008
resolution	10bits
Sampling rate	2GS/s
Maximum input power before coding saturation	-2dBm
Absolute maximum input power	2dBm
bandwidth	[DC – 3.3GHz]
VSWRmax	1.2
Specified ENOB for $F_{in} = [1.1 - 2GHz]$ @ $-1dBFS$	[7.4 – 7.6]bits @2.2GS/s

component 32: digitizer Neptune VXS2

Tektronix (www.tek.com)	DSA 71254
Characteristics	
Max sampling frequency	50GS/s
Analog bandwidth	[DC – 12.5GHz]
channels	4
resolution	8bits – (11bits with averaging)
Max record length	50MS/s
Specified ENOB	5.4bits
Max input power	27dBm
Pass band flatness	$\pm 0.5dB$ up to 6.25GHz
Settings	
Sampling frequency	6.125GS/s
Voltage range	50mV/div

component 33: high speed digitizer DSA 71254

8. 1st local oscillator

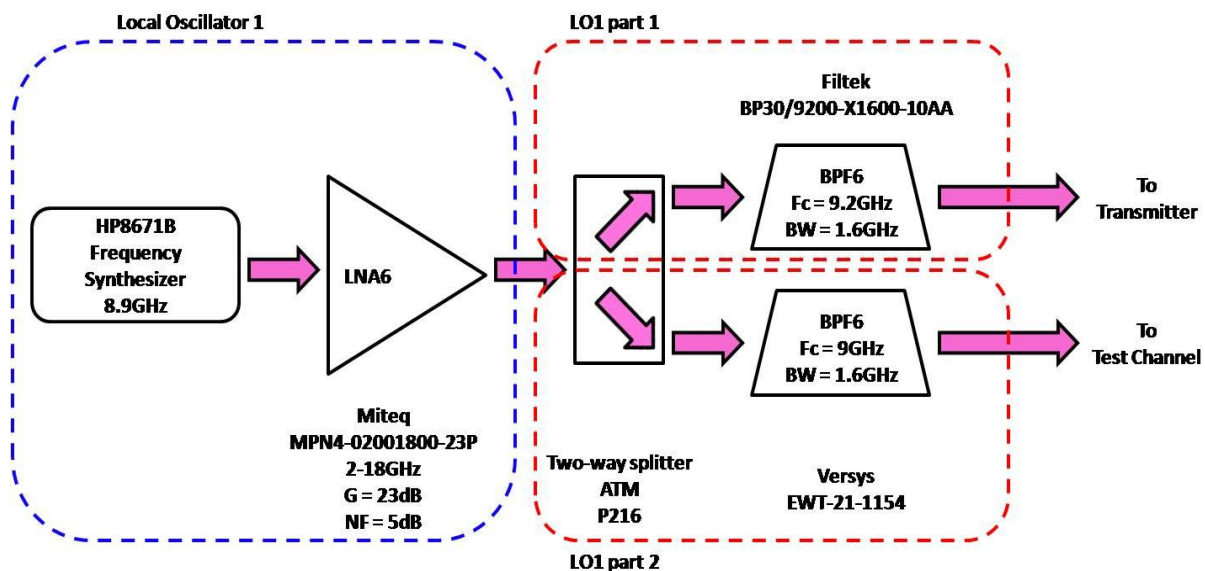


Figure 93: Detailed architecture of the 1st Local Oscillator

A frequency synthesizer (component 34) is used to generate the 8.9GHz frequency. The amplifier (component 6) is driven in saturation to get as much power as possible at the output. The signal is then fed to a two-way splitter (component 35). Both signals are filtered (part 1 by component 36 and part 2 by component 18) to remove the 2nd harmonic before feeding the signals to the transmitter upconverter (Figure 87) and to the test channel downconverter (Figure 92).

Agilent (www.home.agilent.com)	HP8671B
Characteristics	
Frequency Setting	8.9GHz
External reference	10MHz from AWG7102
Output power setting	XXdBm (maximum available)

component 34: frequency synthesizer HP8671B

The amplifier is a MPN4-02001800-23P. Refer to component 6 on page 9-20

ATM (www.atmmicrowave.com)	P216
Characteristics	
Frequency range	[8 – 12.4GHz]
Isolation	20dB
VSWR _{in}	1.35
VSWR _{out}	1.3
Insertion loss	0.5
Amplitude balance	±0.2dB
Phase balance	±2°

component 35: two-way splitter P216

The filter leading to the test channel downconverter is an EWT-21-1154. Refer to component 18on page 9-25.

FILTEK (www.filtekkfilters.com)	BP30/9200-X1600-10AA
---	----------------------

Characteristics – comb line filter	
Center Frequency	$F_c = 9.2GHz$
Bandwidth	$BW = 1.6GHz$
Number of sections	10
Insertion Loss	0.68dB
VSWR	1.5
Rejection > 50dB	$F_{low} = 7.6GHz - F_{high} = 10.7GHz$

component 36: filter BP30/9200-X1600-10AA

J. Parking Experiment Model

At the Onera Palaiseau site, five floors below the lab there is a parking lot. This outdoor area was chosen to test the radar. The set-up is shown below in Figure 94. This area was modeled in order to evaluate a realistic power budget based on antenna characteristics and terrain.

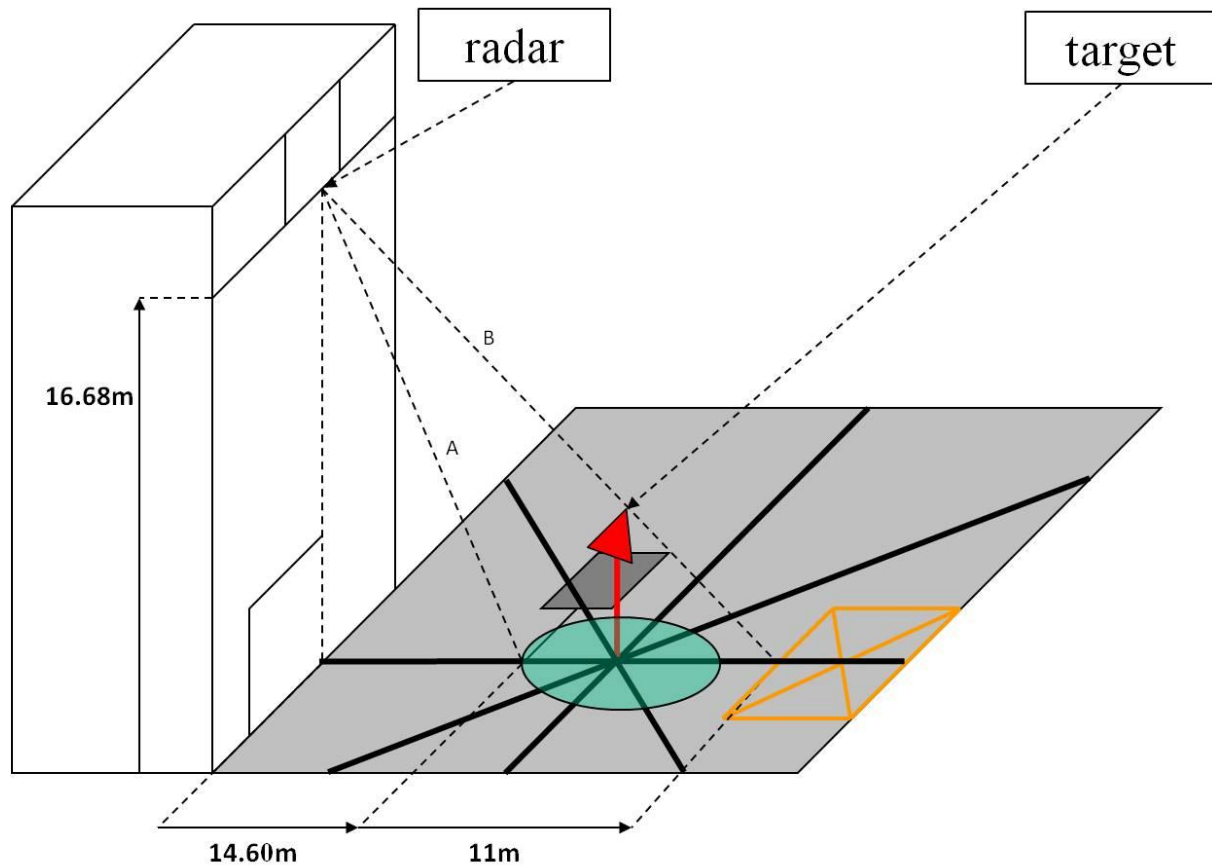


Figure 94: set-up for the parking experiment

The horn antennas are located 16.68m above the ground level and the fixed targets are placed at least at 15m from the building, this way the antennas are not tilted at a sharp angle because the grating lobes would be directed towards the building walls, causing strong reflections. The target used to test the radar system was a 0.7m triangle corner reflector, whose RCS is given by Equation 27:

Equation 27: Triangle Corner Reflector RCS

$$\sigma_{max} = \frac{4\pi L^4}{3\lambda^2}$$

Where L is the triangle dimension in m, λ is the wavelength in m.

With Equation 27, the RCS for this target @ 10.4GHz is 30.5dBsqm. Since the antennas are 1.5m apart and the targets are at least at 20m from the antennas, using the ovals of Cassini, the power budget can be calculated with the monostatic equation instead of the bistatic equation for simplicity.

Equation 28: Monostatic Signal to Noise Ratio

$$SNR = \frac{P_{av} G_{tx} G_{rx} \lambda^2 \sigma}{(4\pi)^3 D^4 L (kTB) F}$$

Where P_{av} is the emitted average power in Watts, G_{tx} is the transmitter antenna gain, G_{rx} is the receiver antenna gain, λ is the wavelength, σ is the target RCS in square meters, D is the radial distance from the radar to the target in meters, L is the radar system loss coefficient, k is the Boltzmann constant, T is the temperature in Kelvin, B the bandwidth in Hz and F the radar system noise figure.

Since the antennas are fixed, as the target moves inside the illuminated area, it also moves inside the antenna gain pattern. A sinc^2 approximation of the antenna gain pattern was used and is shown in Equation 29.

Equation 29: sinc^2 approximation of the horn antenna gain pattern

$$G(\theta_{az}, \theta_{el}) = G_o \times \left(\text{sinc}^2 \left(-2.8 \left(\frac{\theta_{az}}{\theta_{az3dB}} \right) \right) + \text{sinc}^2 \left(-2.8 \frac{\theta_{el}}{\theta_{el3dB}} \right) \right)$$

Where θ_{az} and θ_{el} are respectively the azimuth and elevation angles in rads, θ_{az3dB} and θ_{el3dB} are respectively the azimuth and elevation beamwidth equal to 0.265rads (14.85 °) and 0.325rads (18.04 °), G_o is the maximum gain in the direct line of sight.

The SNR with 20dBm emitted power and a triangle corner reflector of RCS 30.5dB is compared when the target is in the line of sight and when it is travelling in the antenna gain pattern in the radar axis, the result is shown in Figure 95. It can be observed that the power levels are significantly lower than the hypothesis when the target is always in the antenna line of sight. Both curves meet at 27m which matches the antenna maximum gain. Also this SNR is expressed only over one pulse so integration should improve detection capabilities. The calibrator was thus placed at this point on the ground, 27m from the antenna. It should be kept in mind that a moving target will display power fluctuations while passing through the scene as shown in Figure 95.

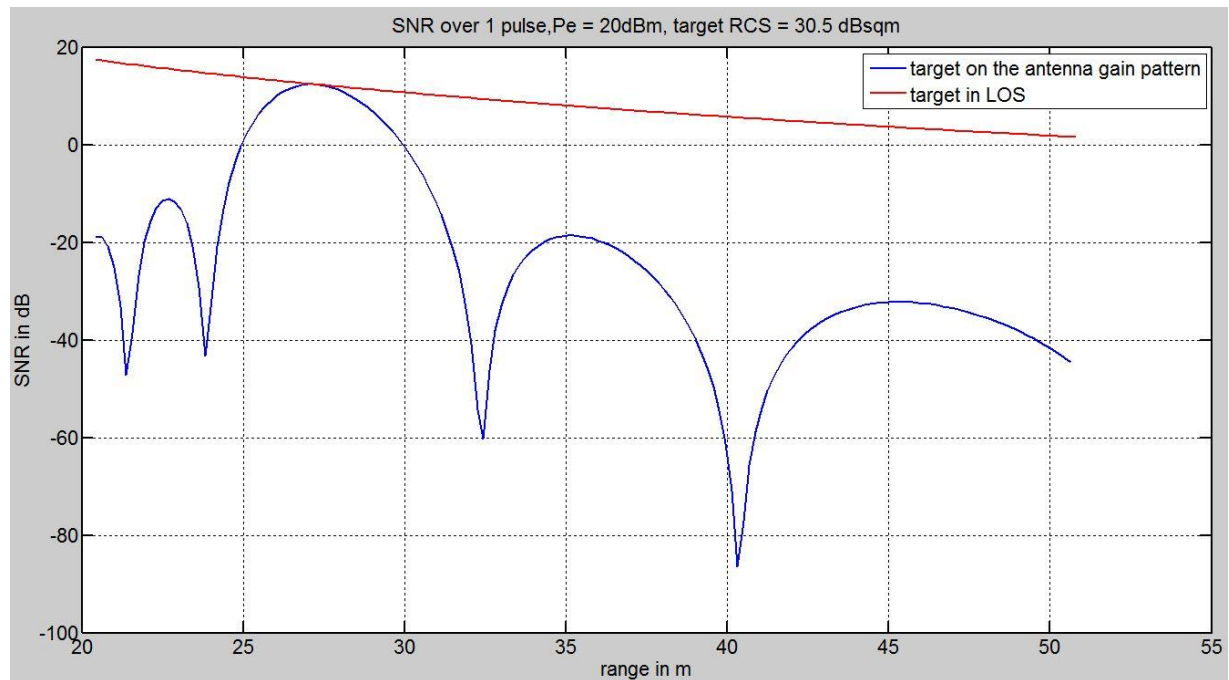


Figure 95: Difference between target in line of sight and target travelling inside the antenna gain pattern

Another aspect of the experiment that needs to be taken into account is the clutter power. However, we must first determine the clutter power from the scene geometry shown in Figure 96 and the antenna characteristics. For this calculation, we need to determine the clutter nature and its RCS, the clutter surface (Equation 15) with respect to distance and the grazing angle.

Equation 30: clutter surface calculation (13)

$$S_n = \theta_{az,n} (2A_n \delta A_n + \delta A_n^2) \text{ where } A_n = \sqrt{D_n^2 + H^2} \text{ and } \delta A_n = A_{n+1} - A_n$$

Where A_n is the projection of the radial distance on the ground in m, δA_n is the difference between two successive projected radial distances in m, H is the radar antenna height in m, D_n the radial distance target-antenna in m, $\theta_{az,n}$ is the azimuth angle including the antenna inclination (53°) in rads.

The RCS in dBm/sqm is $\gamma = -12 \text{ dBsqm/sqm}$ in Xband, this data comes from Onera's database on clutter RCS. Then Equation 31 for moderate grazing angles is used to calculate the relative clutter RCS with respect to the grazing angle.

Equation 31: relative clutter RCS with respect to grazing angle (13)

$$\sigma_n = \gamma \times \sin(\psi_n) \text{ where } \psi_n = \frac{\pi}{2} - \theta_{az,n}$$

Incorporating this clutter RCS in Equation 28 with a range dependent RCS and simplifying the calculation by assuming a constant gain over the entire clutter area equal to the maximum gain, we get the following Clutter to Noise Ratio (CNR) in Figure 97. Since maximum antenna gain over the clutter area was assumed, this simulation is overestimating the clutter power. However, the clutter power is insignificant compared to the noise power and can thus be neglected.

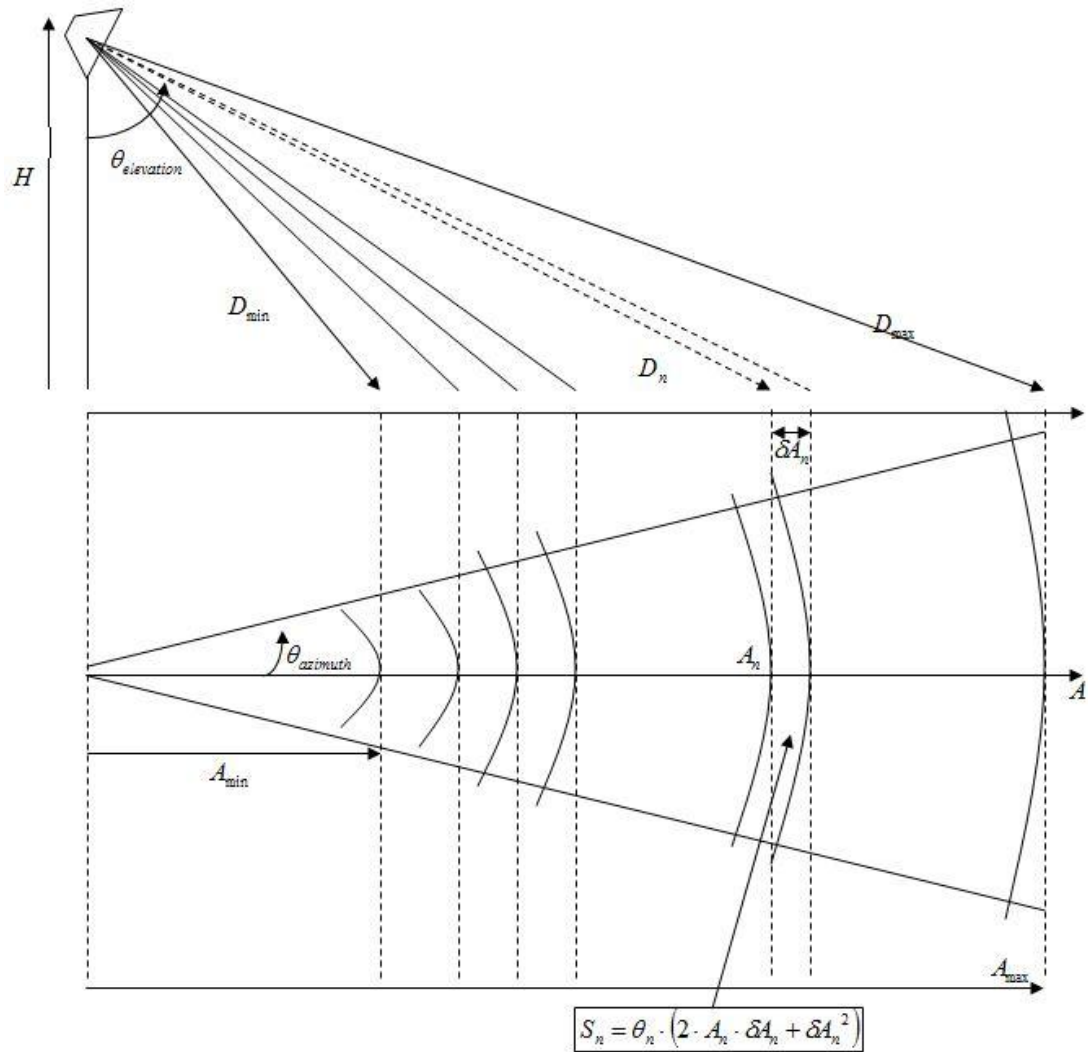


Figure 96: antenna main beam footprint for clutter calculation

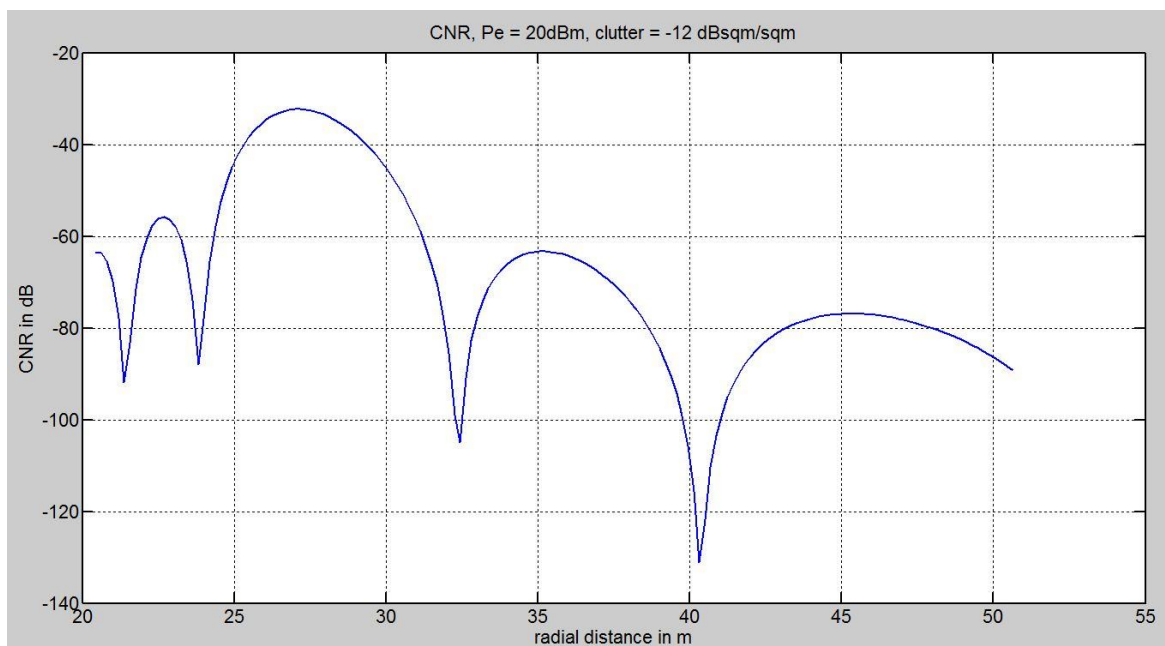


Figure 97: Clutter to Noise ratio over the Parking area

K. RMS quantization noise floor

The quantization noise floor or maximum achievable signal to noise ratio is.

Equation 32: Maximum SNR achievable per ADC channel

$$SNR_{max} = 6.02 \times ENOB + 1.76 \text{ (dB)}$$

Where $ENOB$ is the effective number of bits.

$$\begin{aligned} ENOB_{Neptune\ VXS\ 2} &= 7.4\text{bits} \ \& \ SNR_{Neptune\ VXS\ 2} = 46.3\text{dB} \\ ENOB_{DSA\ 71254} &= 5.4\text{bits} \ \& \ SNR_{DSA\ 71254} = 34.26\text{dB} \end{aligned}$$

This value is calculated with the entire noise in the Nyquist band. The processing gain obtained by filtering either analogically or digitally the useful bandwidth must be added and is shown in Equation 33.

Equation 33: Processing gain

$$G_{processing\ gain} = 10 \times \log_{10} \left(\frac{F_s}{2 \times BW} \right)$$

Where F_s is the sampling frequency and BW is the signal useful bandwidth.

The signals will have bandwidth from 800MHz down to 1MHz, thus the processing gain will be respectively [0.95dB – 30dB]. When observing the sampled data in the frequency domain, the FFT process also contributes to the process gain. The FFT noise floor is lower than the quantization noise floor.

Equation 34: FFT gain

$$G_{FFT} = 10 \times \log_{10} \left(\frac{M}{2} \right)$$

Where M is the FFT length. This will have to be considered when evaluating the signal SNR from the frequency domain. Thus the gain over one pulse will vary from 30dB for a 500ns pulse to 210dB for a 1ms pulse.

Using bandpass sampling raises the noise power even if we had a perfect antialiasing filter. All the noise aliased between DC and the pass band contributes to the degradation of the signal to noise ratio. (115). The antialiasing filter is used to reduce the out of band (OOB) noise power, thus $N_0 \ll N_p$. In our case the antialiasing filter crosses over the Nyquist bands so the OOB noise power will degrade the SNR. Bandpass sampling with a factor of m will approximately multiply the OOB noise by $2m$ (116). Considering the worst case scenario when $N_0 = N_p$.

Equation 35:bandpass sampling losses caused by aliased noise

$$D_{SNR} = 10 \times \log_{10} \left(1 + \frac{2mN_0}{N_p} \right) = 4\text{dB when } m = \frac{f_i}{f_s} = \frac{1.5\text{GHz}}{2\text{GHz}} = 0.75$$

Where N_p is the in band noise power, N_0 is the out of band (OOB) noise power, f_i is the signal carrier frequency and f_s is the sampling frequency.

The ADC’s maximum SNR (117) (118) (119) for a given aperture time jitter is time-invariant.

Equation 36: SNR limitation caused by the total RMS aperture jitter

$$SNR_{jitter} = -10 \times \log_{10} \left(\frac{\int_{-\infty}^{\infty} S(f) df}{2 \int_{-\infty}^{\infty} S(f) (1 - e^{-2(\pi f \sigma_j)^2}) df} \right)$$

Where $S(f)$ is the power density function, σ_j is the total RMS aperture jitter is the carrier frequency.

The limitation in SNR is estimated from digitizers specifications in Table 21.

	RMS jitter σ_j	Dynamic range
Neptune VXS II	[160fs – 200fs]	[54.5dB – 56.5dB]
DSA71254	450fs	45.8dB

Table 35: estimated digitizer dynamic range

L. Micro-Doppler Experiment

Most of the experiments were realized with moving targets along the 45° axis traced on the parking because the moving parts are better exposed to the electromagnetic waves and thus the micro-Doppler are more visible on radar images.

In Figure 98, a radar experiment with a pedestrian is described, the pedestrian is sprinting at a very fast pace at 45° towards the radar. In this image, the optical and radar view are matched to explain the phenomena observed in radar view.

The color scale is normalized to the calibrator reflection power level. A typical RCS for a pedestrian is between -10 and 0dBsm and the calibrator has a 30.5dBsm. So the color scale with a max level at -60dB relative to the calibrator reflection power level is coherent since the sprinter isn't oriented directly towards the radar.

First of all, the velocity is the radial velocity. The radar doesn't measure any other velocities with these measurements. The negative velocities indicate that the target moves away from the radar and the positive velocities that the target moves towards the radar. The radar image shows a target at 0m from the calibrator position which is coherent with the optical image where the line is graduated every 2m. The target also displays a mean radial velocity of 4m/s (≈ 14.4 km/h) which gives about 20km/h in absolute speed, which is coherent with a sprint.

Also the micro-Doppler shown on the images allows observing the limbs relative velocities with respect to the body's mean velocity. From the radar image, two limbs are distinguished moving away from the radar the top micro-Doppler trace indicates the relative speed of the right leg that pushes the body forward and thus appears to move away from the radar when compared to the torso's movement. From the radar point of view the legs are lower than the arms, the left arm swings backward as the right leg pushes forward to hold balance. On the other hand, the left leg is thrown ahead for the next step thus displaying positive velocity as relative to the torso it is moving faster. The left arm swings forward for balance.

In Figure 99, the car slowly circles around the center of the scene. The radar view displays a large mass moving away from the radar corresponding to the car frame at -2m/s radial velocity which corresponds to -13km/h in absolute speed. This is coherent with a very slow moving car. Two wheels are visible on the radar view as well as in the optical image. The micro-Doppler on the wheels is almost symmetrical because the car frame partially masks the wheels. If you consider a rotating wheel, the velocity at the front of the wheel is the same in absolute value as the velocity at the rear side of the wheel. This explains the quasi symmetry of the micro-Doppler on the image (88).

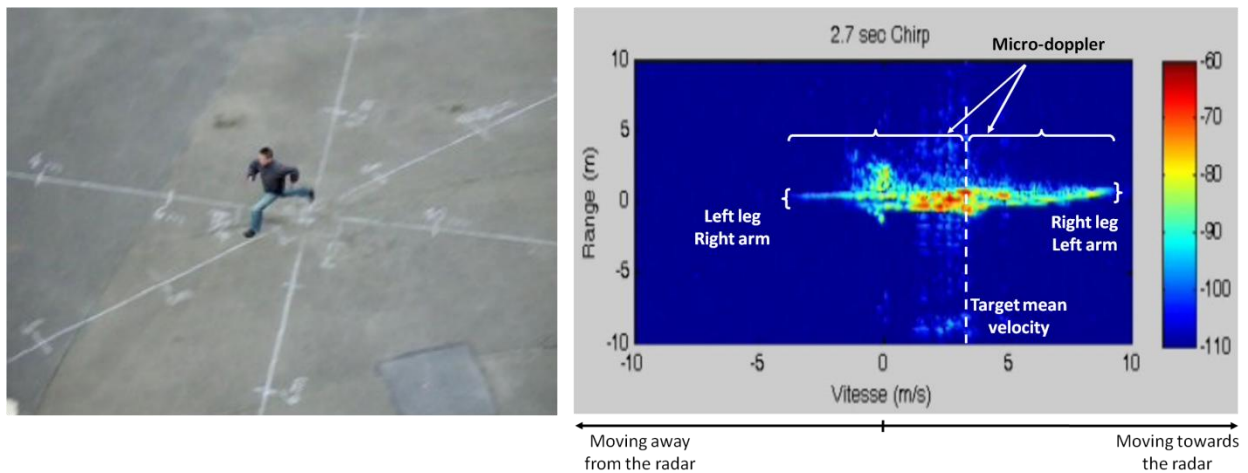


Figure 98: a pedestrian sprinting on the 45° axis (left) optical camera view (right) radar view

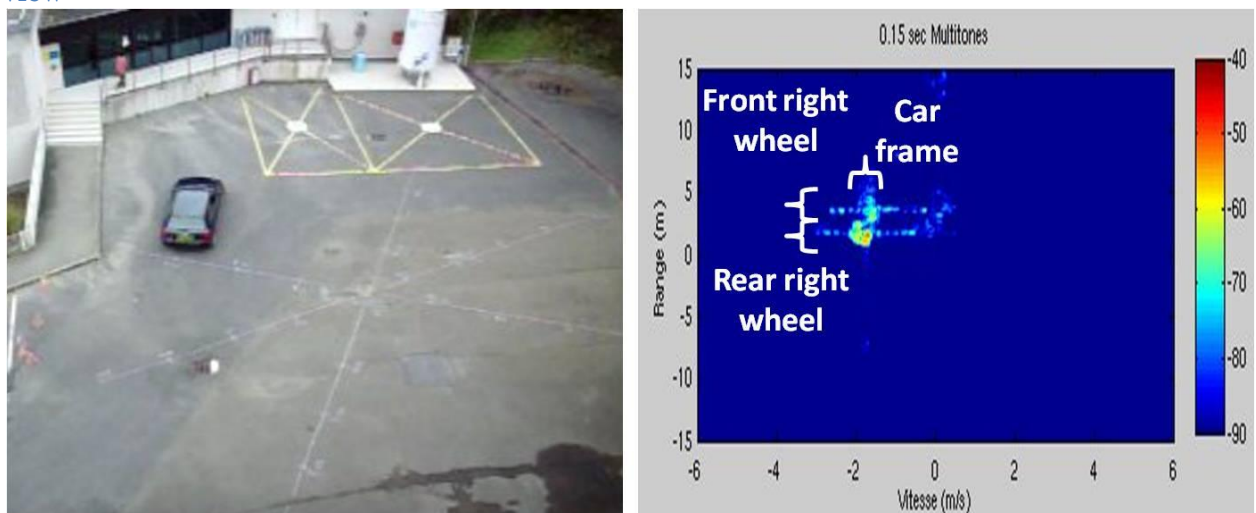


Figure 99: a car circling very slowly around the center of the scene (left) optical camera view (right) radar view

The micro-Doppler experiments were used at first to compare the waveforms. Several experiments were conducted with cars, bikes and pedestrians. But the synchronization and reproducibility of the experiments couldn't be guaranteed as shown in Figure 100. In this figure, the synchronization and reproducibility issues are illustrated. The car on a straight line in (a) isn't synchronized: the position is off by 1m between the two experiments and the mean velocity is also off by about 0.5m/s. And in the other 3 experiments (b) with a sprinter, (c) with a cyclist and (d) two joggers, the synchronization and reproducibility was only approximative despite repeated tries. Plus the man power required for these experiments prohibits long tryouts. Furthermore, the acquisition time would drop considerably when increasing the pulse length so this is unfeasible.

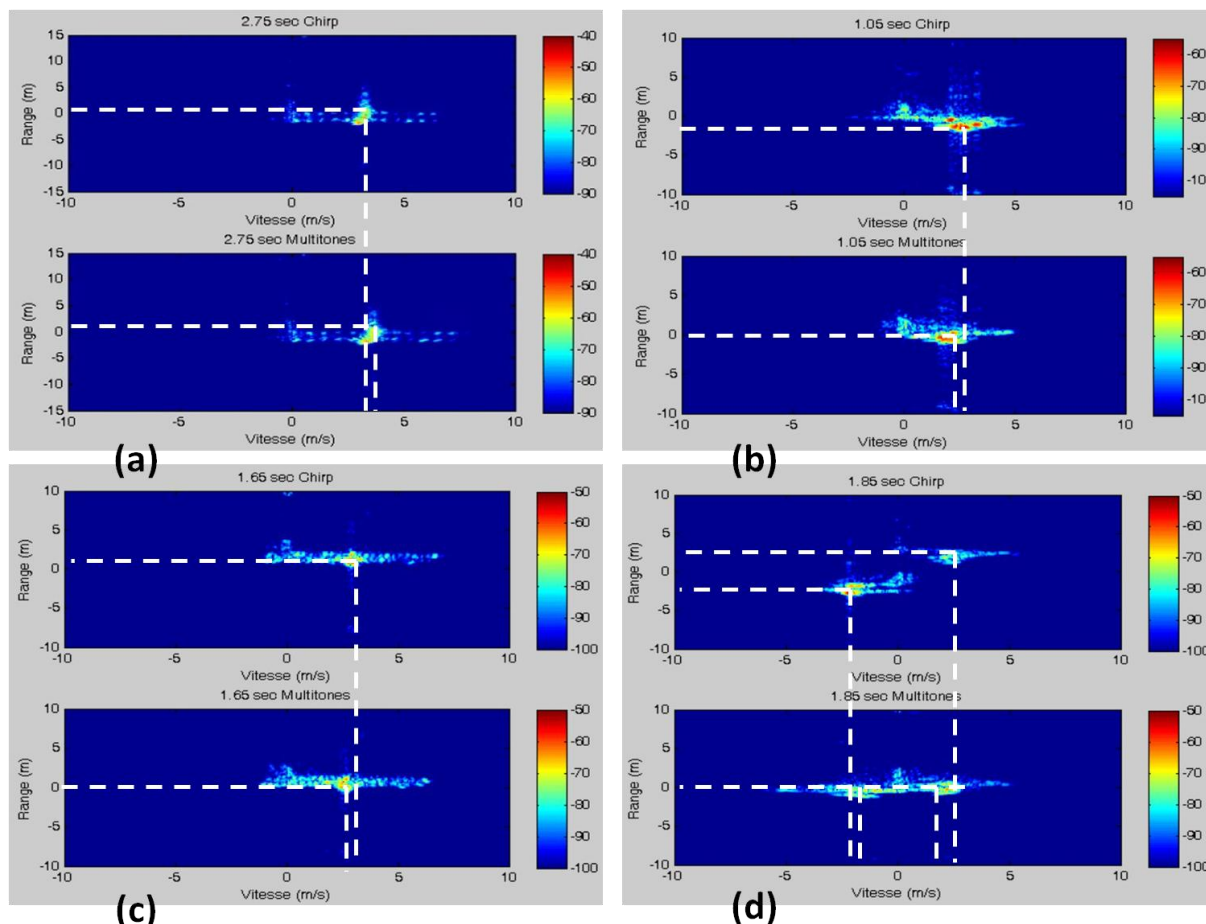


Figure 100: synchronization and reproducibility issues with experiments on moving targets on a straight line over the 45° axis (a) car (b) sprinter (c) cyclist in free wheel (d) two joggers on

A rotating fan seems like a good alternative. The rotation is constant and the reproducibility can be better controlled. The synchronization may not be guaranteed but over the integration time, the difference shouldn't be too great. Furthermore the range walk is no longer a problem since the target has moving parts but remains static. The radar view of the experiment looked promising at first glance.

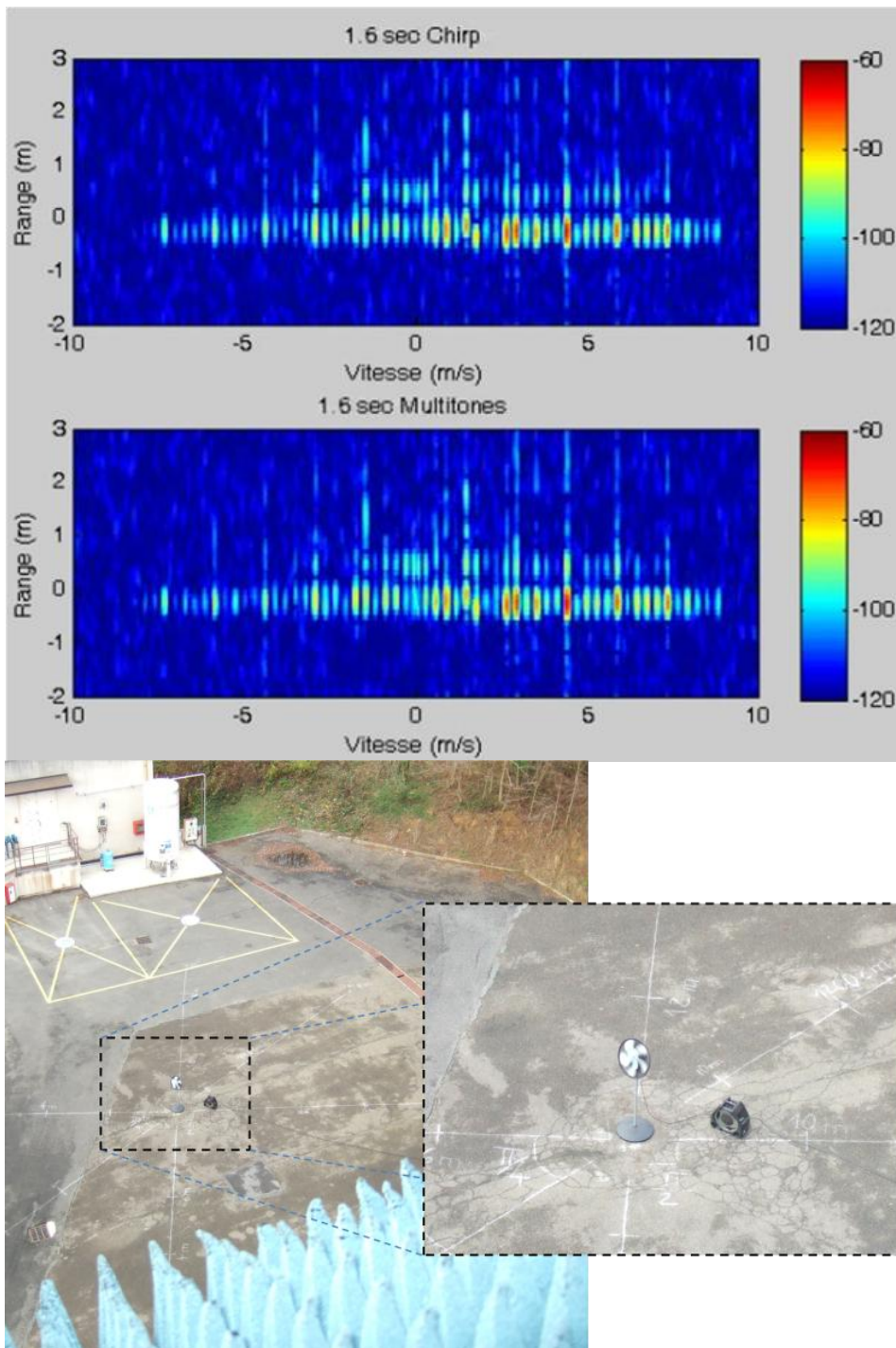


Figure 101: Doppler experiment with rotating fan facing forward on the 45° axis

However on that day, it was very windy and the fan stand was waving. And a fine analysis of the resulting measurement wasn't viable for comparison again as shown in Figure 102. There is a real need for reproducibility to compare the waveforms.

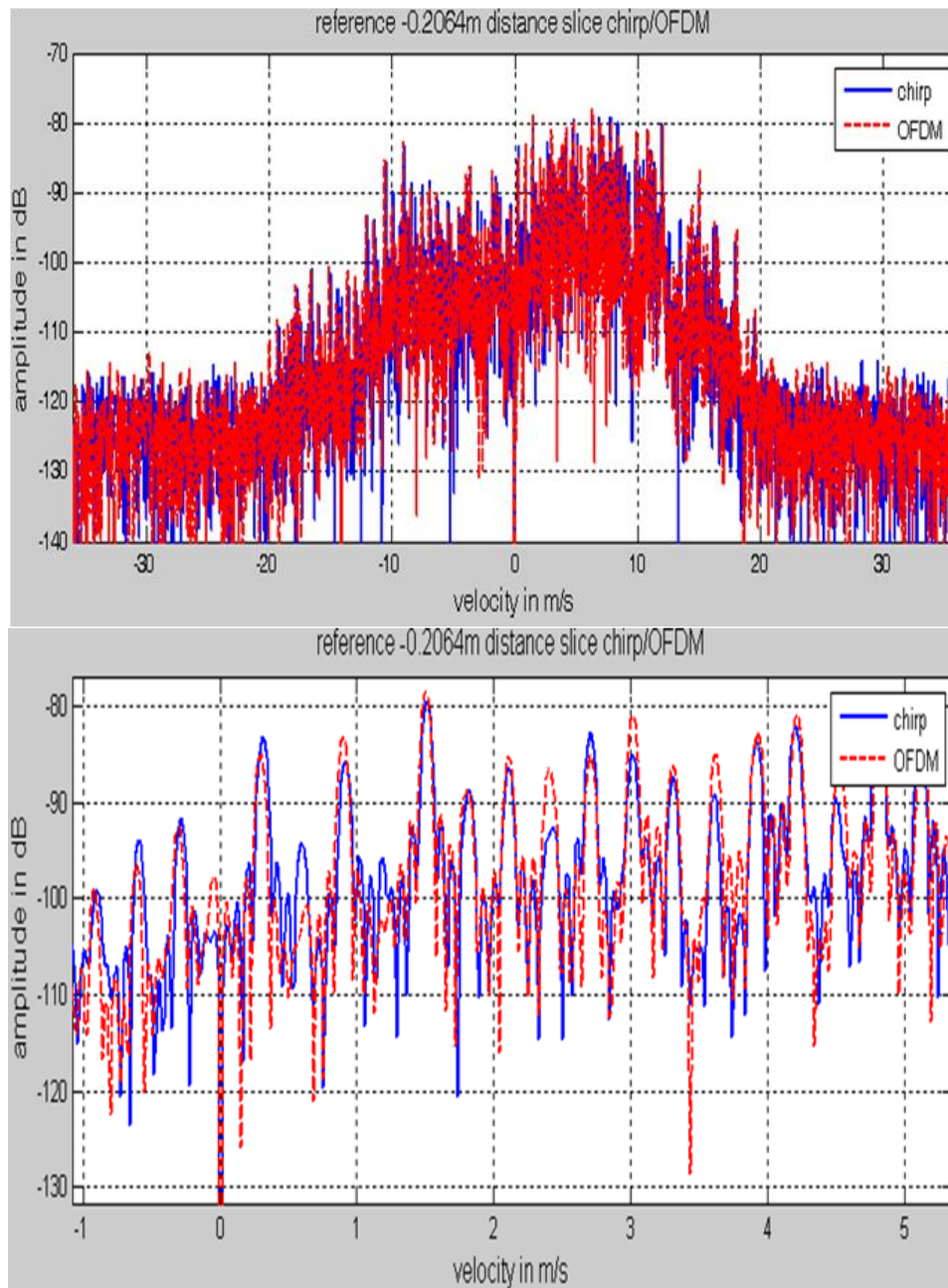


Figure 102: distance cut at -0.2064m of radar view (left) full distance cut (right) zoom of left view (Figure 101)

An automaton might be able to reproduce exactly the movements but a mean to match the start of the consecutive acquisition would still be necessary. In other words, moving targets are interesting to observe the Doppler effects but can't be used as a valid base to compare the waveforms with the equipment at hand.

M. Amplifier gain measurement and input power range for the saturation experiment

The amplifier ITS electronics PA-95105-4050 (component 12) was characterized in gain with respect to input power using a Vector Network Analyzer.

The vector network analyzer is first calibrated using the calibration kit from DC to 18GHz. Then the attenuators used for the amplifiers are first measured alone to determine a reference S_{21} as shown in Figure 103, using a sweep from 9GHz up to 12GHz. This sweep power ranges from -35dBm to 0dBm to determine the gain versus input power. The center frequency 10.4GHz was chosen to trace the gain versus input frequency Figure 104.

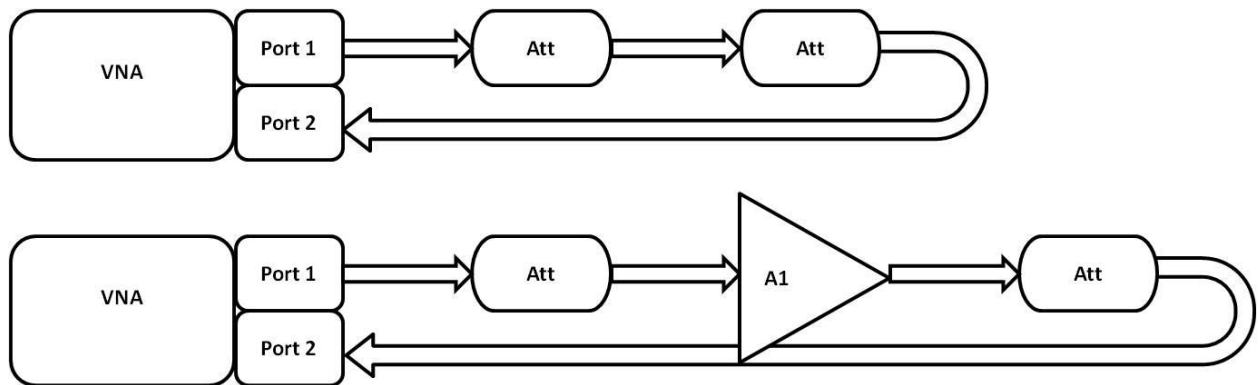


Figure 103: vector network analyzer measurement setup (top) reference measurement (bottom) amplifier gain measurement

Equation 37: Gain versus input power

$$G(P_{in}) = S_{21_{Att+Amp}}(P_{in}) - S_{21_{ref}}(P_{in})$$

The results of the gain characterizations for the amplifier is shown in Figure 104. The input power range should be $IP_{1dB} \pm 6dB$. Thus for PA-95105-4050, the range should be $-17dBm \pm 6dB$. These ranges should cover both the common knowledge of optimum 6dB IBO in telecommunications and saturation states to allow us to determine the optimum radar operating point.

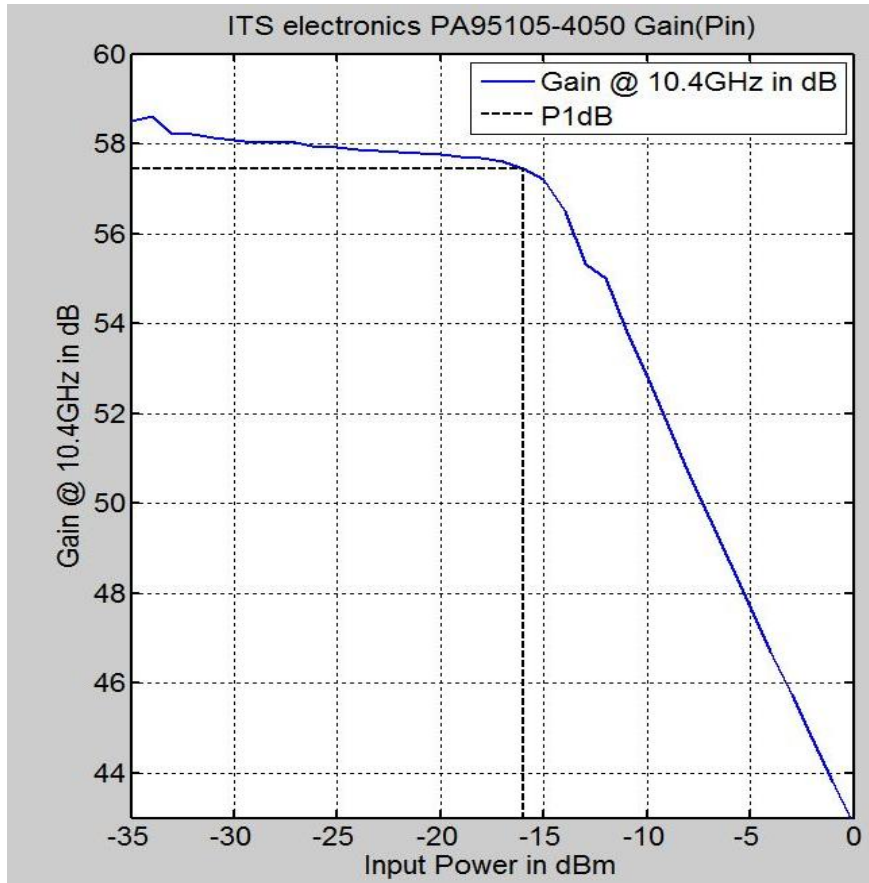


Figure 104: IP1dB and gain for saturation experiment: amplifier ITS electronics PA-95105-4050

N. Stability

PRP ►		500ns		5 µs		50 µs		500 µs		1ms	
BW ▼	Stab	MT	upC	MT	upC	MT	upC	MT	upC	MT	upC
1MHz	Mean	X	X	X	X	-44.2	-43.7	-43	-41.6	-49.4	-44.8
	Min	X	X	X	X	-32.11	-32.4	-33.2	-35.6	-40.8	-38.2
10MHz	Mean	X	X	-42.7	-41.9	-40.1	-43	-43.2	-43.4	-45.6	-51
	Min	X	X	-31.5	-27	-31.5	-33.9	-33.8	-35.1	-35.3	-44.15
150Hz	Mean	-42.3	-42.3	-38.6	-42.2	-41.2	-42.1	-43.3	-39.4	-44.1	-47.3
	Min	-29.6	-29.4	-28.8	-30	-31	-31.8	-35.2	-33.5	-34.8	-38.5
800MHz	Mean	-41.6	-39	-43.4	-42.4	-44.3	-43.8	-43.5	-43.5	-44.8	-46.7
	Min	-28.2	-27.9	-31	-29.6	-34.1	-32	-33.9	-38.3	-36.5	-35.4

Table 36: relative error in dB in amplitude and phase of the peak of the impulse response with a digital reference – raw

PRP ►		500ns		5 µs		50 µs		500 µs		1ms	
BW ▼	Stab	MT-upC									
1MHz	Mean	X		X		-0.48		-1.43		-4.56	
	Min	X		X		-0.32		2.45		-2.61	
10MHz	Mean	X		-0.8		2.03		2.16		5.41	
	Min	X		-4.45		1.85		1.2		8.86	
150Hz	Mean	0.01		3.62		0.92		-3.9		3.2	
	Min	-0.15		1.49		0.83		-1.71		3.76	
800MHz	Mean	-2.59		-1.01		-0.51		0		1.92	
	Min	-2.48		-1.42		-2.02		4.38		-1.09	

Table 37: difference in dB between multitones and Chirp in relative error in amplitude and phase of the peak of the impulse response with a digital reference – raw

PRP ►		500ns		5 µs		50 µs		500 µs		1ms	
BW ▼	Stab	MT	upC	MT	upC	MT	upC	MT	upC	MT	upC
1MHz	Mean	X	X	X	X	-43.3	-43.4	-42.3	-41.5	-48.4	-43.5
	Min	X	X	X	X	-31.4	-31.9	-31.6	-34	-37.9	-36.9
10MHz	Mean	X	X	-42.6	-41.8	-39.8	-43	-41.2	-42.8	-46.3	-48.2
	Min	X	X	-31.4	-26.9	-30.4	-32.9	-34.1	-34.2	-36.1	-40.5
150Hz	Mean	-42.2	-42.3	-38.5	-42.2	-40	-42	-40.7	-38.8	-43.4	-44.6
	Min	-29.4	-29.4	-28.7	-30.3	-30.4	-31.5	-33.6	-32.7	-33.4	-35.7
800MHz	Mean	-41.6	-39	-43.4	-42.2	-44	-43.5	-42.7	-42.3	-43.5	-47.1
	Min	-28.2	-27.9	-31.1	-29.5	-33.8	-31.7	-33	-35.2	-35	-35.6

Table 38: relative error in dB in amplitude and phase of the peak of the impulse response with a digital reference – Hamming

PRP ►		500ns		5 µs		50 µs		500 µs		1ms	
BW ▼	Stab	MT-upC									
1MHz	Mean	X		X		0.09		-0.85		-4.88	
	Min	X		X		0.53		2.46		-0.97	
10MHz	Mean	X		-0.73		3.13		1.58		1.86	

	Min	X	-4.47	2.46	0.09	4.45
150Hz	Mean	1.71	3.72	1.94	-1.9	1.19
	Min	-0.03	1.64	1.07	-0.87	2.32
800MHz	Mean	-2.6	-1.21	-0.49	-0.39	3.63
	Min	-3.2	-1.59	-2.07	2.24	0.66

Table 39: difference in dB between multitones and Chirp in relative error in amplitude and phase of the peak of the impulse response with a digital reference – Hamming

PRP ►		500ns		5 µs		50 µs		500 µs		1ms	
BW ▼	Stab	MT	upC	MT	upC	MT	upC	MT	upC	MT	upC
1MHz	Mean	X	X	X	X	-43.9	-43.7	-43.4	-41.6	-48.7	-44.8
	Min	X	X	X	X	-31.8	-32.4	-33.1	-35.6	-40.8	-38.2
10MHz	Mean	X	X	-42.7	-41.9	-41	-43	-43.3	-43.4	-45.6	-51
	Min	X	X	-31.5	-27	-31.5	-33.4	-33.9	-35.1	-35.2	-44.5
150Hz	Mean	-42.2	-42.3	-38.6	-42.2	-41	-42.1	-43.2	-39.5	-44	-47.3
	Min	-29.5	-29.4	-28.8	-30.4	-30.9	-31.7	-35	-33.6	-34.6	-38.5
800MHz	Mean	-41.4	-38.9	-43.4	-42.5	-44.5	-43.8	-43.8	-43.7	-44.9	-47.2
	Min	-28.1	-27.9	-31	-29.6	-33.8	-32.2	-34.1	-38.3	-36.9	-35.5

Table 40: relative error in dB in amplitude and phase of the peak of the impulse response with a measured reference – raw

PRP ►		500ns		5 µs	50 µs	500 µs	1ms
BW ▼	Stab	MT-upC		MT-upC	MT-upC	MT-upC	MT-upC
1MHz	Mean	X	X	X	-0.17	-1.77	-3.89
	Min	X	X	X	0.63	2.49	-2.61
10MHz	Mean	X	X	-0.77	1.97	0.15	5.43
	Min	X	X	-4.43	1.86	1.24	9.39
150Hz	Mean	0.09	0.09	3.61	1.05	-3.77	3.3
	Min	-0.12	-0.12	1.57	0.83	-1.49	3.87
800MHz	Mean	-2.47	-2.47	-0.88	-0.62	-8.02	2.27
	Min	-0.17	-0.17	-1.39	-1.54	4.11	-1.34

Table 41: difference in dB between multitones and Chirp in relative error in amplitude and phase of the peak of the impulse response with a measured reference – raw

PRP ►		500ns		5 µs		50 µs		500 µs		1ms	
BW ▼	Stab	MT	upC	MT	upC	MT	upC	MT	upC	MT	upC
1MHz	Mean	X	X	X	X	-43.3	-43.4	-42.1	-41.5	-48	-43.5
	Min	X	X	X	X	-31.4	-32	-31.6	-34.1	-37.9	-36.9
10MHz	Mean	X	X	-42.6	-41.9	-39.9	-43	-41.3	-42.8	-46.2	-48.4
	Min	X	X	-31.4	-27	-30.5	-33	-34.2	-34.2	-36	-40.8
150Hz	Mean	-42.3	-42.3	-38.5	-42.2	-40	-42	-40.5	-38.8	-43.3	-44.6
	Min	-29.6	-29.4	-28.7	-30.3	-30.4	-31.5	-33.5	-32.8	-33.3	-35.7

800MHz	Mean	-41.4	-38.9	-43.4	-42.4	-44.1	-43.6	-42.8	-42.7	-43.5	-47.5
	Min	-28.1	-27.9	-31	-29.5	-33.5	-31.8	-33.1	-35.4	-35	-35.6

Table 42: relative error in dB in amplitude and phase of the peak of the impulse response with a measured reference – Hamming

PRP ►		500ns	5 µs	50 µs	500 µs	1ms
BW ▼	Stab	MT-upC	MT-upC	MT-upC	MT-upC	MT-upC
1MHz	Mean	X	X	0.13	-0.69	-4.49
	Min	X	X	0.56	2.46	-0.97
10MHz	Mean	X	-0.65	3.13	1.44	2.2
	Min	X	-4.41	2.47	0	4.79
150Hz	Mean	-0.01	3.66	1.99	-1.73	1.29
	Min	-0.18	1.6	1.07	-0.7	2.4
800MHz	Mean	-2.5	-0.95	-0.58	-0.37	3.97
	Min	-0.17	-1.5	-1.67	2.2	0.61

Table 43: difference in dB between multitones and Chirp in relative error in amplitude and phase of the peak of the impulse response with a measured reference – Hamming

PRP ►		500ns		5 µs		50 µs		500 µs		1ms	
BW ▼	Stab	MT	upC	MT	upC	MT	upC	MT	upC	MT	upC
1MHz	Mean	X	X	X	X	0.3	-0.01	-0.34	0	0.68	0.01
	Min	X	X	X	X	0.27	-0.04	-0.04	0	0	0
10MHz	Mean	X	X	0	-0.02	-0.06	0	0	-0.01	0.04	0.02
	Min	X	X	0.03	0.02	-0.03	-0.04	-0.04	0	0.1	-0.43
150Hz	Mean	0.07	0	0	0	0.1	-0.02	0.1	-0.02	0.11	0.01
	Min	0.02	-0.01	0.02	-0.06	0.03	0.03	0.1	-0.12	0.19	0.07
800MHz	Mean	0.21	0.09	0.04	-0.09	-0.11	0	-0.28	-0.21	-0.1	-0.44
	Min	0.12	0.04	0.06	0.03	0.3	-0.17	-0.26	0	-0.35	-0.1

Table 44: difference in dB between relative errors on stability obtained with measured reference and digital reference – raw

PRP		500ns		5 µs		50 µs		500 µs		1ms	
BW ▼	Stab	MT	upC	MT	upC	MT	upC	MT	upC	MT	upC
1MHz	Mean	X	X	X	X	0.05	0	0.15	0	0.39	0
	Min	X	X	X	X	0	-0.03	0	0	0	0
10MHz	Mean	X	X	0.01	-0.07	0	0	0	0.03	0.1	-0.24
	Min	X	X	0.03	-0.02	-0.03	-0.04	-0.04	0.04	0.05	-0.28
150Hz	Mean	-0.12	0.06	-0.05	0.01	0.05	0	0.13	-0.04	0.05	-0.04
	Min	-0.16	-0.01	0	0.03	0.03	0.03	0.08	-0.07	0.08	0
800MHz	Mean	0.14	0.05	0.05	-0.21	-0.1	0	-0.12	-0.14	-0.05	-0.38
	Min	0.12	-0.02	0.06	-0.02	0.29	-0.1	-0.11	-0.15	-0.05	0

Table 45: difference in dB between relative errors on stability obtained with measured reference and digital reference - Hamming

0. Saturation Measurements

1. PMEPR

Bandwidth ►		1MHz	10MHz	150MHz	800MHz
impulse response with simulated reference					
Chirp	PMEPR	4	4	3.95	4.5
	Range	[3.93;4.45]	[3.9;4.12]	[3.91;3.97]	[4.31;5.84]
MT	PMEPR	4.4	4.4	4.1	4.5
	Range	[4.15;4.8]	[4.06;5.55]	[3.96;4.59]	[4.45;4.61]
Error Chirp $\left \frac{meas}{sim} \right $	Mean	1	1	0.87	0.4
	Range	[0.92;1.44]	[0.88;1.11]	[0.83;0.89]	[0.12;1.67]
Error MT $\left \frac{meas}{sim} \right $	Mean	-1.1	-1.1	-1.3	-0.8
	Range	[-1.38;-0.6]	[-1.49;0.22]	[-1.58;-0.76]	[-1.04;-0.64]
Error $\left \frac{MT}{upC} \right $	Range	[-0.25;0.88]	[-0.04;1.59]	[0;0.66]	[-1.36;0.3]
impulse response with measured reference					
Chirp	PMEPR	3.3	3.4	4.2	6.4
	Range	[3.2;4.43]	[3.18;4.39]	[3.92;4.54]	[6.16;6.86]
MT	PMEPR	5	5.5	5.1	6.2
	Range	[3.32;5.69]	[4.31;6.98]	[4.6;5.76]	[5.38;6.94]
Error Chirp $\left \frac{meas}{sim} \right $	Mean	0.3	0.3	1.2	2.3
	Range	[0.19;1.42]	[0.17;1.38]	[0.84;1.46]	[1.93;2.645]
Error MT $\left \frac{meas}{sim} \right $	Mean	-0.5	-0.3	-0.2	0.8
	Range	[-1.92;-0.15]	[-0.93;1.42]	[-0.66;0.22]	[0.08;1.546]
Error $\left \frac{MT}{upC} \right $	Range	[0.52;2.37]	[1.34;3.65]	[0.57;1.82]	[-0.87;0.09]
Error between impulse response with meas ref and impulse response with sim ref wrt impulse response with sim ref					
Chirp Error	$\frac{IR_{meas_ref}}{IR_{sim_ref}}$	[-0.8;0.44]	[-0.81;0.36]	[-0.04;0.57]	[0.35;2.52]
MT Error	$\frac{IR_{meas_ref}}{IR_{sim_ref}}$	[-0.84;1.49]	[-0.63;2.69]	[0.14;1.79]	[0.93;2.47]

Table 46: Measurement results on PMEPR in dB

2. Power efficiency

Bandwidth ►		1MHz	10MHz	150MHz	800MHz
impulse response with simulated reference					
	Power efficiency	87	92	96	97.5
	Range	[71.05;96.77]	[75.6598;83]	[86.63;99.58]	[96.49;99.16]

]]]
Error $\frac{ meas - sim }{sim}$	Mean	8	5	0	0
	Range	[1.28;25.08]	[0;13.64]	[-6.77;0.9]	[-0.4;0.3]
Error $\frac{ MT - upC }{upC}$	Range	[4.3;18.13]	[1.2;12.7]	[0.23;1.96]	[0.69;1.03]
	impulse response with measured reference				
	Power efficiency	70	80	94	97.5
	Range	[27.86;77.6]	[36.33;90.55]	[85.08;97.97]	[96.37;98.98]
Error $\frac{ meas - sim }{sim}$	Mean	-15	-6	-2	0
	Range	[-68.62;-10.99]	[-61.94;8.9]	[-8.56;-0.68]	[-0.23;0.4]
Error $\frac{ MT - upC }{upC}$	Range	[-2.81;3.41]	[-38.5;19.58]	[-0.9;3.38]	[0.6;1.93]
	Error between impulse response with meas ref and impulse response with sim ref wrt impulse response with sim ref				
Error	$\frac{IR_{meas_ref} - IR_{sim_ref}}{IR_{sim_ref}}$	[-62.92;-8.6]	[-60.03;-4.31]	[-2.87;-1.27]	[-0.36;0.82]

Table 47: Measurement results on power efficiency in %

3. Mainlobe 3dB width

Bandwidth ►		1MHz	10MHz	150MHz	800MHz
impulse response with simulated reference					
	3dB width	≈133m	≈14m	≈0.9m	≈0.3m
	Range	±6m	±4m	+7.5cm	±7.5cm
Error $\frac{ meas - sim }{sim}$	Mean	≈2%	≈8%	≈1.7%	≈81.82%
	Range	±3%	±16%	[0;8.5]%	[-45.5;0]%

Error $\left \frac{MT - upC}{upC} \right $	Range	<6.1%	<30%	<8.3%	<33.3%
impulse response with measured reference					
	3dB width	≈134m	≈14m	≈0.9m	≈0.3m
	Range	±7m	±3	7.5cm	0
Error $\left \frac{meas - sim}{sim} \right $	Mean	≈1.5%	≈8%	≈1.7%	≈81.82%
	Range	±3%	±16%	[0;8.5%]	0%
Error $\left \frac{MT - upC}{upC} \right $	Range	<6.3%	<36%	<8.5%	0%
Error between impulse response with meas ref and impulse response with sim ref wrt impulse response with sim ref					
Error	$\frac{IR_{meas_ref} - IR_{sim_ref}}{IR_{sim_ref}}$	<5.5%	<15.3%	<8.3%	<33.33%

Table 48: Measurement results on 3dB main lobe width

4. Sidelobes' amplitudes

Bandwidth ►		1MHz	10MHz	150MHz	800MHz
impulse response with simulated reference					
	left sidelobe amplitude	≈-13dB	≈-10.5dB	≈-14dB	≈-21dB
	Range	[-1.1;2.7]dB	[-17.8;9.5]dB	[-3.3;2.7]dB	[-3.6;3.8]dB
Error $\left \frac{meas}{sim} \right $	Mean	≈1dB	≈2.5dB	≈-1dB	≈-8dB
	Range	[-1.5;2.5]dB	[-9.6;9.8]dB	[-2.6;2.8]dB	[-4.3;5]dB

Error $\left \frac{MT}{upC} \right $	Range	[-3.4;1.4]dB	[-14.9;11.5]dB	[-5.8;4.1]dB	[-7.7;3.2]dB
impulse response with measured reference					
	left sidelobe amplitude	≈-13dB	≈-11.5dB	≈-13dB	upC≈-13dB MT≈-21dB
	Range	[-1.7;2.4]dB	[-10;8.4]dB	[-2.7;2.2]dB	[-2.5;2.5]dB
Error $\left \frac{meas}{sim} \right $	Mean	≈0.5dB	≈3dB	≈0.5dB	upC≈0 MT≈-7.5
	Range	[-1.9;2.7]dB	[-10;8.7]dB	±2.2dB	[-2.7;2.3]dB
Error $\left \frac{MT}{upC} \right $	Range	[-3.7;0.5]dB	[-14.8;14.6]dB	[-4.9;3.7]dB	[-10.1;-5.6]dB
Error between impulse response with meas ref and impulse response with sim ref wrt impulse response with sim ref					
Error	$\frac{IR_{meas_ref}}{IR_{sim_ref}}$	[-2.03;0.5]dB	[-1.3;1.8]dB	[0.4;2.2]dB	[-4.7;7.5]dB

Table 49: Measurement results on left sidelobe amplitude

Bandwidth ►		1MHz	10MHz	150MHz	800MHz
impulse response with simulated reference					
	right sidelobe amplitude	≈-13dB	≈-13.5dB	≈-11.5dB	upC≈-5dB MT≈-8.3dB
	Range	[-0.5;1.5]dB	[-8.3;7.8]dB	[-2;2.3]dB	[-1.6;2.2]dB
Error $\left \frac{meas}{sim} \right $	Mean	0.3dB	0dB	2dB	upC≈8dB MT≈5dB
	Range	[-0.5;1.5]dB	[-3.2;13.1]dB	[-2;1.9]dB	[-1.4;2.5]dB
Error $\left \frac{MT}{upC} \right $	Range	[-1.9;1.3]dB	[-4.6;14]dB	[-2.8;2.7]dB	[-5.7;-1.8]dB
impulse response with measured reference					
	right sidelobe amplitude	≈-13dB	≈-13.5dB	≈-11dB	upC≈-9dB MT≈-15dB

	Range	[-1.1;1.4]dB	[-8.3;7.8]dB	[-8.7;1.5]dB	[-1.2;2.4]dB
Error $\left \frac{meas}{sim} \right $	Mean	0dB	0dB	2dB	upC≈4dB MT≈-1.5dB
	Range	[-1;1.4]dB	[-3.4;13.1]dB	[-8.6;1.8]dB	[-1.2;2.5]dB
Error $\left \frac{MT}{upC} \right $	Range	[-2;0.3]dB	[-4.4;14]dB	[-8.1;1.9]dB	[-8;-3.4]dB
Error between impulse response with meas ref and impulse response with sim ref wrt impulse response with sim ref					
Error	$\frac{IR_{meas_ref}}{IR_{sim_ref}}$	[-1;1.3]dB	[-3.6;1.4]dB	[0;0.8]dB	[-7.1;-2.9]dB

Table 50: Measurement results on right sidelobe amplitude

5. Sidelobes' positions

Bandwidth ►		1MHz	10MHz	150MHz	800MHz
impulse response with simulated reference					
	left sidelobe distance	≈-215m	≈-21m	≈-1.35m	≈-0.45m
	Range	[-34.7;11.4]m	[-12.5;5.8]m	±7.5cm	-15;7.5cm
Error $\left \frac{meas - sim}{sim} \right $	Mean	1%	5%	3%	45%
	Range	[-4.2;16.5]%	[-29.2;58.6]%	[-10.3;5.3]%	[-27.8;56.6]%
Error $\left \frac{MT - upC}{upC} \right $	Range	<17.1%	<50.3%	<11.8%	<33.3%
impulse response with measured reference					
	left sidelobe distance	≈-212m	≈-21m	≈-1.425m	≈-0.3m
	Range	[-9.4;9.2]m	[-13.2;4.3]m	±7.5cm	[-7.5;0]m
Error $\left \frac{meas - sim}{sim} \right $	Mean	1%	-4%	0%	11.1%
	Range	[-6;3.6]%	[-10.7;59.8]%	[-5.5;5.2]%	[0;27.8]%

Error $\left \frac{MT - upC}{upC} \right $	Range	<6.5%	<37%	<5.6%	<20%
Error between impulse response with meas ref and impulse response with sim ref wrt impulse response with sim ref					
Error	$\frac{IR_{meas_ref} - IR_{sim_ref}}{IR_{sim_ref}}$	<8.4%	<10.4%	<11.8%	<55.6%

Table 51: Measurement results on left sidelobe position

Bandwidth ►		1MHz	10MHz	150MHz	800MHz
impulse response with simulated reference					
	right sidelobe distance	≈218m	≈22m	≈1.425m	upC≈0.225m MT≈0.3m
	Range	[-5.4;53.7]m	[-2.8;2.4]m	[-15;7.5]cm	0m
Error $\left \frac{meas - sim}{sim} \right $	Mean	2%	3%	1%	upC≈16.7% MT≈11.1%
	Range	[-3;25.2]%	[-11.9;12.6]%	[-10.4;5.2]%	0%
Error $\left \frac{MT - upC}{upC} \right $	Range	<23%	<17.5%	<11.1%	<33.3%
impulse response with measured reference					
	right sidelobe distance	≈222	≈22	≈1.425	≈0.3
	Range	[-6.8;7.9]m	[-2;2.4]m	±7.5cm	[0;7.5]cm
Error $\left \frac{meas - sim}{sim} \right $	Mean	1.5%	1%	0%	11.1%
	Range	[-2.2;2.7]%	[-11.2;13.8]%	±5.2%	[0;27.7]%
Error $\left \frac{MT - upC}{upC} \right $	Range	<4.5%	<19.3%	<11.1%	<25%
Error between impulse response with meas ref and impulse response with sim ref wrt impulse response with sim ref					

Error	$\frac{IR_{meas_ref} - IR_{sim_ref}}{IR_{sim_ref}}$	7.1%	17.6%	<11.8%	<66.7%
-------	--	------	-------	--------	--------

Table 52: Measurement results on right sidelobe position

Chapter 10. Bibliography

1. Onera, the French Aerospace Lab, www.onera.fr.
2. *Le projet R.I.A.S., une Nouvelle Approche du Radar de Surveillance Aérienne*. J. Dorey, Y. Blanchard, F. Christophe, 1984, L'Onde Electrique, Vol. 64, pp. 15-20.
3. *R.I.A.S., Radar à Impulsions et Antenne Synthétique*. J. Dorey, G. Garnier, G. Auray, Colloque international sur le radar, 1989.
4. *Experimental results on RIAS digital beamforming radar*. A.-S. Luce, H. Molina, D. Muller, V. Thirard, 1992, Radar 92 - International Conference, pp. 74-77.
5. *Passive detection using digital broadcasters (DAB, DVB) with COFDM modulation*. D. Poullin, 2005, IEE Proceedings -Radar, Sonar and Navigation, Vol. 152, pp. 143-152.
6. *L'utilisation active des COFDM en radar multistatique*. D. Poullin, 2006, REE, pp 36-42.
7. *Recent progress in Passive Coherent Location (PCL) concepts and technique in France using DAB or FM broadcasters*. D. Poullin and M. Flecheux, 2008, RADAR '08 - IEEE proceedings of Radar Conference. pp. 1-5.
8. *HYCAM: A RCS Measurement and Analysis System for Time-Varying Targets*. Y. Paichard, and J.-C.Castelli, P. Dreuillet, G. Bobillot, 2006, IMTC 2006 - IEEE proceedings of Instrumentation and Measurement Technology Conference, pp. 921-925.
9. *Microwave Camera for Multi-Dimensional Analysis of the RCS of Time-Varying targets*. Y. Paichard, 2007, PhD thesis, University of Paris 11.
10. *Hertzian-wave projecting and receiving apparatus adapted to indicate or give warning of the presence of a metallic body, such as a ship or a train, in the line of projection of such waves*. C. Hülsmeier, 1904, patent 13170.
11. *History of Radar*, J. Schneider, 2003, Lockheed Martin presentation on Radar at the Arizona State University.
12. *Radar signals*. N. Levanon, E. Mozeson, 2004, editor John Wiley & Sons
13. *Physique et théorie du radar*, J. Darricau, 2005, editor Sodipe.
14. *Improvement in target detection performance of pulse coded Doppler radar based on multicarrier modulation with fast Fourier transform (FFT)*. N. N. S. S. R. K. Prasad, V. Shameem, U. B. Desai, S. N. Merchant, 2004, IEE Proceedings -Radar, Sonar and Navigation, Vol. 151, pp. 11-17.
15. *Radar handbook*. M.I. Skolnik, 1991, editor Mc Graw Hill.
16. *Evolution de la conception radio: de la radio logicielle à la radio intelligente*. C. Moy, 2008, Habilitation à Diriger la Recherche, Université de Rennes I.

17. *Software defined radio: architectures, systems and functions*. M. Dillinger, K. Madani, N. Alonistioti, 2003, editor John Wiley & Sons.
18. *Mutual interference in OFDM-based spectrum pooling systems*. T. Weiss, J. Hillenbrand, A. Krohn, and F.K. Jondral. 2004. Proceedings of IEEE Vehicular Technology Conference, pp. 1873-1877.
19. *Cognitive radio modulation techniques*. I. Budiarto, H. Nikookar and L. Ligthart, November 2008, Signal Processing Magazine, IEEE , Vol. 25 Issue 6, pp. 24-34.
20. *Synthesis of Band-Limited Orthogonal Signals for Multichannel Data Transmission*. R.W. Chang, 1966, Bell System Technical Journal, Vol. 45, pp. 1775-1796.
21. *Performance of an Efficient Parallel Data Transmission System*. B.R. Saltzberg, 1967, IEEE Transactions on Communications, Vol. 15, pp. 805-811.
22. *Theoretical Study of Performance of an Orthogonal Multiplexing Data Transmission Scheme*. R.W. Chang and R.A. Gibby, 1968, IEEE Transactions on Communications, Vol. 16, pp. 529-540.
23. *Data Transmission by Frequency-Division Multiplexing Using the Discrete Fourier Transform*. S.B. Weinstein and P.M. Ebert, 1971, IEEE Transactions on Communications, Vol. 19, pp. 628-634.
24. *Frequency Domain Data Transmission Using Reduced Computational Complexity Algorithms*. A. Peled and A. Ruiz, 1980, ICASSP'80 - Proceedings of the IEEE International Conference on Acoustics, pp. 964-967.
25. *An Orthogonally Multiplexed QAM System Using the Discrete Fourier Transform*. B. Hirosaki, 1981, IEEE Transactions on Communications, Vol. 29, pp. 982-989.
26. ANSI standard T1.413-1995 - Customer Installation Interfaces — Asymmetric Digital Subscriber Line (ADSL) Metallic Interface, 1995.
27. *Fundamentals of Coding for Broadcast OFDM*. R. Wesel, 1995, Proceedings of the 29th Asilomar Conference on Signals, Systems & Computers.
28. *An introduction to Ultra Wideband Communication Systems*. J.H. Reed, 2005, editor Prentice Hall.
29. *Train of diverse multifrequency radar pulses*. N. Levanon, 2001. Proceedings of IEEE Radar Conference, pp. 93-98.
30. *Conceptual design of a dual-use radar/communication system based on OFDM*. D. Garmatyuk and J. Schuerger, 2008, MILCOM 2008 - Proceedings of IEEE Military Communications Conference, pp. 1-7.
31. *Orthogonal Frequency Division Multiplexing for Wireless Communications* Ye Li, G.L. Stüber, 2006, editor Springer

32. *An Overview of Peak-to-Average Power Reduction Techniques For Multicarrier Transmission*. S.H. Han, J.H. Lee, 2005, Modulation, Coding and Signal Processing for Wireless Communications, Vol. 12, pp. 56-65.
33. ERO Frequency Information System, www.efis.dk
34. European Telecommunications Standard Institute., www.etsi.com
35. IEEE standards, standards.ieee.org
36. *Doppler properties of polyphase coded pulse compression waveforms*. F.F. Kretschmer, B.L. Lewis, 1983, IEEE Transactions on Aerospace and Electronic systems, Vol. AES-19, pp. 521-531.
37. *OFDM waveforms for frequency agility and opportunities for Doppler processing in radar*. G. Lellouch, P. Tran, R. Pribic and P. van Genderen, 2008, RADAR '08 - Proceedings of IEEE Radar Conference, pp. 1-6.
38. *Silent Sentry A New Type of Radar*. B.D Nordwall, 1998, Aviation Week & Space Technology, Vol. 30, pp. 70-71.
39. *Target tracking using television-based bistatic radar*. P.E. Howland, 1999, IEE Proceedings - Radar, Sonar and Navigation, Vol. 146, pp. 166-174.
40. *Simulated Imaging Performance of UWB SAR Based on OFDM*. D.S Garmatyuk, 2006. Proceedings of IEEE International Conference on Ultra-Wideband. pp. 237-242.
41. *On the Capability of a Radar Network to Support Communications*. G. Lellouch and H. Nikookar, 2007, Proceedings of 14th IEEE Symposium on Communications and Vehicular Technology in the Benelux, pp. 1-5.
42. *Design of a Multifrequency FMCW Radar*. M. Jankiraman, B.J. Wessels and P. van Genderen, 1998, Proceedings of 28th European Microwave Conference, Vol. 1, pp. 584-589.
43. *Pandora multifrequency FMCW/SFCW radar*. M. Jankiraman, B.J. Wessels, B. J. and P. Van Genderen, 2000, Proceedings of the IEEE 2000 International Radar Conference, pp. 750-757.
44. *Radar and data communication fusion with UWB-OFDM software-defined system*, D. Garmatyuk, K. Kauffman, 2009, ICUWB 2009 - Proceedings of IEEE International Conference on Ultra-Wideband, pp. 454-458.
45. *Wideband OFDM system for radar and communications*. D. Garmatyuk et al., 2009, Proceedings of IEEE Radar Conference, pp. 1-6.
46. Open Air Interface - IDROMel, www.openairinterface.org
47. *Dynamic Range Improvements in Radar Systems using Transmitter Linearisation*. D. Pennington, 2004, 1st EMRS DTC Technical Conference - Edinburgh, Vol. C15.

48. *Dynamic Range Enhancements in Radar Systems*. B.J. Harker, 2005, 2nd EMRS DTC Technical Conference – Edinburgh, Vol. A10.
49. *Dynamic Range Enhancements for Radars and RF Systems*. B.J. Harker, Z. Dobrosavljevic, Dr. E.P. Craney, A.D. Chadwick, Dr. S. Hayward, Dr. R. Penney, M.S. Cole, Professor R.A. Belchert, 2008, 5th EMRS DTC Technical Conference - Edinburgh, Vol. B16.
50. *Dynamic Range Enhancements in Radar Systems*. B.J. Harker, 2006, 3rd EMRS DTC Technical Conference - Edinburgh, Vol. A23.
51. *Dynamic range improvements and measurements in radar systems*. B.J. Harker, Z. Dobrosavljevic, E.P. Craney, S. Miles, R.A. Belcher and J.Chambers, 2007, IET Radar - Sonar Navigation, Vol. 1 issue 6, pp. 398-406.
52. *OFDM Transmitter Power Amplifier and PAR Reduction Performance: Measurement and Simulation*.S. Gifford, J.E. Kleider, S. Chuprun, 2002, Proceedings of MILCOM 2002, Vol. 1, pp. 591-595.
53. *An Effective Iterative Clipping for Coded CI/OFDM Systems over the Nonlinearity of SSPA*. K. Anwar, T. Hara and M. Okada. 2008, PIMRC 2008 - IEEE International Symposium on Personal, Indoor and Mobile Radio Communications, pp. 1-5.
54. *Linearization of Power amplifiers by baseband digital predistortion for OFDM transmitters*. D. Bondar, D. Budimir and B. Shelkovnikov, 2008, CriMiCo'2008 - 18th International Crimean Conference on Microwave & Telecommunication Technology, Sevastopol, Crimea, Ukraine, pp. 270-271.
55. *A Tunable Pre-Distorter for Linearization of Solid State Power Amplifier in Mobile Wireless OFDM*. R.J.P. de Figueiredo, B.M. Lee, 2005, IEEE Symposium on Emerging Technologies: Circuits and Systems for 4G Mobile Wireless Communications, pp. 84-87.
56. *Increasing TWTA multi-carrier saturated power with limiters and linearizers*. A. Katz, 1999, IEEE Microwave Theory and Techniques Society Digest, pp. 337-340.
57. *An Efficient Technique for Reducing PAPR of OFDM System in the Presence of Nonlinear High Power Amplifier*. H. Sakran, M. Shokair , A.A. Elazm, 2008, ICSP 2008 - Proceedings of international conference on signal processing, pp. 1749-1752.
58. *A new peak-to-average power reduction technique in the OFDM system using u-law compander*. H. Sakran, M. Shokair, A.A. Elazm, 2008, ISWCS '08 - IEEE International Symposium on Wireless Communication Systems, pp. 386-390.
59. *A discussion of the effects of amplifier back-off on OFDM*. B. J. Dixon, R. D. Pollard and S. Iezekiel, 1999, High Frequency Postgraduate Student Colloquium, pp. 14-19.
60. *Clip correction in wireless LAN receivers*. R. Rietman, J.P. Linnartz, E.P de Vries, 2008, EuWiT 2008 - European Wireless Technology, Amsterdam, Netherlands, pp. 174-177.

61. *Impacts of Narrowband Interference on OFDM-UWB Receivers: Analysis and Mitigation*. K. Shi, Y. Zhou, B. Kelleci, T.W. Fischer, E. Serpedin, A.I. Karsilayan, 2007, IEEE Transaction on Signal Processing, Vol. 55 issue 3, pp. 1118-1128.
62. *Analog to digital converter resolution of multi-band OFDM and pulsed-OFDM ultra wideband systems*. E. Saberinia, A.H. Tewfik, K.-C. Chang, G.E. Sobelman, 2004, 1st International Symposium on Control, Communications and Signal Processing, pp. 787-790.
63. *Feasibility study of a multi-carrier dual-use imaging radar and communication system*. D. Garmatyuk, J. Schuerger, Y.T. Morton, K. Binns, M. Durbin, J. Kimani, 2007, EuRAD 2007 - Proceedings of European Radar Conference, pp. 194-197.
64. *Comparison between linear FM and phase-coded CW radars*. N. Levanon, B. Getz, 1994, IEE Proceedings -Radar, Sonar and Navigation, Vol. 141 issue 4, pp. 230-240.
65. *Removing autocorrelation sidelobes by overlaying orthogonal coding on any train of identical pulses*. E. Mozeson, N. Levanon, 2003, IEEE Journal on Aerospace and Electronic Systems, Vol. 39 issue 2, pp. 583-603.
66. *Diverse radar pulse-train with favourable autocorrelation and ambiguity functions*. E. Mozeson, N. Levanon, 2002, RADAR 2002, Proceedings of IEEE radar conference, pp. 172-176.
67. *Multifrequency radar signals*. N. Levanon, 2000. Proceedings Record of the IEEE 2000 International Radar Conference, pp. 683-688.
68. *Multicarrier radar signals with low peak-to-mean envelope power ratio*. E. Mozeson, N. Levanon, 2003, IEE Proceedings -Radar, Sonar and Navigation, Vol. 150, pp. 71-77.
69. *Multicarrier radar signal - pulse train and CW*. N. Levanon, E. Mozeson, 2002, IEEE Journal on Aerospace and Electronic Systems, Vol. 38 issue 2, pp. 707-720.
70. *Doppler Tolerance of OFDM-coded Radar Signals*. G.E.A. Franken, H. Nikookar and P. van Genderen, 2006, EuRAD 2006 - Proceedings of 3rd European Radar Conference, pp. 108-111.
71. *Solving Doppler ambiguity by Doppler sensitive pulse compression using multi-carrier waveform*. R.F. Tigrek, W.J.A. de Heij, P. van Genderen, 2008, EuRAD 2008 - Proceedings of European Radar Conference, pp. 72-75.
72. *Wideband OFDM pulse burst and its capabilities for the Doppler processing in radar*. G. Lellouch, R. Pribic, P. van Genderen, 2008, Proceedings of International Conference on Radar, pp. 531-535.
73. *Waveform analysis and design*. N. Levanon, 2008, RADAR '08 - Proceedings of IEEE Radar Conference, p. 1.
74. Tekmicro, www.tekmicro.com.
75. Stratix V, www.altera.com.

76. Virtex 6, www.xilinx.com.
77. PXIexpress rack, Rack RAID storage disk drives, www.ni.com.
78. Pin switches, www.paciwave.com.
79. Electro-mechanical switches, www.jfwindustries.com.
80. *Digital techniques for wideband receivers*, J.B. Tsui, 2004, second edition, editor : Scitech Publishing Inc.
81. *Multitone signals with low crest factor*. S. Boyd, 1986, IEEE transactions on circuits system, Vols. CAS-33, pp. pp 1018-1022.
82. Commission, Federal Communications. FCC 02-48. 2002.
83. ITU. UN regulatory body for Telecommunications.
84. *Radar and communication waveform: Wideband ambiguity function and narrowband approximation*. M. Ruggiano, and P. van Genderen, 2007, Proceedings of IET International Conference on Radar Systems, pp. 1-5.
85. *Wideband ambiguity function and optimized coded radar signals*. M. Ruggiano and P. van Genderen, 2007, EuRAD 2007 - Proceedings of European Radar Conference, pp. 142-145.
86. Tektronix, www.tek.com.
87. Filtek, www.filtekkfilters.com.
88. *Analyse de l'effet micro-Doppler de cibles mobiles en imagerie radar*. A.Ghaleb, 2009, PhD thesis, Telecom ParisTech. 2009.
89. *Radar High Resolution Range & Micro-Doppler Analysis of Human Motion*. L. Vignaud, A. Ghaleb, J. Le Kerneec, J.M. Nicolas, 2009, Radar 2009- SEE international radar conference, pp 1-6.
90. *A refined Micro-Doppler Analysis of pedestrians in ISAR imaging*. A. Ghaleb, L. Vignaud, J.M. Nicolas, 2008, EUSAR 2008 - 7th European Conference on Synthetic Aperture Radar, pp 1-4.
91. *Waveshaping of multicarrier signal for data transmission over wireless channels*. H. Nikookar, and R. Prasad, 1997, IEEE 6th International Conference on Universal Personal Communications Record Conference Record, pp. 173-177.
92. *OFDM Wireless LANs: A Theoretical and Practical Guide*. J. Terry, J. Heiskala, 2002, editor: Sams Publishing.

93. *Effect of clipping and filtering on the Performance of OFDM*. X. Li, Jr L.J. Cimini, 1998, IEEE Communication Letters, Vol. 2 issue 5, pp. 131-133.
94. *Peak-to-Average Power Reduction for OFDM by Repeated Clipping and Frequency Domain Filtering*. J. Armstrong, 2002, Electronic Letters, Vol. 38, pp. 246-247.
95. *Complementary Series*. M. Golay, 1961, IEEE Transactions on Information Theory, Vol. 7, pp. 82-87.
96. *Peak-to-Mean Power Control in OFDM, Golay Complementary Sequences, and Reed–Muller Codes*. J.A. Davis, J. Jedwab, 1999, IEEE Transaction on Information Theory, Vol. 45, pp. 2397-2417.
97. *On the Existence and Construction of Good Codes with Low Peak-to-Average Power Ratios*. K.G. Paterson, V. Tarokh, 2000, IEEE Transactions on Information Theory, Vol. 46, pp. 1974-1987.
98. *Generalized Reed-Muller Codes and Power Control in OFDM Modulation*. K. Patterson, 2000, IEEE Transactions on Information Theory, Vol. 46, pp. 104-120.
99. *A Simple Encodable/Decodable OFDM QPSK Code with Low Peak-to-Mean Envelope Power Ration*. C.V. Chong, V. Tarokh, 2001, IEEE Transactions on Information Theory, Vol. 47, pp. 3025-3029.
100. *Block Coding Scheme for Reduction of Peak to Mean Envelope Power Ratio of Multicarrier Transmission Scheme*. A.E. Jones, S.K. Barton, 1994, Electronic Letters, Vol. 30, pp. 2098-2099.
101. *OFDM with Reduced Peak-to-Average Power Ratio by Optimum Combination of Partial Transmit Sequences*. S.H. Müller, J.B. Huber, 1997, Electronic Letters, Vol. 33, pp. 368-369.
102. *Adaptive PTS Approach for Reduction of Peak-to-Average Power Ratio of OFDM Signal*. C. Tellambura, A.D.S. Jayalath, 2000, Electronic Letters, Vol. 36, pp. 1226-1228.
103. *Peak-to-Average Power Ratio Reduction of an OFDM Signal Using Partial Transmit Sequences*. Jr. L.J. Cimini, N. R. Sollenberger, 2000, IEEE Communication Letters, Vol. 4 issue 3, pp. 86-88.
104. *Improved Phase Factor Computation for the PAR Reduction of an OFDM Signal Using PTS*. C. Tellambura, 2001, IEEE Communication Letters, Vol. 5 issue 4, pp. 135-137.
105. *PAPR Reduction of OFDM Signals Using a Reduced Complexity PTS Technique*. S.H. Han, and J.H. Lee, 2004, IEEE Signal Processing Letters, Vol. 11, pp. 887-890.
106. *A Comparison of Peak Power Reduction Schemes for OFDM*. S.H. Müller, J.B. Huber, 1997, GLOBECOM'97 - Proceedings of IEEE Global Communication Conference, pp. 1-5.

107. *Reducing the Peak-to-Average Power Ratio of Multicarrier Modulation by Selected Mapping*. R. W. Bäuml, R. F. H. Fisher, and J. B. Huber, 1996, *Electronic Letters*, Vol. 32, pp. 2056-2057.
108. *SLM Peak-Power Reduction without Explicit Side Information*. H. Breiling, S.H. Müller–Weinfurtner, J.B. Huber, 2001, *IEEE Communication Letters*, Vol. 5, pp. 239-241.
109. *Reducing the Peak-to-Average Power Ratio in OFDM by Cyclically Shifting Partial Transmit Sequences*. G. R. Hill, M. Faulkner, and J. Singh, 2000, *Electronic Letters*, Vol. 36, pp. 560-561.
110. *Peak to Average Power Reduction for OFDM Schemes by Selective Scrambling*. P. Van Eetvelt, G. Wade, and M. Tomlinson, 1996, *Electronic Letters*, Vol. 32, pp. 1963-1964.
111. *Reducing the Peak-to-Average Power Ratio of Orthogonal Frequency Division Multiplexing Signal through Bit or Symbol Interleaving*. A.D.S Jayalath, C. Tellambura, 2000, *Electronic Letters*, Vol. 36 issue 13, pp. 1161-1163.
112. *Peak to Average Power Reduction for Multicarrier Modulation*. J. Tellado, J.M Cioffi, 1998, *GLOBECOM'98 - Proceedings of IEEE Global Communication Conference*
113. *PAR Reduction in OFDM via Active Constellation Extension*. B.S. Jones, D.L. Krongold, 2003, *IEEE Transactions on Broadcasting*, Vol. 49, pp. 258-268.
114. *Electromagnetic Waves and antennas*. S.J. Orfanidis, 2008, editor: Rutgers University.
115. *The theory of bandpass sampling*. R.G. Vaughan, N.L. Scott, D.R. White. 1991, *IEEE transactions on Signal Processing*, Vol. 39 issue 9, pp. 1973-1984.
116. *Design and performance of a wideband sub-sampling front-end for multi-standard radios*. M.R. Yuce, A. Tekin, W. Liu, 2008, *International journal of electronics and communications*, Vol. 62, pp. 41-48.
117. *Trait é d' électricité - th éorie et traitement des signaux*. F. Coulon, 1998, editor: presses polytechniques et universitaires romandes.
118. *Aperture Jitter Effects in Wideband ADC systems*. H. Kobayashi, M. Morimura, K. Kobayashi, Y. Onaya, 1999, *Proceedings of the 38th international conference on Instrumentation, Control, Information Technology and System Integration*, pp. 1089-1094.
119. *The Effects of Aperture Jitter and Clock Jitter in Wideband ADCs*. G. Fettweis, M. Löhning, 2007, *Journal of Computer Standards & Interfaces - Elsevier Science Publishers B. V.*, Vol. 29, pp. 11-18.
120. *Aperture Synthesis with a Non-Regular Distribution of Interferometer Baselines*. J.A. Högbom, 1974, *Astronomy and Astrophysics Supplement*, Vol. 15, p. 417.
121. *De la radio logicielle à la radio intelligente*, J. Palicot, 2010, editor: HERMES.
122. *Cognitive radar*. S. Haykin, 2006, *IEEE Signal processing magazine*, pp 31-40